Department of Materials Science

PhD program in Materials Science and Nanotechnology
Cycle XXXI

From nanosized to single site zinc-based activators for rubber vulcanization process

Mostoni Silvia

Registration number: 810913

Supervisor: Prof. Roberto Scotti

Industrial tutor: Dott.ssa Raffaella Donetti

Coordinator: Prof. Marco Bernasconi

ACADEMIC YEAR 2017/2018

Contents

Glossary

A-SiO$_2$	Silica particles functionalized with APTES
APTES	(3-aminopropyl)triethoxysilane
AR	Aspect Ratio
ATR-FTIR	Attenuated Total Reflection – Fourier Transform Infrared Spectroscopy
B.E.T.	Brunauer Emmett Teller
BR	Butadiene Rubber
CBS	N-Cyclohexyl-2-benzothiazole sulphenamide
CHA	Cyclohexylamine
CHNS	Elemental analysis
CPMAS	Cross-Polarization Magic Angle Spinning
D-SiO$_2$	Silica particles functionalized with EDTMS
DDD	1,2-dodecanediol
ΔW	Weight loss registered in a specific range of temperature
EDTMS	N-[3-(Trimethoxysilyl)propyl]ethylendiamine
EPR	Electron Paramagnetic Resonance
G*	Complex modulus
G′	Elastic modulus
G′′	Dissipative modulus
HRTEM	High Resolution Transmission Electron Microscopy
ICP-AES	Inductively Coupled Plasma Atomic Emission Spectroscopy
IR	Isoprene Rubber
LS	Layered Silicate
M$_{min}$	Minimum torque
M$_{max}$	Maximum torque
M-SiO$_2$	Silica particles functionalized with MPTMS
M$_{CH}$-SiO$_2$	Silica particles functionalized with MPTMS, synthesis performed in cyclohexane
m-ZnO	Micro-crystalline ZnO

MBT	Mercaptobenzothiazole
MCV	Model Compound Vulcanization
MPTMS	(3-Mercaptopropyl)tri-methoxysilane
MS	Mass Spectroscopy
MW	Molecular weight
N_A	Avogadro's number
NC	Nanocomposite
NMR	Nuclear Magnetic Resonance
NP	Nanoparticles
ODA	Octadecylamine
ODE	1-octadecene
phr	Parts per Hundred Rubber
Ph-TAD	Phenil-triazolidinone
PS	Polystyrene
SA	Stearic acid
Sep	Sepiolite
SSA	Specific Surface Area
tanδ	Dissipative factor
TEOS	Tetraethyl orthosilicate
TESPD	Bis(3Triethoxysilylpropyl)disulfide
TGA	Thermo Gravimetric Analysis
TME	2,3-dimethyl-2-butene
XPS	X-Ray Photoelectron Spectroscopy
XRD	X-Ray Diffraction
ZA	Zinc Acetate
ZnA-SiO$_2$	Zn(II) centres dispersed onto SiO$_2$ particles
ZnO/SiO$_2$	ZnO NPs dispersed onto SiO$_2$ particles

Introduction

Rubber nanocomposites (NCs) are commonly used materials in tyre industry. Their mechanical properties result from the synergetic interactions between polymer chains and reinforcing filler nanoparticles (NPs), whose addition provides an added value in materials properties not displayed by the individual phases. Carbon black and silica are typically filler NPs employed to produce rubber NCs for tyres.

The mechanical properties of rubber NCs are further increased thanks to the vulcanization reaction, a consolidated large-scale process used to improve elasticity, tensile strength and abrasion of rubber materials. Sulphur vulcanization is based on the formation of cross-links between the polymer chains through mono-, bi- and poly-sulphide bridges. In the industrial perspective, the enhancement of the vulcanization rate and cross-linking efficiency is a fundamental requirement to increase the productivity, while reducing the energy and time consumption. Accelerators, as sulphenamides or thiazoles, activators, as inorganic oxides or hydroxides, and co-activators, generally fatty acids, are generally utilized to increase the efficiency of the reaction, significantly reducing the reaction temperature and improving the mechanical properties of the final material. Due to the presence of all these species, the reaction is characterized by a highly complex mechanism with many consecutive reaction steps. Consequently, despite the long history of the vulcanization process, the role of the activators and accelerators and the nature of the intermediate active complexes are not yet fully understood, and the real total control of the process is still a scientific and technological challenge.

In this process, a main role is recognized to zinc oxide (ZnO), the worldwide used activator of vulcanization, intensively employed in the rubber industrial production, in particular for tyres applications. This is due to an advantageous kinetic of the reaction and to a direct impact on the nature of the cross-linked structures, with the achievement of higher cross-linking densities. The global

demand per year of ZnO is estimated 15 million tons, (data of 2010), with a ZnO content in tyres corresponding to 3-5 phr (parts per hundred rubber). Nevertheless, its extended use is connected to a very important environmental issue, that nowadays drives towards a safer reduction of ZnO content in tyres. According to ECHA classification, ZnO is classified toxic for the aquatic environment (R50-53); as zinc is released during production, service conditions, disposal and recycling of rubber products, an excess of zinc concentration in the environment can be generated. Reducing zinc content in tyres products would represent a benefit from the environmental point of view, to reduce the consequent potential negative effects on the ecosystem. Besides, the recycling treatment of end-of-life tyres would benefit of the reduction of ZnO amount, to produce high quality regenerated rubber. Finally, thanks to the more environmentally friendly mentality diffused in the recent years, an important economic aspect would be involved, due to the increased demand for low environmental impact products.

In the literature, several alternatives have been proposed to reduce or substitute ZnO in rubber materials, based on the use of different zinc complexes or involving other metal oxides; nevertheless, at the moment no alternative solutions are available in the market or are going to be applied. In a recent work, Susanna et al.[1], proposed a possible solution by supporting ZnO NPs on the surface of silica NPs reinforcing filler (ZnO/SiO$_2$), claiming that higher vulcanization efficiencies could be achieved by using half of the traditional amount of micro-crystalline ZnO (m-ZnO) used in the industrial processes. This material, called double function filler, behaving both as reinforcing filler and as activator for vulcanization, showed that a higher dispersion of zinc oxide inside the rubber matrix would favour a more efficient vulcanization process.

Aim of the thesis

In this scenario, the aim of the Thesis was to develop innovative zinc-based activators for rubber vulcanization process, in order to reduce the amount of m-

ZnO conventionally used in the industrial process and to decrease the zinc leaching during the preparation and use of the material, keeping a high vulcanization efficiency. The introduction of innovative activators was based on the concept of a higher dispersion of the activator inside the rubber matrix, achieved with the double function filler (ZnO/SiO_2). The work aimed at the introduction of dispersed and more active zinc sites, moving from the dispersion of ZnO NPs onto the surface of silica particles to isolated zinc centres, exploiting SiO_2 as a tool to increase the dispersion. Zinc centres were studied with the purpose of creating heterogeneous single catalytic sites on the surface of silica, stable enough to be maintained during the vulcanization reaction and the interaction with the other involved species. For this reason, single zinc sites ($ZnA-SiO_2$) anchored on silica surface were synthesized, to exploit the advantages derived from the higher distribution, while increasing the availability and reactivity of the activator towards the other vulcanization reagents.

In the first part, the work was focused on the synthesis of the two different materials. The synthesis of ZnO/SiO_2 was performed by a sol-gel procedure, based on the hydrolysis and condensation of a zinc precursor in a basic environment. $ZnA-SiO_2$ was synthesized through a two-step reaction, in which silica was pre-functionalized with a grafting agent ((3-aminopropyl)triethoxysilane, APTES) and then reacted with a zinc precursor. The formation of ZnO NPs and Zn(II) centres anchored to SiO_2 and their relative structural properties were deeply investigated in both cases, through morphological, structural and surface analyses, to be aware of the nature of the zinc-based activators.

Lately, the two materials were tested as activators for the vulcanization process of polyisoprene rubber (IR) NCs and their properties compared to the behaviour of m-ZnO, focusing on the assessment of vulcanization efficiency in the presence of different activators. Moreover, the influence of the introduction of $ZnA-SiO_2$ and ZnO/SiO_2 on rubber NCs was evaluated in terms of the mechanical

properties of vulcanized rubber NCs, their cross-linking densities and their morphological properties.

Later on, the effect of the nature of the activators on the reaction mechanism was studied, in order to understand how the process of formation of the cross-linking products and the mechanism of interaction between the vulcanization agents are modified by the introduction of more dispersed zinc-based activators. A main focus was dedicated to the influence of ZnA-SiO$_2$ material on the mechanism of the reaction, since the introduction of anchored isolated zinc centres was supposed to likely modify the mechanism, compared to m-ZnO and ZnO NPs, especially due to the possible behaviour of Zn(II) centres as heterogeneous catalytic sites on the surface of SiO$_2$. The possible promotion of the catalytic process in the proximity of the SiO$_2$ surface was investigated both in terms of reaction mechanism and of the local distribution of the cross-linking inside the rubber NCs.

At last, the activity of the two activators was studied in relation to their structural parameters: by suitably tuning the structural properties of ZnO/SiO$_2$ and ZnA-SiO$_2$, the influence of the nature of the two activators was further evaluated in the determination of their reactivity.

Finally, the two zinc-based activators were applied in different systems compared to the IR NCs, in order to enlarge the number of possible applications of these materials in the rubber field and in the preparation of rubber NCs.

Structure of the thesis

The research described in the Thesis is subdivided with the following structure:

In *Chapter 1*, a general scenario on tyres circular economy is described, focusing on the possible modifications that can be introduced during production, use and disposal phase to make the life cycle of tyres more sustainable. Later, a focus on the vulcanization process is presented, with a particular attention to the possible strategies that could be followed to reduce the environmental impact of tyres

industries products, especially referring to the advantages and problems related to the use of ZnO as activators in the vulcanization process.

In *Chapter 2*, the syntheses of two innovative double function fillers are illustrated (ZnA-SiO$_2$ and ZnO/SiO$_2$) and the materials characterized to define the structure and the composition of the zinc-based activators.

In *Chapter 3*, the use of the materials as activators in IR NCs is described, compared to m-ZnO; their influence in the vulcanization efficiency and the effects on the properties of vulcanized rubber NCs studied, focusing on their mechanical, cross-linking densities and morphological properties.

In *Chapter 4*, the mechanism of vulcanization is investigated in the presence of the two activators, connecting the discussion to the mechanism reported in the literature in the presence of m-ZnO.

In *Chapter 5*, the influence of Zn(II) centres in the promotion of the vulcanization process inside the rubber matrix was evaluated, by analysing the cross-linking distributions inside the vulcanized rubber NCs and the mechanical properties of the NCs.

In *Chapter 6*, the reactivity of the zinc-based activators was further analysed as a function of their structural properties. The role of the structural parameters was evidenced by suitably changing the structure of the materials and evaluating the reactivity of the final products.

In *Chapter 7*, to extend the range of systems in which the two activators could be applied, the combination of the anisotropic support effect with the higher reactivity of ZnO NPs and zinc centres was studied; moreover, the application of Zn/SiO$_2$ as a possible double function filler to increase the filler/rubber interactions in organically modified polymers was considered.

Finally, *Chapter 8* sums up the main results and reports the conclusion of the investigation.

Bibliography

1.   Susanna, a., Armelao, L., Callone, E., Dirè, S., D'Arienzo, M., Di Credico, B., Giannini, L., Hanel, T., Morazzoni, F. & Scotti, R. ZnO nanoparticles anchored to silica filler. A curing accelerator for isoprene rubber composites. *Chem. Eng. J.* **275**, 245–252 (2015).

1

Towards a more sustainable industrial production of tyres

A focus on the vulcanization process

1.1 Sustainability of tyre life cycle

The production of tyres is one of the most innovative technologies introduced in the last century. Although it has been more than one hundred years from their first invention, several studies are still concerned with the optimization of their composition and performances. The first concept of a tyre found its origin back to the XIX century, when William Thomson developed a first inflatable rubber support, to be applied to wheels, in order to make the rolling process of wheels more favourable. This invention was patented in 1847,[1] but the real popularity of tyres came later, due to the parallel growth of the modern automotive market. The possibility to travel faster and farther, the easiness of transportation of more and more goods within shorter time, contribute to the extraordinary development of both the automotive and tyre market, that are today two driving fields in the global economy.

As a confirmation of the success of tyre market, the annual production of tyres was reported to be more than one billion units in 2010[2-5], with a market diffused worldwide; almost 88% of the total number of tyres are nowadays produced by the most developed countries, including Europe, USA, Japan and India. Besides, by 2024, the global market is forecast to reach two and a half billion units, doubling the number of available tyres in the world in just fourteen years[6].

Nowadays, tyres are constituted by very complex materials, whose composition is the result of the long history of tyre industries, whose work was focused on the optimization of the mechanical properties and performances. Several parts of the tyre contribute to its final structure, each composed of different materials. Rubber, the main component, is usually reinforced with additional substances of distinct nature, that cooperate in determining its structure.

In the last few years, tyre market has started to face some drawbacks, that have attracted the attention of the society mainly from an environmental point of view. The main concern related to tyres is that, due to the high complexity of their structure, the high number of ingredients and the use of thermal

treatments for their production, tyres could not be decomposed to re-obtain the raw materials; closing the circular economy of tyres is still one of the biggest challenges in this century.

The impressive numbers of the annual production, are connected to i) the consumption of a large amount of natural resources and energy during the production phase and ii) the generation of a huge amount of discarded tyres (End of Life Tyres, ELTs), defined as tyres not suitable anymore to responding to the requirements for use on the road, due to tear or irreparable damages[7]. Thus, in the recent years, many efforts have been concentrated on the development of innovative techniques to handle ELTs, regulated by European legislation, to reduce the wastefulness of resources and promote the recycling of the existing materials[2,5].

Further implications have been connected lately to the absence of a circular economy: the substances enclosed in tyres could not be recovered after use, but on the contrary they were shown to be easily released both during the production and use phase (due to tyre tread consumption), and finally disposal[8]. Moreover, recent scientific studies have highlighted that most of these substances can be toxic for the environment and can affect the whole ecosystem, especially in the urban areas. As a result, a large part of the scientific research in this field is nowadays focused on the reduction or substitution (totally or partially) of the more toxic materials conventionally used on tyre production, based on risks assessment forms for each component.

Consequently, in the XXI century, working in the tyre market has assumed multiple aims: produce high performant tyres, deal with the scarceness of natural resources and minimize the pollution coming from production, use and disposal phases. Facing these problems can be done by either developing suitable methods to treat ELTs, in order to reduce the wastefulness of natural resources or reconsidering tyre compositions, to decrease the amount of toxic substances that contribute to pollution in all life steps of tyres.

In the next paragraphs, the above-mentioned aspects will be further discussed, starting from the concept of the circular economy, and focusing on a more detailed description of causes and consequences of the absence of tyre circular economy; later on, the possible pathways that can be covered to solve the environmental issues of an inadequate circular economy in the different phases of tyre life cycle will be reported, highlighting what have been done so far and the future perspectives.

1.1.1 The concept of circular economy

Materials life cycles can be generally decomposed into four subsequent phases: selection of raw materials, design and production of the products, use and at last the collection of ends of life materials, for the disposal/recovery step. In the last century, these four phases were usually organized in a classical linear model, called the "take-make-dispose" model, in which after the selection and use of raw materials for the production of goods and service, the only treatment reserved for the end of life materials was their disposal (Figure 1.1)[9]. This model was based on the accessibility of huge amount of resources and energies and was characterized by the production of directly proportional quantities of waste materials.

Only in the recent years, the increased scarcity of the raw materials and the elevated numbers of wastes to be treated, has grown a higher environmental awareness on the necessity to develop alternative systems, that could lead to more sustainable materials life cycles. Several regulations were introduced in the last years, aiming at a higher control of waste production and management. The main changes compared to the "take-make-dispose" method, were definitely introduced in a European Directive, published on November 19th, 2008 (Directive 2008/98/EC), in which a new framework legislation for handling of waste in the European community was established. One main point introduced by this regulation, as explained by Uruburu *et al.*[10], was the concept of "hierarchy of waste", in which different priority levels were asserted, when

handling with end of life materials. In this perspective, waste formation needs to be avoided; otherwise, materials must be treated starting with re-using techniques, followed by recycling and energy recovery procedures, removing as far as possible their disposal, that can be considered only in case all the other options are not possible[11]. The classical pyramid presentation of waste management proposed by this regulation is shown in Figure 1.2.

Linear economy *vs* **Circular economy**

Take   Make   Dispose

Raw materials

Production

Use

Recover
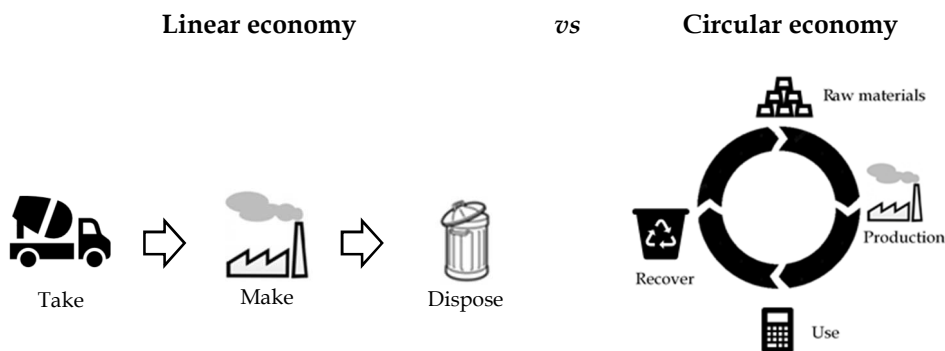
Figure 1.1. Scheme of the linear economy model in comparison to the circular economy model.

Starting from the new century, the attention of both the scientific and non-scientific community has started to focus on the development of a different model for the development and management of products, called Circular Economy (CE), that in few years substituted the older linear concept of materials life cycles[12].

The CE can be defined as an economic self-sustained system, in which fluxes of materials are transferred continuously and entirely from one phase to the others of their life cycles. The expression refers to an alternative idea on the production and use of goods and services, based on the possibility that all the economic systems behave as alive organisms, in which the nutrients are assumed, elaborated and reinserted in the biological and technical cycles after usage. In this perspective, a recurrent concept is the necessity of developing closed circular economy of the materials, so that the raw materials can be exploited for

the generation of products but can also be recovered at the end of the products life cycle, to be used again for other purposes (Figure 1.1). The main advantages of a closed circular economy are the complete elimination of waste materials, because of the total recovery of materials at the end of life and the reduction of the use of natural resources, whose availability has decreased due to the inconsiderate usage in the last century.
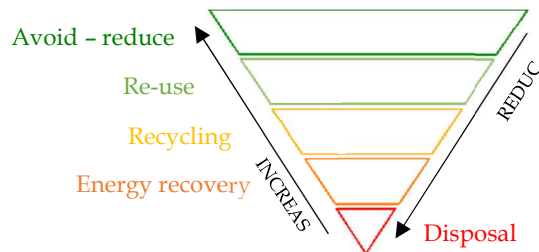
Figure 1.2. Pyramid of waste management proposed in the European regulation 2008/98/EC[10].

The development of closed circular economies has become an urgent issue for all the available products in the market and the production processes. By reconsidering all the phases of the materials life cycles (from the design, to production, consume and end of life treatments), it is necessary to pick up every opportunity to limit the use of new raw materials and energy as input of the cycles and minimize the production of wastes as outputs. In the following, a focus on the development of CE concept in tyre field is presented. Present situation and challenges are described.

1.1.2 Development of tyre circular economy

As for other fields, tyre market has started to put efforts towards the closure of the circular economy only in the recent years. In the last century, the typical linear model described before, was usually applied to tyre life cycle, and disposal of tyres at the end of their life was a common practice. Stockpiling tyres in huge landfills for years and decades was a reality all over the world. In 1992,

in Europe the number of disposed End of Life Tyres (ELTs) was more than 65% of the European production[13].

Though, at the beginning of the nineties, the presence of huge areas dedicated to landfills for tyres became an emergent issue, both for environmental and social reasons: the large areas needed for their disposal, the non-biodegradability and durability of tyres, the possible release of toxic substances expected from the erosion of tyres, the risks associated to their flammability, were the main problems that arose at that time. Tyre manufacturers were also facing growing environmental pressure from the general public and other stakeholders concerning illegal dumping and historic stockpiles. For these reasons, the introduction of re-using and recycling processes of dismissed tyres became more and more important and the development of the circular economy started to take place in this field.

In Europe, a first change towards CE was introduced in 1999, when disposal of tyres on landfills was declared outlawed (European Directive 1999/31/EC); stockpiling in landfills was further prohibited in the next years, both for whole tyres (July 2003) and ground tyres (July 2006), with the exception of bicycle tyres and tyres with an external diameter of more than 1400 mm. European member states were promoted to transpose European directives into local legislations, leaving the countries free to set national initiatives to reach the European targets[7,14]. In addition, a supplementary regulation (End of Life Vehicle Directive 2000/53/EC) on procedures for vehicles withdrawn from service, forced automotive companies to remove tyres before vehicles are scrapped, so that tyres can be recycled[13]. As a result, 96% of used tyre were recovered or recycled in Europe in 2010, an impressive result compared to the initial value of 35% registered in 1992 (Figure 1.3). This result is particularly positive if compared with the recovering percentage achieved for paper (72.2%) and plastic (58%) measured in the same year[15,16]. Finally, Europe has shown better results compared to Japan (91%) and USA (89%), establishing as one of the most advanced regions in the world in the recovery and recycling of used tyres.

Figure 1.3. Status of ELT recovery in 2013 in Europe. In green: area with > 90% recovery[5].

In the meantime, several re-using, recycling and energy recovery procedures have been developed to treat ELTs. A first distinction between part-worn tyres and ELTs was introduced[5], the former being defined as re-usable tyres, after a re-treading process; whereas, the latter were defined as tyres not suitable for their original purpose, neither as they are (second hand tyres) nor using re-treading techniques, but necessarily subjected to recycling techniques.

So far, both recycling and energy recovery technologies were developed on shredded or grinded tyres, with sizes starting from 150 mm for a large shred, to 2.5 – 4 mm after granulation and 0.8 – 2.5 mm for a pulverisation process, available for several purposes[7,17]. Typical recycling applications of tyres have been developed in the civil engineering field, for example road construction, drainage materials, sound barrier, insulation, but also with bitumen and asphalt [18,19]. Furthermore, ELTs were exploited for energy recovery procedures, as fuel sources (Tire-Derived Fuel, TDF) in the cement industry, steel plants or in thermal power station (especially widespread in the US and Japan, but not in Europe)[7,20]. The use and emissions limits of TDF were lately regulated by a European legislation (Directive 2000/76/EC), especially for cement kilns, in

which the use of TDF cannot exceed the 20% of total fossil fuel required in the manufacture of cement [21,22]. Between the other possible recycling treatments of tyres, lately also the so-called pyrolysis and gasification, thermal degradation processes of shred or granulated tyre to intermediate valuable products, such as oils, gases and syngas were introduced[23].

Nevertheless, nowadays a closed circular economy of tyres has not been achieved yet. The recovery of the raw materials starting from the end of life tyres is still one of the biggest challenges of this century. The main reason of the hard development of a closed CE for tyres can be assigned to their high complex composition, whose properties and performances are usually achieved through the combined use of different raw materials and thermal processes. In fact, tyres are highly engineered structural composites, whose performances can be designed to fit with vehicle manufacturers' ride, handling and traction criteria, together with quality safety and performance expectation of the customer[24]. The selection of suitable raw materials, design and production phases of the products are fundamental steps in the realization of performant tyres.

Consequently, in tyre field more efforts are required to obtain a closed CE. Three main different pathways can be followed to increase the sustainability of tyre life cycle: i) a direct improvement on ELTs treatments, by the introduction of innovative treatment techniques, in order to finally be able to re-obtain the raw materials, starting from the final product; ii) improvement of tyre performances, in order to reduce the contribution of tyres to the automotive generated pollution; iii) re-consideration of tyre composition and processes used to produce tyres, in order to simplify the complex composition of tyres and consequently the possible treatments of ELTs.

In the next paragraph, these possible paths are considered. Present and future perspectives will be presented in the three cases.

1.1.3 Improve tyre life cycle sustainability

Making tyre life cycle more sustainable means moving towards the production of materials with a low environmental impact, through the consumption of a low amount of natural resources and with a reduced generation of waste materials. All these changes are aimed at the generation of a closed tyre life cycle, based on the new concept of the circular economy of materials.

The sustainability of tyre life cycle can be improved from the present situation by properly modifying the steps involved in their life cycle, reconsidering the main phases involved. Main modifications could be introduced in different moment of tyre life cycle, including the selection of raw materials/production, use and recover phases of tyres.

Starting from the first phases, the selection of raw materials and the production processes used at the industrial level could be refined in order to make both the processes and the final products more sustainable. A proper change of the composition of tyres, through the introduction of innovative more eco-friendly materials, would contribute both to the reduction of the use of available raw materials in the world and to the possible development of materials that could be treated as ELTs more easily. Recently, in this context, several studies have been concentrated on the introduction of possible alternative ingredients for tyre composition.

One of the main problems regarding the selection of raw materials is that nowadays several components that are currently used for tyre production, have been classified as toxic materials and responsible for the emission of toxic by-products during production, use and disposal phases of tyres. Among them, one example is the presence of oils, used to facilitate the processing procedures of tyres, but that can be related to the emission of Polycyclic Aromatic Hydrocarbons (PAH), during the energy recovery processes[25]. Since ELTs are always processed as complex resources and used in their entirety as shred, granulate or powder, toxic substances that are introduced in the first steps of

tyre life cycle, will accompany tyre in all their secondary applications. Moreover, the emission of toxic by-products could take place also in the production and use phases, especially due to tyre tread consumption. As an example, high concentrations of benzothiazole molecules were detected in the environment as a result of their production and use during the rubber vulcanization process, with toxic effects to the aquatic environment and micro-organisms[26]. Besides, aquatic pollution was declared ascribable to high concentrations of zinc oxide too, whose main source was connected to tyre industries. To solve this problem, a major revision on the composition of tyres has become necessary; the substitution or reduction of contents of the more toxic substances is now mandatory in order to minimize or completely eliminate their leaching phenomena. This pathway goes through a deep analysis on the role of each component inside tyres, to achieve high awareness on the possible candidates to replace the present components, at the same time keeping high the performances of tyres, required both by the producers and customers. On this basis, both the substitution or reduction processes, could lead to the formulation of highly performing and more sustainable tyres, characterized by a lower environmental impact.

Regarding the use phase of tyre life cycle, efforts have been focused on the production of tyres that could promote a reduction of pollutants emissions during their use for the automotive market. Beyond the possible emission of toxic by-products due to the tread consumption of tyres, one main point is the contribution of tyres to the high fuel consumption of vehicles and consequently to the emission of carbon dioxide. This contribution is connected to the necessity of the vehicles to overcome the tyre rolling resistance, in other words the effort required by the vehicles' engine to keep a tyre rolling. The main contributor to rolling resistance is the process known as hysteresis, the energy loss that occurs as a tyre rolls through its footprint. This loss happens whenever a tyre contacts a road surface, but it can be minimized as much as possible, operating on the microscopic structure of tyres. For this reason, the development of the low

rolling resistance tyres has attracted much attention in the scientific community[27,28]. The use of these innovative tyres could reduce fuel consumption up to 10% of the present consumption, with great benefit for drivers' economy and with environmental benefits, driving towards the direction of more sustainable tyres for usage in the automotive market.

In this sense, a few years ago, Europe adopted a new legislation, the European Tyre Labelling Regulation (EC/1222/2009), that forces tyre industries to display information on the fuel efficiency (Figure 1.4), together with wet grip properties and rolling noise of tyres, when the tyres are sold to the customers. The aim was to increase the safety, the environmental and economic efficiency of road transport by promoting fuel-efficient and safe tyres with low noise levels.
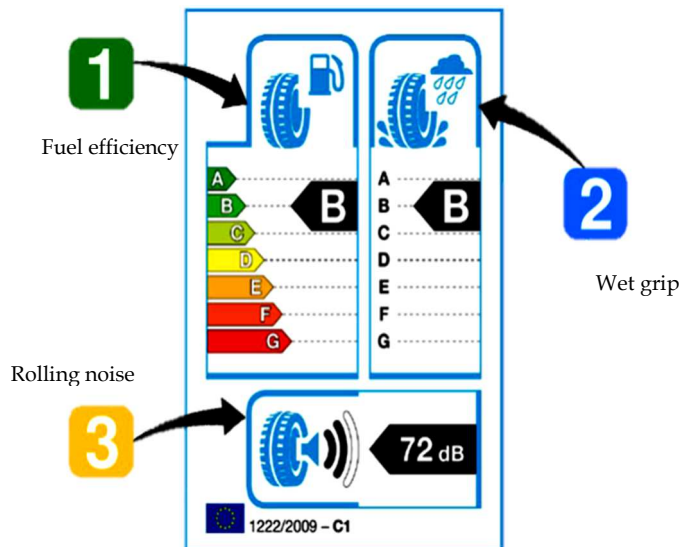
Figure 1.4. European Tyre Labelling introduced in 2009.

Finally, concerning the recovery phase of tyre life cycle, the introduction of innovative ELTs treatment methods would represent a further improvement towards the elimination of the stockpiled waste tyres and the possible recover of the raw materials. Considering that ELTs were estimated to be 17 million tonnes

in 2010[13], but higher estimations are forecast for the next years, following the imposed trend by the production process, the treatment of ELTs is still a priority from the sustainability point of view. Several processes are nowadays under investigation, in order to decompose tyres. One of the main studies is directed to the development of the so-called devulcanization process, that relies on the use of bacteria, ultrasounds or microwave, to facilitate the breakage of covalent bond inside the structure of tyres (sulphur-sulphur and carbon-sulphur bonds), typically formed during the production (mainly during vulcanization). Nowadays only a small number of operating systems with small capacity are available, but this process has a great potential in the reformation of the raw materials.

In this Thesis, the attention has been focused on the first steps of tyre life cycle, that are represented by the selection of the raw materials and the production processes of tyres. In particular, the study has concentrated on the actual industrial production plans and the possible modifications that can be introduced into tyre composition to make tyres more sustainable materials to be inserted into the environment. In the following, a discussion about the present composition of tyres and the processes used for their production is reported. Vulcanization process is presented in detail, as it represents the main industrial process investigated in the Thesis. Lately, a focus on zinc oxide (ZnO) is illustrated, as it is a catalyst for the vulcanization reaction, whose substitution and reduction in tyres is the main goal of this Thesis work.

1.1.4 Industrial production of tyres

The present situation about tyre composition and production at the industrial level is here reported, in order to develop a higher awareness on the high number of ingredients that are used in tyre formulations, their role and the possible modifications that may be introduced in tyre production, with the perspective of producing more sustainable tyres, with a lower environmental impact.

In a typical tyre, the main component is the rubber, also called elastomer, whose properties by itself are not useful until mixed with proper additives and treated with a thermal process, called vulcanization. Elastomers are elastic materials, composed of long and flexible chains with a coiled and kinked structure, that can be stretched, giving rise to an aligned result under stress. For this reason, elastomers are characterized by unique properties, such as low hardness, high elasticity and high elongation at break. In the field of tyres, both natural (NR) and synthetic rubber (isoprene, IR; styrene, SR; butadiene, BR) are used. Due to the large production of tyres, the major global use of rubber is dedicated to tyre applications (Figure 1.5).
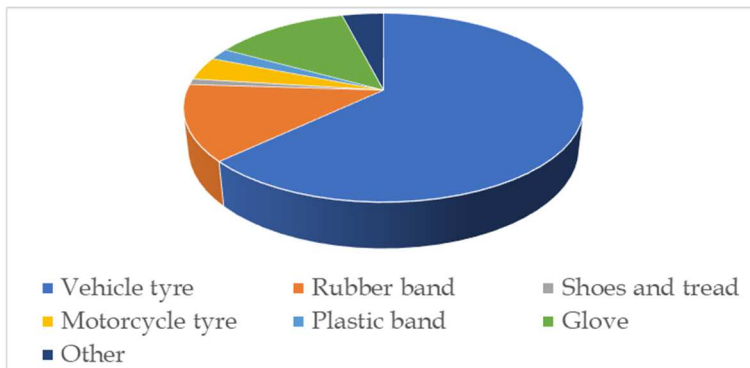
Figure 1.5. Natural Rubber consumption in 2012 by finish products[29].

Depending on the type of rubber products and on the desired properties, various ingredients with a specific function can be used and the selection of them is the first step to achieve the desirable physical and chemical properties. The selected formulation is built up on a drum and then heat, at controlled pressure, in a press. Different formulations are usually employed together in a tyre, positioned in specific locations inside the drum, on the basis of the properties of the specific formulation (hardness, tensile strength, wear resistance, etc.) and thus, on the specific part of the tyre that they will constitute (tread, bead, etc.).

A typical tyre formulation is reported in Table 1.1. The amount of each ingredient is expressed in phr (Parts per Hundred Rubber), that means parts per one hundred by weight of the rubber polymer.

Table 1.1. Typical rubber composition used for large scale rubber compounding for tyre applications.

Rubber composition

Ingredient	Quantity (phr)
Elastomer	100
Filler	30-40
Processing aid (oils, plasticizers)	2
Antidegradant	2
Vulcanization agent (sulphur)	2-4
Accelerator	2-3
Activator (usually used together with co-activator)	3-5

Fillers and vulcanization agents play a main role in determining the mechanical properties of rubber. Fillers are typically nanosized materials (1-100 nm, Figure 1.6), classified as black (mainly carbon black) or white fillers (silica, carbonates, silicates, clays) and used as reinforcing materials.

The interactions between filler nanoparticles (NPs) and elastomer chains in the rubber, together with the large interfacial area, are the main characteristics of the nanocomposites (NCs), that represents an added value to the materials properties, not showed by neither conventional composite (composed of microsized fillers) nor the two separated phases.

Recently, the innovation process towards more sustainable tyres have driven the attention towards the use of natural nanofillers, in order to substitute the synthetic materials, as silica and carbon black, generally used in the industrial production. As an example, natural layered silicates have been studied as

nanofillers, showing high reinforcement of rubber materials, by using highly available natural materials[30,31].
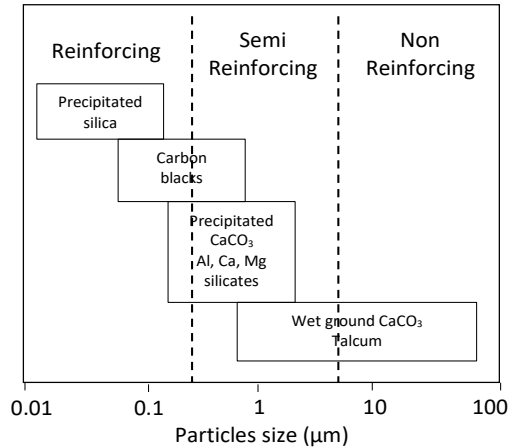
Figure 1.6. Classification of the reinforcement properties of fillers, based on their size.

On the other hand, vulcanization agents are employed to form a chemical cross-link between polymer chains. Vulcanization process usually follows the mixing step, in which the rubber is mixed with all the ingredients, including filler NPs and vulcanizing agents. In the case of sulphur as vulcanizing agent (Table 1.1), the cross-link is determined by the formation of poly-sulphide bridges that chemically connect the polymer chains. Several catalysts are required to enhance the vulcanization efficiency and rate, including accelerators (sulphenamides, thiazoles, thiurams, etc.), activators (metal oxides, such as zinc or magnesium oxide) and co-activators (fatty acids). This process guarantees the construction of a polymer network, that together with the filler networking and filler-rubber interactions, enables the achievement of the desired properties.

Historically, the introduction of these catalysts has been optimized considering the performances achieved during the vulcanization process; as explained later, accelerators, activators and co-activators all contribute to the determination of the vulcanization efficiency and rate, and the interaction between these species

is fundamental to create active intermediate species that allows the formation of polymer cross-link. Only recent studies have highlighted that these substances, especially organic accelerator species and inorganic activators, can be toxic from an environmental point of view (especially for the aquatic environment), especially connected to their possible release during all the phases of tyre life cycle[26,32]. Thus, recently, several studies have been focused on the vulcanization process and the possible use of alternative materials, keeping high vulcanization efficiency. Nevertheless, the substitution of these materials has revealed not to be an easy process, due to the complex mechanism in which such materials are involved and the high performances requested to put a more sustainable environmentally friendly material on the market.

Finally, in a typical product, processing aids and antidegradants are employed to improve the efficiency of mixing procedures and to extend the product life, respectively. Innovative studies are now focused on the use of eco-friendly and natural oils, promoting also in this case the substitution of synthetic materials with natural and available sources[33].

In this general background, in this Thesis, a close attention was addressed to the vulcanization process and in particular to the use of zinc oxide as activator of the process. As shown in the following paragraphs focused on vulcanization, the addition of this activator is fundamental to get the highest efficiencies of the process, but environmental drawbacks are related to its presence in the rubber formulation. The advantages and drawbacks of zinc oxide in this process will be described in details, explaining the more recent environmental issue emerging in the rubber field.

1.2 Vulcanization process

As mentioned before, the vulcanization reaction is a highly employed industrial method to increase the mechanical properties of rubber NCs, thanks to the formation of a polymer three-dimensional network inside the matrix (Figure 1.7). In its most popular version, sulphur is used as vulcanizing agent and the network corresponds to the formation of poly-sulphide bridges that chemically connect the polymer chains, forming a cross-linked structure. The number and the length of sulphide bridges (from one to eight sulphur atoms per each bridge) determine the cross-linking degree of the final material and consequently the macroscopic mechanical properties, such as the elastic recovery stiffness or the toughness (Figure 1.8)[34,35].
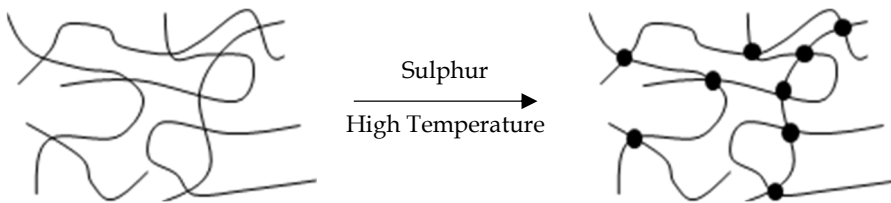
Figure 1.7. Formation of the three-dimensional network inside rubber NCs through the vulcanization process.
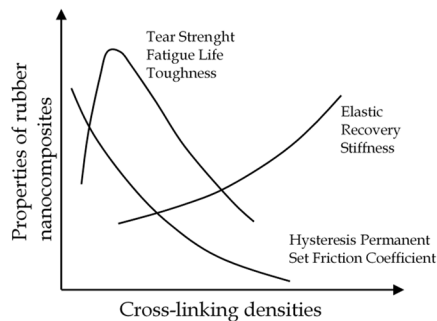
Figure 1.8. Macroscopic properties of rubber composites influenced by the increase of the cross-linking density.

An efficient vulcanization process in tyre industries needs i) enough time elapsing before cross-linking starts (delay time, called scorch time, t_{scorch}), in order to easily manage the material, shaping, forming and flowing in the mold; ii) a high rate of cross-linking formation, as high as possible, measured during the curing time; iii) high value of cross-linking degree in the final materials (high values of maximum torque (M_{max})); iv) low reversion degree after the reaction is completed, in the overcuring phase, but a preferential achievement of the plateau region. The so-called vulcanization curve (Figure 1.9) shows the typical scorch, vulcanization and overcuring phases that can be distinguished during the process and the respective parameters that are measured in the different phases.
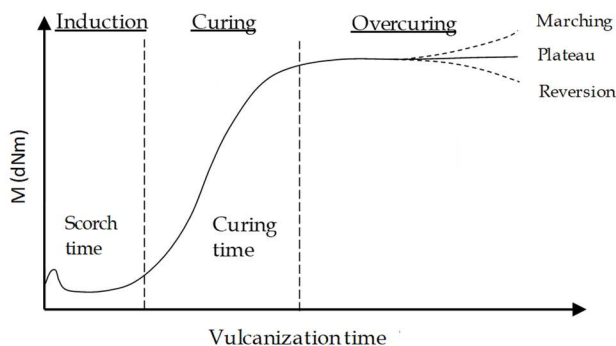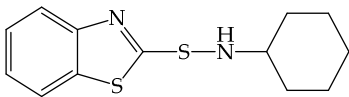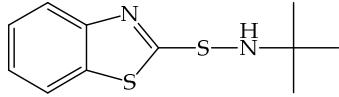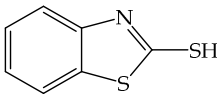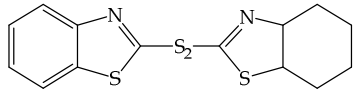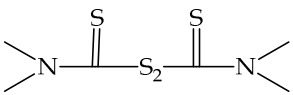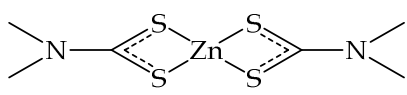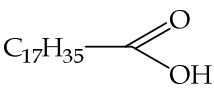
Figure 1.9. A typical vulcanization curve of rubber NCs.

Activators, accelerators and co-activators are typical terms used in the rubber field, generally adopted to refer to those materials that represent the catalysts of the reaction. Their addition was historically connected to the necessity to reduce the reaction time and the energy consumption by tyre industries, increasing at the same time the reaction efficiency[36,37]. As an example, the reaction time was reduced from 6 hours to 30 minutes (T = 142°C), by introducing these catalysts, moving from 1850 to 1920. Typical accelerators and co-activators are shown in Table 1.2.

The advantages of the use of these materials lied also in the reduction of the amount of sulphur needed and in the modification of the distribution of cross-links formed between polymer chain.

Table 1.2. Commonly used accelerators and co-activators in the vulcanization process.

Accelerators

Benzothiazole sulphenamide

N-cyclohexylbenzothiazole sulphenamide

N-tert-butylbenzothiazole-2-sulphenamide

CBS

TBBS

Benzothiazole

2-mercaptobenzothiazole

2,2'-dithiobenzothiazole

MBT

MBTS

Thiuram

Dithiocarbamate

Tetramethylthiuram disulphide

Zinc dimethyldithiocarbamate

ZDMC

TMTD

Co-activators

Stearic acid

$C_{17}H_{35}$

or other saturated fatty acids

SA

In the literature, all these species are supposed to interact in the first part of the reaction, to form active intermediate species, considered responsible of the catalytic promotion of the vulcanization process[38,39]. In fact, the cross-linking between polymer chains is generally connected to the interaction of the polymer

with the active species formed between activators, co-activators, accelerator and sulphur, in which sulphur is more available to react and with a higher tendency to bind to the rubber material, compared to the bare sulphur.

The mechanism of the reaction, the formation of the active intermediate agents and their nature is deeply discussed in the next section.

1.2.1 Vulcanization mechanism

The vulcanization reaction is characterized by a very complex mechanism, composed of several reactions going on all at the same time. Surface chemistry, heterogeneous catalysis, polymeric reactions, coordination compound formation, are examples of the reactions that are involved in the rubber NC vulcanization. Due to this high complexity, in the literature several studies were focused on the reaction mechanism, in the attempt of identifying the intermediate species and to evaluate the role of each component inside the reaction. Despite the long history of vulcanization, its reaction mechanism is still not yet fully understood, also due to an additional problem related to the difficulties in using traditional analytical techniques in the analysis of real elastomeric systems.

To solve this experimental problem, in several works the study of the mechanism has been often accomplished through the exploitation of model systems, in which the elastomeric materials are substituted by simple monomeric molecules[40,41]: these systems guarantee higher purities, reduced amounts of secondary products and more simple structures that allow the use of analytical methods in the study of the reactions going on during the process.

Morrison and Porter's first attempt to describe the vulcanization mechanism was determinant in this field and still represents nowadays one of the more accredited mechanism[42]. In their scheme, they proposed that the reaction could be divided in following steps, as showed in Figure 1.10. They further suggested that the activator, co-activator, accelerator and sulphur interact in the first steps of the reaction, leading to the formation of active complexes (active accelerator

complex and sulphurating agent), that interact with the polymer chains in the subsequent phases. Moreover, they advised that the formation of sulphur connection between polymer chains would start from long poly-sulphide products, with a progressive degradation towards shorter sulphide bridges, through a shortening process.

Activator + co-activator + accelerator

Active accelerator complex

+ sulphur or
sulphur donor

Polymer chain (RH)   +   Active sulphurating agent

Cross-linking intermediates

Cross-linking poly-sulphide products

Shortening of sulphur bridges

Final cross-linking products
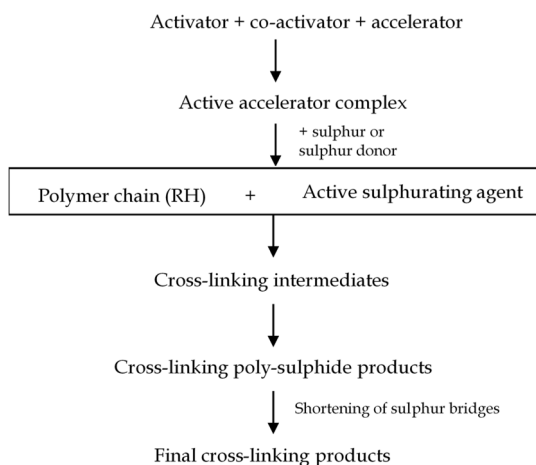
Figure 1.10. Scheme of vulcanization reaction, proposed by Morrison and Porter, in 1984[42].

The same main guidelines of this scheme were proposed by successive studies, although the partition of the reaction steps was a little changed moving from authors to authors. Ghosh *et al.*[43] introduced a division of the vulcanization mechanism in three sub-categories; the first step called accelerator chemistry leads to the formation of active sulphurating agents; later on, the cross-linking chemistry and post-crosslinking chemistry involve the formation of cross-linking intermediates and products, respectively. Other perspective was presented by Ignatz-Hoover[44], regarding the vulcanization mechanism in the presence of sulphenamide accelerator, that still re-mark the same general scheme.

Although the general mechanism is accepted by the main part of the scientific community, the debate is focused on the exact reactions that take place in all the

different steps and on the identification of precise nature of the intermediate species that are supposed to be generated during the reaction mechanism.

In this general scenario, a main role is always assigned to the activator and in particular to zinc oxide, the most used activator of the reaction. Zinc ions are supposed to be fundamental in the mechanism for the interaction with the other reagents of the vulcanization process and to achieve highly efficient vulcanization reaction. Nevertheless, a high number of drawbacks have been related to zinc oxide. Advantages and drawbacks of zinc oxide in rubber NCs are explained in the following section.

1.3 Zinc oxide

Micro-crystalline ZnO acts as activator of the rubber vulcanization process, increasing the rate and the efficiency of the process. The amount of ZnO in rubber (3-5 phr) conventionally used by tyre industries, makes tyre production the primary use of ZnO in the world[45,46]. With a global annual production of 25 million tons reported in 2010[47], more than 50% is used in rubber[47-49] (Figure 1.11).
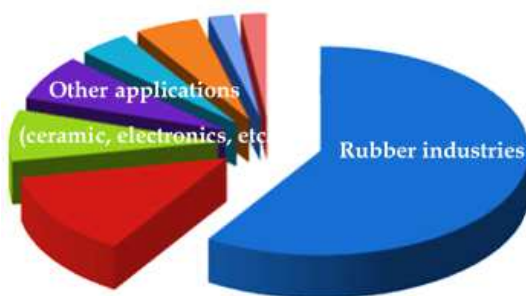
Figure 1.11. Partition of zinc oxide applications in 2010[50].

1.3.1 Role of zinc in the vulcanization reaction

ZnO plays a main role both in the first steps of the reaction and during the last formation and shortening reactions of the cross-linking products[51].

The main point about zinc oxide reactivity is that the main species in the reaction is not ZnO, in which zinc ions are entrapped in a closed lattice alternated with oxygen atoms, but free zinc ions. The presence of the co-activators (mainly fatty acids as stearic acid) creates free Zn^{2+} centres, coordinating them, in the so-called "solubilization of Zn^{2+}" step, as reported in several mechanisms[51,52]. Stearic acid is supposed to form with zinc ions a zinc-stearate complex, whose structure is generally reported as shown in Figure 1.12. The so-formed Zn^{2+} centres interact in a second step with the accelerator and sulphur to create the active sulphurating agents.
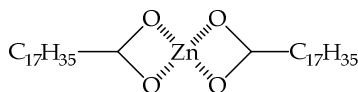
Figure 1.12. Structure of zinc-stearic acid complex reported in the literature. In this structure, two stearic acid molecules coordinate one zinc atom through a chelating coordination.

An interesting observation was reported by Heideman et al.[53] regarding the reactivity of the presumed zinc-stearate complex: when the authors tried to substitute ZnO with different zinc complexes, including zinc stearate, the vulcanization was subjected to a detrimental effect, despite a zinc-stearate complex is supposed to be formed during the first step of the reaction. Strongly reduced cross-linking densities were achieved by introducing zinc stearate, instead of ZnO and stearic acid. Although the authors did not give any possible explanations, this study evidenced that the nature and role of the intermediate species still needs to be clarified.

Subsequently, zinc ions are believed to: i) fasten the generation of very active intermediate complexes, ii) determine the nature of the cross-linking products, through a direct impact of zinc on the shortening process of sulphur bridges in the cross-linking products[51]. These observations were mainly deduced comparing the reaction mechanisms in the presence and in the absence of ZnO. Coran suggested that zinc ions are able to form very active complexes with the accelerators, even more reactive than the free accelerator, towards sulphur[34]. The presence of zinc was also supposed to facilitate the insertion of zinc in the active accelerator complex to form the active sulphurating agents: in a benzothiazole catalysed reaction (MBTS accelerator), the coordination of zinc to the accelerator (Figure 1.13) would facilitate the opening of sulphur-carbon bond, favouring the insertion of sulphur. Morgan *et al.*[41] also suggested that ZnO would facilitate the opening of sulphur rings, leading to an easier availability of sulphur towards the interaction with the active accelerator complex.
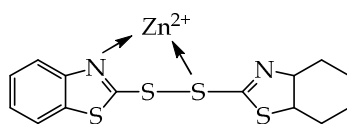
Figure 1.13. Zinc coordination to a TBBS molecules, to form the active accelerator complex.

Moreover, the possible coordination of zinc with other moieties, for example carboxylate ligands (from stearic acid) or amine groups (released from accelerators as sulphenamides) could potentially be able to increase the stability of the active sulphurating agents (Figure 1.14a). Other possible coordination could imply a coordinative bond, instead of covalent bonds of zinc towards the other involved species (Figure 1.14b).
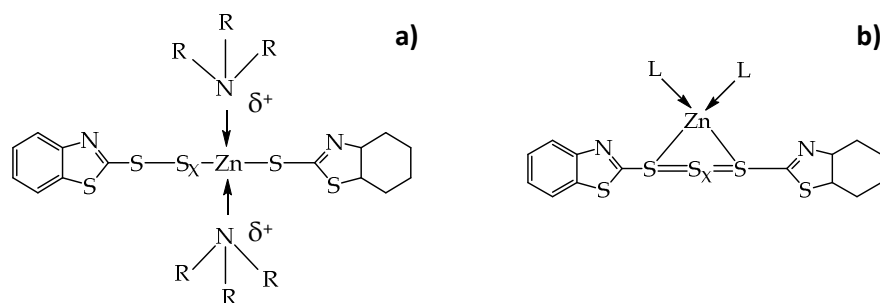
Figure 1.14. Stabilized active sulphurating agents created in the presence of ZnO and a sulphenamide accelerator, through the coordination of zinc atom to two amino groups, derived from the breakage of accelerator molecules. In a) zinc is covalently bond to the ligands; in b) no covalent bonds are supposed to form with the accelerator moieties.

The intermediate and final cross-linking products are formed through the interaction of the active sulphurating agents at the allylic sites of the polymer unsaturation. Thus, these zinc-based complexes must be stable enough to be formed at the first stages of the reaction, but at the same time, reactive towards the polymer; in other words, the zinc-sulphur bond must be stable enough, but not so strong to hinder the subsequent reaction of the sulphur chain with the polymer. The stability of a bond can be discussed in first approximation in terms of bond dissociation energies, defined as the standard state enthalpy change (ΔHf_{298}) involved in the breakage of the considered bond. Tabulated value of ΔHf_{298} for zinc-sulphur bond is 205 kJ mol^{-1}; comparing this value with the tabulated ΔHf_{298} Cu-S, equal to 285 kJ mol^{-1}, it can be easily deduced that copper is more likely to form more stable bonds with sulphur and the introduction of copper instead of zinc could have a detrimental effect on the vulcanization process, due to highly stable intermediate species.

Finally, the increased efficiency of the shortening process of sulphide bridges in cross-linking intermediates and products in the presence of Zn ions, could be explained by supposing that Zn^{2+} ions are able to coordinate these products,

influencing the energies involved in sulphur-sulphur (S-S) chains. In general S-S bond is a labile bond, that tends to decompose, by thermal treatment, giving rise to shorter sulphur connections by increasing the reaction time. As explained in the literature, in a sulphenamide accelerated vulcanization, zinc coordinate to the nitrogen of the benzothiazole group and to a sulphur atom in the sulphur chain: this type of coordination weakens a S-S bond that is farther from the accelerator moiety, thus decreasing the length of sulphur chains of the cross-linking intermediate, that will coordinate to another polymer chain (Figure 1.15). Instead, in the absence of Zn^{2+}, the more labile S-S bond would be the one closest to the accelerator molecules.

Cross-linking intermediate
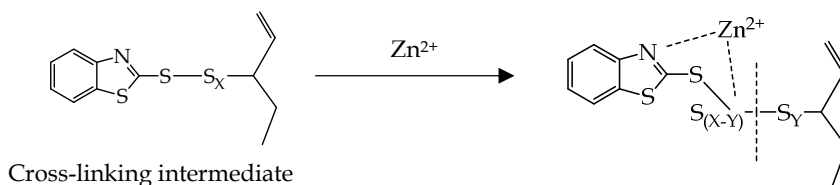
Figure 1.15. Coordination of Zn^{2+} to cross-linking intermediates allows weakening of sulphur-sulphur bond, closer to the polymer molecules, instead of the accelerator moiety.

As a conclusion, in this section the vulcanization mechanism has been shown and the role of ZnO explained; ZnO influences several steps of the vulcanization reaction, affecting both kinetic parameters and the properties of the vulcanization products. After the formation of Zn^{2+} centres (through the solubilization with stearic acid), various zinc complexes are involved in the first steps of the reaction, in which the coordination of zinc to the co-activator, accelerator and sulphur is necessary to further accelerate the reaction with the polymer in the following steps of reaction.

1.3.2. Drawbacks of ZnO in tyre formulations

One main industrial issue of ZnO in tyre formulation is connected to its hydrophilic character, that is opposed to the hydrophobic properties of the

polymer chains; this characteristic hinders a fine distribution of ZnO in the elastomer, requiring high amount of ZnO to achieve homogeneous vulcanization diffusion.

The widespread and expanding production and use of ZnO increases the potential leaching to the environment. Councell *et al.*[54] reported that in 1999 the quantity of zinc released by tyre wear in the U.S. was estimated to be 10 to 11 thousand metric tons; in a long term period, starting from 1936 to 1999, the estimation arose up to 235 thousand tons of released zinc. Callender et al.[55] further evaluate that anthropogenic zinc concentration well correlated with traffic density, by analysing sediment cores in Georgia and Florida; besides, approximately 60% of the total load of zinc in the lower South San Francisco bay was estimated to derive from tyre-wear particles[56]. The same issue was highlighted in Europe: both in Swedish and Great Britain, at the end of the nineties, the amount of zinc originated from tyre tread to the environment was calculated of about 150 tons per year[57,58].

Due to the high amount of released zinc involved, zinc leaching from tyres contributes to strongly increase the natural concentration of zinc in the environment: exceeding environmentally harmless levels of zinc concentration were measured worldwide, both in surface-water and soils, including some European rivers and soil road boarders alongside motorways[59-61].

Although zinc is a natural essential element, its properties are strictly related to its concentration, that should be above a minimum concentration to supply organisms' needs (including humans), but below a maximum concentration, above which zinc becomes toxic. Several limits have been established to define the maximum concentration allowed, especially in water: for example, the U.S. Environmental Protection Agency (EPA) has set the drinking water limit for Zn at 5 mg/L; as dissolved Zn, the maximum allowed concentration in water have been set by EPA at 120µg/L[62,63]. In Europe, the Netherlands first initiated the need for an international European review process on the potential risks of zinc

related to the aquatic environment[64]. The European regulation ended up with a risk assessment form for zinc metal and zinc compound in 1994 (EC 1488/94). Bodar *et al.*[59] reported the predicted no effect concentrations added values, without natural background (PNEC$_{add}$, Table 1.3) of zinc calculated in different ecosystems, including surface-water, sediments and soils. In the various environmental compartments, zinc may be speciated as zinc ions (mainly in water), zinc salt (such as zinc sulphide) in sediments, zinc metal or other zinc compounds (zinc oxide). In each compartment, the PNEC$_{add}$ must have different values, based on the main speciation of zinc. Measurements of the effective zinc concentration in Europe, in the different compartments, identified effective concentrations to PNEC values exceeding unity, both for the aquatic, sediment and soils compartments, at local and regional scale.

Table 1.3. PNEC$_{add}$ values estimated for different environmental compartments[59].

Ecosystem	PNEC$_{add}$
Surface-water (µg/L; dissolved)	7.8
Sediment (mg/kg dry wt)	37
Soil micro-organisms (mg/kg dry wt)	27
Soil, plants/invertebrates (mg/kg dry wt)	26

Further studies focused on the classification of the main species that could be affected by high concentrations of zinc and on the mechanisms that are involved. Brunner *et al.*[65] concluded that ZnO toxicity in water involves both ZnO particulate and solubilized species, through distinct mechanisms of action[32]: partially solubilisation of Zn^{2+} ions from ZnO particles was first proven to contribute to zinc cytotoxicity[65,66]; besides, as ZnO can behave as photocatalyst, it was recognized as a source of radical oxidized species under irradiation with high energy (equal or above its band gap energy). Toxicity of ZnO was studied starting from bacteria, till human beings: adverse effects were determined both for terrestrial and aquatic organisms, with a special concern to

aquatic species (such as *D. magna*), whose toxic effects can be identified at concentrations as low as less than 1 mg /L. Studies were extended in other countries outside Europe, on various marine and terrestrial species[60,61,67,68], highlighting once again a main concern to the aquatic environment and to marine organisms, including fishes.

The above described environmental issue about micro-crystalline ZnO, has driven the attention of the scientific research towards the development of innovative methods to reduce or substitute the amount of ZnO introduced in tyre composition. Total removal of ZnO has been set aside, due to the high improvement to the vulcanization efficiency, not achieved in the absence of ZnO. Several studies have been published in the recent years, proposing possible alternative zinc based materials to ZnO as activators for rubber vulcanization process[38,69-73]. The use of more dispersed forms of zinc oxides or the introduction of zinc complexes have been evaluated on the vulcanization efficiency. Other studies have focused on the possible use of other metals oxides, such as magnesium oxide or blends of the two metals[40,74,75]. A more detailed explanation of the attempts reported so far in the literature are presented in the next paragraph.

1.3.3 Reduction or substitution of ZnO in the vulcanization reaction

So far, both advantages and drawbacks of micro-crystalline ZnO as activator in rubber vulcanization process were examined. Despite the fundamental role of ZnO in the vulcanization mechanism (especially of Zn^{2+}), its hydrophilic character opposed to the hydrophobic properties of rubber causes an inadequate diffusion in the matrix, leading to the use of high amount of ZnO; consequently, environmental problems, connected to the leaching of both reacted and unreacted ZnO in the environment are generated. Moreover, the presence of high amount of ZnO hinders the formation of high-quality regenerated rubber.

Aiming at solving these drawbacks, reducing the zinc content inside the rubber materials could be placed as a possible contribution to the general movement

towards the production of more sustainable materials and the closure of CE for tyres. For this reason, the development of innovative activators with high reactivity in the vulcanization process, could promote the creation of high performant and more eco-friendly tyres.

In the literature, several attempts are reported, in which ZnO was partially or totally substituted by different species. Heideman et al.[53,76] presented several possible solutions in his study about zinc complexes. The complexes were generically supposed to increase the dispersion of Zn^{2+} ions, ready to interact with the other species. Some improvements were connected to the use of zinc glycerolate, instead of zinc stearate, but no chemical explanation for the experimental results was suggested. Przybyszewska *et al.*[72] suggested the use of other zinc complexes, such as zinc acetylacetonate as well as zinc chelates with 1,3-diketones, but a slight decrease in cross-linking densities of vulcanizates and a lower efficiency were achieved, even though the mechanical properties were almost preserved. Other zinc complexes were further tested, including zinc monometacrylate[77], without promising results. With the same idea of increasing the availability of zinc ions, zinc loaded clays were tested inside the vulcanization reaction, with almost comparable efficiency, but using reduced amount of Zn[70].

Further studies are related to the use of other metal oxides: although some papers do not achieve promising vulcanization efficiencies using metal as magnesium oxide (MgO) or beryllium oxide (BeO)[75], other authors claim the possible substitution of ZnO with calcium or magnesium oxide can lead to positive results in the vulcanization[74,78]. Guzman *et al.*[79] also suggested a possible interaction between Zn and Mg could lead to a cooperation in the vulcanization, with improved kinetic of reaction.

A possible reduction of micro-crystalline ZnO content was shown with the introduction of nano-ZnO. Roy et al.[80] demonstrated that by increasing the surface area of ZnO (thanks to the nanometric size), a higher amount of ZnO

would be able to interact with the accelerator, thus reducing the amount of required ZnO in the rubber NC. On this basis, several studies developed materials in which NPs of ZnO (ZnO NPs) were dispersed onto different supports, in order to have a double effect: on one hand, the increased surface areas, on the other hand, the use of the support would guarantee a better dispersion of ZnO inside the composite[71,73,81,82].

Of particular interest is the work published by Susanna et al.[73], in which ZnO NPs were supported onto the surface of silica particles (ZnO/SiO$_2$), realizing the so-called double function filler, a material that can behave simultaneously as reinforcing filler (thanks to the presence of SiO$_2$) and as a vulcanization activator. This material has already demonstrated higher vulcanization efficiencies, using only half of the amount of ZnO generally employed during the industrial process. Moreover, the final rubber composites have shown higher cross-linking densities and improved mechanical properties, promoting as a possible candidate for the industrial substitution of ZnO. By developing and using this material, the authors have proved that a higher dispersion of ZnO inside the rubber matrix can promote a higher efficient vulcanization process.

In this Thesis, ZnO/SiO$_2$ has been considered as a starting point for the subsequent development of innovative zinc-based materials that can be used as activators for the vulcanization process, as explained in the next paragraph.

1.3.4 Development of single sites zinc-based activators

The concept of double function filler, that is based on the high dispersion of zinc through silica filler in rubber materials, was exploited in this Thesis for the development of new activators, with the aim of reducing the zinc content in rubber, through the introduction of more reactive zinc species and producing more sustainable rubber materials for tyre application.

In the new materials, as a further progressive improvement of the reactivity of the double function filler, the dispersion of single zinc centres on silica was

considered. Two main reasons can be defined to justify the introduction of isolated zinc centres instead of ZnO in the structure of the double function filler.

First, the design of the catalyst was based on a deep knowledge of the fundamentals of the vulcanization reaction, to get the best catalysts for the process. In the previously explained reaction mechanism, it was clearly shown that the main actors in the vulcanization reaction are the zinc ions, generated after the interaction with the co-activator. On this basis, the insertion of zinc centres was developed to increase the kinetic of the reaction, by avoiding the first step of generation of zinc centres, because already available in the system. Having in mind the general scheme of the vulcanization mechanism (Figure 1.10), the addition of zinc centres was foreseen to increase the initial availability of zinc towards the reaction. As a further consequence, the addition of the co-activator was eliminated, due to the early and high availability of the zinc centres, already at the beginning of the reaction. Moreover, the reactivity of zinc towards the other vulcanization reagents (accelerator and sulphur) was supposed to be suitably modulated, thanks to a different chemical neighbourhood of zinc centres and their spatial distribution inside the rubber matrix.

In addition, the dispersion of zinc centres onto the silica surface was developed in order to exploit the advantages coming from the introduction of a heterogenous catalytic system. In the presence of zinc oxide, the reactivity of zinc could be described as a homogeneous catalysis, that proceeds thanks to the formation of zinc complexes, able to diffuse inside the rubber matrix. In this case, zinc centres were introduced aiming at the formation of heterogeneous catalytic sites on the surface of silica; in other words, one goal was the creation of stable zinc isolated single sites, that could be stable enough to be maintained during the vulcanization reaction and the interaction with the other involved species.

In the literature, several studies are related to the use of supported single metal sites as catalyst for processes of different nature[83-86]. In general, a higher number of examples is reported for precious metals NPs (palladium, platinum, gold, etc.) dispersed on porous materials, for gas phase reactions[87]. Most of the industrial processes also make use of catalytic heterogeneous materials, that are generally represented by supported NPs. Other examples report the use of supported organometallic complexes, immobilized on suitable structural supports, in which the metal centres can behave as catalytic sites, mimicking the reactivity of the natural metal structures, as enzymes[87-91]. In this kind of materials, several studies demonstrated that the catalytic activity and the selectivity can be optimized by studying the structure of the active sites; for this reason, most of the studies are nowadays focused on the preparation of heterogeneous catalysts, with a very precise structure.

In this Thesis, the use of suitable zinc complexes was exploited to anchor zinc centres onto the surface of silica ($ZnA\text{-}SiO_2$). The zinc centres were dispersed using proper linkers, that could create covalent bonds both with the support and the metal centres. Even though non-covalent interactions are often exploited for the creation of catalytic metal centres on the surface of the supports (such as Van der Waals interactions between the metal and the support), the creation of more stable covalent bonds was preferred here, in order to increase the stability of the heterogeneous metal centres during the vulcanization process.

In the next chapters, the synthesis and application of the two double function fillers as activators for the vulcanization reaction was investigated. Both ZnO/SiO_2 and $ZnA\text{-}SiO_2$ were considered in this study, to examine the effect given by the transition from dispersed ZnO NPs towards dispersed zinc centres onto the surface of silica nanofiller in the reaction and in the determination of the mechanical properties of rubber NCs. After a first phase of synthesis and characterization of the two materials, to assess their structural and morphological properties, a deep investigation of their reactivity was realized.

Influences on both the properties of rubber NCs and on the kinetic and mechanistic aspects of the reaction were considered.

1.4 Bibliography

1.   Thomson, R. W. Carriage Wheel. *United States Patent Office* **5**, (1847).

2.   WBCSD. End-of-Life Tires. *Management* (2010).

3.   Bhansali, G. & Brokers, S. Tyre Industry. **18**, 1–7 (2010).

4.   Rubber Manufacturers Association. Scrap Tire Markets in the United States, 9th biennal report. 105 (2009).

5.   ETRMA. End-of-life Tyre Report 2015. 36 (2015).

6.   Global Industry Analyst, I. Developments in Modern Tire Engineering Including Innovations n Tire Tread Pattern Technology to Drive Growth in the Global Tires Market. 1–2 (2018). Available at: www.strategyr.com/MarketResearch/ViewInfoGraphNew.asp?code=MCP-2798.

7.   Ramos, G., Alguacil, F. J. & López, F. A. The recycling of end-of-life tyres. Technological review. *Rev. Metal.* **47**, 273–284 (2011).

8.   Wagner, S., Hüffer, T., Klöckner, P., Wehrhahn, M., Hofmann, T. & Reemtsma, T. Tire wear particles in the aquatic environment - A review on generation, analysis, occurrence, fate and effects. *Water Res.* **139**, 83–100 (2018).

9.   Stahel, W. R. Circular economy. *Nature* **531**, 435–438 (2016).

10.   Uruburu, Á., Ponce-Cueto, E., Cobo-Benita, J. R. & Ordieres-Meré, J. The new challenges of end-of-life tyres management systems: A Spanish case study. *Waste Manag.* **33**, 679–688 (2013).

11.   Commission, E. *Communication from the commission to the european parliament, the council, the european economic and social committee and the committee of the regions.* (2016).

12.   Wysokinska, Z. The 'new' environmental policy of the European Union: a path to development of a circular economy and mitigation of the negative effects of climate change. *Comp. Econ. Res.* **19**, 57–73 (2016).

13.   Sienkiewicz, M., Kucinska-Lipka, J., Janik, H. & Balas, A. Progress in used tyres management in the European Union: A review. *Waste Manag.* **32**, 1742–1751 (2012).

14.   Torretta, V., Rada, E. C., Ragazzi, M., Trulli, E., Istrate, I. A. & Cioca, L. I. Treatment and disposal of tyres: Two EU approaches. A review. *Waste Manag.* **45**, 152–160 (2015).

15.   PlasticsEurope Market Research Group (PEMRG) / Consultic Marketing & Industrieberatung GmbH. Plastics – the Facts 2017. 16 (2017). doi:10.1016/j.marpolbul.2013.01.015

16.   European Declaration on Paper Recycling. Monitoring Report 2014 European Declaration on Paper Recycling Paper Recycling. 1–8 (2014).

17.   Eldin, N. N. & Senouci, A. B. Rubber-tire particles as concrete aggregate. *J. Mater. Civ. Eng.* **5**, 478–496 (1993).

18.   Dobrotă, D. & Dobrotă, G. An innovative method in the regeneration of waste rubber and the sustainable development. *J. Clean. Prod.* **172**, 3591–3599 (2018).

19. Shu, X. & Huang, B. Recycling of waste tire rubber in asphalt and portland cement concrete: An overview. *Constr. Build. Mater.* **67**, 217–224 (2014).

20. Machin, E. B., Pedroso, D. T. & de Carvalho, J. A. Energetic valorization of waste tires. *Renew. Sustain. Energy Rev.* **68**, 306–315 (2017).

21. Chou, H. L., Lu, C. K., Chang, J. R. & Lee, T. M. Use of waste rubber as concrete additive. *Waste Manag. Res.* **25**, 68–76 (2007).

22. Conesa, J. A., Gálvez, A., Mateos, F., Martín-Gullón, I. & Font, R. Organic and inorganic pollutants from cement kiln stack feeding alternative fuels. *J. Hazard. Mater.* **158**, 585–592 (2008).

23. Martínez, J. D., Puy, N., Murillo, R., García, T., Navarro, M. V. & Mastral, A. M. Waste tyre pyrolysis - A review. *Renew. Sustain. Energy Rev.* **23**, 179–213 (2013).

24. Brewer, H. The Pneumatic Tire. *Natl. Highw. Traffic Saftey Adminstration* 231–285 (2006). doi:10.1109/54.970421

25. Torretta, V., Rada, E. C., Ragazzi, M., Trulli, E., Istrate, I. A. & Cioca, L. I. Treatment and disposal of tyres: Two EU approaches. A review. *Waste Manag.* **45**, 152–160 (2015).

26. De Wever, H. & Verachtert, H. Review paper biodegradation and toxicity of benzothiazoles. *Water Res.* **31**, 2673–2684 (1997).

27. Barrand, J. & Bokar, J. Reducing tire rolling resistance to save fuel and lower emissions. *SAE Int. J. Passeng. Cars-Mechanical Syst.* **1**, 9–17 (2008).

28. Guerinon, B. US Patent No 9,987,884 B2, Tire having low rolling resistance. (2018).

29. Thai Automobile Tyre Manufacturers Association. Natural Rubber Consumption, TATMA. (2013). Available at: http://tatma.org/content-NaturalRubberConsumption-4-2102-4705-1.html.

30. Arroyo, M., López-Manchado, M. A. & Herrero, B. Organo-montmorillonite as substitute of carbon black in natural rubber compounds. *Polymer (Guildf).* **44**, 2447–2453 (2003).

31. Giannelis, E. P. Polymer Layered Silicate Nanocomposites. *Adv. Mater.* **8**, 29–35 (1996).

32. Ma, H., Williams, P. L. & Diamond, S. A. Ecotoxicity of manufactured ZnO nanoparticles - A review. *Environ. Pollut.* **172**, 76–85 (2013).

33. Dasgupta, S., Agrawal, S. L., Bandyopadhyay, S., Mukhopadhyay, R., Malkani, R. K. & Ameta, S. C. Eco-friendly processing oils: A new tool to achieve the improved mileage in tyre tread. *Polym. Test.* **28**, 251–263 (2009).

34. Coran, A. Y. Vulcanization. in *Science and Technology of Rubber* (ed. Eirich, E. R.) 291 (Ed. Academic Press, 1978).

35. Coleman, M. M., Shelton, J. R. & Koenig, J. L. Sulfur Vulcanization of Hydrocarbon Diene Elastomers. *Ind. Eng. Chem. Prod. Res. Dev.* **13**, 154–166 (1974).

36. Alliger, G. & Sjothun, J. I. *Vulcanization of Elastomers: Principles and Practice of Vulcanization of Commercial Rubbers*. (Reinhold, 1964).

37. Mark, J. E., Erman, B. & Roland, M. *The science and technology of rubber*. (Academic Press, 2013).

38. Nieuwenhuizen, P. J. Zinc accelerator complexes. Versatile homogeneous catalysts in sulfur vulcanization. *Appl. Catal. A Gen.* **207**, 55–68 (2001).

39. Nieuwenhuizen, P. J., Sandjaj, T. & Van Veen, J. M. Homogeneous zinc(II) catalysis in accelerated vulcanization I. Reaction-stage modeling and cross-link formation. *Rubber Chem. Technol.* **71**, 750–765 (1998).

40.   Guo, C., Zhou, L. & Lv, J. Effects of expandable graphite and modified ammonium polyphosphate on the flame-retardant and mechanical properties of wood flour-polypropylene composites. *Polym. Polym. Compos.* **21**, 449–456 (2013).

41.   Morgan, B. & Mcgill, W. J. 2-Mercaptobenzothiazole as Accelerator for 2 , 3-Dimethyl-2-butene. *J. Appl. Polym. Sci.* **76**, 1377–1385 (2000).

42.   Morrison, N. J. & Porter, M. Temperature Effects on the Stability of Intermediates and Crosslinks in Sulfur Vulcanization. *Rubber Chem. Technol.* **57**, 63–85 (1984).

43.   P. Ghosh, S. Katare, P. P. Sulfur Vulcanization of Natural Rubber for Benzothiazole Accelerated Formulations. *Rubber Chem. Technol.* **76**, 592–693 (2003).

44.   Ignatz & Hoover. Review of vulcanization chemistry. *Rubber world* **220**, (1999).

45.   Moezzi, A., McDonagh, A. M. & Cortie, M. B. Zinc oxide particles: Synthesis, properties and applications. *Chem. Eng. J.* **185–186**, 1–22 (2012).

46.   Das, A., Wang, D.-Y., Leuteritz, A., Subramaniam, K., Greenwell, H. C., Wagenknecht, U. & Heinrich, G. Preparation of zinc oxide free, transparent rubber nanocomposites using a layered double hydroxide filler. *J. Mater. Chem.* **21**, 7194 (2011).

47.   International rubber study group. *Statistical summary of world rubber situation. Rubber Stat Bull* (2011).

48.   International Zinc Association-Zinc oxide Information Center. (2011). Available at: http://www.znoxide.org/index.html.

49.   Perl, A. Annual Minerals Review, Zinc Oxide. *Am. Ceram. Soc. Bull.* **76**, 140 (1997).

50.   Chemicals used in rubber industry. (2016). Available at: blog.chemtradeasia.in/chemicals-used-in-rubber-industry.

51.   Heideman, G., Datta, R. N., Noordermeer, J. W. M. & van Baarle, B. Activators in Accelerated Sulfur Vulcanization. *Rubber Chem. Technol.* **77**, 512–541 (2004).

52.   Musto, P., Larobina, D., Cotugno, S., Straffi, P., Di Florio, G. & Mensitieri, G. Confocal Raman imaging, FTIR spectroscopy and kinetic modelling of the zinc oxide/stearic acid reaction in a vulcanizing rubber. *Polymer (Guildf).* **54**, 685–693 (2013).

53.   Heideman, G., Noordermeer, J. W. M., Datta, R. N. & Van Baarle, B. Various ways to reduce zinc oxide levels in S-SBR rubber compounds. *Macromol. Symp.* **245–246**, 657–667 (2006).

54.   Councell, T. B., Duckenfield, K. U., Landa, E. R. & Callender, E. Tire-wear particles as a source of zinc to the environment. *Environ. Sci. Technol.* **38**, 4206–4214 (2004).

55.   Callender, E. & Rice, K. C. The urban environmental gradient: Anthropogenic influences on the spatial and temporal distributions of lead and zinc in sediments. *Environ. Sci. Technol.* **34**, 232–238 (2000).

56.   Program, S. C. V. N. S. C. *Source Identification and Control Report.* (1992).

57.   Wolfenden, I. & British Energy Agency. *Tyres report.* (2001).

58.   Lander, L. & Lindestrom, I. *Swedish Environmental Research Group, Fryksta.* (1998).

59.   Bodar, C. W. M., Pronk, M. E. J. & Sijm, D. T. H. M. The European Union risk assessment on zinc and zinc compounds: the process and the facts. *Integr. Environ. Assess. Manag.* **1**, 301–319 (2005).

60.   Suman, T. Y., Radhika Rajasree, S. R. & Kirubagaran, R. Evaluation of zinc oxide nanoparticles toxicity on marine algae chlorella vulgaris through flow cytometric, cytotoxicity and oxidative stress analysis. *Ecotoxicol. Environ. Saf.* **113**, 23–30 (2015).

61.   Lopes, S., Ribeiro, F., Wojnarowicz, J., Lojkowski, W., Jurkschat, K., Crossley, A., Soares, A.

M. V. M. & Loureiro, S. Zinc oxide nanoparticles toxicity to Daphnia magna: Size-dependent effects and dissolution. *Environ. Toxicol. Chem.* **33**, 190–198 (2014).

62. U.S. Environmental Protection Agency. *National Recommended Water Quality Criteria.* (1999).

63. U.S. Environmental Protection Agency. *National Secondary Drinking Water Regulations.* (1984).

64. Cleven, R., Janus, J., Annema, J., Sloof, W. & Environment, N. I. of P. H. and the. *Integrated criteria document zinc.* (1993).

65. Brunner, T. J., Wick, P., Manser, P., Spohn, P., Grass, R. N., Limbach, L. K., Bruinink, A. & Stark, W. J. In vitro cytotoxicity of oxide nanoparticles: Comparison to asbestos, silica, and the effect of particle solubility. *Environ. Sci. Technol.* **40**, 4374–4381 (2006).

66. Heinlaan, M., Ivask, A., Blinova, I., Dubourguier, H. C. & Kahru, A. Toxicity of nanosized and bulk ZnO, CuO and TiO2 to bacteria Vibrio fischeri and crustaceans Daphnia magna and Thamnocephalus platyurus. *Chemosphere* **71**, 1308–1316 (2008).

67. Naito, W., Kamo, M., Tsushima, K. & Iwasaki, Y. Exposure and risk assessment of zinc in Japanese surface waters. *Sci. Total Environ.* **408**, 4271–4284 (2010).

68. Shaw, B. J. & Handy, R. D. Physiological effects of nanoparticles on fish: A comparison of nanometals versus metal ions. *Environ. Int.* **37**, 1083–1097 (2011).

69. Taghvaei-Ganjali, S., Malekzadeh, M., Abbasian, A. & Khosravi, M. Effects of different activator systems on cure characteristics and physicomechanical properties of a NR/SBR blend. *Iran. Polym. J. (English Ed.* **18**, 415–425 (2009).

70. Heideman, G., Noordermeer, J. W. M. & Datta, R. N. Zinc Loaded Clay As Activator in Sulfur Vulcanization : *Rubber Chem. Technol.* **77**, 336–355 (2004).

71. Lin, Y., Chen, Y., Zeng, Z., Zhu, J., Wei, Y., Li, F. & Liu, L. Effect of ZnO nanoparticles doped graphene on static and dynamic mechanical properties of natural rubber composites. *Compos. Part A Appl. Sci. Manuf.* **70**, 35–44 (2015).

72. Przybyszewska, M., Zaborski, M., Jakubowski, B. & Zawadiak, J. Zinc chelates as new activators for sulphur vulcanization of acrylonitrile-butadiene elastomer. *Express Polym. Lett.* **3**, 256–266 (2009).

73. Susanna, a., Armelao, L., Callone, E., Dirè, S., D'Arienzo, M., Di Credico, B., Giannini, L., Hanel, T., Morazzoni, F. & Scotti, R. ZnO nanoparticles anchored to silica filler. A curing accelerator for isoprene rubber composites. *Chem. Eng. J.* **275**, 245–252 (2015).

74. Roy, K., Alam, M. N., Mandal, S. K. & Debnath, S. C. Preparation of zinc-oxide-free natural rubber nanocomposites using nanostructured magnesium oxide as cure activator. *J. Appl. Polym. Sci.* **132**, 1–7 (2015).

75. Heideman, G., Noordermeer, J. W. M., Datta, R. N. & Van Baarle, B. Effect of metal oxides as activator for sulphur vulcanisation in various rubbers. *KGK Kautschuk Gummi Kunststoffe* **58**, 30–42 (2005).

76. Heideman, G., Noordermeer, J. W. M., Datta, R. N. & van Baarle, B. Effect of Zinc Complexes as Activator for Sulfur Vulcanization in Various Rubbers. *Rubber Chem. Technol.* **78**, 245–257 (2005).

77. Henning, S. K. *Reduced Zinc Loading : Using Zinc Monomethacrylate to Activate Accelerated Sulfur Vulcanization.* (2007).

78. Roy, K., Alam, M. N., Mandal, S. K. & Debnath, S. C. Development of a suitable nanostructured cure activator system for polychloroprene rubber nanocomposites with enhanced curing, mechanical and thermal properties. *Polym. Bull.* **73**, 191–207 (2016).

79. Guzman, M., Reyes, G., Agullo, N. & Borros, S. Synthesis of Zn/Mg oxide nanoparticles

and its influence on sulfur vulcanization. *J. Appl. Polym. Sci.* **119**, 2048–2057 (2011).

80. Roy, K., Alam, M. N., Mandal, S. K. & Debnath, S. C. Sol-gel derived nano zinc oxide for the reduction of zinc oxide level in natural rubber compounds. *J. Sol-Gel Sci. Technol.* **70**, 378–384 (2014).

81. Lin, Y., Zeng, Z., Zhu, J., Chen, S., Yuan, X. & Liu, L. Graphene nanosheets decorated with ZnO nanoparticles: Facile synthesis and promising application for enhancing the mechanical and gas barrier properties of rubber nanocomposites. *RSC Adv.* **5**, 57771–57780 (2015).

82. Alam, M. N. & Potiyaraj, P. Precipitated Nano Zinc Hydroxide on the Silica Surface As an Alternative Cure Activator in the Vulcanization of Natural Rubber. *Rubber Chem. Technol.* **90**, 714–727 (2017).

83. Corma, A. & Garcı, H. Lewis acids from conventional homogeneous to green homogeneous and heterogeneous catalysis. *Chem. Rev.* **103**, 4307–4365 (2003).

84. Campanati, M., Fornasari, G. & Vaccari, A. Fundamentals in the preparation of heterogeneous catalysts. *Catal. Today* **77**, 299–314 (2003).

85. Vi, P., Jackson, S. D., Kelly, G. J. & Webb, G. Supported Metal Catalysts ; Preparation , Characterisation , and Function. *Technology* **234**, 225–234 (1998).

86. Yang, X. F., Wang, A., Qiao, B., Li, J., Liu, J. & Zhang, T. Single-atom catalysts: A new frontier in heterogeneous catalysis. *Acc. Chem. Res.* **46**, 1740–1748 (2013).

87. Nava, R., Halachev, T., Rodríguez, R. & Castao, V. M. Synthesis, characterization and catalytic behavior of a zinc acetate complex immobilized on silica-gel. *Appl. Catal. A Gen.* **231**, 131–149 (2002).

88. Jones, C. W., McKittrick, M. W., Nguyen, J. V. & Yu, K. Design of silica-tethered metal complexes for polymerization catalysis. *Top. Catal.* **34**, 67–76 (2005).

89. Benessere, V., Cucciolito, M. E., Esposito, R., Lega, M., Turco, R., Ruffo, F. & Di Serio, M. A novel and robust homogeneous supported catalyst for biodiesel production. *Fuel* **171**, 1–4 (2016).

90. Comerford, J. W., Hart, S. J., North, M. & Whitwood, A. C. Homogeneous and silica-supported zinc complexes for the synthesis of propylene carbonate from propane-1,2-diol and carbon dioxide. *Catal. Sci. Technol.* **6**, 4824–4831 (2016).

91. Rimoldi, M. & Mezzetti, A. Site isolated complexes of late transition metals grafted on silica: Challenges and chances for synthesis and catalysis. *Catal. Sci. Technol.* **4**, 2724–2740 (2014).

2

Preparation of the
zinc-based activators

In this chapter, the synthetic procedures and the characterization techniques used for the preparation of the activators are illustrated. Two sections are presented: first, the synthesis of ZnO nanoparticles onto the surface of silica particles (ZnO/SiO$_2$) is reproduced and optimized, starting from the experimental sol-gel method reported in the literature[1]. The characterization confirms the achievement of ZnO NPs formation, distributed onto the surface of the silica support. In the second section, the procedure for the generation of zinc centres anchored to silica (ZnA-SiO$_2$) is described; the structure of the isolated zinc centres coordinated by the anchoring agents was deeply investigated through structural and surface characterizations.

2.1 Preparation of ZnO/SiO$_2$

ZnO/SiO$_2$ is synthesized following the procedure reported by Susanna *et al.*[1]. This reaction is classified in the field of wet chemistry and exploits a sol-gel method, based on the hydrolysis and condensation reactions of a zinc precursor to form *in situ* ZnO NPs in the presence of SiO$_2$ nanoparticles (Figure 2.1a). The procedure was further optimized modifying the basic condition and the reaction time in order to get reproducible and high reaction yields, as explained in the next paragraph.

2.1.1 Synthesis of ZnO/SiO$_2$

Materials: precipitated SiO$_2$ Zeosil MP1165 from Rhodia (specific surface area 160 m^{2}g^{-1}); all the other materials from Sigma Aldrich: zinc acetate dihydrate (Zn(CH$_3$COO)$_2$·2H$_2$O, ≥ 98%), sodium hydroxide (NaOH, 98%), ethanol (EtOH, puriss, p.a., absolute, ≥ 99.8%).

Experimental procedure: 70 mL of a basic solution of EtOH is first prepared (C$_{NaOH}$ reported in Table 2.1.) and heated at 65°C. After complete dissolution of NaOH (10 minutes, Figure 2.1b), suitable amount of Zn(CH$_3$COO)$_2$·2H$_2$O (ZnA) is added and left under vigorous stirring for suitable time (t, Figure 2.1b). Table 2.1 reports the amounts of reactants and the t values used for the preparation of the

different samples. The purpose was to synthesize samples with an effective ZnO percentage below 10 wt% to get small and very well distributed NPs on silica; above this value, ZnO NPs are reported to more easily aggregate to form crystalline structures on SiO_2 particles[1].

Lately, 1.0 g of SiO_2 is added to the solution and the suspension is stirred for 20 minutes (Figure 2.1b) to favour the hydrolysis and condensation and the formation of ZnO NPs on silica surface (see later); the ZnO/SiO_2 particles are then filtered, washed three times with fresh ethanol and dried 12 hours in an oven at 80°C.
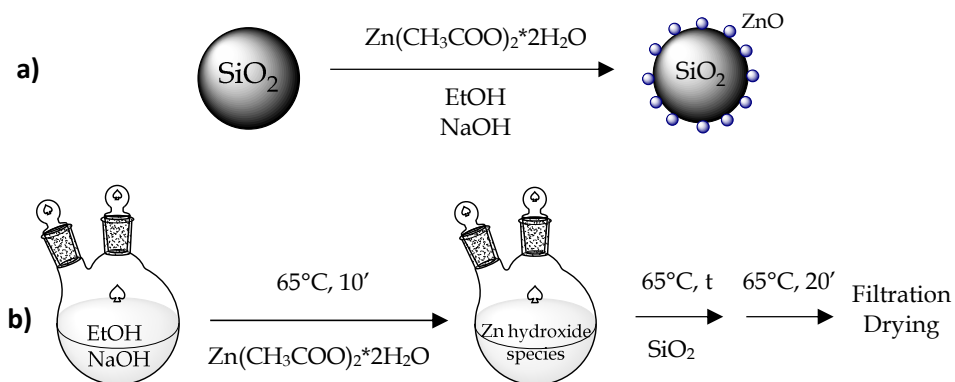
Figure 2.1. a) Scheme of the reaction for the formation of ZnO NPs on the surface of SiO_2 particles and b) its experimental setup.

Table 2.1. Parameters varied during the optimization process of the reaction, referred to the synthesis of 1 g of SiO$_2$. On the right experimental results of ICP analysis.

Sample	m ZnA (g)	C$_{NaOH}$ (M)	t (min)	Nominal ZnO (wt%)	Measured ZnO (wt%)	Reaction yield (%)
ZnO/SiO$_2$_0.04	0.33	**0.04**	5	12.2	4.0	**33**
ZnO/SiO$_2$_0.10	0.33	**0.10**	5	12.2	10.0	**82**
ZnO/SiO$_2$_0.40	0.33	**0.40**	5	12.2	8.5	**70**
ZnO/SiO$_2$_5′	0.33	0.10	**5**	12.2	10.0	**82**
ZnO/SiO$_2$_10′	0.33	0.10	**10**	12.2	10.0	**82**
ZnO/SiO$_2$_20′	0.33	0.10	**20**	12.2	10.4	**85**

Table 2.2. Optimized reaction conditions used for the preparation of two samples with different ZnO loading (4 and 10 wt%). On the right experimental results from ICP analysis.

Sample	m ZnA (g)	C$_{NaOH}$ (M)	t (min)	Nominal ZnO (wt%)	Measured ZnO (wt%)	Reaction yield (%)
ZnO/SiO$_2$_4%	0.13	0.10	5	5.0	4.1	82
ZnO/SiO$_2$_10%	0.33	0.10	5	10.0	9.9	81

2.1.2 Optimization of the synthesis of ZnO/SiO$_2$

The synthetic procedure was optimized through the evaluation of the reaction yields obtained in different experimental conditions (Table 2.1.). ICP-AES was used to quantify the real amount of ZnO deposited on SiO$_2$. Two parameters were changed: NaOH concentration and reaction time t, after the addition of zinc precursor to the basic ethanol solution containing SiO$_2$ (Table 2.1.). These parameters were chosen considering that the deposition of ZnO NPs onto the surface of SiO$_2$ strictly depends on the equilibrium formation of zinc hydroxo-species in basic solution[2]. As shown in Figure 2.2 at high basicity the formation of soluble hydroxo-zincate Zn(OH)$_3^-$ and Zn(OH)$_4^{2-}$ is favoured. The formation of these species is fundamental to promote the condensation of the zinc species

and reactivity towards the surface silanol groups of SiO_2. Consequently, the identification of an optimal NaOH concentration is of primary importance.
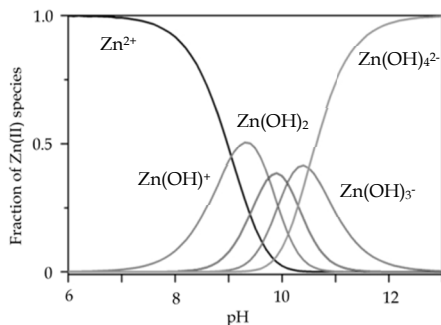
Figure 2.2. Equilibrium between Zn(II) hydroxo and hydroxide species dependent on the basicity in water solution.

Besides, the process of formation of the zinc hydroxo complexes must reach the equilibrium before the addition of SiO_2 particles. Thus, the time t must be long enough to allow the achievement of the equilibrium conditions. Three reaction times t were tested (5, 10, 20 min), to assess the best conditions required for the equilibrium to be reached.

ICP-AES analysis demonstrated that NaOH concentration plays the main role in the determination of the reaction yields (Table 2.1.), achieving the highest reaction yield (80%) at $C_{NaOH} = 0.10$ M. At lower NaOH concentration (0.04 M), the basicity is probably not enough to guarantee the quantitative formation of soluble hydroxo species; whereas, at the highest basicity (0.40 M), NaOH could both stabilize zinc complexes in solution and create local surface modification of SiO_2, that were responsible for the lower reaction yield.

Instead, reaction time t did not show to affect the ZnO loadings in the investigated time range. The reaction yield was over 80% already after 5 minutes, demonstrating that the zinc precursor solution is already at equilibrium conditions.

In conclusion, it was demonstrated that by controlling the experimental conditions, it was possible to synthesize very reproducible samples, with reaction yields higher than 80%. Optimal NaOH concentration for the synthesis of ZnO/SiO_2 was fixed at 0.10 M. The reaction time t was recognized as a non-significant parameter in the determination of the reaction yield and it was fixed at 5 minutes, the shorter time necessary for the formation of a reproducible equilibrium in precursor solution. Using these experimental conditions, SiO_2 samples with two ZnO loadings (4 and 10 wt%) were synthesized by using different amounts of zinc precursor (Table 2.2) and fully characterized to confirm the properties of the synthesized ZnO/SiO_2 materials, as reported in a previous paper[1].

2.1.3 Characterization of ZnO/SiO_2

$ZnO/SiO_2\_4\%$ and 10% were characterized to confirm the morphological and structural properties of the synthesized materials, checking their properties with those reported by Susanna *et al.*[1]. ZnO amount was measured by ICP-AES; structural, optical and morphological characterizations of ZnO NPs on SiO_2 were performed with FTIR-ATR spectroscopy and XRD diffraction, UV-Vis reflectance and TEM analysis, respectively (details reported in the Appendix).

ICP-AES. The ZnO loadings (wt%) calculated from ICP-AES measurements of the zinc content are reported in Table 2.2. The results are similar to the expected ones[1], corresponding to reaction yields of 80%, demonstrating high reproducibility.

FTIR spectroscopy. FTIR-ATR analysis proved that SiO_2 surface was modified by supporting ZnO NPs, bonded to SiO_2 through the formation of Si-O-Zn bonds (Figure 2.3).
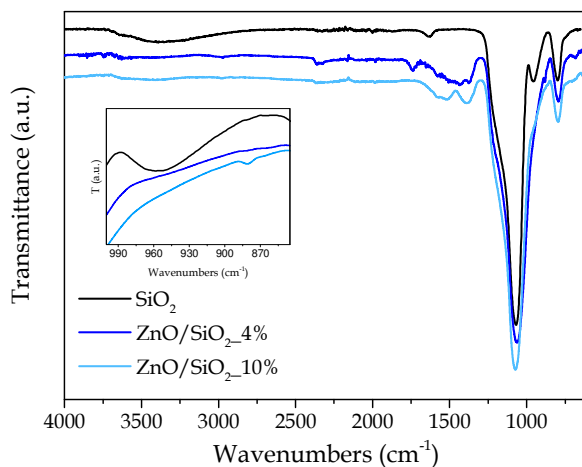
Figure 2.3. FTIR-ATR spectra of the ZnO/SiO$_2$ samples compared to bare SiO$_2$; in the inset, the peaks related to Si-OH stretching vibrations are highlighted.

In fact, the typical peak at 954 cm^{-1} of bare SiO$_2$, attributed to the stretching vibration of Si-OH bond, shifted to higher wavenumbers (965 cm^{-1}), due to a partially substitution of surface OH groups with a symmetric Si-O-Zn bond. As a result, this peak became a shoulder of the strong peak at about 1050 cm^{-1} (Si-O-Si stretching vibration).

X-Ray diffraction. The structural characterization of ZnO/SiO$_2$ was performed using the X-Ray Diffraction technique (Figure 2.4). The main broad peak at $2\theta = 23$ was assigned to amorphous silica; no other peaks due to crystalline ZnO wurtzite phase could be detected in the spectra, confirming the amorphous structure of ZnO NPs.
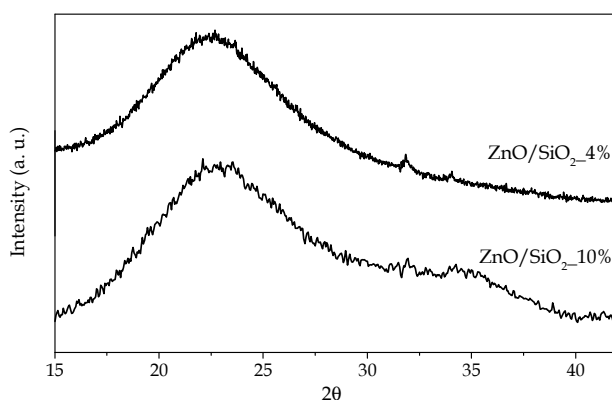
Figure 2.4. XRD diffractograms registered for ZnO/SiO$_2$_4% and ZnO/SiO$_2$_10%. No peaks related to ZnO crystalline phase are detected.

UV-Vis reflectance. Reflectance UV-Vis analysis gave two main information on the nature of ZnO/SiO$_2$ samples (Figure 2.5): first, the presence of the absorption edge typical of ZnO in both samples confirmed the presence of ZnO on SiO$_2$ surface (the band gap of micro-crystalline ZnO, m-ZnO, is ~3.2 eV)[3]. Besides, the UV-Vis measurements allowed the calculation of the magnitude of the band gaps of ZnO NPs, using the Kubelka-Munk equation (as shown in the Appendix). The observed blue-shift of the absorption edge energy from that of ZnO for ZnO/SiO$_2$_10% and ZnO/SiO$_2$_4%, proved the nanometric sizes of ZnO particles on SiO$_2$ in this samples and the progressive decrease of ZnO NPs sizes[4], by reducing the amount of ZnO.
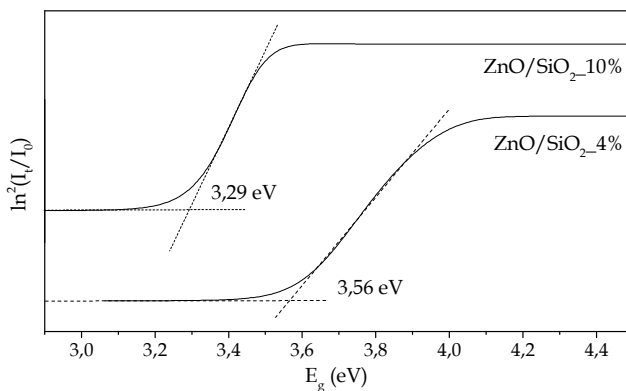
Figure 2.5. UV-Vis reflectance spectra of ZnO/SiO_2. In the spectra the band gap energies calculated for the two samples are reported.

Morphological study: TEM microscopy. Morphological analysis was employed to confirm the size of ZnO NPs on SiO_2. In Figure 2.6., as an example, the TEM images of $ZnO/SiO_2\_10\%$ are shown, proving the nanometric size of ZnO NPs. In $ZnO/SiO_2\_10\%$, 30 nm SiO_2 NPs were decorated by 6-8 nm ZnO NPs, whereas smaller ZnO NPs (4-5 nm, data not reported) were evident in $ZnO/SiO_2\_4\%$, confirming the previous data obtained in the UV-Vis reflectance analysis.
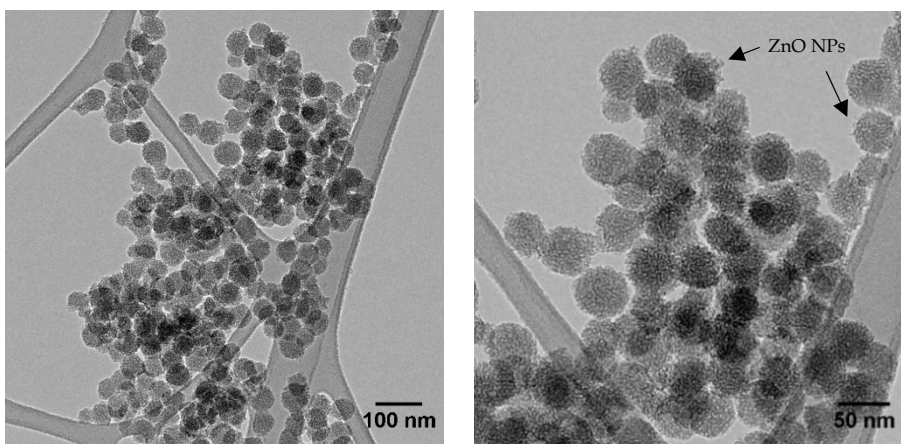
Figure 2.6. TEM images of $ZnO/SiO_2\_10\%$at two different magnification (x20k on the left, x40k on the right).

2.1.4 Summary on ZnO/SiO$_2$ preparation

Two samples of ZnO/SiO$_2$ at different ZnO loadings (4% and 10%) were synthesized according to a reported procedure[1], optimized for obtaining high yield and reproducibility.

In the synthetic procedure, a main role was assigned to the NaOH concentration, that favours the condensation of ZnO NPs in the presence of SiO$_2$ particles. Amorphous ZnO NPs of 4-5 to 8 nm were deposited onto the SiO$_2$ surface in samples ZnO/SiO$_2$_4% and ZnO/SiO$_2$_10%, respectively (detected from UV-Vis and TEM analyses), with the formation of Si-O-Zn bond that covalently connect ZnO NPs to SiO$_2$ (FTIR).

The material will be used as activators for tests in rubber NCs, together with ZnA-SiO$_2$, whose synthesis and characterization are described in the next section. Through this analysis, the activity of the double function fillers, in the form of ZnO NPs and Zn(II) centres was evaluated in comparison to m-ZnO.

2.2 Preparation of ZnA-SiO$_2$

The catalyst ZnA-SiO$_2$ constituted by Zn(II) centres anchored to SiO$_2$ NPs was prepared using anchoring agents with two terminal functional groups, able to bind both to SiO$_2$ surface and to coordinate Zn(II) centres. Trialkoxysilanes are good candidates as anchoring agents: the alkoxy units can easily condensate with the hydroxyl groups on SiO$_2$ surface, forming Si-O-Si bonds and liberating the respective alcohol by-products; in the meantime, the terminal groups can be suitably tuned, to favour the coordination with Zn(II) centres.

Functional groups containing heteroatoms are suitable linkers of Zn(II) centres, due to the intrinsic tendency of Zn to be coordinated by oxygen, nitrogen or sulphur atoms , e.g. in natural compounds as the enzymes[5,6]. Amine groups are well known to coordinate Zn in many different compounds[7,8]. In the present work, the amino silane (3-aminopropyl)triethoxysilane (APTES) was used as anchoring agent for the synthesis of ZnA-SiO$_2$ NPs. A two step-reaction was developed: i) a previous step of SiO$_2$ functionalization, followed by ii) the reaction with a zinc precursor (zinc nitrate hexahydrate) to generate isolated single Zn centres anchored to the SiO$_2$ surface.

2.2.1 Synthesis of ZnA-SiO$_2$

Materials: precipitated SiO$_2$ Zeosil MP1165 (specific surface area 160 m^{2}g^{-1}) was obtained from Rhodia; (3-aminopropyl)triethoxysilane (H$_2$N(CH$_2$)$_3$Si(OC$_2$H$_5$)$_3$, 99%, APTES) was purchased from Sigma Aldrich; zinc nitrate hexahydrate (Zn(NO$_3$)$_2$·6H$_2$O, 99%) and toluene (99%) from Alfa Aesar; ethanol (EtOH, puriss, p.a., absolute, ≥ 99.8%) from Sigma Aldrich.

Experimental procedure: the scheme of reaction is shown in Figure 2.7.
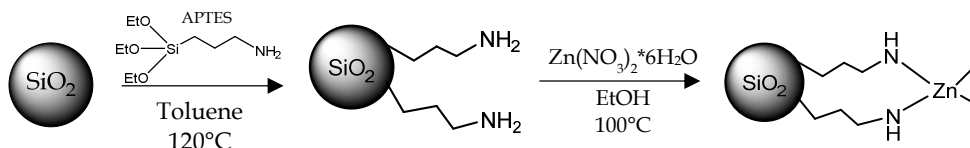
Figure 2.7. Scheme of the reaction used for the formation of zinc centres on SiO_2.

a) *SiO_2 NPs functionalization with APTES*. SiO_2 powder (1.0 g) is dispersed under stirring in 24 mL of toluene for ten minutes at 120°C; then a suitable amount of APTES (Table 2.3) is added to the SiO_2 suspension, kept under stirring for 24 hours. The amount of APTES was varied to different molar ratios APTES/ surface silanol groups of SiO_2 (as estimated by TGA, see paragraph 2.2.2). SiO_2 functionalization proceeds by hydrolysis and condensation of APTES molecules on the silica surface. Finally, the suspension is cooled down at room temperature and the powder recovered by centrifugation, washed twice with fresh toluene and dried at 80°C for 12 hours.

Hereafter, these samples are labelled A_X-SiO_2, where A is for APTES and X indicates the molar ratios of APTES over hydroxyl groups of silica (n_{APTES}/n_{OH} sup.).

Table 2.3. Amounts of APTES used for the functionalization of silica NPs (per each gram of SiO2), associated with different molar ratios of APTES over surface silanol groups of silica.

	X ($n_{APTES}/n_{OH\ sup.}$)		Y (n_{Zn}/n_{APTES})
	0.17		0.5
A_X-SiO_2	0.33	$Zn_Y A_X$-SiO_2	1.0
	0.50		2.0
	1.00		

b) *Zn(II) anchoring to SiO_2*. 1.0 g of A_X-SiO_2 is dispersed under stirring in 50 mL of ethanol for 20 minutes at 100°C; later, $Zn(NO_3)_2 \cdot 6H_2O$ is added. The amount of zinc precursor was varied based on the amount of silane molecules linked on the SiO_2 NPs surface (as calculated by TGA analysis, see paragraph 2.2.2), by

varying the molar ratio between Zn and APTES molecules as indicated in Table 2.3. The reaction is carried out for 2 hours and after cooling down, the powder is separated by centrifugation and washed twice with fresh ethanol, to eliminate the unreacted salt. Then the powder is dried at 80°C for 12 hours.

Hereafter, these samples are labelled $Zn_Y A_X\text{-}SiO_2$, where Y indicate the molar ratios of Zn over APTES (n_{Zn}/n_{APTES}) used in the reactions with each $A_X\text{-}SiO_2$ sample.

2.2.2 Characterization of $A_X\text{-}SiO_2$ samples

The study of the $A_X\text{-}SiO_2$ structure is reported in this paragraph. The knowledge of structure and composition of these intermediates are determinant for the subsequent anchorage of Zn(II) centres onto SiO_2 surface.

The real APTES functionalization of SiO_2 was confirmed by FTIR and solid-state NMR, using a pulse sequence technique (Cross Polarization Magic Angle Spinning, CPMAS) and was quantified by TGA and elemental analysis (CHNS). The specific surface area (SSA) of SiO_2 NPs was measured before and after functionalization by nitrogen physisorption, to verify whether the surface functionalization affects the SSA values. The experimental details are reported in the Appendix.

FTIR spectroscopy. The real SiO_2 functionalization with APTES was highlighted by comparing FTIR spectra of functionalized samples to the spectrum of bare SiO_2 (Figure 2.8). First, the partial substitution of SiO_2 hydroxyl groups due to the formation of bonds between SiO_2 and the silane, was evidenced by the shift of the stretching mode of Si-O-H at 954 cm^{-1} to higher wavenumbers, becoming a shoulder of the main peak at 1068 cm^{-1} (Si-O-Si stretching vibration), as already seen with ZnO/SiO_2. Besides, two more peaks at 2864 and 2948 cm^{-1} attributed to the symmetric and asymmetric stretching of CH_2 groups of the APTES propyl chain were present. The intensities of these latter peaks strictly depend on the

amount of APTES in the reaction, suggesting that different degrees of functionalization of silica can be achieved in these experimental conditions.
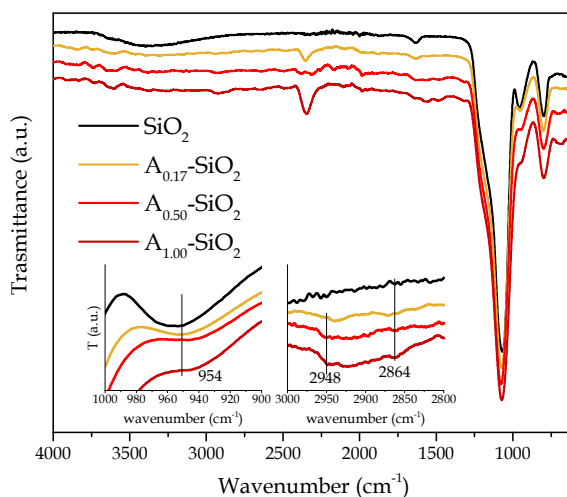
Figure 2.8. FTIR spectra of three functionalized A_X-SiO$_2$ samples.

TGA and CHNS analyses. The quantification of the organic ligands on the surface of SiO$_2$ was determined using TGA analysis combined to CHNS measurements.

TGA profiles of A_X-SiO$_2$ compared to bare SiO$_2$, showed higher weight loss percentages in the range of temperatures between 150 and 1000°C ($\Delta W_{150-1000}$) due to i) the combustion of the organic functional groups bonded to SiO$_2$ surface; ii) the desorption of residual chemisorbed silanol groups as water (Figure 2.9). The latter was the only contribution of bare SiO$_2$. The trend of the weight loss percentages in A_X-SiO$_2$ was strictly dependent on the amount of APTES used in the reaction, confirming the effective functionalization of silica (Table 2.4.). In particular, the weight loss increased up to $A_{0.50}$-SiO$_2$, then remains comparable in the sample at the highest APTES content ($A_{1.00}$-SiO$_2$). This observation evidences that a saturation of silica surface occurred, even increasing the precursor APTES, so that no more silane molecules can bind to SiO$_2$ and the coverage degree achieved a plateau region.
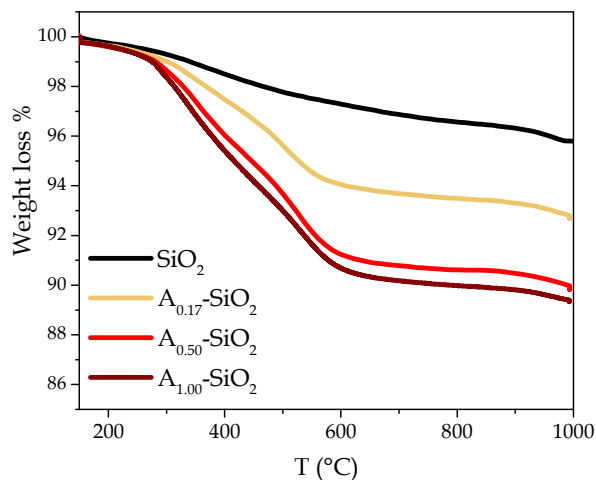
Figure 2.9. TGA thermograms of A_X-SiO$_2$ samples, reported between 150 and 1000°C.

The estimation of the moles of silane effectively deposited onto silica was calculated considering that the weight loss registered in the range 150-1000°C ($\Delta w_{150-1000°C}$) is determined by two contributions, due to both the organic ligands and the chemisorbed silanol groups. $\Delta w_{150-1000°C}$ can be expressed as follows:

$$\Delta w_{150-1000°C} = n_R \cdot MW_R + \frac{n_{OH}(g_{SiO_2}) \cdot w_{SiO_2(1000°C)} - n_R}{2} \cdot MW_{H_2O} \qquad (2.1)$$

where n_R is the number of APTES moles, MW_R is the molecular weight of the APTES residue bond to silica surface (58 g mol^{-1}), n_{OH} is the mole of OH groups on SiO$_2$ surface determined by a previous TGA measurement on bare SiO$_2$ (equal to 0.0052 mol g^{-1}), $w_{SiO_2(1000°C)}$ is the weight of silica measured at 1000°C after the TGA analysis is completed and MW_{H_2O} is the molecular weight of water. From the previous equation, the number of moles of silane n_R can be derived:

$$n_R = \frac{2 * \Delta w_{150-1000°C} - n_{OH} * w_{SiO_2(1000°C)} * MW_{H_2O}}{2MW_R - MW_{H_2O}} \qquad (2.2)$$

Starting from this equation, the weight percentage of silane on SiO_2 (wt%) was calculated as follows:

$$\text{weight percentage APTES} = \frac{n_R \cdot MW_R}{w_{SiO_2(1000°C)}} \tag{2.3}$$

By comparing the effective coverage degrees with the nominal values, calculated from the amount of APTES used during the reaction, the reaction yields were calculated. Moreover, an evaluation of the number of molecules of APTES over silica surface, that gives an idea of the coverage degree of SiO_2 was possible through the following equation:

$$\frac{\text{n. molecules}}{\text{surface(nm}^2)} = \frac{N_A * n_R}{\frac{n_{SiO_2} * MW_{SiO_2}}{S_{BET}} * 10^{18}} \tag{2.4}$$

where N_A is the Avogadro's number, MW_{SiO2} is the molecular weight of silica (60 g mol^{-1}), S_{BET} is the specific surface area of bare SiO_2 (160 m^2 g^{-1}) and n_R is the number of APTES moles, calculated in (2).

The calculated silane percentages, reaction yields and the estimated number of APTES over silica surface are reported in Table 2.4. Each value is calculated as the average value of three samples, with the relative standard deviations.

Table 2.4. Experimental weight loss percentages between 150-1000°C measured from TGA profiles of the four functionalized samples and bare silica. From this data, the coverage degrees, reaction yields and an estimation of number of APTES molecules over silica surface were calculated.

Sample	% weight loss (150-1000°C)	Silane percentage (wt %)	Reaction yield	Number of APTES molecules/nm^2
SiO_2	4.2	-	-	-
$A_{0.17}$-SiO_2	7.1 ± 0.1	3.2 ± 0.1	99	2.3 ± 0.1
$A_{0.33}$-SiO_2	8.0 ± 0.2	6.2 ± 0.2	95	4.4 ± 0.2
$A_{0.50}$-SiO_2	10.4 ± 0.2	7.6 ± 0.2	76	5.2 ± 0.2
$A_{1.00}$-SiO_2	10.6 ± 0.3	7.8 ± 0.3	41	5.3 ± 0.3

The quantification of APTES molecules was further performed by CHNS measurements on A_X-SiO$_2$ (Table 2.5). The nitrogen content obtained from CHNS is comparable in the range of the experimental error with that calculated by TGA, considering nitrogen derived only from anchored APTES. The values were calculated as the main values between the measurements made on three samples. This analysis confirmed the good estimations calculated by TGA.

Table 2.5. Weight percentage of nitrogen measured by CHNS analysis and determined through the previous quantification with TGA.

Sample	N% (from TGA)	N% (from CHNS)
SiO$_2$	-	0.03 ± 0.01
A$_{0.17}$-SiO$_2$	0.75 ± 0.12	0.90 ± 0.15
A$_{0.33}$-SiO$_2$	1.45 ± 0.28	1.38 ± 0.22
A$_{0.50}$-SiO$_2$	1.78 ± 0.28	1.51 ± 0.19
A$_{1.00}$-SiO$_2$	1.84 ± 0.30	2.01 ± 0.31

From the experimental results it can be concluded that the maximum weight percentage of APTES over SiO$_2$ was about 8wt%; above this value, a dramatical drop of the reaction yields took place. At the same time, the estimated average number of APTES molecules over SiO$_2$ surface ranged between two and six on squared nanometres of SiO$_2$ surface depending on the coverage degree (Table 2.4). This calculation allowed to reasonably suppose that Zn(II) centres could bind to the amino groups of silanes, with a coordination that could involve more than one amino group. The number of molecules cannot reasonably exceed six molecules over square nanometre of silica surface, due to either steric hindrance or electrostatic repulsion. Another possible explanation may be the low number of still non-reacted hydroxyl groups which reduces the binding points on silica surface.

Based on the amount of hydroxyl groups on the silica surface (see TGA analysis), a preliminary hypothesis about the APTES bonding on SiO$_2$ can be

formulated. Considering that each APTES molecule may bind through one to three ethoxy groups reacting with the hydroxyl groups of silica, in the case of a homogenous coverage of the surface, the maximum number of APTES moles bound to silica should be from equal to one third of the OH moles of silica, depending on the way of linking. The very high reaction yield obtained with the sample $A_{0.33}$-SiO_2 (1 APTES mole every 3 OH moles), suggested that all the previously suggested ways of linking may be possible. Instead, the lower reaction yields of sample $A_{0.50}$-SiO_2 and especially of $A_{1.00}$-SiO_2 suggested that APTES molecules have a preferential binding model to silica through two to three bonds for each molecule, excluding the possibility of a one-bond based APTES-silica system.

Solid state NMR. Based on these considerations, solid state NMR technique was used to further characterized the link of APTES molecules to SiO_2 NPs. This analysis was performed in collaboration with Professor Diré, Department of Industrial Engineering, University of Trento. Only $A_{0.17}$-SiO_2 and $A_{0.50}$-SiO_2 samples were analysed, as an example of functionalized samples, compared to bare SiO_2. ^{29}Si-CPMAS experiments shows the typical spectrum of SiO_2 with Q^4, Q^3 and Q^2 units (Figure 2.10.), where Q^X represents the typical units due to Si-O and Si-OH bonding modes available for Si on bare SiO_2 surface. The spectra of A_X-SiO_2 showed the same signals of SiO_2 pattern with the addition of T^3 and T^2 units, due to APTES, where T^X are the additional units due to Si-OR bonds on the surface of SiO_2 (Figure 2.10.). The amount of T units increased with the amount of functionalizing agents, confirming the previous observations about the weight percentage of silane over SiO_2.

The comparison among the CPMAS spectra pointed out that the Q^3/Q^4 ratio decreased significantly from pure SiO_2 to the APTES-functionalized silica (Table 2.6), suggesting the consumption of Si-OH surface groups due to functionaliza-tion. In agreement with that, T/Q ratio decreases with the amount of APTES (Table 2.6), highlighting that the amount of grafted APTES increases

proportionally to the nominal concentration. Besides, the ratio T^2/T^3 decreased, suggesting that APTES molecules are likely bound to silica with at least two or even three bonds for each molecule, in agreement with the hypothesis from the TGA results. ^{29}Si-CPMAS spectra evidenced also a partial substitution of the -OH groups with -OEt according to the upfield shift of Q^2 units from 90 ppm to 92-94 ppm in A_X-SiO_2.
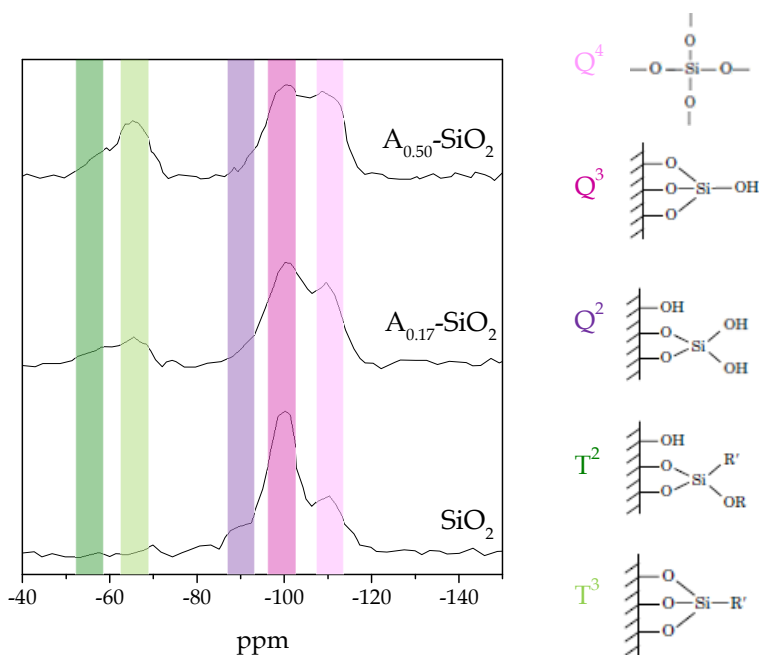
Figure 2.10. CPMAS experiments (^{29}Si frequency) performed on bare SiO_2 and on two functionalized sample with APTES. On the right the representations of the typical units available on the surface of bare (Q^4, Q^3 and Q^2) and functionalized SiO_2 (T^3 and T^2).

Table 2.6. Semi-quantitative results of ^{29}Si-CPMAS experiments.

Sample	$(Q^2+Q^3)/Q^4$	T/Q	T^2/T^3
$A_{0.17}$-SiO_2	1.53	0.19	0.94
$A_{0.50}$-SiO_2	1.11	0.35	0.45

In ^{13}C-CPMAS spectra, the APTES addition caused the appearance of typical resonances of the propyl chain of APTES and signals due to residual ethoxy groups that are not completely consumed after condensation. This analysis further confirmed the functionalization of SiO_2 surface with APTES.

Specific surface area. The surface area values (SSA) measured by B.E.T. method for the functionalized samples (Table 2.7.) showed that the functionalization reduces the SSA of bare silica, probably due to the occlusion of silica pores by the organic ligands.

Table 2.7. Decreased SSA values measured by B.E.T. method for the functionalized samples.

Sample	SSA ($m^2\ g^{-1}$)
SiO_2	160
$A_{0.17}$-SiO_2	107
$A_{0.33}$-SiO_2	109
$A_{0.50}$-SiO_2	107
$A_{1.00}$-SiO_2	106

2.2.3 Summary on A_X-SiO_2 characterization

From the previous characterization, it can be concluded that SiO_2 NPs were successfully functionalized with APTES ligands (FTIR); the functionalization can be suitably tuned on the basis of the quantity of APTES introduced in the reaction, up to a maximum of ~ 8wt% of APTES over SiO_2 corresponding to ~ 6 molecules/nm^2 (TGA and CHNS analysis). Each APTES molecule is bonded to silica surface through two to three covalent bonds (solid state NMR); the functionalization beyond 8wt% is probably hindered from the steric hindrance of the APTES molecules.

Finally, the APTES surface coverage degree and the reciprocal distance between the anchored ligands are suitable for the coordination of Zn(II) centres. For the preparation of the activators, only those A_X-SiO_2 samples prepared with the high reaction yields were used. For this reason, $A_{1.00}$-SiO_2 sample was not employed in the following reaction with the zinc precursor and will not be discussed in the next section.

2.2.4 Characterization of Zn_YA_X-SiO_2

In this section, Zn_YA_X-SiO_2 were characterized, after the reaction of the Zn precursor with A_X-SiO_2. First, FTIR, TGA and CHNS analyses already performed on A_X-SiO_2 (see paragraph 2.2.2) were repeated, to assess the possible influence of the Zn coordination reaction on the structure of the A_X-SiO_2. No structural modifications of A_X-SiO_2 were detected (data not reported).

The coordination of Zn(II) centres to the APTES ligands was confirmed through ICP analysis and studied by solid-state NMR, X-Ray Photoelectron Spectroscopy (XPS) and Electron Paramagnetic Resonance (EPR), using copper(II) atoms as paramagnetic probe for studying the coordination. Experimental details are illustrated in the Appendix.

ICP analysis. Zn_YA_X-SiO_2 samples were prepared by reaction of A_X-SiO_2 with three different amounts of zinc precursor (zinc/amine molar ratios equal to 0.5; 1.0, 2.0, Table 2.3) to establish the extent of zinc that could interact with functionalized silica and to understand the preferential coordination of the metal. The amounts were chosen considering that the quantity of zinc correspond to a coordination with the amino groups 1:2 (zinc/amine molar ratio 0.5), 1:1 (ratio 1.0) or to an excess of stoichiometric zinc (ratio 2.0), supposing that Zn(II) cannot directly bind to SiO_2 surface.

ICP results on Zn_YA_X-SiO_2 are reported in Table 2.8. From this data, the real Zn content of Zn_YA_X-SiO_2 NPs was noticed to be independent on the amount of zinc precursor used in the reaction and not influenced by the molar ratios n_{Zn}/n_{APTES}

(Y). The coverage degree of silica with APTES was the main parameter that affected the amount of Zn linked to silica.

Table 2.8. Weight percentage of zinc measured by ICP analysis for the Zn_YA_X-SiO_2 samples.

Samples	Y (n_{Zn}/n_{APTES})	Effective Zn (wt%)
$Zn_YA_{0.17}$-SiO_2	0.5	1.6 ± 0.1
	1.0	
	2.0	
$Zn_YA_{0.33}$-SiO_2	0.5	2.3 ± 0.2
	1.0	
	2.0	
$Zn_YA_{0.50}$-SiO_2	0.5	3.1 ± 0.2
	1.0	
	2.0	

Starting from the Zn wt%, the main number of zinc atoms distributed on the surface of A_X-SiO_2 was calculated using equation (2.4), considering that S_{BET} for Zn_YA_X-SiO_2 was equal to 107 m^2g^{-1}. In Table 2.9. the estimation of the number of Zn molecules (from ICP) and APTES molecules (from TGA, Table 2.4.) on silica surface and their relative ratios are shown.

Table 2.9. Number of Zn and APTES molecules calculated for the three Zn(Y)A(X)-SiO_2 samples.

Samples	Zn (molecules nm^{-2})	APTES (molecules nm^{-2})	Zn/APTES (molecules nm^{-2})
$Zn_YA_{0.17}$-SiO_2	1.3 ± 0.1	2.3 ± 0.1	0.56
$Zn_YA_{0.33}$-SiO_2	2.0 ± 0.2	4.4 ± 0.2	0.46
$Zn_YA_{0.50}$-SiO_2	2.58 ± 0.2	5.2 ± 0.2	0.50

The estimation of Zn/APTES ratio on SiO_2 is an indication that Zn is mainly bonded to SiO_2 thanks to APTES molecules, forming Zn(II) centres anchored to silica surface, and suggest the way of coordination of the metal centres with the amino groups. As Zn/APTES molecules nm^{-2} is almost equal to 0.5 for each sample, it can be deduced that each Zn(II) is likely to be coordinated by two amine groups. Moreover, this coordination is stable and not affected by the presence of an excess of zinc precursor in the reaction.

Consequently, the structure of the zinc centres on SiO_2 in Zn_YA_X-SiO_2 was proposed, as shown in Figure 2.11. As Zn atoms are typically tetracoordinated[8], it was supposed that two positions were occupied by APTES molecules, while the other ones may be occupied by more labile groups, such as hydroxyl, water or nitrate groups, coming from either the reaction surnatant or zinc precursor.
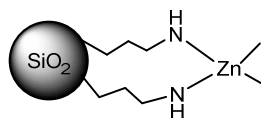
Figure 2.11. Proposed structure of zinc centres on SiO_2 surface: each zinc centres is coordinated by two anchoring agent molecules (APTES); the other two positions of zinc are supposed to be occupied by two different groups, as hydroxyl or nitrate groups, residual from the reaction.

Solid state ^{1}H-NMR. Solid state ^{1}H-NMR analysis of Zn_YA_X-SiO_2 was performed to determine the effective formation of a Zn-N bond with the amine groups of APTES, supporting the information from the ICP analysis. The analyses were realized in collaboration with Professor Diré, University of Trento (Italy).

In Figure 2.12, the spectra of $Zn_{0.5}A_{0.50}$-SiO_2 was reported of in comparison with that of $A_{0.50}$-SiO_2. These spectra are reported as an example of the functionalized samples, since the same patterns were detected for all Zn_YA_X-SiO_2 and A_X-SiO_2.

^{1}H-NMR spectrum of A_X-SiO_2 shows sharp peaks at 3.4, 1.2 and 0.7 ppm, due to the methylene protons of the propyl chain. The protons of the -NH_2 groups

show a main peak at 1.9 ppm. 5.2 and 1.0 ppm peaks are probably connected to some residual ethoxy groups from the functionalization reaction.

In $Zn_{0.5}A_{0.50}$-SiO_2, the peak of NH_2 protons (1.9 ppm) totally disappeared and the signal of the amino-group downfield shifts up to 7.3 ppm and broadens. No other change in the spectra was detected. In agreement with the calculation of Sun Ha Kim et al.[9] this behaviour can be related to the Zn^{2+} interaction with the amino groups, thus confirming the effective coordination of zinc centres to the amino groups of APTES.
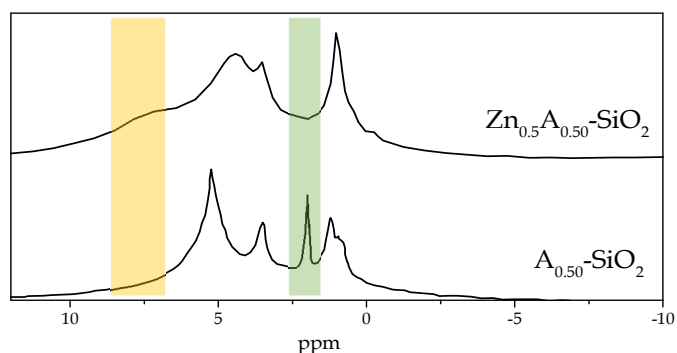
Figure 2.12. ^{1}H-NMR spectra of $Zn_{0.5}A_{0.50}$-SiO_2 compared to $A_{0.50}$-SiO_2; the peak related to NH_2 group of APTES molecules is substituted by a broad peak shifted at 7.3 ppm.

XPS spectroscopy. XPS was used to assess the surface composition of the Zn_YA_X-SiO_2 samples. This analysis was performed in collaboration with Prof. Lidia Armelao, of University of Padova. Detailed scans were recorded for C1s, O1s, N1s, Si2p, Zn2p regions. No further elements were detected. As for solid state NMR, samples $Zn_{0.5}A_{0.50}$-SiO_2 and $A_{0.50}$-SiO_2 were reported as an example of the functionalized samples, since the same patterns were detected for all Zn_YA_X-SiO_2 and A_X-SiO_2.

The atomic composition measured for $A_{0.50}$-SiO_2 and $Zn_{0.5}A_{0.50}$-SiO_2 samples are reported in Table 2.10.

Table 2.10. Atomic composition measured by XPS analysis

Samples	C %	O %	Si %	Zn %	N tot %	NH %	NO$_3$ %
SiO$_2$	3.15	70.90	25.95	-	-	-	-
A$_{0.50}$-SiO$_2$	19.64	53.38	22.21	-	4.76	4.76	-
Zn$_{0.5}$A$_{0.50}$-SiO$_2$	16.09	55.15	20.13	2.58	6.05	4.32	1.73

As expected, after functionalization an additional contribution to due nitrogen can be detected (NH%); besides, after reaction with the zinc precursor, zinc and nitrogen contribution are both evident. Regarding nitrogen, two main components were highlighted for N1s, ascribed to one organic and one inorganic contributions, that are represented by the amino groups of APTES molecules and nitrate groups originated from zinc precursor, respectively. Thus, this analysis suggested that nitrate groups are likely to coordinate zinc centres. Further structural information was collected by analysing the ratios between zinc and the two nitrogen components, reported in Table 2.11.

Table 2.11 Zn/NH and Zn/NO$_3$ ratios calculated from the atomic composition reported in Table 2.10.

Samples	Zn/NH	Zn/NO$_3$
Zn$_{0.5}$A$_{0.50}$-SiO$_2$	0.6	1.5

The value of Zn/NH ratio calculated from XPS analysis confirmed the previous estimation calculated from ICP measurement, in which the Zn/NH ratio was equal to 0.5 for the same sample. This result further validated the structure of Zn(II) centres, bonded to two amine groups of APTES molecules; besides, based on the value of Zn/NO$_3$ ratio, it was assessed that zinc could be partially coordinate with nitrate groups.

The presence of these labile groups coordinated to zinc centres represents an added value to the structure of this activator: in fact, it can be supposed that

these groups can be easily exchanged during the catalytic reaction, with other molecules or groups that are involved in the reaction, such as accelerator molecules or moieties.

EPR on a copper (Cu^{2+}) substituted material. EPR is a very useful technique to get structural information on paramagnetic species as transition metal ions with unpaired electrons. Zinc (II) is diamagnetic. On the contrary, copper (II) ions with d9 configuration, are paramagnetic and typically subjected to many EPR studies[10], to obtain information about the coordination environment of the metal centres with different ligands including possible metal-metal interactions.

In this study, Cu(II) was exploited as paramagnetic probe in substitution of Zn(II), in order to get an indirect information about the coordination structure of the metal centres with APTES. Even if the reactivity and the symmetry of the Zn(II) and Cu(II) are not the same, the study of the coordination of the Cu(II) centres with A_X-SiO_2 material in the same condition as Zn(II), allowed to further insight the role of anchoring ligand of APTES in A_X-SiO_2 after the addition of a metal precursor was assessed.

The analysis required the synthesis of $Zn_{Y-J}Cu_JA_X$-SiO_2 material, in which copper nitrate was used as a probe in small concentration, in addition to zinc nitrate in the second step of the reaction (Y = 0.49, J = 0.1, Y = 0.5, Figure 2.7.); the other synthetic parameters were not changed.

EPR spectra of $Zn_{0.49}Cu_{0.1}A_{0.50}$-$SiO_2$ showed a resonance line attributed to a monomeric Cu(II) species in axial symmetry with $g_{\parallel}$ = 2.26, $g_{\perp}$ = 2.06 and the hyperfine coupling constant $A_{\parallel}$ = 185 G (Figure 2.13a), where the magnetic tensor values are consistent with tetragonally elongated or square-planar or square pyramidal ions with two nitrogen ligands and two oxygen ligands in the equatorial positions[11,12].
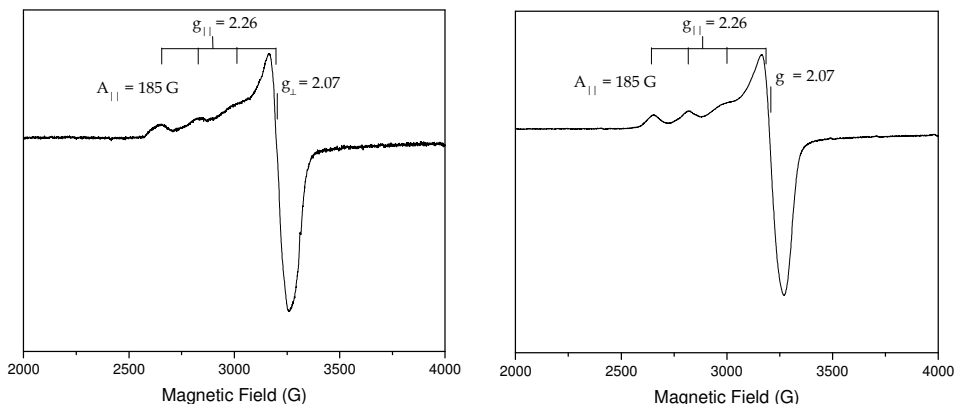
Figure 2.13. EPR spectra recorded at 123 K of a) $Zn_{0.49}Cu_{0.1}A_{0.50}$-$SiO_2$ and b) $Cu_{0.5}A_{0.50}$-SiO_2 NPs.

The same spectrum was recorded in a sample in which the total Zn content was substituted with Cu ($Cu_{0.5}A_{0.50}$-SiO_2), with a higher signal to noise ratio, confirming the coordination of copper ions as explained before.

These results show that Cu(II) are anchored to silica as isolated copper centres, without any metal-metal interactions; besides, it was supposed that only two nitrogen ligands bond can exist for every single Cu(II) centre, confirming that APTES molecules are close enough to coordinate one single metal centre and that, at the same time, no more than two APTES ligands are available for each centre, neither from the same SiO_2 particle nor from other vicinal SiO_2 particles. The presence of two oxygen ligands suggest the possible interaction of these centres with other species, such as water molecules, hydroxyl groups or nitrate groups (through the oxygen atom), as previously foreseen.

2.2.5 Summary on Zn_YA_X-SiO_2 characterization

Through the interaction of a Zn precursor (zinc nitrate hexahydrate) with APTES functionalized SiO_2, the formation of isolated Zn(II) centres bonded to SiO_2 was achieved. The coordination of each Zn(II) centre to SiO_2 takes place through the interaction of two molecules of APTES (anchoring agents). The other two free positions of tetracoordinated Zn(II) centres are likely occupied by

more labile groups as nitrate deriving from zinc precursors or by hydroxyl or water molecules. The loading of $Zn(II)$ over SiO_2 is strictly dependent on the previous functionalization step and can be suitably tuned by changing the functionalization degree of SiO_2. The highest coverage degree of APTES on SiO_2 (~8wt%) leads to the highest zinc loading (up to 3.1 wt%).

Three Zn_YA_X-SiO_2 samples with different Zn loading were selected and synthesized: $Zn_{0.5}A_{0.17}SiO_2$, $Zn_{0.5}A_{0.33}$-SiO_2 and $Zn_{0.5}A_{0.50}$-SiO_2. These samples will be tested as activators for the vulcanization reaction in the next chapter, comparing their activity to m-ZnO and ZnO/SiO_2.

2.3 Bibliography

1.   Susanna, a., Armelao, L., Callone, E., Dirè, S., D'Arienzo, M., Di Credico, B., Giannini, L., Hanel, T., Morazzoni, F. & Scotti, R. ZnO nanoparticles anchored to silica filler. A curing accelerator for isoprene rubber composites. *Chem. Eng. J.* **275**, 245–252 (2015).

2.   Reichle, R. A., McCurdy, K. G. & Hepler, L. G. Zinc Hydroxide: Solubility Product and Hydroxy-complex Stability Constants from 12.5–75 °C. *Can. J. Chem.* **53**, 3841–3845 (1975).

3.   Zhou, J., Zhao, F., Wang, Y., Zhang, Y. & Yang, L. Size-controlled synthesis of ZnO nanoparticles and their photoluminescence properties. *J. Lumin.* **122–123**, 195–197 (2007).

4.   Monticone, S., Tufeu, R. & Kanaev, A. V. Complex Nature of the UV and Visible Fluorescence of Colloidal ZnO Nanoparticles. *J. Phys. Chem. B* **102**, 2854–2862 (1998).

5.   Karsisiotis, A. I., Damblon, C. F. & Roberts, G. C. K. A variety of roles for versatile zinc in metallo-??-lactamases. *Metallomics* **6**, 1181–1197 (2014).

6.   Morán-Barrio, J., González, J. M., Lisa, M. N., Costello, A. L., Dal Peraro, M., Carloni, P., Bennett, B., Tierney, D. L., Limansky, A. S., Viale, A. M., *and others*. The metallo-β-lactamase GOB is a Mono-Zn(II) enzyme with a novel active site. *J. Biol. Chem.* **282**, 18286–18293 (2007).

7.   Parkin, G. Synthetic Analogues Relevant to the Structure and Function of Zinc Enzymes. *Chem. Rev.* **104**, 699–767 (2004).

8.   Molenveld, P., Engbersen, J. F. J. & Reinhoudt, D. N. Synthesis of a dinuclear Zn-II-calix[4]arene enzyme model with additional general base groups - Catalytic activity in phosphate diester transesterification. *Eur. J. Org. Chem.* **1999**, 3269–3275 (1999).

9.   Kim, S.-H., Han, O.-H., Kim, J.-K. & Lee, K.-H. Multinuclear Solid-state NMR Investigation of Nanoporous Silica Prepared by Sol-gel Polymerization Using Sodium Silicate. *Bull. Korean Chem. Soc.* **32**, 3644–3649 (2011).

10.   Pilbrow, J. R. *Transition ions electron paramagnetic resonance.* (Clarendon Press, 1990).

11.   Peisach, J. & Blumberg, W. E. Structural implications derived from the analysis of electron paramagnetic resonance spectra of natural and artifical copper proteins. *Arch. Biochem. Biophys.* **165**, 691–708 (1974).

12.   Hathaway, B. & Billing, D. E. The electronic properties and stereochemistry of mono-nuclear complexes of the copper (II) ion. *Coord. Chem. Rev.* **5**, 143–207 (1970).

3

Vulcanization tests

in rubber nanocomposites

The development of innovative activators, included in the general scenario of progressing towards more environmentally friendly materials, can hit the big time only if it brings about improvements in the performances of vulcanized rubber NCs. Both the vulcanization efficiency and the mechanical properties of the rubber NCs need to be enhanced, especially referring to the industrial available products.

The effect of the proposed activator ZnA-SiO$_2$ on the vulcanization process of rubber is illustrated in this chapter, focusing both on the process efficiency and on its effect on the determination of the mechanical properties of rubber. In this study, commercial m-ZnO, usually employed in the industrial vulcanization process of rubber for tyres application, is used as reference sample. ZnO/SiO$_2$ is further applied as activator for comparison. This material has already shown that the activator morphology and dimensions could play a role in setting the properties of the vulcanization process. Besides, as it is formed of dispersed ZnO NPs, it represents an intermediate situation between the use of massive m-ZnO and of a single-site system of Zn(II) centres, as activators in the rubber NCs.

In this chapter, the preparation of vulcanized isoprene rubber (IR) NCs performed with the different zinc-based activators is reported; then, a description about the parameters that determines the vulcanization process efficiency and the final mechanical properties is presented; finally, an investigation on the effects of the three activators in the vulcanization reaction is explored, in terms of vulcanization efficiency and mechanical, structural and morphological properties of rubber NCs.

3.1 Rubber compounding and processing

To produce commercial rubber materials with suitable technical properties, the identification of an appropriate rubber formulation of polymers and additives (compounding) and the set of operations pertinent to the mixing procedure (processing) are fundamental steps.

As mentioned before, the achievement of high performant products requires the addition of several ingredients to the raw elastomer or blend of elastomers, that contribute through different mechanisms to the formation of a network, determinant for the final mechanical properties. Among them, reinforcing fillers, the package of vulcanization agents, antioxidants, preservatives, etc., are typical examples (paragraph 1.1.4). Both the intrinsic properties and the compatibility of potential new ingredients with the rubber formulation are parameters taken into account when choosing for a new component. As an example, until 20 years ago the difficult mixing process of SiO_2, a nanosized reinforcing filler, in rubber matrix hindered its large employment. Only the further addition of suitable compatibilizing agents, molecules that chemically bind to the surface hydroxyl group of SiO_2, increasing its hydrophobic character and creating a covalent bond with the matrix, allowed the development of this new technology, with good impact on properties as rolling resistance and wet grip. Typical compatibilizing agents are silane molecules as bis[3-(triethoxysilyl)propyl]tetrasulfide (TESPT) or Bis[3-(triethoxysilyl)propyl]disulfide (TESPD), that generally require a usage temperature of about 140°C, to efficiently bind to SiO_2.

Together with the composition and primary structure of rubber materials, the degree of homogeneity of all these ingredients inside the formulation takes on great importance to enhance the resistance of the material and reduce the extent of the weakness points. Plasticizers and oils are generally added to increase the molecular mobility and reduce the mass viscosity, favouring the dispersion of the ingredients; moreover, subsequent mixing phases are usually employed, to guarantee a homogeneity as high as possible.

These principles of rubber compounding and processing were used for the preparation of the rubber (NCs) with the three different activators of vulcanization previously described. A three-steps mixing procedure was used to increase the homogeneity, without the addition of oils to reduce the variables in the systems. In accordance with the common procedure to produce silica/rubber NCs, bare SiO_2 was used together with TESPD as compatibilizing agent; instead, no addition of any compatibilizing agents was carried out with $Zn(Y)A(X)$-SiO_2 NPs, as NPs are already functionalized with silane molecules coordinating Zn(II) centres. The detailed preparation of rubber NCs is described in the next paragraph.

3.2 Preparation of IR rubber NCs

Materials: cis-1,4-polyisoprene rubber (IR) was purchased from Nizhnekamskneftechim Expor; bis(3-triethoxysilylpropyl)disulphide (TESPD) from Aldrich; antioxidant N-(1,3-dimethylbutyl)-N′-phenyl-p-phenylenediamine (6PPD), Santoflex-6PPD from Flexsys; the curing agents were purchased as follows: stearic acid (Stearina TP8) from Undesa; N-cyclohexyl-2-benzothiazole sulfenamide (CBS), Vulkacit CZ/X from Lanxess; sulphur Creso from Redball Superfine; ZnO (wurtzite, specific surface area 5 m^2 g^{-1}) from Zincol Ossidi.

3.2.1 Silica/IR NCs preparation procedure by using Zn_YA_X-SiO_2

Silica/IR NCs were prepared by mixing IR, Zn_YA_X-SiO_2 as filler, antioxidant 6-PPD and the curing agents CBS and S_8. No m-ZnO and stearic acid (SA) were added as activator and co-activator, since Zn(II) ions are already present and they were supposed to be already available to react. No TESPD was used, due to the previous functionalization of SiO_2.

The ingredients were mixed in a Brabender Plasti-Corder lab station internal mixer (65 mL mixing chamber, 0.6 filling factor, 60 rpm rotor speed), using a three-steps procedure. At first, IR was masticated into the mixing chamber at 90°C and Zn_YA_X-SiO_2 was added. After 3 minutes of mixing, required for the

filler incorporation in IR matrix, the antioxidant (6-PPD, 2.0 phr) was added. In the second step, the composites were reloaded into the mixing chamber at a temperature of 90°C and CBS (3.0 phr) and S_8 (1.6 phr) were added (2 minutes of mixing). In the last step the composites were further mixed in a two-rolling mill at 50°C for 3 minutes, to improve the homogeneity of the composites.

The composites were then vulcanized in a hydraulic press at 170 °C and 100 bar for 5 minutes (frequency = 1.670 Hz, Angle = 6.980%).

Hereafter, the cured NCs will be called $W\_Zn_YA_X$-SiO_2/IR where Y and X indicate the molar ratios used for the preparation of the Zn_YA_X-SiO_2 samples as previously reported, and W is the Zn content in the NCs in phr (Table 3.1). The highest Zn content used in the NCs (1.49 phr, that corresponds to 1.85 phr of ZnO) is about half of the conventional amount of Zn generally used in the industrial production (3-5 phr). The lowest Zn contents (1.08 and 0.68 phr) were chosen to get a more extended overview of the influence of Zn content on the vulcanization efficiency. NCs were prepared keeping constant the amount of silica, in order to reduce the number of variables that could affect the vulcanization performances.

Table 3.1. Composition expressed in phr of $W\_Zn_YA_X$-SiO_2/IR NCs at different zinc content, prepared using Zn_YA_X-SiO_2 samples with different coverage degrees (X and Y).

	Zn_YA_X-SiO_2					SiO_2	SA	TESPD
	X	Y	phr	Zn content (W)	SiO_2 content			
	0.17	0.5	45.4	0.68	43	-	-	-
$W\_Zn_YA_X$-SiO_2/IR	0.33	0.5	47.0	1.08	43	-	-	-
	0.50	0.5	48.1	1.49	43	-	-	-

3.2.2 Silica/IR NCs preparation procedure by using ZnO/SiO_2

Silica/IR NC was prepared using $ZnO/SiO_2\_4\%$ for the comparison of the activator properties with Zn_YA_X-SiO_2/IR NCs.

The preparation procedure was similar to that described for Zn_YA_X-SiO_2/IR NCs (3.2.1), modifying the experimental conditions of the first step of the mixing process where $ZnO/SiO_2\_4\%$ NPs and SA were mixed with IR at 145°C, followed by bare SiO_2, TESPD and 6PPD. The other steps remained unchanged.

A NC labelled $ZnO/SiO_2\_4\%\_IR$, was prepared with a Zn and SiO_2 content equal to 1.49 and 43 phr, respectively (Table 3.2).

This Zn content was chosen as the optimal one for the comparison between the activators since it was demonstrated to give the best performances in terms of vulcanization efficiency. The Zn loading of 4wt% for ZnO/SiO_2 NPS was chosen because the total amount of SiO_2 from NPS containing 1.49 phr of Zn, corresponds to the desired filler loading (43 phr) without any eventual addition of bare silica, as for Zn_YA_X-SiO_2 NPs in 3.2.1.

Table 3.2. Composition expressed in phr of the samples prepared with $ZnO/SiO_2\_4\%$; Zn and SiO_2 contents are equal to the three W_ Zn_YA_X-SiO_2/IR NCs.

	$ZnO/SiO_2\_4\%$			SiO_2	SA	TESPD
	phr	SiO_2 content	Zn content (W)			
$ZnO/SiO_2\_4\%\_IR$	44.8	43	1.49	-	2	3.4

3.2.3 Silica/IR NCs preparation procedure by using m-ZnO

References m-ZnO/IR NCs were prepared using conventional m-ZnO as activator, for the comparison with Zn_YA_X-SiO_2/IR.

The synthetic procedure was similar to that described for Zn_YA_X-SiO_2/IR (paragraph 3.2.1), modifying the experimental conditions of the first step of the

mixing process, where bare SiO_2 Zeosil 1165 and TESPD were mixed with IR at 145°C, followed by 6PPD, m-ZnO and SA (co-activator). The other steps remained unchanged., Hereafter, the samples prepared with m-ZnO will be called W_ZnO/IR, where W is the amount of Zn expressed in phr in the composite. These reference samples were characterized by an equal content of Zn (W) and SiO_2 to the respective $W\_Zn_YA_X$-SiO_2/IR NCs, to minimize the parameters that could play a role in affecting the vulcanization process and ascribe the differences only to the activators' morphology (Table 3.3).

Table 3.3. Composition expressed in phr of the reference samples prepared with m-ZnO and bare SiO_2; Zn and SiO_2 contents are equal to the three $W\_Zn_YA_X$-SiO_2/IR NCs.

	ZnO	Zn content (W)	SiO_2	SA	TESPD
	0.85	0.68	43	2	3.4
W_ZnO/IR	1.34	1.08	43	2	3.4
	1.85	1.49	43	2	3.4

3.3 Properties of the vulcanization process and vulcanized rubber NCs

The vulcanization process leads to the formation of a polymer network inside the polymer matrix, represented by sulphur cross-linking bridges between polymer chains[1]. The increased number of connections causes an increased cross-linking density in the rubber, that corresponds to a higher viscosity of the system and it is generally measured as a higher resistance of the material to a cyclic stress. By vulcanizing rubber specimens through the Rubber Process Analyzer (RPA) instrument, at constant stress frequency, the increased torque modulus values are recorded during vulcanization time, in the so-called vulcanization curves[2].

The main parameters that can be extrapolated from the curves are:

- the scorch time, the time in which the modulus exceeds the minimum value and starts to increase;

- the minimum torque (M_{min}) and the maximum torque (M_{max}), the lowest and maximum values of torque registered during the vulcanization curves, in N.m.; the former is equal to the viscosity of the compound heated to vulcanization curve, whereas the latter is the value of the vulcanized compound shear modulus at the given temperature;

- vulcanizate torque interval ΔM, given in N.m., representing the difference between the maximum and minimum torques ($M_{max} - M_{min}$);

- optimum time of vulcanization t_{90}, the time required for reaching 90% of the maximum achievable torque or network density, at the given temperature.

In a typical vulcanization curve, the modulus starts to increase after an induction period (scorch time) and keeps on growing (curing time) until a plateau is formed[3]. In some cases, a reversion process may be responsible for a reduction of the modulus after reaching the maximum torque. An optimal reaction is characterized by the achievement of high M_{max}, at very low time (t_{90}): thus, the higher ΔM and the lower t_{90}, the more the vulcanization process is highly efficient. In the industrial production of vulcanized rubber NCs, also the scorch time assumes a high technical importance, as the rubber needs to be suitably worked before the vulcanization get started.

Once the vulcanization process is completed, vulcanized rubber NCs behave as viscoelastic materials. As they are deformed, a fraction of energy is elastically stored, whereas the remaining is dissipated as heat (hysteresis loss). The main properties that describe the viscoelastic behaviour are G' (storage modulus), G'' (loss modulus) and tanδ (dissipative factor). From these properties, it is possible to derive the mechanical response of rubber under dynamic loading conditions (e.g. simulating the operative conditions of a tire).

In a typical oscillatory dynamic-mechanical test, the application of an oscillatory shear strain γ of angular frequency ω, results in a sinusoidal stress σ, as expressed in the following equation:

$$\gamma(t) = \gamma_o + \sin(\omega t) \qquad (3.1)$$

$$\sigma(t) = \sigma_o + \sin(\omega t + \delta) = \sigma_o \left[\sin(\omega t)\cos(\delta) + \cos(\omega t)\sin(\delta)\right] \qquad (3.2)$$

where δ is the phase angle. $\sigma(t)$ can be separated into two contributions: $\sigma_o\sin(\omega t)\cos(\delta)$ is the component of the stress in-phase with the strain and $\sigma_o\cos(\omega t)sen(\delta)$ is the 90° out of phase component.

Indicating $\sigma_o \cos(\delta) = \sigma_{o'}$ and $\sigma_o\sin(\delta) = \sigma_{o''}$, G' and G'' can be defined as follows:

$$G' = \frac{\sigma_o{}'}{\gamma_0} \qquad\qquad G'' = \frac{\sigma_o{}''}{\gamma_0} \qquad (3.3)$$

where G' and G'' contribute to the determination of G^*, a complex modulus expressed as an in-phase elastic component (G') and an out-phase dissipative component (G''). G^* is expressed as:

$$G^* = G' + iG'' \qquad (3.4)$$

The ratio between G'' and G', called $\tan\delta$ (dissipative factor), expresses the energy lost in a cyclic deformation. Both G' and G'' depends on the frequency and on the temperature.

Referring to rubber NCs for tyres application, these properties are strictly connected to the macroscopic behaviour of rubber NCs, such as wear resistance, wet traction and rolling resistance[4,5]. As an example, the trend of $\tan\delta$ with the frequency determines two main properties of rubber NCs: at low frequency, the lower the value of $\tan\delta$, the lower the rolling resistance. On the other hand, at high frequencies, the higher $\tan\delta$, the lower the elastic behaviour and the higher the wet traction. Thus, the measurement of G', G'' and $\tan\delta$ at different frequency and temperature conditions would be essential to know the behaviour of the analysed NCs in the real application.

In this Thesis, as one of the main goals was the production of low rolling resistance tyres, with low environmental impact, G', G'' and $\tan\delta$ were evaluated for vulcanized NCs at low frequency, aiming at the reduction of $\tan\delta$.

tanδ could be reduced either by increasing the values of G′ or reducing G′′ at low frequency.

G′ is reported to be affected by both strain-independent and strain-dependent contributes[6,7] (Figure 3.1): the former are the hydrodynamic effect (related to the filler volume fraction), the polymer network (due to polymer entanglements and physical and chemical cross-links of the polymer chains) and the in-rubber structure (connected to the immobilization of rubber on filler particles and to filler rubber interaction, in case of silica dependent on the coupling silane). The strain-dependent behaviour is responsible of the non-linear decreasing of G′ increasing the strain and is generally connected to the presence of the network of reinforcing filler[8].
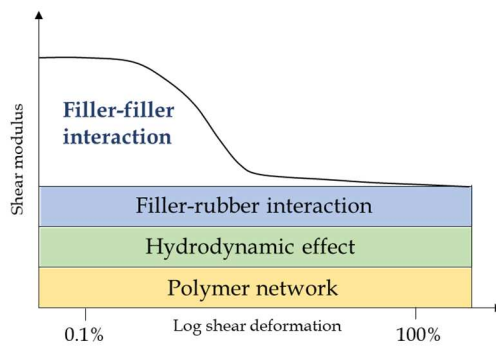
Figure 3.1. Representation of a stress-strain curve describing the strain independent and dependent (Payne Effect) contributions on rubber reinforecement.

Both reinforcing filler and vulcanization process can participate to the enhancement of G′ due to the formation of networks inside the structure; more precisely, the vulcanization participate at all strain values, because it contributes to the formation of the polymer network (strain-independent contribution); a reinforcing filler contributes to increase G′ at low strain values (G′$_0$), whereas at intermediate values of strain, G′ shows a decrease due to the hysteretic breakdown of the filler network formed by filler NPs joined together or through polymer layers. This reduction is known as Payne Effect. One possible way to

reduce the Payne effect is the improvement of filler-rubber interaction, for example, in the case of SiO_2, thanks to the addition of coupling agents.

In the present Thesis, the substitution of a system in which nano-SiO_2 is used as reinforcing filler together with m-ZnO as activator of vulcanization, with the so-called double function fillers could have a double effect on the mechanical properties of rubber NCs and especially on G′. With both ZnO/SiO_2 and Zn_YA_X-SiO_2 an increased vulcanization efficiency could shift the G′ curve towards higher values, changing the strain-independent contribution given by the polymer network. Besides, especially with Zn_YA_X-SiO_2 NPs, the presence of a different filler-rubber interface could modify the strain-dependent contribution, that is filler-rubber interaction and Payne Effect.

3.4 Study of the vulcanization process of IR NCs with different activators

In this paragraph, the rheological, dynamic-mechanical and morphological characterization of the rubber NCs vulcanization process is reported.

First, the vulcanization curves for all the prepared NCs were described and discussed based on the nature of the activator and on the Zn content. Moreover, the vulcanized samples were characterized from a dynamic-mechanical point of view, measuring G′, G′′ and tanδ.

The cross-linking densities were calculated using a swelling procedure experiment, to confirm the effectiveness of the vulcanization process. Finally, the morphology of the NCs was studied, using TEM analysis, to assess whether the modification of silica surface modify the filler/rubber interaction and consequently the distribution of SiO_2 in the rubber matrix.

3.4.1 Vulcanization curves

The vulcanization curves of NCs with Zn_YA_X-SiO_2 compared with those with ZnO/SiO_2_4% and m-ZnO are reported in Figure 3.2. The comparison was

performed at a Zn content equal to 1.49 phr, as this amount was the most performant in the investigated range of concentration (as shown later from the comparison of $W\_ Zn_YA_X\text{-}SiO_2/IR$).

The vulcanization curve of $1.49\_Zn_{0.5}A_{0.50}\text{-}SiO_2/IR$ showed the best performances. In Table 3.4. it is shown that ΔM was increased of 30% and t_{90} was half of the value of m-ZnO, demonstrating a very high vulcanization efficiency. Besides, $ZnO/SiO_2\_4\%/IR$ showed a halfway through behaviour between $1.49\_ZnO/IR$ and $1.49\_Zn_{0.5}A_{0.50}\text{-}SiO_2/IR$. When ZnO NPs are supported on SiO_2, the achieved M_{max} was the same as m-ZnO, but t_{90} was highly reduced (Table 3.4.). This behaviour suggested that ZnO/SiO_2 NPs are more reactive compared to m-ZnO, so that the interaction with the other vulcanization agents (starting from stearic acid) is faster and the cross-linking network can be formed in a shorter time. At the same time, the even lower t_{90} of $Zn_YA_X\text{-}SiO_2/IR$ NCs suggested that this activator is more reactive compared to the other two activator systems due to the availability to react of the single site Zn centres with the curatives and the reaction proceeds faster.
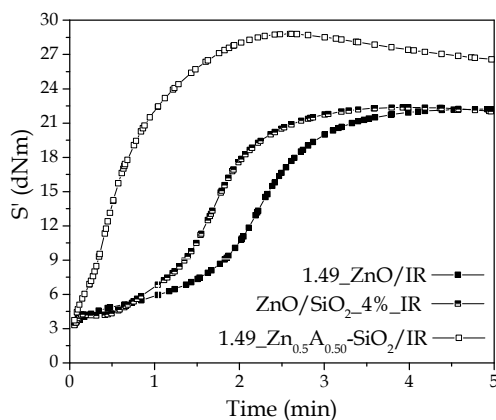

Figure 3.2. Vulcanization curves registered using three activators: ■ m-ZnO; ▬ $ZnO/SiO_2\_4\%$; □ $Zn_{0.5}A_{0.50}\text{-}SiO_2$. The three NCs have the same Zn and SiO_2 content.

Table 3.4. Vulcanization characteristics for $W\_Zn_YA_X-SiO_2/IR$, compared to the reference W_ZnO/IR and $ZnO/SiO_2\_4\%\_IR$.

NCs		M_{max} (dNm)	M_{min} (dNm)	ΔM (dNm)	t90 (min)
W (phr)	Sample				
0.68	$ZnA-SiO_2/IR$	16.0	2.9	13.1	1.7
	ZnO/IR	17.0	3.0	14.0	1.6
1.08	$ZnA-SiO_2/IR$	19.6	3.2	16.4	1.2
	ZnO/IR	17.2	2.6	14.6	1.9
1.49	$ZnA-SiO_2/IR$	28.8	3.7	25.1	1.6
	ZnO/IR	22.2	3.3	18.9	3.1
	$ZnO/SiO_2\_4\%\_IR$	22.4	3.3	19.1	2.4

From the curves, it can be noticed that the scorch times are different too. The lowest scorch time registered in the presence of $1.49\_ZnA-SiO_2/IR$, is consistent with the structure of this activator as Zn(II) centres are already available at the beginning of the process and in this case, no SA was required to solubilize Zn(II) ions from ZnO; the reaction of the zinc centres with the other vulcanization agents and the polymer can start as the vulcanization temperature is reached (Figure 3.3). As observed, the scorch time increased moving to $ZnO/SiO_2\_4\%$ and $1.49\_ZnO/IR$, because of the first step of interaction between ZnO and SA and *in situ* formation of Zn(II) centres. The initial delay was higher in the presence of m-ZnO, since the larger particles of m-ZnO are less available to react then the very small amorphous ZnO NPs supported on SiO_2, distributed all over the rubber matrix.

The activity of $Zn_YA_X-SiO_2$ NPs was further tested at different concentration of ZnO inside the rubber matrix and compared to the activity of m-ZnO, in order to study its efficiency at different Zn content. The vulcanization curves are shown in Figure 3.3.
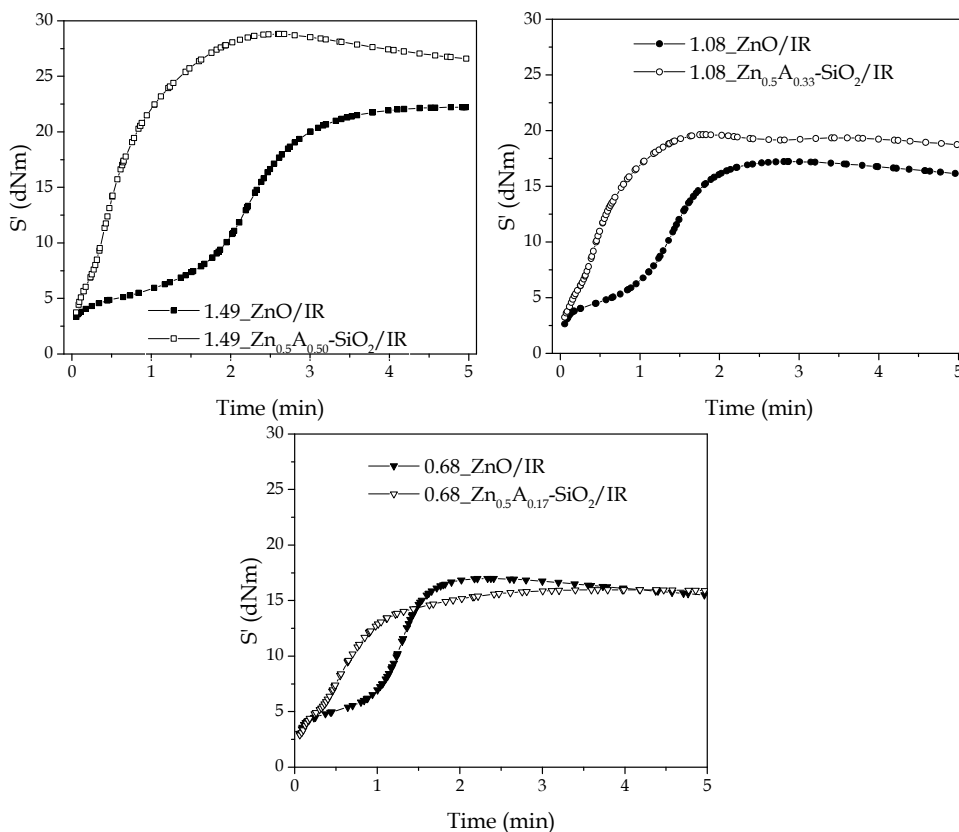
Figure 3.3. Vulcanization curves registered for the W_$Zn_Y A_X$-SiO$_2$/IR, at three different Zn content. Each reference W_ZnO/IR NCs is reported in the same graphs, at equal Zn and SiO$_2$ content.

At all Zn content a more efficient vulcanization was achieved, and a higher activity of the $Zn_Y A_X$-SiO$_2$ NPs was proved, as shown by the very small scorch time registered for the vulcanization curves. This observation confirmed that the reduced scorch times can be related to the higher availability and reactivity of Zn centres at the beginning of the reaction. Besides, higher ΔM were registered in the presence of $Zn_Y A_X$-SiO$_2$ NPs, even though the enhancement compared to the respective m-ZnO reference NC strictly depended on the amount of Zn in the rubber matrix: in fact, the higher the Zn content, the higher the effect in terms of M_{max}, with the sample at W = 1.49 phr the most performant in the applied range of concentrations.

3.4.2 Dynamic-Mechanical properties

The comparison of the dynamic-mechanical properties of NCs prepared using $Zn_YA_X\text{-}SiO_2$ NPs, $ZnO/SiO_2\_4\%$ NPs and the reference activator m-ZnO highlighted that both the two innovative activators can modify the mechanical properties of rubber, leading to an increase of their performance. G′, G″ and tanδ curves of the vulcanized NCs, between 0-10% strain, are reported in Figure 3.4.

The highest reinforcement can be achieved with the $Zn_YA_X\text{-}SiO_2$ NPs at all strain values (highest G′ values), thanks to the highest vulcanization efficiency measured in the vulcanization curves (strain-independent contribution); moreover, at low strain, this activator allows a strong reduction of tanδ values, connected to the high G′ values and to the low G″ values. Whereas, at high strain, the increased G″ values are responsible of the consequent enhancement of tanδ.

Instead, the reinforcement seems to be unchanged with ZnO/SiO_2, compared to m-ZnO; the main advantage of this activator appears the decrease of G″ and consequently tanδ values at all oscillation strain values.
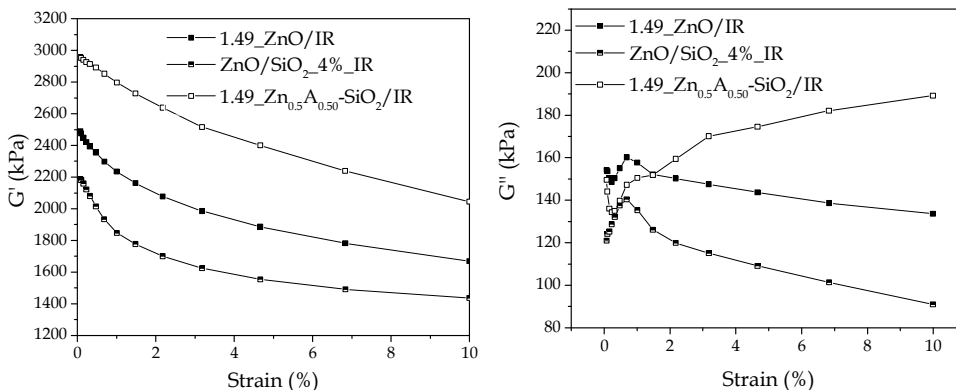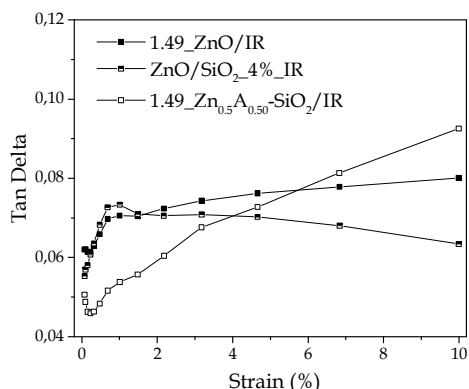
Figure 3.4. G′, G″, tanδ profiles of NCs using three activators: ■ m-ZnO; ■ ZnO/SiO$_2$_4%; □ Zn$_{0.5}$A$_{0.50}$-SiO$_2$ NPs.

By comparing the G′ curve of the NCs with the three activators, a different strain-dependent contribution can be highlighted. In the case of ZnA-SiO$_2$, the Payne Effect remained almost stable compared to 1.49_ZnO/IR. In fact, in 1.49_Zn$_{0.5}$A$_{0.50}$-SiO$_2$/IR, G′$_\infty$ increase as much as G′$_0$ compared to NC in the presence of SiO$_2$ and m-ZnO. This observation suggested that with the new activator the filler-rubber interaction is modified by the presence of Zn(II) centres linked by APTES on silica surface.

With ZnO/SiO$_2$, the Payne Effect seemed to be lower than NC in the presence of SiO$_2$ and m-ZnO, suggesting that in this case, a good filler-rubber interaction can be formed.

From the literature, TESPD (used with SiO$_2$) is supposed to create chemical bonds both with the SiO$_2$ surface and the polymer chains; in the case of Zn$_Y$A$_X$-SiO$_2$ NPs, APTES is certainly chemically bond to SiO$_2$ surface, but it would probably interact with the polymer through Zn(II) centres, thus creating only physical or electrostatic interactions. As it will be demonstrated in the next chapter, Zn(II) centres are not released from SiO$_2$ surface during the vulcanization reaction; it is reasonable to suppose that the presence of these Zn(II) centres can modify the filler-rubber interaction, but also the distribution of the vulcanization degree inside the rubber matrix. Further discussion about

the influence of the activator on the filler-rubber interface and vulcanization distribution, will be presented in Chapter 5.

The different mechanical properties measured in the presence of the three activators demonstrated that by changing the activators' morphology, the properties of rubber NCs can be tuned due to the different reactivity of the activators.

A comparison between the mechanical properties of W_Zn_YA_X-SiO_2/IR NCs with different Zn content is also reported in Figure 3.5. As a result of a more efficient vulcanization, at all Zn content, G'_0 values increased and the whole G' curves are shifted to higher values, probably due to an improved structure of the polymer network inside the NCs structure.
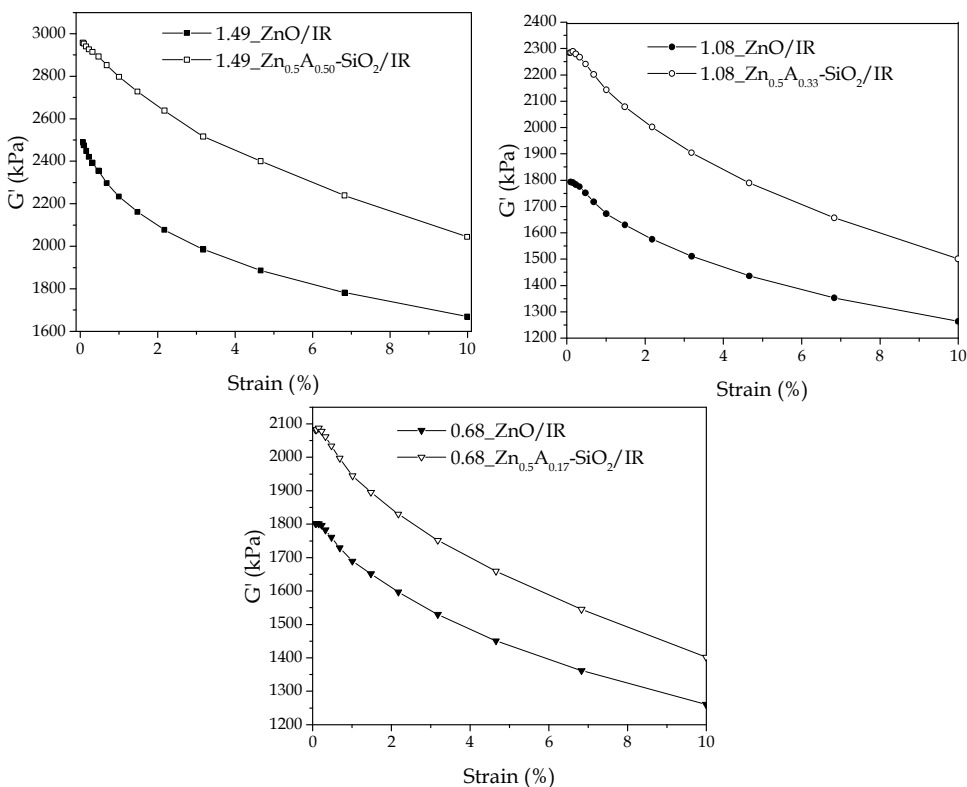
Figure 3.5. G' profiles for W_Zn_YA_X-SiO_2/IR, compared to W_ZnO/IR.

As shown in Table 3.5., G'_0 values increased by increasing the Zn content in the NCs (W), keeping constant the amount of SiO_2, demonstrating a strong effect given by Zn_YA_X-SiO_2 on the vulcanization process and consequently on the mechanical properties of the NCs. As expected, the Payne Effect increased by reducing the amount of Zn in the rubber NCs, as a reduction of Zn content is accompanied by a lower coverage degree of SiO_2 with APTES. The lower amount of APTES left more hydroxyl groups on silica surface, increasing the general hydrophilicity of these NPs and thus their tendency to agglomerate, reducing the filler-rubber interaction.

Table 3.5. Payne effect of $ZnASiO_2$/IR, in comparison to ZnO/IR and ZnO/SiO_2/IR NCs.

NCs		G'_0 (kPa)	$\Delta G'_{3\%-9\%}$ (kPa)
W (phr)	Sample		
0.68	ZnA-SiO_2/IR	2082	322
	ZnO/IR	1801	255
1.08	ZnA-SiO_2/IR	2283	374
	ZnO/IR	1793	239
1.49	ZnA-SiO_2/IR	2958	444
	ZnO/IR	2489	307
	ZnO/SiO_2/IR	2187	182

In general, the mechanical properties of $W\_Zn_YA_X$-SiO_2/IR assumed different behaviours at the lowest and intermediate strains. In fact, at low strain, the increased values of G' were accompanied by a reduction of G'' and tanδ as shown for samples with W = 1.49 and 1.08 (Figure 3.6., Figure 3.7).

Whereas when Zn content was too low (0.68 phr), both G'' and tanδ assumed higher values, probably because of the lower vulcanization efficiency due to the very low Zn content and of the not well distributed SiO_2 NPs due to the low APTES coverage. At intermediate strain, the enhancements of the G'' values were detected at all Zn content and especially the lowest Zn content (and consequently APTES coverage degree (Figure 3.6). The same trend was reflected

by tanδ profiles, whose values are always higher than the reference samples and increased by reducing the Zn content.
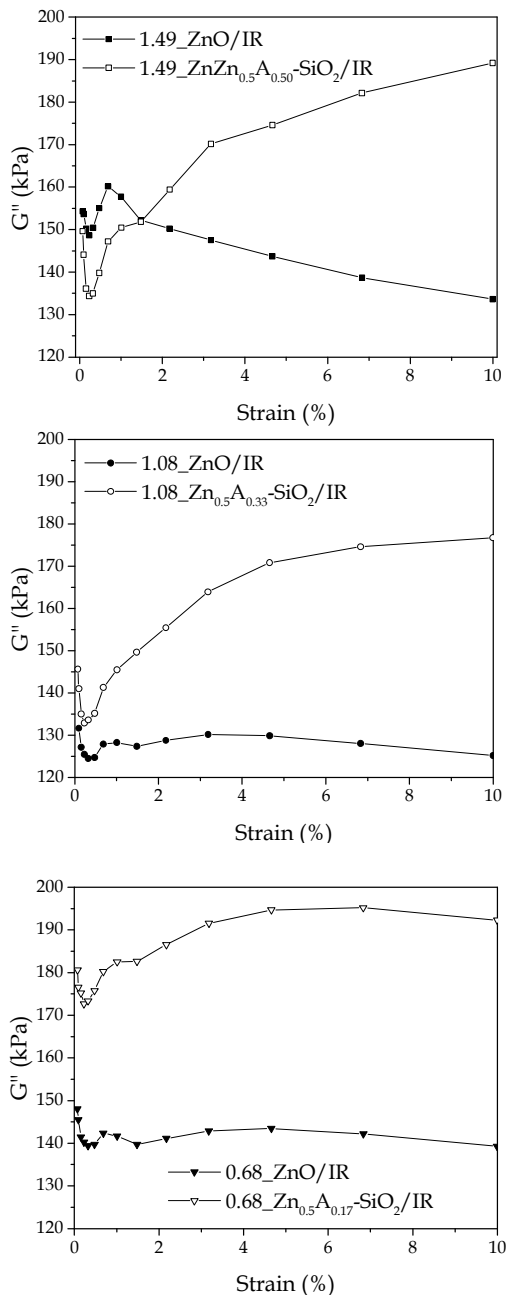
Figure 3.6. G'' profiles for W_Zn$_Y$A$_X$-SiO$_2$/IR, compared to the reference W_ZnO/IR.
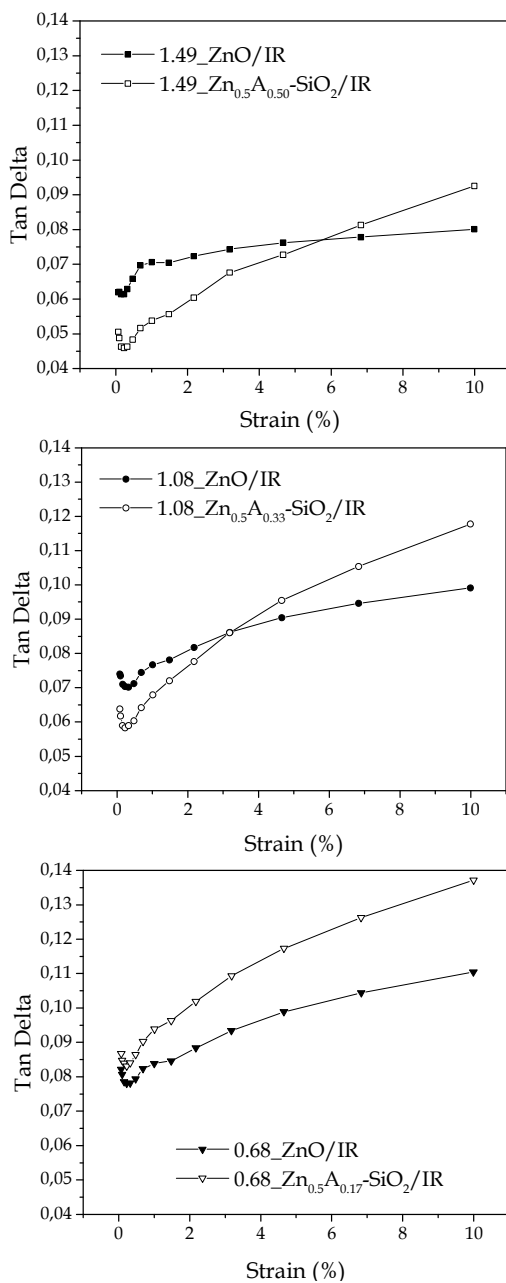
Figure 3.7. Tanδ profiles for W_Zn$_Y$A$_X$-SiO$_2$/IR, compared to the reference W_ZnO/IR.

3.4.3 Cross-linking density

Swelling experiments with toluene were performed in order to get information about the average cross-linking densities of the rubber NCs. In Figure 3.8 the comparison between the NCs prepared with Zn_YA_X-SiO_2, ZnO/SiO_2_4% and the reference activator m-ZnO is reported.
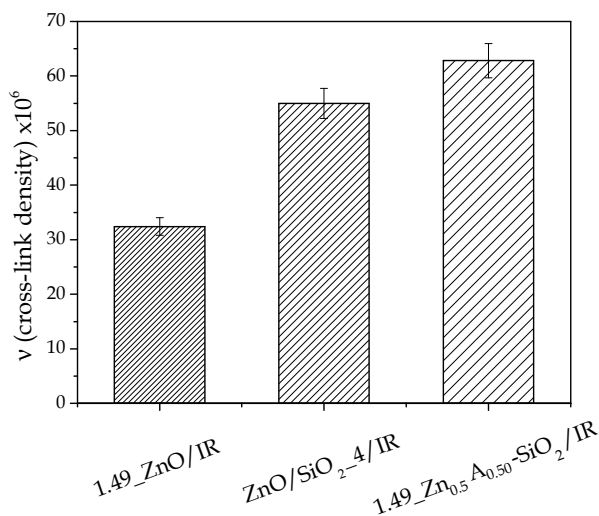
Figure 3.8.   Cross-linking densities measured through swelling experiments for the NCs prepared with the three activators.

The use of ZnO/SiO_2_4% and Zn_YA_X-SiO_2 NPS evidenced a direct impact on the enhancement of the cross-linking densities, that are almost twice the original value obtained in the presence of m-ZnO. This result confirmed the previous observations regarding the higher vulcanization efficiencies achieved through the introduction of new activators. An important factor is that these higher values are achieved by using about half of the ZnO content used in the industrial production, that is enough to reached higher cross-linking degrees inside the rubber matrix.

The cross-linking densities calculated for W_ Zn_YA_X-SiO_2/IR with W = 1.08 and 0.68 phr, were lower than the same NC with W = 1.49 phr, confirming the lower vulcanization efficiency achieved in these two NCs (data not reported).

3.4.4 Morphological TEM analysis

The morphology of the NCs Zn_YA_X-SiO_2/IR, ZnO/SiO_2_4%_IR and m-ZnO/IR (Zn content = 1.49 phr) and the dispersion of the SiO_2 filler inside the rubber matrix were studied through the analysis of TEM images, recorded on NCs thin slices obtained by a cryo-ultramicrotome.
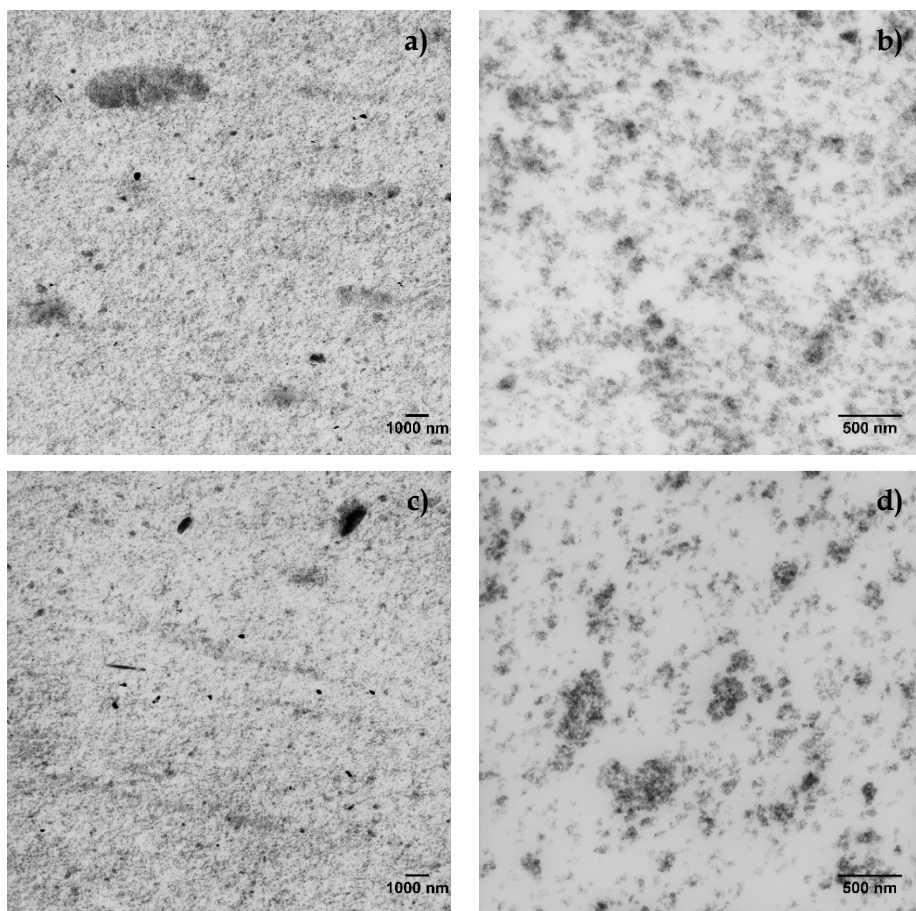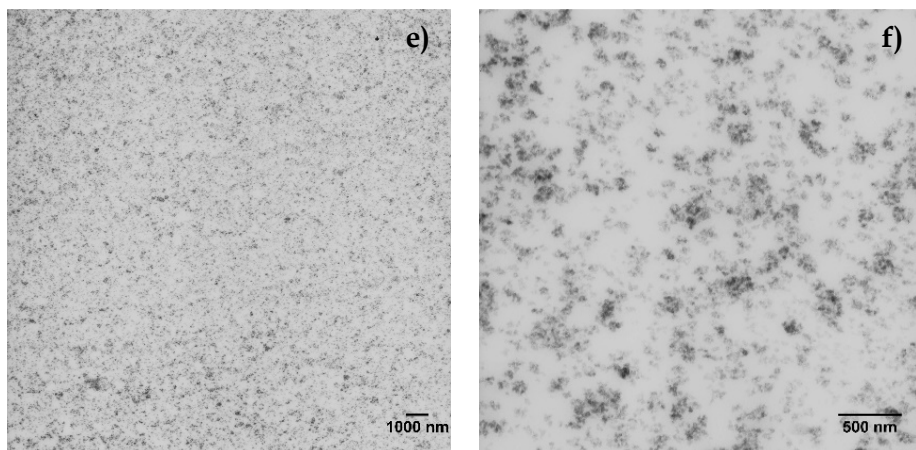
Figure 3.9. TEM images of a, b) 1.49_ZnO/IR, c, d) ZnO/SiO$_2$_4%_IR and e, f) 1.49_Zn$_{0.5}$A$_{0.50}$-SiO$_2$/IR NCs at two different magnification (left x3K, right x20K).

The comparison between the TEM images of the NCs at the highest zinc content, 1.49_Zn$_{0.5}$A$_{0.50}$-SiO$_2$/IR, ZnO/SiO$_2$_4%_IR and 1.49_ZnO/IR, is reported in Figure 3.9. From the images at low magnification a good dispersion of SiO$_2$ inside the rubber matrix was evidenced in all the three cases, with the formation or rare aggregates of SiO$_2$. When Zn$_{0.5}$A$_{0.50}$-SiO$_2$ is used, the dispersion looks better than the reference samples, demonstrating that the surface modification of SiO$_2$ did not decrease the ability of this filler to disperse inside the rubber matrix. At higher magnification, the filler network appears continuous and homogeneous, especially regarding the 1.49_Zn$_{0.5}$A$_{0.50}$-SiO$_2$/IR NC, confirming the good homogeneity of SiO$_2$ dispersion.

A further comparison between W_Zn$_Y$A$_X$-SiO$_2$/IR NCs at different Zn content is reported in Figure 3.10 and Figure 3.11, compared with the reference NCs prepared with m-ZnO at the same zinc content. Compared to the NCs prepared at high Zn content, the dispersion of SiO$_2$ in W_Zn$_Y$A$_X$-SiO$_2$/IR with W = 1.08 and 0.68 phr, progressively get worse, probably due to the lower coverage degree of APTES, associated to the lower Zn content. In fact, in these samples, the dispersion of SiO$_2$ filler inside the rubber matrix is guaranteed by the coverage of SiO$_2$ surface by APTES, without any further addition of

compatibilizing agents (TESPD), as usually done with bare SiO_2 filler. This observation agrees with the previous suggestions from the dynamic-mechanical analysis and the trend of G′ and G′′ values. In fact, at low magnification, several micrometric and elongated agglomerates of SiO_2 become evident when W = 0.68 phr, and at high magnification the filler network looks less continuous then NCs with W = 1.49 and 1.08 phr. The same trend was evident also for the reference samples (W_ZnO/IR with W = 1.08 and 0.68 phr), even if the morphology looks more homogeneous and continuous, compared to the respective Zn_YA_X-SiO_2/IR NCs. This result can be connected to the higher amount of TESPD used in the case of bare SiO_2 (W_ZnO/IR) compared to W_Zn_YA_X-SiO_2/IR, when W is equal to 1.08 or 0.68 phr.
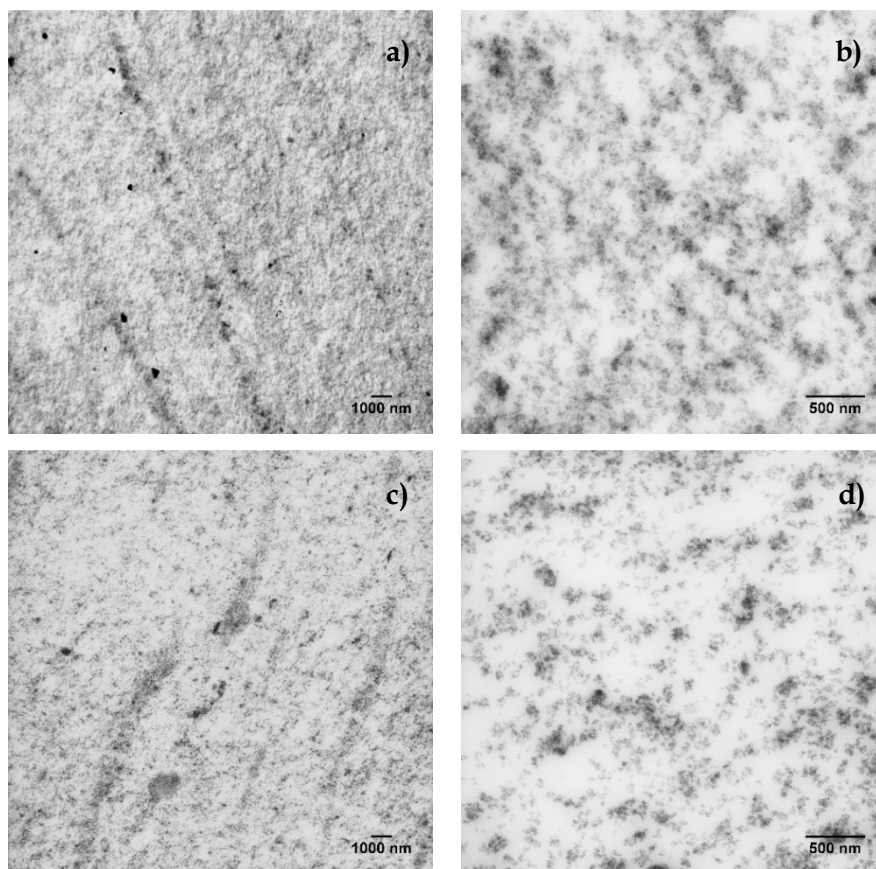
Figure 3.10. TEM images of a, b) 1.08_ZnO/IR, c, d) 1.08_$Zn_{0.5}A_{0.33}$-SiO_2 NCs at two different magnification (left x3K, right x20K).
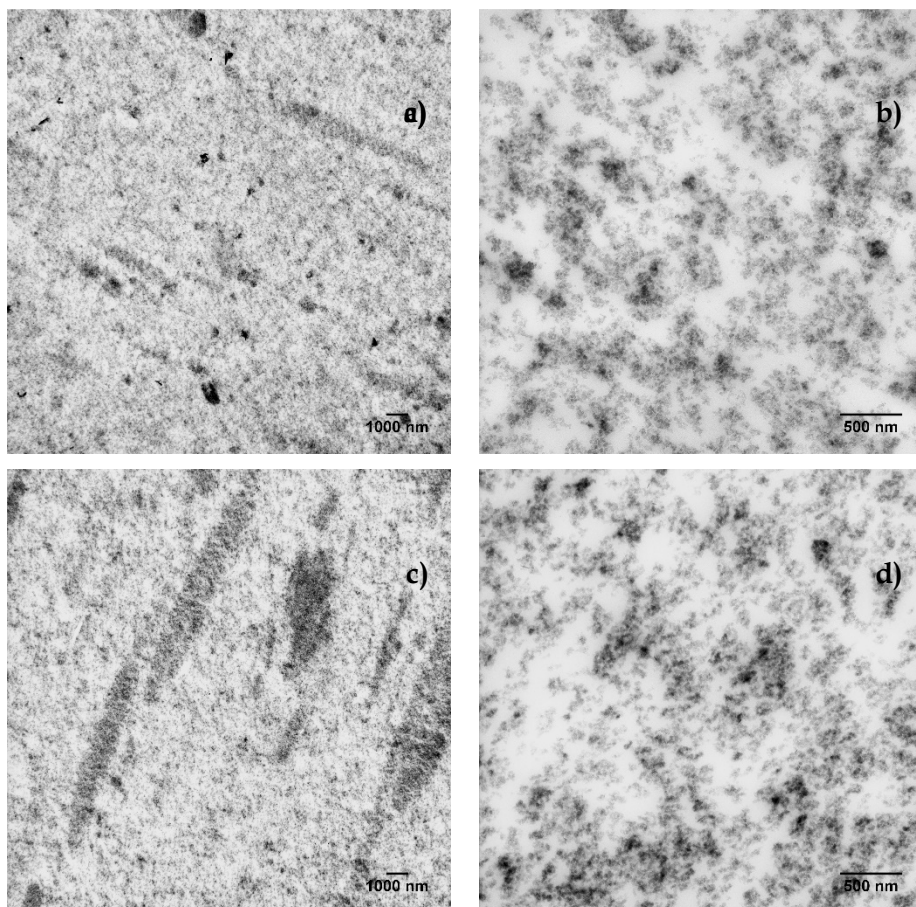
Figure 3.11. TEM images of a, b) 0.68_ZnO/IR, c, d) 0.68_Zn$_{0.5}$A$_{0.17}$-SiO$_2$ NCs at two different magnification (left x3K, right x20K).

3.5 Summary of the vulcanization tests using different activators

In this Chapter the vulcanization tests carried out using different zinc-based activators showed that the activators' morphology plays a main role in the determination of the vulcanization efficiency and the mechanical properties of rubber. Using ZnO/SiO$_2$ and ZnA-SiO$_2$ materials, higher moduli and lowered vulcanization times were registered during the vulcanization reaction, in comparison to m-ZnO; in particular, the very low scorch time measured in the presence of ZnA-SiO$_2$ was consistent with the structural properties of Zn(II) centres, already available at the beginning of the reaction and highly reactive,

without the use of the co-activator. The same result was confirmed by employing Zn_YA_X-SiO_2 NPs with different Zn content in the rubber NCs, that proved the higher reactivity of this material compared to the others.

The improved efficiency of the vulcanization reaction with the two double function fillers had a direct impact on the mechanical properties of rubber NCs, with an increased reinforcement, enhanced cross-linking densities and comparable Payne Effect. This result is particularly important in the case of ZnA-SiO_2 NPs, whose NCs were realized in the absence of any additional compatibilizing agents, achieving at the same time a good dispersion of SiO_2 filler inside the rubber, almost comparable or even improved, compared to the ZnO/IR NCs.

3.6 Bibliography

1. Coleman, M. M., Shelton, J. R. & Koenig, J. L. Sulfur Vulcanization of Hydrocarbon Diene Elastomers. *Ind. Eng. Chem. Prod. Res. Dev.* **13,** 154–166 (1974).

2. P. Ghosh, S. Katare, P. P. Sulfur Vulcanization of Natural Rubber for Benzothiazole Accelerated Formulations. *Rubber Chem. Technol.* **76,** 592–693 (2003).

3. Arroyo, M., López-Manchado, M. A. & Herrero, B. Organo-montmorillonite as substitute of carbon black in natural rubber compounds. *Polymer (Guildf).* **44,** 2447–2453 (2003).

4. Nordsiek, K. H. The integral rubber concept - an approach to an ideal tire tread rubber. *Kautsch. Gummi Kunstst* **38,** 178–185 (198AD).

5. Ward, I. M. & Sweeney, J. *Mechanical properties of Solid Polymers.* (John Wiley & Sons, 2012).

6. Sabu, T. & R., S. *Rubber Nanocomposites: Preparation, properties and applications.* (John Wiley & Sons, 2010).

7. Payne, A. R. & Kraus, G. *Reinforcement of elastomers.* (1965).

8. Fröhlich, J., Niedermeier, W. & Luginsland, H. D. The effect of filler-filler and filler-elastomer interaction on rubber reinforcement. *Compos. Part A Appl. Sci. Manuf.* **36,** 449–460 (2005).

4

Model study of the
vulcanization mechanism

In this chapter the kinetic and the mechanism of vulcanization reaction in the presence of the activator ZnA-SiO$_2$ was studied and compared to those with ZnO/SiO$_2$ and the conventional m-ZnO. In Chapter 3 their application as activators to rubber NCs has already shown that the morphology of the activator plays a main role in the determination of the vulcanization efficiency and the mechanical properties of rubber NCs. Different shaped vulcanization curves, improved cross-linking densities and enhanced mechanical properties were registered moving from m-ZnO to dispersed ZnO NPs and Zn(II) centres onto the surface of silica, suggesting that these activators behave differently during the reaction. Thus, the aim of this study was the investigation of the activators' effect on both the kinetic and the mechanism of the reaction, two distinct parameters that both affect the vulcanization efficiency and the final properties of rubber NCs.

Kinetic and mechanism of vulcanization in the presence of these activators were studied using the so-called "Model Vulcanization Compound" approach, simulating the experimental conditions of rubber NCs in a less complicated system.

In the first part of the chapter, a brief introduction of the used model compound approach and its advantages are illustrated, while in the second part, the results of the application of this method in the study of the reaction kinetic and mechanism are presented.

4.1 Model Compound Vulcanization (MCV)

The Model Compound Vulcanization (MCV) is an extensively used methodology in the elastomer field, to study the reaction products and intermediates of the vulcanization reaction[1,2]. The development of this model approach is connected to the highly complicated experimental conditions required for the study of the vulcanization reaction in the rubber NCs, including the high number of components inside the rubber matrix, the large diversity of the possible cross-linking products, generally formed at low concentrations, the variety of reactions that take place simultaneously due to the high number of reagents involved in the reaction.

This approach permits a simplified study of the reaction mechanism, since the polymer (corresponding to the real system) is substituted by a model compound, generally chosen in order to simulate as much as possible the chemical reactivity of the polymer. Taking advantage of the knowledge developed through the model approach, a description of the real system (the polymer) with complex reactivity can be achieved.

The main advantage of the MCV approach is that the employment of a model compound allows the formation of a more restricted range of cross-linking products, that can be investigated by the more traditional analytical and spectroscopic techniques. Besides, the low complexity of the system favours the identification of possible intermediate complexes that are involved in the reaction. For this reason, generated cross-linking products can be identified and information about the cross-linking mechanism can be collected.

The choice of the model compound represents one of the main steps of the MCV approach, as its reactivity must be as similar as possible to the reactivity of the polymer under investigation. Different parameters are generally considered, such as the number, position and configuration of the double bonds; the potential presence of functional groups; physical properties as fusion and boiling point, solubility of the other vulcanization agents, molecular weight, etc.

Several molecules have been proposed as potential model compounds for MCV[3,4]. Among them, squalene is mainly used in the literature, due to the high boiling point and the high similarity to the major part of the polymers[5]. A simpler compound, as pentene and 2,3-dimethyl-2-butene (TME)[6], with a single double bond and four equivalent methyl groups , is generally chosen when the main goal is the study of the cross-linking formation, so that the number of cross-linking products and intermediates is reduced.

4.2 MCV tests with ZnA-SiO₂, ZnO/SiO₂ and m-ZnO as activators

In this study TME was used as model compound for the polymer IR used for producing rubber NCs (see chapter 3) because of the same tendency to react through the allylic positions with sulphur to form the cross-linking products. Typical cross-linking products are composed of TME molecules , bond to each other thanks to sulphur bridges of different lengths. The presence of four identical allylic positions in TME allows to reduce the range of cross-linking products. The simplest structure of TME cross-linking products is shown Figure 4.1, where only two TME molecules are connected.
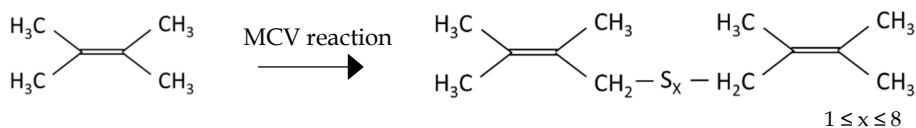
Figure 4.1. Cross-linking products formed during the MCV reaction with TME.

MCV tests with TME were performed to study the distribution of cross-linking products and to identify the reaction intermediates in the presence of ZnA-SiO₂, ZnO/SiO₂ and m-ZnO as activators of vulcanization.

Hereafter the sample for the tests will be called ZnA-SiO₂/TME, ZnO/SiO₂/TME and m-ZnO/TME, respectively.

Materials: TME vulcanization was performed using the same vulcanization agents employed for IR NCs. CBS used as accelerator, Vulkacit CZ/X, was

purchased from Lanxess; S_8 Creso (vulcanizing agent) from Redball Superfine; SA (95%) from Sigma Aldrich; ZnO (wurtzite, specific surface area 5 m^2 g^{-1}) from Zincol Ossidi, TME (2,3-dimethyl-2-butene, 98%) from Sigma Aldrich.

For Mass Spectroscopy analysis: water for HPLC was obtained from Sigma-Aldrich; Acetonitrile for LC-MS by Chromasolv.

4.2.1 TME vulcanization procedure

MCV experiments of TME were performed using the three different activators with the same contents of Zn (1.49 phr) and SiO_2 (43 phr). The amounts of reactants are reported in Table 4.1.

ZnA-SiO_2/TME samples were prepared by mixing CBS (1.6 phr), S_8 (3 phr) and the activator $Zn_Y A_X$-SiO_2 (48.1 phr corresponding to 1.49 phr of Zn) with TME. $Zn_{0.5}A_{0.50}$-SiO_2 was chosen as it showed the highest performances as activator in IR NCs (see paragraph 3.4.1). The reaction was performed in the absence of SA, since the single Zn(II) centres are supposed to be available to directly react with the curatives , as already observed for IR NCs.

ZnO/SiO_2/TME samples were prepared using ZnO/SiO_2_4% (44.8 phr) while the reference sample m-ZnO/TME using m-ZnO (1.85 phr, corresponding to 1.49 phr of Zn) and SiO_2 (43 phr). Both ZnO/SiO_2/TME and m-ZnO/TME required the addition of SA (2 phr), necessary to complex Zn(II) centres when ZnO is used.

Table 4.1. Reagents used for MCV experiments performed with the three activators.

Sample	$Zn_{0.5}A_{0.50}$-SiO_2			ZnO/SiO_2_4%			ZnO	SiO_2	SA	CBS	S_8
	phr	Zn	SiO_2	phr	Zn	SiO_2					
ZnA-SiO_2/TME	48.1	1.49	43		-		-	-	-	1.6	3
m-ZnO/TME		-			-		1.85	43	2	1.6	3
ZnO/SiO_2/TME		-		44.8	1.49	43	-	-	2	1.6	3

4.2.2 Mass Spectroscopy (MS) and ^{1}H-NMR analysis of MCV products

The study of the formation process of the vulcanization products was evaluated at different reaction time as follows.

The reactants were mixed in a 5 mL conical vial at room temperature and the vulcanization reaction was performed in an oil bath at 120°C (optimum vulcanization temperature in TME), in a closed environment. The reaction was carried out at different reaction times (5, 10, 20 min), assuming that 20 minutes is the optimum curing time in TME. After the reaction, the vial was cooled down in a liquid nitrogen bath and the reaction mixture filtered with a porous filter. Aliquots of the filtered liquids were stored at -15°C to preserve their composition before the analysis.

Mass Spectroscopy (MS) and ^{1}H-NMR were used to analyse the liquid samples at different reaction times, to detect the formation of the cross-linking products.

MS experiments operating in positive mode were carried out on cured samples diluted in acetonitrile (1:10 vol:vol); H_2O was added (4 vol%) to favour the protonation of species and an internal standard at fixed concentration (diethylamine, m/z = 74, c= 48 μM) was used to normalize peak intensities of the cross-linking products according to the standard signal.

^{1}H NMR spectra were recorded at 500 MHz on samples dissolved in $CDCl_3$ (1:10 vol:vol). Chemical shifts were determined relative to the residual solvent peak (CDCl3, δ 7.26 ppm).

4.2.3 FTIR and XPS analysis of the interaction of the activators with the curatives in MCV

The study of interaction of the three activators $ZnA-SiO_2$, ZnO/SiO_2 and m-ZnO with the vulcanization agents (SA, CBS, S_8) and the identification of possible intermediate species was carried out by using TME as model compound. The study was performed by adding to TME containing silica, the reactants in the following order: activator and, eventually; co-activator SA; CBS and, finally, S_8

(Table 4.2.). In the case of ZnA-SiO$_2$ NPs, no SA was used and only the interactions with CBS and S$_8$ were studied. In Table 4.2, the different treatments and the labels of the corresponding samples are reported.

Table 4.2. Scheme of the interactions studied between the zinc-based activators and the vulcanization agents SA, CBS and S$_8$.

Activators (in TME)	+ stearic acid	+ stearic acid + CBS	+ stearic acid + CBS + S$_8$
m-ZnO	m-ZnO_SA	m-ZnO_CBS	m-ZnO_S$_8$
ZnO/SiO$_2$	ZnO/SiO$_2$_SA	ZnO/SiO$_2$_CBS	ZnO/SiO$_2$_S$_8$
ZnA-SiO$_2$	-	ZnA-SiO$_2$_CBS	ZnA-SiO$_2$_S$_8$

The relative amounts of reagents were the same reported in Table 4.1; samples were put in a closed conical vial, heated at 120°C for 20 min, then the reaction was quenched with liquid nitrogen and the resulting solution analysed.

Each sample indicated in Table 4.2. was analysed by FTIR-ATR spectroscopy. In particular, useful information was obtained about the interaction of m-ZnO and ZnO NPs with SA (see paragraph 4.3.2) at the beginning of the vulcanization reaction, which of course is absent in ZnA-SiO$_2$/TME.

On the other hand, since in ZnA-SiO$_2$/TME the single-site active Zn(II) centres are anchored on the silica surface, further analyses were carried out by solid-state NMR and XPS to study the changes on the silica surface during the different steps of the MCV reaction. The elemental composition of possible intermediate species and the eventual release from the surface of the zinc centres during vulcanization were investigated. The sampling procedure after each step of reaction with the curatives (Table 4.2) is the following: the dispersion was filtered and the solid part was recovered and washed several times with fresh ethanol to eliminate any traces of unreacted curatives, then it was analysed by solid-state NMR and XPS.

4.3 Results and discussion

The results are presented in two different sections: first the experimental results regarding formation process of cross-linking products in the presence of the different activators is explained, whereas the implications on the reaction mechanism are illustrated in the second part.

4.3.1 Formation of TME cross-linking products

The influence of ZnA-SiO_2 on the process of cross-linking reaction was investigated in the vulcanization of TME, in comparison with ZnO/SiO_2 and m-ZnO. The reaction products were analysed after 5, 10 and 20 minutes by MS and ^{1}H-NMR.

In MS analysis, only the formation of the simplest cross-linking products, composed of two molecules of TME connected through a sulphur bridges, was considered (Figure 4.1). More structured products with more than two TME molecules, were not included in the analysis, since preliminary MS spectra, confirmed that the concentration of higher molecular weight species could be neglected in these experimental conditions.

The list of mass/charge ratio m/z values of the cross-linking products TME-S_X-TME, where $1 \leq X \leq 8$ is the number of sulphur atoms, is reported in Table 4.3.. For each species, two additional peaks are present, corresponding to the partial oxidation of the TME units during the cross-linking reactions and the formation of one or two 2,3-dimethylbutadiene units instead of the TME molecules (with the loss of 2 or 4 Da, respectively, Figure 4.2).

The identification of TME-S_X-TME species for the MS analysis was confirmed by MS-MS experiments of the cross-linking product detected at a specific m/z value. For each species, the detection of the TME ion upon collision-induced dissociation (CID) confirmed the nature of the analysed products (data not reported).

Hereafter, the formula of TME-S_X-TME stands for the sum of the three species with the same length of polysulphide chains S_X.

Table 4.3. Range of m/z values that correspond to TME-S_X-TME products.

X	m/z
1	194-198
2	226-230
3	258-262
4	290-294
5	322-326
6	354-358
7	386-390
8	418-422

Figure 4.2. Cross-linking products composed of one or two 2,3-dimethylbutadiene units generated due to the partial oxidation of TME.

Typical MS spectra obtained operating in positive mode, are reported in Figure 4.3. In the spectra, in addition to the peaks related to the cross-linking products, other compounds present in the system are detected: i) the accelerator CBS (m/z = 265); ii) cyclohexylamine, CHA (m/z = 100) formed after the reaction of CBS with Zn and S_8; iii) a recombination product of mercaptobenzothiazole (MBT) and CHA (m/z = 233) and the MBT dimer (m/z = 332).
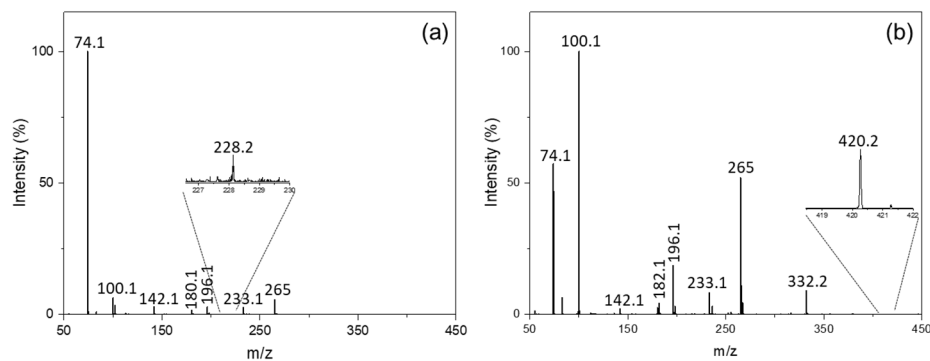
Figure 4.3. MS spectra registered for ZnO/SiO$_2$/TME and ZnO/TME after 5 minutes of reaction.

The relative amount of TME-S$_X$-TME species at different reaction times (5, 10, 20 min) for m-ZnO/TME, ZnO/SiO$_2$/TME and Zn$_{0.5}$A$_{0.50}$-SiO$_2$/TME are reported in Figure 4.4. The intensities are relative intensities (I$_R$), normalized to the intensity of the internal standard diethylamine (experimental procedure, paragraph 4.2.2).

Only the intensities of the same species (e.g. S$_1$) can be compared between the different measurements. This is because the intensities of each species detected in the MS spectra, depend on the volatilization and protonation yields of the single species, that assume specific values for each compound. Thus, each specific has its own intensities during the measurements that can be compared during the reaction time and for the different samples. Nevertheless, no comparison between the intensities of different species can be performed, due to the different properties of the species in the analysis.

In the three samples ZnA-SiO$_2$, ZnO/SiO$_2$ and m-ZnO, at the lowest reaction time (5 min) a distribution of mono-, di- and poly-sulphide cross-linking products is detectable, with a considerable contribution of the long poly-sulphide chains (S$_X$, with X ≥ 4). By increasing the vulcanization time, the length of the poly-sulphide bridges progressively decreases, and the mono-sulphide species becomes almost the only product.
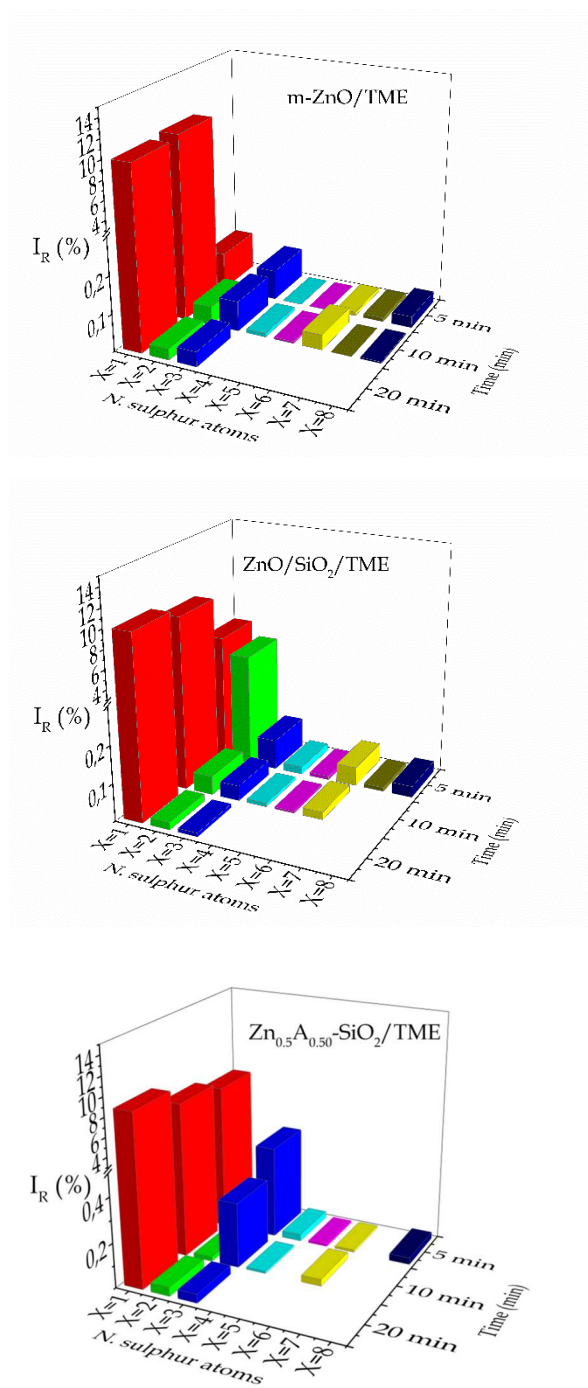
Figure 4.4. Relative intensities of cross-linking products of TME, obtained in the MCV tests in the presence of a) m-ZnO, b) ZnO/SiO$_2$_4%, c) Zn$_{0.5}$A$_{0.50}$-SiO$_2$ NPs.

This observation confirmed that the vulcanization mechanism proceeds through a progressive degradation of long sulphur bridges, formed in the first phase of the cross-linking formation, towards shorter sulphur bridges, through a breaking-down mechanism of the longer poly-sulphide chains. This mechanism is evident with all the three tested activators and agrees with the reaction sequence for the cross-linking formation proposed in the literature[7] (Figure 4.5). In this mechanism, Zn(II) centres are supposed to promote i) the S-S breakage through their coordination to the cross-linking precursor, that can be repeated more than one time, progressively shortening the polysulphide chains; ii) the break-down process of the already formed polysulphide cross-links through the formation of an intermediate adduct between the zinc sulphurating complex and sulphur chains.
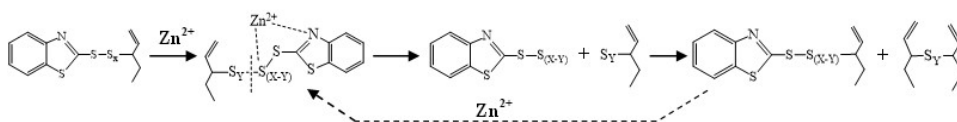
Figure 4.5. Schematic representation of the mechanism of cross-linking formation.

The comparison of the three systems highlighted that when ZnO NPs and Zn(II) centres are dispersed onto the surface of SiO_2, the reactivity is faster than with m-ZnO. In fact, the progressive formation of mono-sulphide chains starting from the poly-sulphide chains is faster and already after 10 minutes the poly-sulphide products are not detected anymore. Whereas, the whole range of TME-S_X-TME products is still present after 10 minutes, in the case of m-ZnO/TME sample. The difference is even more evident with Zn(II) centres, where the intensities of the long-sulphide products are always lower at all reaction times, compared to the other two materials.

The MCV products were further studied with ^{1}H-NMR, to confirm the identification of the vulcanized compounds by MS. As an example, in Figure 4.6, the ^{1}H-NMR of spectra registered for $ZnASiO_2$/TME ZnO/SiO_2/TME and m-

ZnO/TME, after 10 minutes of reaction at 120°C, are reported. A zoom of the region between 3 and 5 ppm highlights the signals referred to the cross-linking products. At lower ppm (2.2-1.8 ppm), the signals due to the CH_3 groups of TME are dominant.
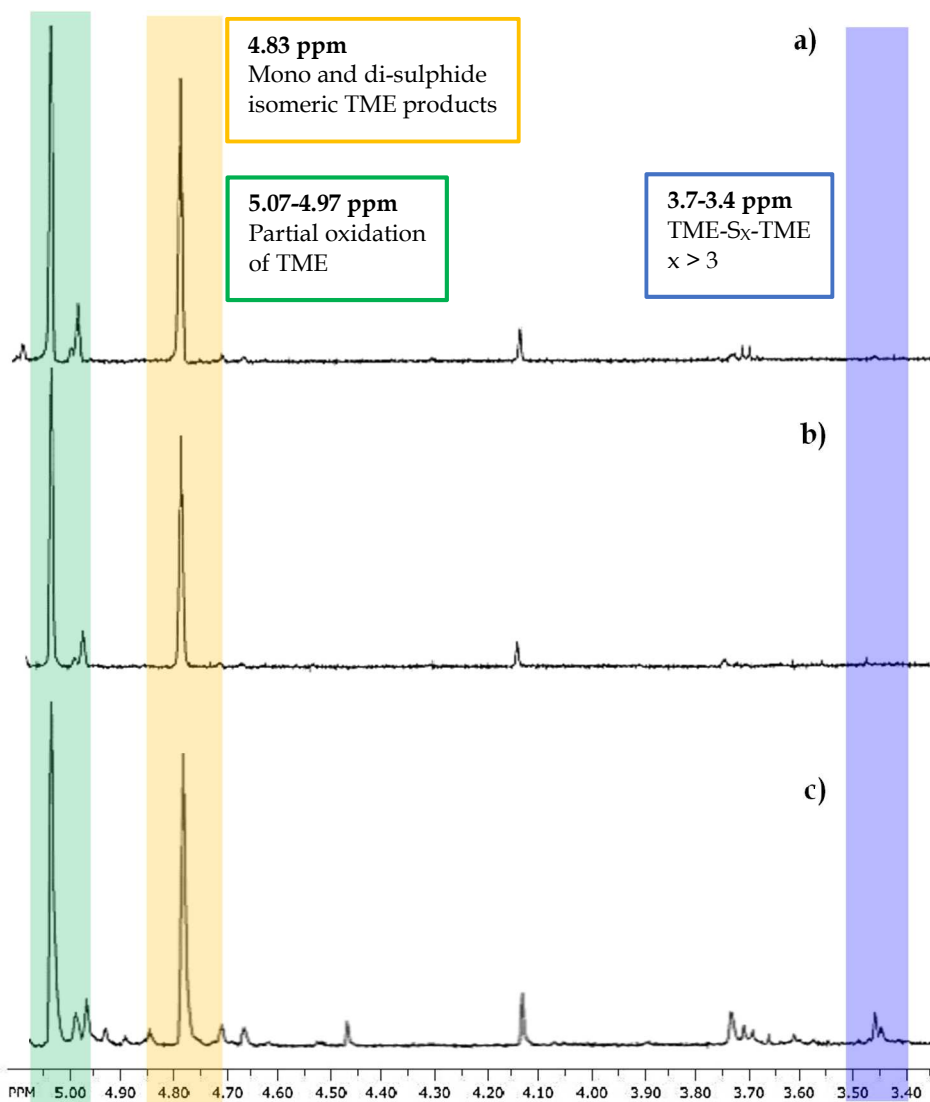
Figure 4.6. ^{1}H-NMR spectra of a) ZnA-SiO$_2$/TME, b) ZnO/SiO$_2$/TME and c) m-ZnO/TME after 10 minutes of reaction.

The ^{1}H-NMR spectra of all the activators present the peaks at 4.83 ppm, related to the formation of isomeric cross-linked TME mono- or disulphide products, formed via allylic substitution during the curing process. Moreover, the signals at 5.07 and 4.97 ppm are associated to a partial oxidation of TME with formation of 2,3-dimetylbutadiene, confirming the MS result observation of TME oxidation in the present experimental conditions.

Poly-sulphide species show typical signals in the range 3.7-3.4 ppm, corresponding to TME-S_X-TME products with x > 3. However, the signals are detected only in the m-ZnO/TME sample after 10 minutes (Figure 4.6a), while it is almost undetectable when ZnO NPs and Zn(II) centres are used as activators (Figure 4.6b,c).

The ^{1}H-NMR investigation confirmed the previous results obtained by MS analysis. First, the results assess that the employment of ZnO/SiO$_2$ and ZnA-SiO$_2$ NPs accelerate the formation of mono- and di-sulphide chains by faster degradation of the poly-sulphide products. Thus, the use of these novel activators compared to the m-ZnO has strong impact on the kinetic of the vulcanization reactions. Moreover, the role of Zn in the degradation mechanism of poly-sulphide chains was highlighted, showing that the use of different activators could pave the way to the formation of more reactive zinc-based intermediate species, more available to further react and coordinate the polysulphide chains, fastening the degradation process.

All these experimental results agree with the results obtained for the vulcanization process of IR NCs, including the improved efficiencies and higher cross-linking densities of ZnA-SiO$_2$/IR and ZnO/SiO$_2$_IR.

4.3.2 Mechanism of interaction with the vulcanization reagents

The study of the interaction of the zinc-based activators with the vulcanization agents follows the scheme reported in Table 4.2. The reagents were left under stirring for 20 min at 120°C (vulcanization conditions in MCV), then were cooled down before FTIR-ATR analysis. The discussion of the results will start from the

comparison between ZnO and ZnO/SiO$_2$ NPs, based on FTIR analysis; ZnA-SiO$_2$ will be considered in the second part, as further analyses were necessary to study its reaction mechanism.

ZnO vs ZnO/SiO$_2$: FTIR-ATR analysis. As a first step, the interaction between m-ZnO and ZnO/SiO$_2$ with stearic acid was studied. In Figure 4.7., the comparison of FTIR of m-ZnO_SA and ZnO/SiO$_2$_SA is reported. In both the spectra, the typical antisymmetric and symmetric stretching vibrations attributed to zinc distearate, which contains four bridging carboxylate groups coordinate to Zn(II) are present (1538 cm^{-1}, 1398 cm^{-1}, Figure 4.7. blue bands). The peaks at 1464 and 1454 cm^{-1} could be assigned to the CH$_2$ scissoring vibration and CH$_2$ bending, respectively. With ZnO/SiO$_2$, additional vibrations in the region of the antisymmetric and symmetric carboxylate stretching are visible, at 1596, 1614, 1625 cm^{-1}.
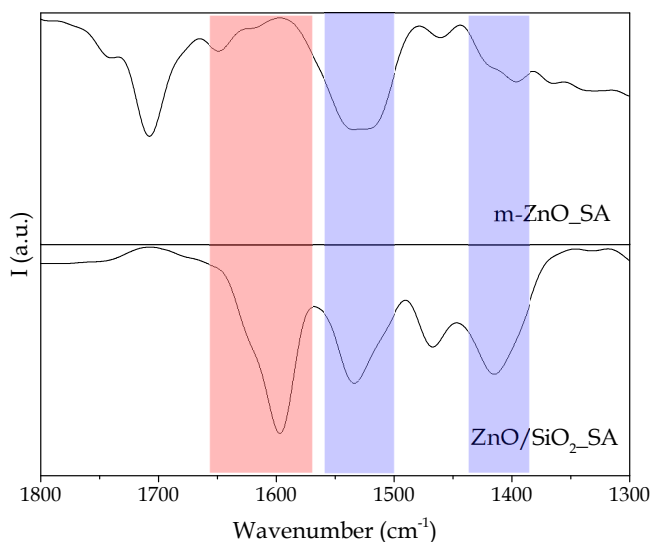
Figure 4.7. FTIR-ATR spectra of m-ZnO_SA and ZnO/SiO$_2$_SA; in blue the peaks related to zinc stearate complex; in red, the peaks connected to the formation of a new zinc complex, detected only with ZnO/SiO$_2$.

As suggested in the literature, these peaks can be attributed to the formation of an additional zinc-stearic acid complex, with a potential bridging coordination of carboxylate units between two metal centres. In fact, the difference between the wavenumbers of the antisymmetric and symmetric modes of carboxylate groups (Δv) can be correlated to the kind of coordination of these groups to the metal centres, that in this case is typical of a bridging coordination. Based on a recent work by Ikeda *et al.*, this complex was further suggested to have 1:1 Zn : stearate molar ratio, with two carboxylate groups bridging two Zn(II) centres and Y groups (OH⁻ or water) completing the Zn coordination (Figure 4.8).As a result, ZnO/SiO_2 has shown to favour a different reaction mechanism compared to m-ZnO, that working simultaneously with the conventional path, could justify the improved reactivity shown in the reaction. The main advantage of this structure could be in the more open structure, in which zinc centres are more available to the reaction with the other vulcanization agents.
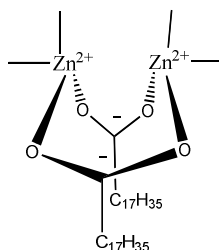
Figure 4.8. Proposed structure of the bridging zinc complex formed in the presence of ZnO/SiO_2 and stearic acid.

The further addition of CBS and S_8 to m-ZnO and ZnO/SiO_2 did not cause any significant changes in the FTIR spectra (Figure 4.9.).
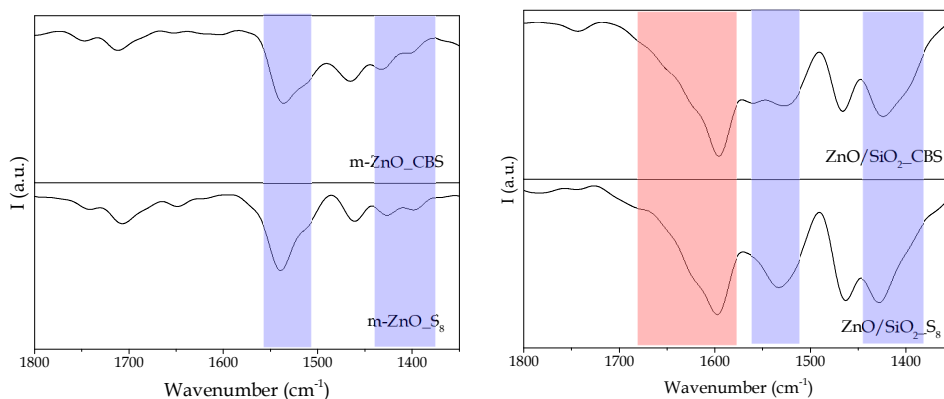
Figure 4.9. FTIR-ATR of MCV samples of m-ZnO (left) and ZnO/SiO₂ (right), after interaction with SA + CBS (up) and SA + CBS + S₈ (down).

None of the expected new signals from the interaction of CBS molecules with Zn, such as the breakage of the S-N bond to generate MBT and CHA, was detected. Furthermore, no disappearance of the peaks of zinc stearate and zinc di-nuclear complex was evidenced, suggesting that part of the stearate ligands may be preserved during the subsequent reaction in the presence of CBS and S_8 and may interact with the other agents through ligands exchange reactions. The open structure of the Zn(II) di-nuclear complex could favour the exchange reactions on the zinc centres, compared to the closed structure of Zn di-stearate.

Finally, the evolution of ZnO/SiO₂ NPs during the reaction mechanism was evaluated, by comparing the FTIR spectra of ZnO/SiO₂ NPs before (see paragraph 2.1.3) and after the interaction with SA, after a filtration procedure from the MCV reaction in TME. In bare ZnO/SiO₂, the peak at 954 cm⁻¹, connected to Si-OH stretching mode, was shifted towards higher wavenumbers in the because of the partial substitution of Si-OH groups with Si-O-Zn bonds (paragraph 2.1.3); whereas, after the addition of SA, this peak was reformed, suggesting that the breakage of Si-O-Zn bonds occurs, in favour of the Si-OH groups (Figure 4.10). This observation confirmed that the interaction between ZnO NPs and SA led to the release of ZnO from SiO₂ NPs, to favour the formation of the active zinc complexes. The reactivity of both m-ZnO and

ZnO/SiO$_2$ relies on the first reaction with SA, fundamental for the catalytic process to occur.
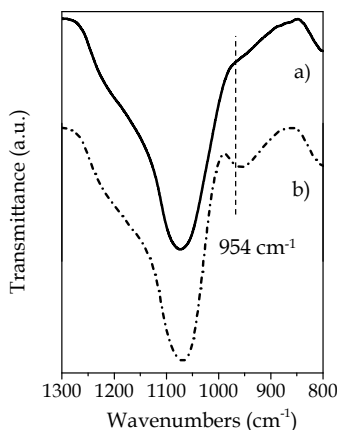
Figure 4.10. FTIR of ZnO/SiO$_2$ before (a) and after (b) reaction with stearic acid (120°C, 20 min).

ZnA-SiO$_2$: FTIR-ATR analysis. The study of the reaction mechanism in the presence of ZnA-SiO$_2$ started from the interaction of the activator with CBS; no SA was used, due to the high availability of the Zn(II) centres in the reaction, as already observed (see paragraph 3.2.1).

FTIR-ATR analysis of ZnA-SiO$_2$_CBS and ZnA-SiO$_2$_S$_8$ samples did not show any additional peaks due to the formation of new zinc complex intermediates. In fact, in the spectra (not reported), only the typical peaks of CBS were detected and no information about Zn(II) centres interaction with the other vulcanization agents could be collected from this analysis. With this activator, the absence of intermediate species with CBS and S$_8$ can be related both to a low sensitivity of the used technique and to the probable low quantities of the formed intermediate species. In fact, these species are likely to be very reactive species that are formed in the neighbourhood of Zn(II) centres, with a very high reactivity but low stability. The structural properties of this material suggest that the intermediate species can be formed directly on the surface of SiO$_2$ particles,

where the Zn(II) centres are located, but can be consumed in a very short time, thanks to the high zinc reactivity.

As for ZnO/SiO_2, the evolution of $ZnA-SiO_2$ NPs during the reaction mechanism was evaluated by comparing the FTIR spectra of $ZnA-SiO_2$ NPs before (see paragraph 2.2.2) and after the interaction with CBS and S_8, after a filtration procedure from the MCV reaction in TME. From the comparison, no evident differences were highlighted (data not reported). This experimental result suggested that the links between Zn(II) centres and SiO_2 surface are not affected by the MCV reaction and that Zn(II) centres could be still bond to the surface of SiO_2 after the interaction with the vulcanization reagents. This suggestion was deeply investigated by a surface analysis of $ZnA-SiO_2\_CBS$ and $ZnA-SiO_2\_S_8$, as explained in the next paragraph.

$ZnA-SiO_2$: surface solid-state analyses. The evolution of $ZnA-SiO_2$ NPs during the vulcanization reaction in MCV was studied by using a specific combination of surface solid-state analyses (XPS and ^1H-solid state NMR), selected due to the nature of this material. The presence of Zn(II) centres anchored to the surface of SiO_2 particles and the suggestion that these centres could be preserved during the reaction mechanism (see paragraph 4.3.2) required the employment of a deeper surface analysis of the material. The analyses were aimed at discovering whether the Zn(II) centres were released from the SiO_2 surface during the reaction mechanism or if stable catalytic sites were formed, able to behave as heterogeneous catalytic sites, binding to CBS and S_8 through the two free positions (occupied by labile groups, as nitrate or hydroxyl groups, as explained before) to form zinc complex intermediates directly on the surface of SiO_2.

Solid state ^1H-NMR spectra of $Zn_{0.5}A_{0.50}-SiO_2$ and $ZnA-SiO_2\_S_8$ are reported in Figure 4.11.. $Zn_{0.5}A_{0.50}-SiO_2\_CBS$ is not shown, because a similar behaviour to $ZnA-SiO_2\_S_8$ was highlighted.
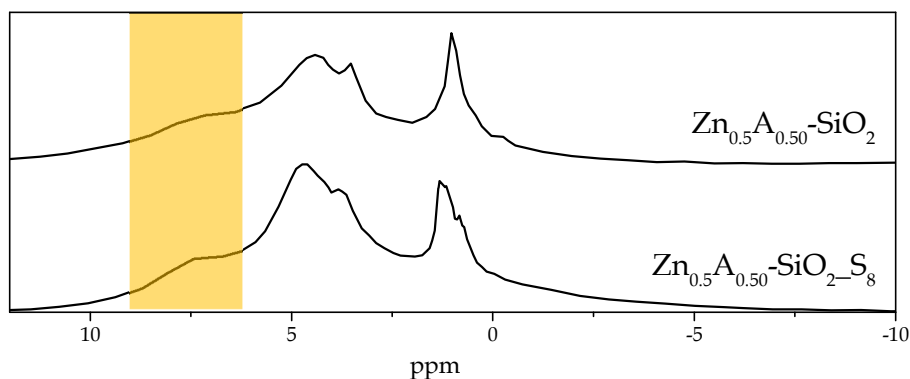
Figure 4.11. Solid state ^{1}H-NMR spectra registered for $Zn_{0.5}A_{0.50}$-SiO$_2$ (up) and $Zn_{0.5}A_{0.50}$-SiO$_2$_S$_8$ (down).

The comparison showed a similar pattern of the two registered spectra. This observation meant that the sample did not change significantly after the interaction with both CBS and S$_8$. In particular, the broad peak at 7.3 ppm, ascribable to the amino group of APTES interacting with Zn^{2+} (detected in Zn$_Y$A$_X$-SiO$_2$ NPs, see paragraph 2.2.4)[8], was still detectable and did not change after CBS and S$_8$ addition. Besides, the peak of free NH$_2$ protons of APTES (1.9 ppm, detected in A$_X$-SiO$_2$ NPs, before the interaction with Zn, see paragraph 2.2.4) was not reformed. These two experimental observations suggested that all the molecules of APTES present on the surface of SiO$_2$ are behaving as grafting agents for Zn(II) centres both before and after the interaction with CBS and S$_8$. Zn(II) centres seemed not to be affected by the reaction with CBS and S$_8$, thus, suggesting that Zn(II) centres behave as heterogeneous catalytic sites on the surface of SiO$_2$.

XPS on ZnA-SiO$_2$_CBS and ZnA-SiO$_2$_S$_8$ samples, was used to determine the surface composition of Zn$_{0.5}$A$_{0.50}$-SiO$_2$ sample after interaction with CBS and S$_8$. Detailed scans were recorded for C1s, O1s, N1s, Si2p, Zn2p regions. The atomic composition measured for ZnA-SiO$_2$_CBS and ZnA-SiO$_2$_S$_8$ samples are reported in Table 4.4., compared to the original ZnA-SiO$_2$, before treatment.

Table 4.4. Atomic composition measured by XPS analysis.

Samples	C %	O %	Si %	Zn %	N tot %	NH %	NO$_3$ %
Zn$_{0.5}$A$_{0.50}$-SiO$_2$	16.09	55.15	20.13	2.58	6.05	4.32	1.73
ZnA-SiO$_2$_CBS	18.48	53.76	19.38	2.78	5.60	4.31	1.29
ZnA-SiO$_2$_S$_8$	19.99	52.60	19.64	2.70	5.08	3.92	1.18

After reaction with CBS and S$_8$, Zn$_{0.5}$A$_{0.50}$-SiO$_2$ remains almost stable and the composition is almost unchanged in both cases. In particular, the weight percentage of Zn on the surface of the sample is constant, meaning that Zn(II) was not release from SiO$_2$ surface due to the reaction with the other agents. According to the indication given by ^{1}H-NMR, the synthesized Zn(II) centres are stable enough to remain on the SiO$_2$ surface, even though they react with the vulcanization agents. The only difference is the amount of NO$_3$% that seems to decrease starting from the bare sample to the other two samples reacted with CBS and S$_8$: this observation is in agreement with the previous suggestion, in which nitrate groups are labile groups that coordinate Zn(II) centres but can be easily exchanged with other groups during the reaction. As a confirmation, the ratios between zinc and the two nitrogen components were calculated (Table 4.5). The Zn/NH ratios are almost stable during the reaction, meaning that no zinc release from the organic amino groups is registered for these samples. Whereas, Zn/NO$_3$ ratios increases from the bare sample to the ZnA-SiO$_2$_CBS and ZnA-SiO$_2$_S$_8$, confirming the possible release of nitrate groups, due to an exchange reaction with CBS and S$_8$. This data was further supported by the presence of sulphur traces detected through this analysis (< 0.2%), that testify the interaction of Zn(II) centres with sulphur-based ligands (CBS and S$_8$), forming very reactive intermediate species, whose formation on the surface of SiO$_2$ is not easily detectable by the used analytical techniques, due to their fast consumption during the reaction.

Table 4.5. Zn/NH and Zn/NO$_3$ ratios calculated from the atomic composition

Samples	Zn/NH	Zn/NO$_3$
Zn$_{0.5}$A$_{0.50}$-SiO$_2$	0.6	1.5
ZnA-SiO$_2$_CBS	0.65	2.2
ZnA-SiO$_2$_S$_8$	0.7	2.3

As a conclusion, ^{1}H-NMR solid state and XPS analyses gave the evidences necessary to assess that Zn(II) centres after the interaction with CBS and S$_8$ remain bond to SiO$_2$ surface through the molecules of APTES as grafting agents. This result confirms the formation of heterogeneous catalytic sites on the surface of SiO$_2$, able to interact with the vulcanization agents through the two available positions previously occupied by nitrate or hydroxyl groups (as confirmed by XPS).

4.4 Summary of the study of the vulcanization mechanism

The MCV approach allowed a deep analysis of the vulcanization mechanisms in the presence of three different activators.

An insight on the process of formation of cross-linking products was given by MS and ^{1}H-NMR analyses, that evidenced an improved process when ZnA-SiO$_2$ and ZnO/SiO$_2$ were applied, compared to m-ZnO. In fact, a progressive degradation of poly-sulphur bridges towards mono- and di-sulphide chains was discovered with all the three activators, that happens faster in the presence of the double function fillers.

The study of the mechanism through FTIR analysis showed up that both m-ZnO and ZnO/SiO$_2$ rely on the solubilization process by SA, that leads to the formation of zinc complexes in solution. With ZnO/SiO$_2$, the release of ZnO NPs from SiO$_2$ takes place at the beginning of the reaction; moreover, a different zinc intermediate species seems to be formed with SA, that could suggest the existence of an additional reaction mechanism developed with ZnO/SiO$_2$.

In the case of ZnA-SiO$_2$, the analysis highlighted the formation of stable Zn(II)centres on the surface of SiO$_2$, during the reaction, whose interaction with the other vulcanization reagents happens with a very different mechanism. No SA is required at the beginning of the reaction, due to the high availability of Zn(II); besides, CBS and S$_8$ are supposed to interact with Zn(II) only in the proximity of SiO$_2$ surface, forming reactive intermediate species that can be consumed in a very short time. No evidences of sulphurating or CBS moieties were detected on SiO$_2$ surface. No Zn(II) release from SiO$_2$ was shown, demonstrating that heterogeneous catalytic Zn isolated sites were synthesized.

The stability of Zn(II) centres is particularly important in the environmental perspective, since it would be connected to a lower zinc leaching from tyre materials. As already explained, one of the main environmental problem in this field is zinc leaching from rubber NCs, due to wear tread during use and disposal phase. Thanks to the introduction of Zn(II) centres that cannot be released from SiO$_2$ surface, Zn leaching could be potentially reduced, decreasing an environmental issue of fundamental importance.

4.5 Bibliography

1. Lautenschlaeger, F. K. Model compound vulcanization - Part I. Basic studies. *Rubber Chem. Technol.* **52**, 213–231 (1978).

2. Anu Mary, J., Benny, G., Madhusoodanan, K. N. & Rosamma, A. Current status of sulphur vulcanization and devulcanization chemistry: Process of vulcanization. *Rubber Sci.* **28**, 82–121 (2015).

3. Nieuwenhuizen, P. J., Timal, S. & Van Veen, J. M. Homogeneous Zinc(II) catalysis in accelerated vulcanization. I. Reaction-stge modeling and cross-link formation. *Rubber Chem. Technol.* **71**, 751–765 (1998).

4. Heideman, G., Datta, R. N., Noordermeer, J. W. M. & Van Baarle, B. Influence of zinc oxide during different stages of sulfur vulcanization. elucidated by model compound studies. *J. Appl. Polym. Sci.* **95**, 1388–1404 (2005).

5. Heideman, G., Noordermeer, J. W. M., Datta, R. N. & Van Baarle, B. Effect of metal oxides as activator for sulphur vulcanisation in various rubbers. *KGK Kautschuk Gummi Kunststoffe* **58**, 30–42 (2005).

6. Versloot, P., Haasnoot, J. G., Reedijk, J., Van Duin, M., Duynstee, F. J. & Put, J. Sulfur vulcanization of simple model olefins, part I: Characterization of vulcanization products of 2,3-dimethyl-2-butene. *Rubber Chem. Technol.* **65**, 343–349 (1991).

7. Susanna, A., D'Arienzo, M., Di Credico, B., Giannini, L., Hanel, T., Grandori, R., Morazzoni, F., Mostoni, S., Santambrogio, C. & Scotti, R. Catalytic effect of ZnO anchored silica nanoparticles on rubber vulcanization and cross-link formation. *Eur. Polym. J.* **93**, (2017).

8. Kim, S.-H., Han, O.-H., Kim, J.-K. & Lee, K.-H. Multinuclear Solid-state NMR Investigation of Nanoporous Silica Prepared by Sol-gel Polymerization Using Sodium Silicate. *Bull. Korean Chem. Soc.* **32**, 3644–3649 (2011).

5

Cross-link distribution

in rubber NCs

In the previous chapters, the isolated Zn(II) centres in Zn_YA_X/SiO_2 were proved to behave as heterogeneous catalytic sites on SiO_2 surface, remaining attached to the anchoring agents of SiO_2, during the whole vulcanization reaction. One main advantage was assigned to the potential reduction of Zn leaching from rubber NCs, with an environmental benefit, as discussed previously.

Another consequence is here discussed. The presence of Zn only on SiO_2 surface in the rubber NCs, forces the interaction of zinc with the vulcanization reagents to take place close to SiO_2 surface and involves the formation of the intermediate Zn complexes in the neighbourhood of SiO_2 particles. As soon as the other vulcanization reagents reach the surface of SiO_2, active Zn complexes are formed and are soon available for the interaction with the polymer chains exposed to SiO_2 surface. Thus, the polymer cross-link formation can be reasonably supposed to start in the proximity of the silica surface, where the Zn(II) centres are located.

This behaviour is potentially really different from m-ZnO, usually used for the industrial rubber NCs, that instead is free to migrate inside the rubber matrix and to promote a homogeneous vulcanization in the whole rubber NCs. A similar behaviour to m-ZnO would be reasonably expected with the use of ZnO/SiO_2, because of the zinc release from SiO_2 after the interaction of ZnO with the co-activator and the possible diffusion of zinc complexes around the rubber NC (chapter 4).

In this chapter, the study of the dependence of the cross-link distribution in the rubber NCs on the nature of the activator, which affects the cross-linking initiation reaction inside the rubber matrix, is reported. For this investigation a morphological analysis of the NCs prepared with the different activators (ZnA/SiO_2, ZnO/SiO_2 and m-ZnO) was performed and the study of the mechanical behaviour of the NCs prepared from ZnA/SiO_2 and m-ZnO was also carried out.

In the first part of the chapter, the discussion about the application of a relatively new method for morphological study, suitable to evaluate the cross-linking

homogeneity, that is the cross-link distribution in the matrix is described. The second section is focused on the characterization of the mechanical behaviour of Zn_YA_X-SiO_2/IR and ZnO/IR NCs and a correlation between the mechanical behaviour/properties and the structural features resulted from the morphological analysis was attempted.

5.1 Morphological study of the cross-link homogeneity

The cross-link distribution in vulcanized rubber NCs was studied through a morphological analysis, based on TEM technique. The peculiarity of the analysis was that rubber NCs were previously swelled in styrene before performing the morphological analysis. Styrene was supposed to diffuse into the vulcanized rubber and to locally swell the rubber differently if there is a different cross-linking degree distribution in the rubber NC: the higher the cross-linking degree of the composite, the lower the tendency of the material to be swollen by styrene. After performing styrene polymerization, the residual double bonds of the polymer chains were let to react with OsO_4.

In case of high cross-link degrees, the lightly swollen rubber appeared as a dark area in a TEM image, due to the high concentration of Os atoms on the corresponding rubber double bonds. In case of low cross-link degree, the swollen rubber appeared as a light area in a TEM image, due to a low concentration of Os atoms on the corresponding rubber material. By the dark area distribution in the rubber NCs, a scheme of the cross-link distribution was hypothesized.

In the following the experimental procedure used for this analysis is reported and the morphology of the samples discussed, in terms of cross-link distribution inside the rubber NCs. The comparison was performed between the IR NCs prepared with $Zn_{0.5}A_{0.50}$-SiO_2, ZnO/SiO_2_4% and m-ZnO, with a Zn content equal to 1.49 phr. An additional comparison was lately carried out between Zn_YA_X-SiO_2/IR samples, at different Zn content (0.68, 1.08, 1.49 phr).

The analysis was performed in collaboration with Dr. Conzatti, from National Research Council (CNR) of Genova, for the study of the Macromolecules (ISMAC).

5.1.1. Experimental procedure

Materials: styrene (≥ 99%), methylethylketone, ethanol (EtOH, puriss, p.a., absolute, ≥ 99.8%), benzoyl peroxide solution (Luperox®AFR40, 40 wt% in dibutyl phthalate), osmium tetroxide (ReagentPlus, 99.8%) were all purchased from Sigma Aldrich.

Procedure: Before TEM analysis, rubber NCs were previously treated through a swelling method with styrene. The procedure is schematically shown in Figure 5.1.
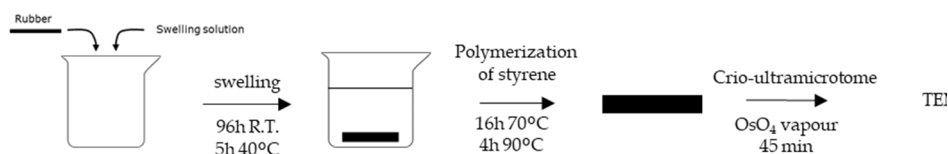
Figure 5.1. Schematic representation of the swelling procedure followed for cross-linking study using TEM analysis.

At the beginning, a rubber extraction pre-treatment was performed in methylethylketone/EtOH (70/30 v/v) for 12h, followed by a drying procedure at 40°C for 12h. The swelling of rubber NCs was realized by immersing a small sample of rubber NC (1x1 cm) in a swelling solution, composed of styrene and benzoyl peroxide (70/30 v/v, used as polymerization initiator). The material was left in the solution for 96h at room temperature and 5h at 40°C. This time was supposed to be enough for the swelling solution to penetrate inside the rubber matrix and discriminate different swelling behaviours due to different cross-linking degrees.

The swollen rubber was then heated at 70°C for 16h and at 90°C for 4h to polymerize styrene. All the samples appeared bigger after the polymerization process and immersed into a PS matrix, confirming the efficient polymerization procedure. Thin rubber slices, to be used for TEM analysis, were cut with the cryo-ultramicrotome, at -77K. The selective contrast with OsO_4 was performed by leaving the rubber slices for 45 minutes in a small container under OsO_4 vapours atmosphere.

As a first step, TEM images were collected after performing rubber swelling and styrene polymerization, to verify the efficient styrene diffusion in the whole rubber matrix. The comparison between the TEM images collected before and after the rubber interaction with OsO_4 vapours allowed to evaluate the cross-link distribution.

5.1.2 Experimental results about cross-linking distribution through TEM analysis

TEM images of the swollen rubber NCs before reaction with OsO_4 vapours confirmed that the experimental procedure was optimal for styrene to penetrate in the rubber materials. This observation was repeated for all the rubber NCs prepared in the presence of the three activator materials.

As an example, the TEM images of the swollen 1.49-ZnO/IR are reported in Figure 5.2 at two different magnifications. The presence of polymerized styrene is confirmed by noticing that in the swollen NCs, the silica agglomerates are more dispersed than they are in the sample of the same material before swelling the rubber in styrene (Chapter 3, morphological study of rubber NCs).
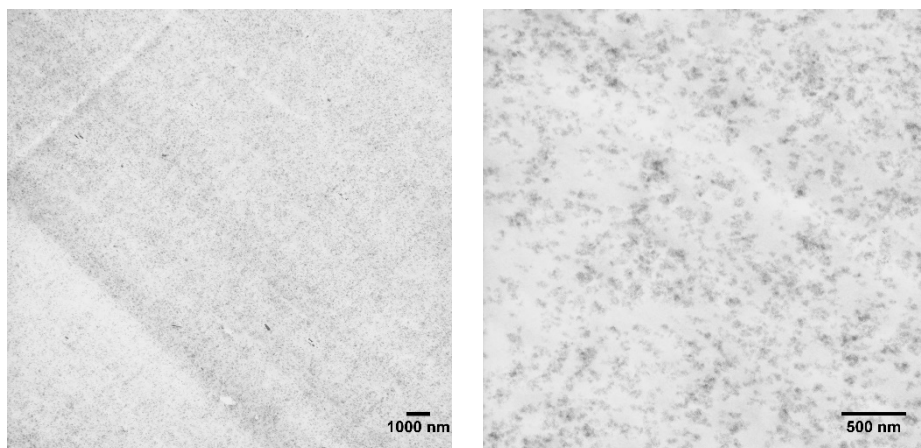
Figure 5.2. TEM images of 1.49_ZnO/IR NC after rubber swelling with styrene and styrene polymerization, at two magnifications (x3k on the left, x20k on the right) .

The TEM images registered for the different IR NCs (differing in the type of activator adopted and having the same Zn content equal to 1.49 phr) treated with OsO_4, are compared in Figure 5.3 to evaluate the cross-link homogeneity of the respective NCs.
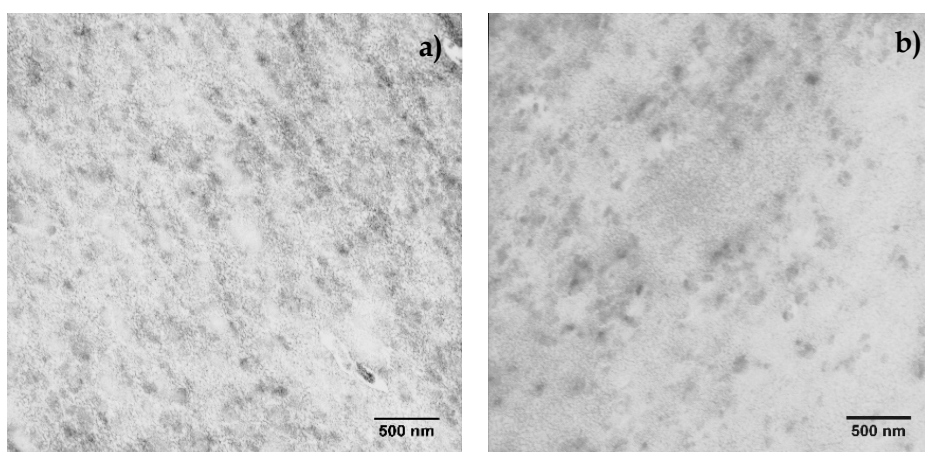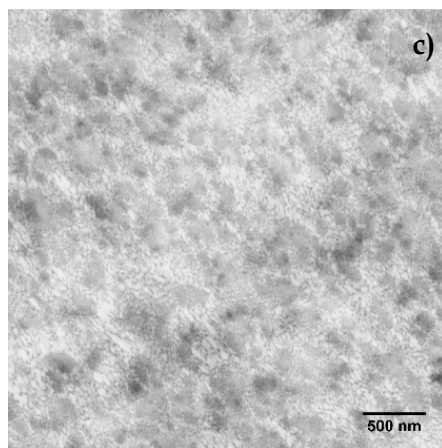
Figure 5.3. TEM images of a) 1.49_ZnO/IR, b) ZnO/SiO$_2$_4%_IR and c) 1.49_Zn$_{0.5}$A$_{0.50}$-SiO$_2$/IR after contrast with OsO$_4$ vapours.

1.49_ZnO/IR seemed highly cross-linked and the cross-linking seemed to be homogeneous in the analysed sample, with a very uniform distribution of the size of the cross-linking network (Figure 5.3a). Darker (polymer chains) and lighter (PS) areas were homogeneously distributed in the images, together with silica aggregates, in the form of circular dark structures, so that the cross-link seemed to be formed in all the regions inside the matrix, without any preferential orientation. This observation confirmed that the vulcanization process was efficient in the presence of m-ZnO, leading to the formation of a highly homogeneous polymeric network.

A similar result was obtained for ZnO/SiO$_2$_4%_IR, which showed a homogeneous distribution of dark and light regions in the relevant TEM image (Figure 5.3b). Moreover, the cross-linking degree of ZnO/SiO$_2$_4%_IR seemed to be slightly higher than that of 1.49_ZnO/IR, as the higher general darkness of the material in the TEM image suggests. This result is in agreement with the higher cross-linking densities measured in Chapter 3, for ZnO/SiO$_2$_4%_IR.

In 1.49_Zn$_{0.5}$A$_{0.50}$-SiO$_2$/IR, circular dark structures were evident, probably corresponding to silica aggregates. In-between these structures, dark cross-link mesh areas can be seen (Figure 5.3c); the distribution of these dark areas seems

different compared to that of the other two NCs, as denser dark regions appear closed to the circular dark regions (probably due to the sub-micrometric silica aggregates). The light areas closed by the dark lines (elastomeric chains) can be connected to PS entrapped inside the material.

In this sample, an indication of a nonhomogeneous cross-link distribution seemed quite evident, with a very high cross-link degree in regions close to the SiO_2 particles, that gradually decreases moving towards the bulk region of the rubber NC, far away from the SiO_2 aggregates. Besides, the presence of some PS islands (white zones) suggested that the cross-linking was less efficient in these regions of the rubber NC. Thus, in $1.49\_Zn_{0.5}A_{0.50}$-SiO_2/IR, a very high cross-linking degree was detected, but with a less homogeneous cross-link distribution in the network. The TEM results are consistent with the results previously reported about the reaction mechanism proposed , which suggests that Zn(II) centres behave as possible heterogeneous catalytic sites on the surface of SiO_2. In fact, considering that Zn(II) centres could exchange their labile ligands (hydroxide or nitrate groups) with the accelerator molecules and sulphur directly on SiO_2 surface, a consequent formation of the active Zn complexes, as active sulphurating agents, would happen close to the surface of SiO_2 particles. In this case the starting of the cross-linking process at the surface of SiO_2 particles, where the active intermediate species are formed, should occur. The different mechanism of reaction promoted by the presence of the heterogeneous catalytic sites on the surface of SiO_2 particles could promote a different distribution of the cross-linking structure.

As a confirmation, the analysis was repeated on the $W\_Zn_YA_X$-SiO_2/IR and W-ZnO/IR samples at different W values (Zn content = 1.49, 108, 0.68 phr); this analysis was performed in order to understand whether different coverage degrees of SiO_2 particle with APTES and Zn in Zn_YA_X-SiO_2 samples could influence the distribution of the cross-link inside the rubber matrix. In principle, a lower amount of Zn should promote a less efficient vulcanization process, both using m-ZnO and Zn_YA_X-SiO_2 as activators; moreover, the same phenomena

should be detected in all the W_Zn_YA_X-SiO_2/IR NCs regarding the cross-link distribution, but with a lower impact in those samples with a lower Zn content, compared to 1.49_$Zn_{0.5}A_{0.50}$-SiO_2/IR.

The results of W_Zn_YA_X-SiO_2/IR with W equal to 1.08 and 0.68, are shown in Figure 5.4, in comparison with two reference samples prepared with m-ZnO, at the same Zn content. First, after the swelling procedure with PS, the silica aggregates looked more distant, as a confirmation of the efficient introduction of styrene in the rubber matrix, as obtained before (data not reported). Moreover, after the completion of swelling procedure, the cross-linking process appeared much less efficient in the presence of reduced Zn content, as expected; in particular the two rubber NCs prepared with W = 0.68 (Figure 5.4c,d) were characterized by few and larger meshes in the structure, as a synonym of the lower vulcanization promotion by lower Zn amount.

Besides, similar observations already reported for the comparison between 1.49_$Zn_{0.5}A_{0.50}$-SiO_2/IR and 1.49_ZnO/IR were noticed at lower Zn content. In fact, with all the W_Zn_YA_X-SiO_2/IR samples, a different distribution of the cross-linking was evident, since the cross-link seemed denser in the proximity of SiO_2 particles (Figure 5.4b,d). On the contrary, all W-ZnO/IR samples showed a good homogeneity of the cross-linking structure in the matrix (Figure 5.4a,c).
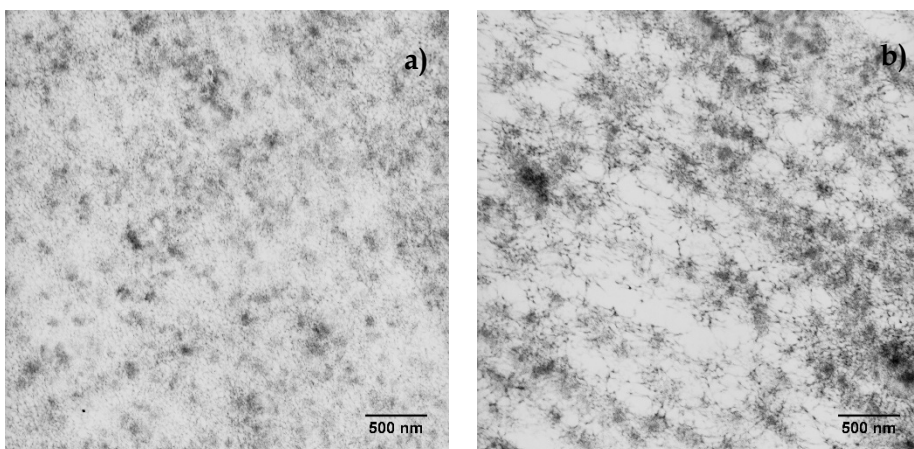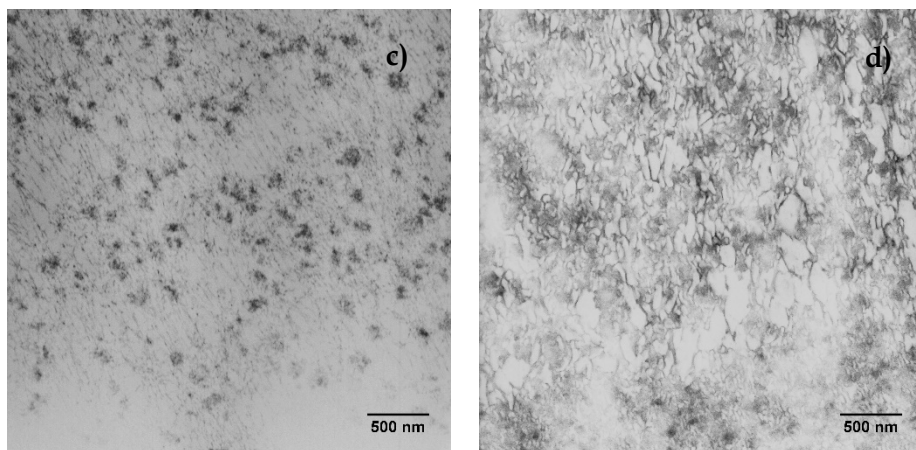
Figure 5.4. TEM images of a) 1.08_ZnO/IR, b) 1.08_Zn$_{0.5}$A$_{0.33}$-SiO$_2$/IR, c) 0.68_ZnO/IR and d) 0.68_Zn$_{0.5}$A$_{0.17}$-SiO$_2$/IR after contrast with OsO$_4$ vapours.

In conclusion, the TEM analysis after swelling with styrene allowed to study the structure of the cross-link inside the rubber matrix, in the presence of different activators of vulcanization. The experimental procedure showed up good swelling efficiencies, able to discriminate different cross-linking degrees. The use of OsO$_4$ vapours allowed a good contrast between polymer chains and PS, with the possibility to study the distribution of PS as a function of the cross-linking degrees.

The main difference was noticed in the presence of W_Zn$_Y$A$_X$-SiO$_2$/IR, where highly efficient cross-linked regions were detected very close to SiO$_2$ particles (darker areas), with a gradual reduction of the density of the cross-link moving towards the bulk region of rubber matrix. This observation is in agreement with a different reaction mechanism promoted in the presence of heterogeneous catalytic Zn(II) sites dispersed on the surface of SiO$_2$ particles. Moreover, it further confirms the formation of stable Zn centres on SiO$_2$ surface, previously suggested in the study of the reaction mechanism (Chapter 4). This phenomenon was evident at all the studied Zn content in rubber (1.49, 1.08, 0.68 phr), even though a less efficient cross-linking formation was achieved in the presence of low Zn

content, as expected from the literature. In fact, low levels of cross-link degrees were detected also in the reference samples, with m-ZnO, at low Zn content (1.08 and 0.68 phr), due to the less catalytic activity that can be achieved with lower Zn contents.

Starting from this morphological study, the different behaviour showed by W_Zn_YA_X-SiO_2/IR was further analysed in terms of the mechanical properties of rubber NCs. In fact, a different cross-link distribution inside the rubber matrix could strongly influence the response of the materials to mechanical imposed stresses, that is connected to the ability of the materials to deform and adapt to external deformation inputs. These responses strictly depend on the internal polymer network, the filler-filler and filler-rubber interaction inside the rubber matrix. In this context, 1.49_$Zn_{0.5}A_{0.50}$-SiO_2/IR sample was used as a selected sample between W_Zn_YA_X-SiO_2/IR, to study the mechanical behaviour from low strains up to high values (fracture), in comparison to a sample in which m-ZnO was used as activator (1.49_ZnO/IR sample). The analysis is shown in the next paragraph.

5.2 Effect of vulcanization procedure on the mechanical behaviour of rubber NCs

The mechanical behaviour of 1.49_$Zn_{0.5}A_{0.50}$-SiO_2/IR is here studied compared to the reference sample (1.49_ZnO/IR), in the attempt to connect the effects of the different vulcanization process and cross-linking distribution to the mechanical properties of rubber NCs.

This study was performed in collaboration with Prof. Claudia Marano, from Politecnico of Milano. The investigation can be divided into four main parts, depending on the mechanical properties that were studied and on the kind of techniques applied: i) mechanical characterization at small strains (Dynamic-Mechanical Analysis, DMA and Payne Effect), ii) mechanical characterization at high strain (uniaxial tensile tests), iii) loading-unloading tests and iv) fracture

phenomenology and toughness determination (fracture tests).

5.2.1 Experimental procedure

Rubber compounds were first calendared at 50° C, to avoid any flow induced anisotropy. An amount of about 40 g of the uncured material was then placed in the centre of a hydraulic press mould used for rubber sheet production, to enable the rubber to flow in all the directions when pressure was applied. The materials were vulcanized for 5 minutes at 170°C. A pressure of 9.8 MPa was applied during the vulcanization. These curing conditions were supposed to guarantee complete vulcanization. Sheets of 200 x 180 x 1 mm were obtained.

Prismatic specimens (40 x 25 x 1 mm), used for dynamic-mechanical analysis and dumbbell specimens (gauge length and width of 20 a 5 mm respectively) used for uniaxial tensile tests, were cut from the vulcanized rubber sheets.

Pure shear specimens for fracture tests were obtained using a proper mould. As shown in Figure 5.5, specimens were characterized by two strips of higher thickness necessary to clamp the specimen in a special aluminium clamp designed to avoid the sample's sleeping out from the clamps that occurs when a pneumatic clamping system is used. Rubber vulcanization of these specimens was carried out keeping the compound at 170°C for 5 minutes, as before.

Figure 5.5. Test settings for fracture tests.

Mechanical testing

1. Dynamic-mechanical analysis (DMA)

Dynamic-mechanical properties were measured with a TA RSA III analyser. The

143

experiments were performed in tension applying a static deformation (ε_s) on which a dynamic strain (ε_d) having an amplitude of 0.1% of the actual length of the specimen, was superposed at a frequency of 10 Hz (Figure 5.6). The static deformation ε_s was increased by step from 0.05% up to about 200%. For each compound the storage modulus (E′) was measured as a function of ε_s.
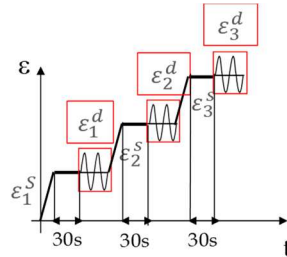
Figure 5.6. Experiment setup for DMA analysis.

2. Uniaxial tensile tests

Uniaxial tensile tests were performed in a Hounsfield dynamometer equipped with a 5 KN cell and with a mechanical extensometer necessary for the measurement of the specimen elongation in its gauge length and thus to obtain the strain, ε. A pneumatic system was used to clamp the specimen. A displacement rate of 50 mm/min was applied, corresponding to a nominal strain rate $\dot{\varepsilon} = 3.57$ min^{-1}.

The output data were used to obtain:

• the nominal stress as:

$$\sigma_n = \frac{F}{A_0} \tag{4.1}$$

where A_0 is the applied load and A_0 is the cross section of the undeformed specimen;

• the nominal strain as:

$$\varepsilon_n = \frac{(L - L_0)}{L_0} \tag{4.2}$$

where L is the extensometer actual gauge length, L_0 is the initial gauge length and λ is the ratio between L and L0, defined as draw ratio. The values of load and specimen elongation were also worked out to derive the reduced stress, σ^*:

$$\sigma^* = \sigma_n \cdot (\lambda - \frac{1}{\lambda^2}) \tag{4.3}$$

3. Loading-unloading test

Loading-unloading cycles in tensile loading conditions were performed on an Instron screw driven dynamometer equipped with a 10 kN cell. Pure shear specimens were used (Figure 5.7). Tests were carried out at constant temperature of 23°C and at a displacement rate of 50 mm min^{-1}, corresponding to $\dot{\varepsilon}$ = 2.63 mm^{-1}.
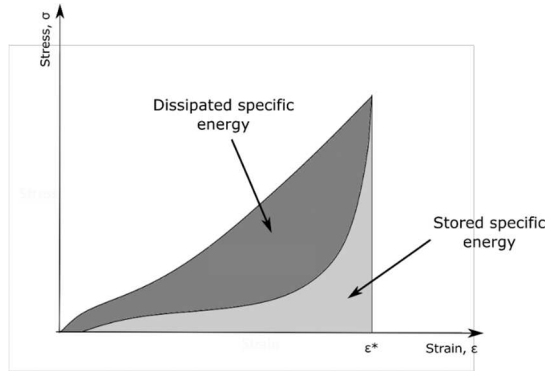
Figure 5.7. Schematic representation of a loading/unloading test and determined dissipated and elastically stored energy.

From each loading-unloading curve, it was possible to calculate:

• the total deformation specific energy as:

$$u_{total} = \int \sigma_{load} d\varepsilon \tag{4.4}$$

- the elastically stored specific energy as:

$$u_{stored} = \int \sigma_{unload} d\varepsilon \qquad (4.5)$$

- the dissipated specific energy obtained as:

$$u_{dissipated} = u_{total} - u_{stored} \qquad (4.6)$$

4. Fracture tests

Fracture tests were carried out using notched pure shear specimens, whose dimensions are reported in Figure 5.5. The edge notch, with a length a = 22 mm, was introduced with a razor blade. A water-based silver paint was sprayed on each sample to create a speckle pattern for strain measurement through Digital Image Correlation Analysis (DIC).

Fracture tests were performed on an Instron screw driven dynamometer equipped with a 10 kN load cell. All tests were performed at a constant displacement rate of 50 mm min^{-1}. The tests were video-recorded to evaluate the time of crack initiation, to study the fracture phenomenology and to measure the local strain. To characterize the fracture properties of materials it was applied a fracture mechanics approach and the integral J at fracture onset, J_C, was used as a measure of material fracture toughness. J_C, was determined following Kim and Joe[1]:

$$J_c = \eta \frac{U_c}{B(W - a_0)} \qquad (4.7)$$

where U_c is the area under the force-displacement curve up to the fracture onset, B and W are the specimen thickness and width and a_0 is the initial crack length; η is a shape factor that changes with respect to the geometry and for pure shear configuration it is equal to 1.

5.2.2 Experimental results on the mechanical behaviour of rubber NCs

1. DMA

In Figure 5.8 the storage modulus E' is plotted as a function of the applied static strain ε_s, for 1.49_ZnO/IR and 1.49_Zn$_{0.5}$A$_{0.50}$-SiO$_2$/IR.
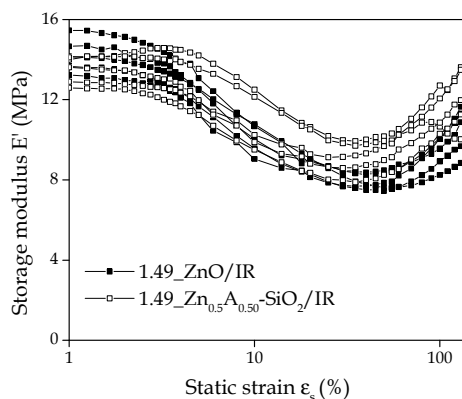
Figure 5.8. Storage modulus as a function of the static appllied strain.

In both the two samples, E' decreased starting from the application of low strain (E'$_{low\ strain}$), as the strain increased, due to the rupture of filler-filler and filler-polymer interactions which, in literature, is referred to the "Payne effect"[2]. In this trend, E' keeps on reducing until a minimum value (E'$_{min}$) is achieved at a certain strain level ($\varepsilon_{@E'min}$), that could be related to the maximum chain extensibility and strain induced crystallization. This latter parameter is determined by the degree of chemical and 'physical' cross-links and by the contribution of the rigid silica inclusions.

Figure 5.9 reports, for the two materials, the mean values of $\varepsilon_{@E'min}$ and the storage moduli E'$_{low\ strain}$ and E'$_{min}$. Even though data were somehow dispersed for both the samples, it could be observed that: i) 1.49_Zn$_{0.5}$A$_{0.50}$-SiO$_2$/IR had a lower $\varepsilon_{@E'min}$ than 1.49_ZnO/IR, suggesting that the polymer in 1.49_Zn$_{0.5}$A$_{0.50}$-SiO$_2$/IR can be more easily oriented than that in 1.49_ZnO/IR, so that E'$_{min}$ is achieved at

lower applied strain; ii) $E'_{low\ strains}$ was fairly the same for the two materials; (iii) E'_{min} is higher for 1.49_$Zn_{0.5}A_{0.50}$-SiO_2/IR than for 1.49_ZnO/IR.
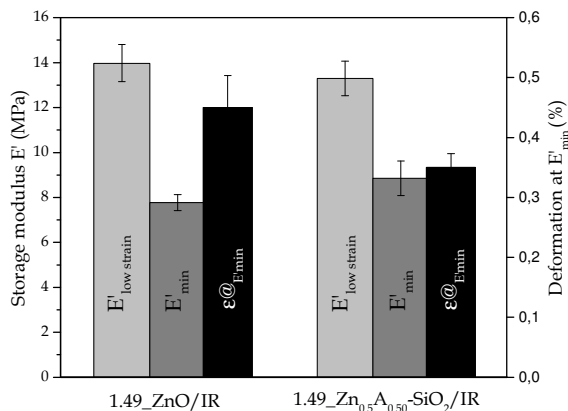
Figure 5.9. Storage modulus E′ at low strain ($E'_{low\ strain}$) and minimum E′ (E'_{min}) measured for the two rubber NCs; on the right axis, the strain values correspondent to the minimum E′ ($\varepsilon@_{E'min}$) are reported.

These results indicate that 1.49_$Zn_{0.5}A_{0.50}$-SiO_2/IR has a lower Payne Effect than 1.49_ZnO/IR and highlighted different behaviours compared to the preliminary tests performed in shear loading conditions, reported in paragraph 3.4.2 and indicating that 1.49_$Zn_{0.5}A_{0.50}$-SiO_2/IR has a higher Payne effect than 1.49_ZnO/IR. Further tests in shear loading conditions should be performed to increase the statistical strength of the result obtained.

Nevertheless, the difference in $\varepsilon_{@E'min}$ values is consistent with the different cross-link densities calculated in paragraph 3.4.3: as expected the higher the cross-linking density, the lower $\varepsilon_{@E'min}$. 1.49_$Zn_{0.5}A_{0.50}$-SiO_2/IR has a lower $\varepsilon_{@E'min}$ than 1.49_ZnO/IR because it has a higher cross-linking degree.

2. Uniaxial tensile tests

In Figure 5.10a, the stress strain curves related to uniaxial tensile tests are reported for the two materials.
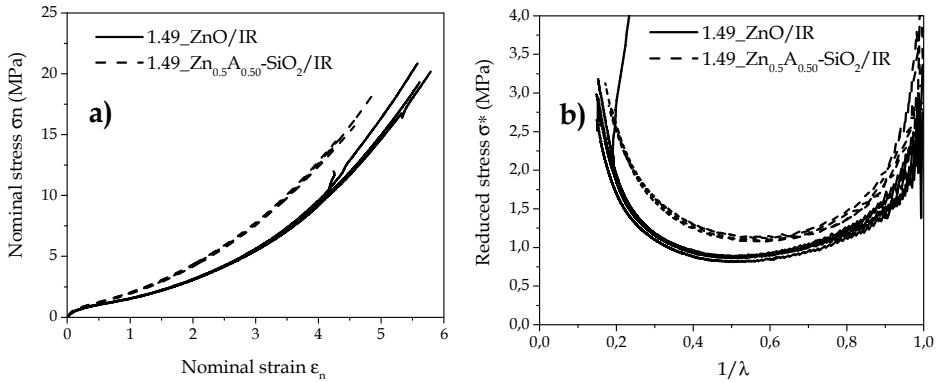
Figure 5.10. a) Stress-strain curves registered for the uniaxial tensile tests; b) Mooney Rivlin plots for the two materials.

As suggested by the DMA tests, the two materials had a similar behaviour up to strain of 0.7, while at higher strains 1.49_ZnO/IR showed a lower rigidity than 1.49_$Zn_{0.5}A_{0.50}$-SiO_2/IR.

By plotting the reduced stress σ* versus the inverse of the draw ratio, $\frac{1}{\lambda}$, the Mooney Rivlin plot could be obtained[3] (Figure 5.10b). The curves showed the typical shape reported in the literature for loaded rubber nanocomposites, with a minimum of reduced strain (σ*min) at a certain value of λ and ε, at which an upturn happens and the values of σ* start to re-increase. The strain at which the reduced stress upturn (ε@σ*upturn) is defined as the strain at which the maximum chain extension is reached in the monotonically loaded rubber network[4]. In Figure 5.11, ε@σ*upturn is reported for the two materials: coherently with DMA results, ε@σ*upturn was lower for 1.49_$Zn_{0.5}A_{0.50}$-SiO_2/IR than 1.49_ZnO/IR and this is consistent with the calculated values of the cross-linking densities, reported in paragraph 3.4.3.
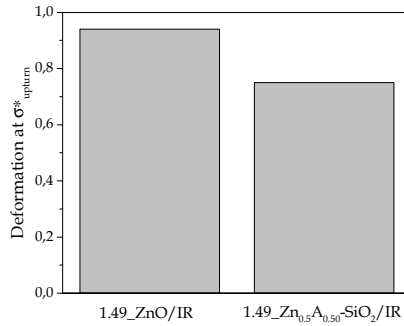
Figure 5.11. $\varepsilon@_{\sigma^*upturn}$ measured for the two materials.

3. Loading-unloading test

In Figure 5.12 the loading-unloading curves recorded for different values of the applied strain are reported for the two materials: for 1.49_$Zn_{0.5}A_{0.50}$-SiO_2/IR a smaller range of deformation was explored due to sample fracture occurring for lower strain than 1.49_ZnO/IR sample.
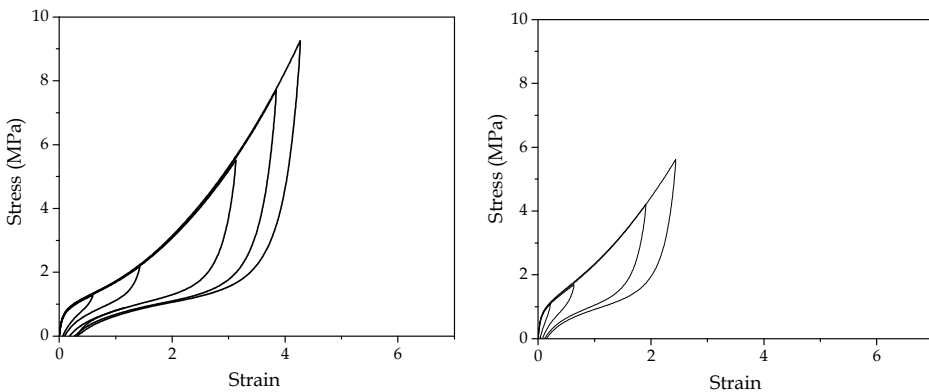
Figure 5.12. Loading-unloading curves used for the two materials.

In the curves, it could be observed that for both the materials a residual strain (ε_{res}) was measured at the end of the unloading step. As shown in Figure 5.13, ε_{res} increased with the applied strain during the loading-unloading tests (ε_{app}) and, at least in a strain range up to 2.5, it seemed to be not dependent on the material type.
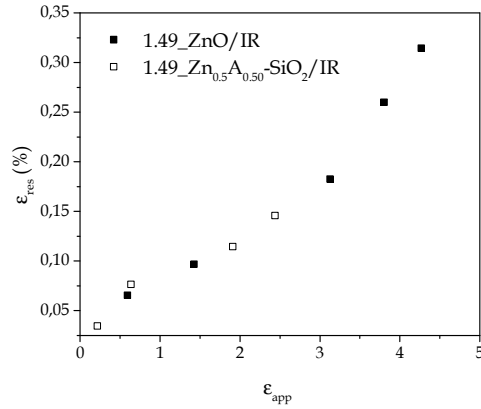
Figure 5.13. Residual strain measured at the end of the unloading step for the two materials.

Figure 5.14 shows the strain dependence of the specific overall (U_{tot}), stored (U_{st}) and dissipated (U_{diss}) deformation energies.
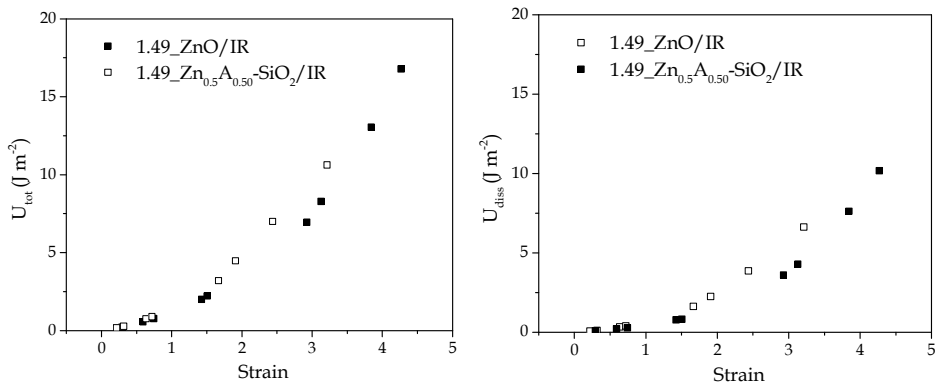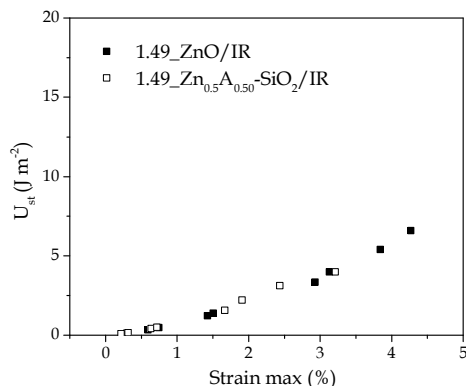
Figure 5.14. Specific overall (U_{tot}), stored (U_{st}) and dissipated (U_{diss}) deformation energies for the two materials.

By comparing the involved energies with the two materials, in the explored deformation range, U_{tot} was always detected slightly higher for 1.49_$Zn_{0.5}A_{0.50}$-SiO_2/IR than for 1.49_ZnO/IR; this behaviour could be associated mainly to the higher energy dissipation (U_{diss}) in 1.49_$Zn_{0.5}A_{0.50}$-SiO_2/IR.

In Figure 5.145 the ratio between the dissipated energy and the overall energy is reported versus the applied strain: at strains lower than 100% both the materials dissipate about 40% of the overall deformation energy while at higher strain about 60% of the deformation energy is dissipated.

Further it can be observed that the dissipated energy fraction seems to be a little higher for 1.49_$Zn_{0.5}A_{0.50}$-SiO_2/IR than for 1.49_ZnO/IR. Furthermore 1.49_$Zn_{0.5}A_{0.50}$-SiO_2/IR resulted to dissipate more energy than 1.49_ZnO/IR in the range of strain explored (data not reported). These results suggest that the strain induced dissipation mechanisms are different or differently involved in the deformation of the two filled networks.
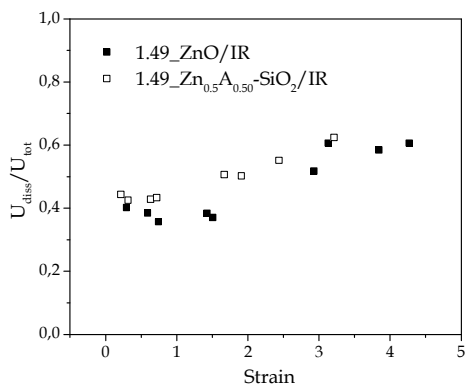
Figure 5.15. Calculated U_{diss}/U_{tot} for the two rubber NCs.

4. Fracture tests

In Figure 5.16 the force-displacement curves recorded during fracture tests are reported for $1.49\_Zn_{0.5}A_{0.50}$-SiO_2/IR (a) and 1.49_ZnO/IR (b), respectively.
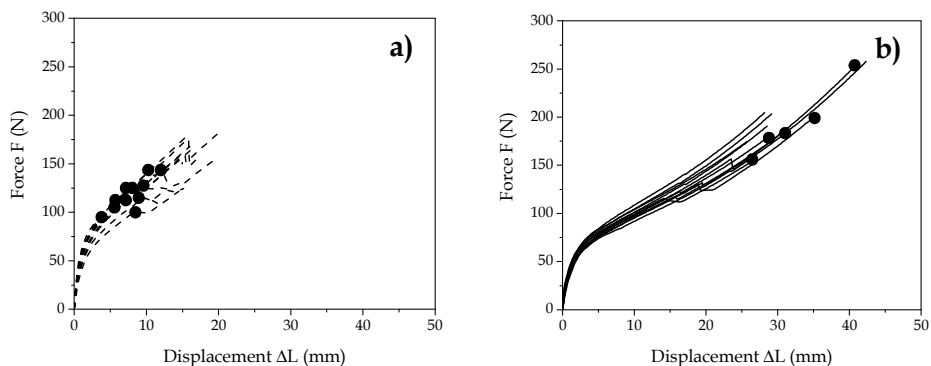
Figure 5.16. Force-displacement curves recorded for the two sample during the fracture tests.

The two materials showed a very different fracture phenomenology. In $1.49\_Zn_{0.5}A_{0.50}$-SiO_2/IR, the onset of a crack which, as expected, propagates on the notch plane (forward crack) was observed. Whereas, in 1.49_ZnO/IR, sideways cracks propagating in the loading direction formed before the onset and propagation of a forward crack took place. This observation confirmed the different nature of the vulcanized materials and of their relative internal structure.

In fact, the formation of sideways cracks or forward cracks is reported in literature and the preferential pathway has been correlated with the strain induced strength anisotropy of the material at the tip of the crack where, due to stress concentration, the material is highly strained and oriented.

In Figure 5.17, video-recording frames corresponding to the forward crack onset are reported, as an example, for 1.49_ZnO/IR (a, b) and 1.49_ $Zn_{0.5}A_{0.50}$-SiO$_2$/IR (c). Referring to 1.49_ZnO/IR, it can be observed that the sideways cracks, indicated by an arrow, are very little and sometimes their propagation did not occur as symmetrically as expected with respect to the notch plane (Figure **5.17** b). Referring to 1.49_ $Zn_{0.5}A_{0.50}$-SiO$_2$/IR, the forward crack propagation often occurred on a plane different from the notch plane.
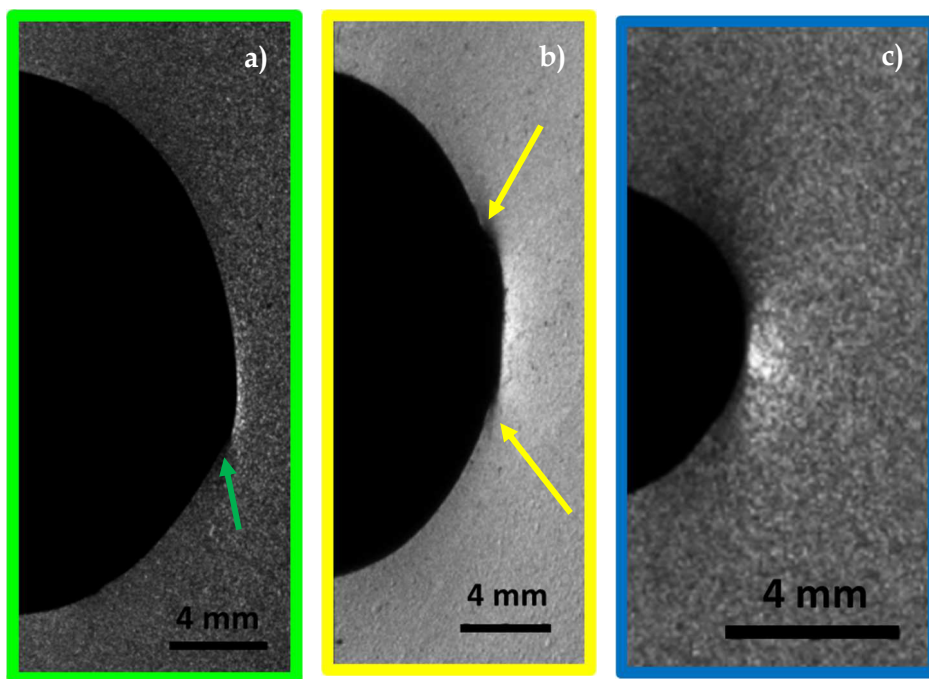
Figure 5.17. Video-recording frames of the forward crack onset of the ZnO/IR (a,b) and $Zn_{0.5}A_{0.50}$-SiO$_2$/IR (c).

In Figure 5.18, the mean values of fracture toughness are reported for the two materials. Fracture toughness standard deviations was very high for both the

samples, with a poor reproducibility.

Nevertheless, as a first preliminary result, from the comparison, it was observed that fracture toughness was lower for 1.49_ $Zn_{0.5}A_{0.50}$-SiO_2/IR than 1.49_ZnO/IR. This result was consistent with the previous observations. In fact, sideways cracks formation is related to molecular orientation at the crack tip which reinforce the crack itself: high deformations are thus applied to the material in the whole specimen, not only at the tip of the crack but in the whole specimen as well and, if material deformation is energy dissipating, material fracture toughness will be high. When sideways cracks do not form, only the material at the tip of the crack is highly deformed at fracture onset and material fracture toughness will be low, due to the fact that the energy dissipated in the sample is very little.
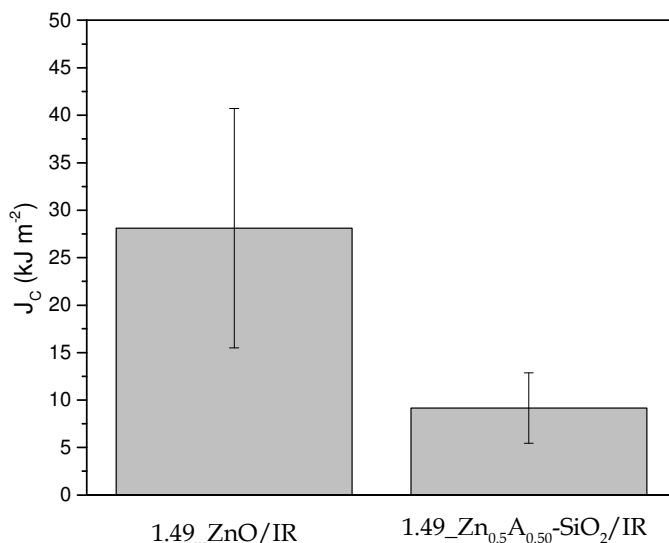
Figure 5.18. Toughness values for the two materials.

In conclusion, the mechanical behaviour of two rubber NCs was studied performing different tests, starting from experiments performed at low strains up to the fracture ones. It is interesting to highlight that the mechanical behaviour of the two NCs was significantly different over the whole range of strain explored

in relation to their different structure: it would be worthwhile studying the effect of structural parameters variation for a better prediction of structure-property correlation for these materials.

5.3 Summary on the cross-link distribution in the rubber NCs

The influence of the use of different activators of vulcanization on the distribution of the cross-link in the rubber matrix has been evaluated. This study was strictly related to the study of the mechanism of the vulcanization process, illustrated in Chapter 4, as it highlights that by introducing activators of different nature that behave through different reaction mechanisms, the morphological and mechanical properties of rubber NCs can be tuned.

In particular, the analysis showed that the introduction of Zn(II) centres as heterogeneous catalytic sites on SiO_2 surface promoted a cross-link formation that started from SiO_2 particles and diffuse all over the rubber matrix. This phenomenon was connected to higher cross-linked areas around the silica aggregates (as shown TEM investigation) and a less uniform distribution of the cross-link in the NC. The polymer network was completely changed compared to the reference m-ZnO/IR and ZnO/SiO_2_IR NCs, whose cross-link distribution was highly homogeneous, in connection to the different reaction mechanism, that goes through the formation of zinc complexes diffused in the matrix.

The differences evidenced in the morphological study were later connected to a different mechanical behaviour of the Zn_YA_X-SiO_2/IR NCs, in the whole range of explored strain values. In this study it was again highlighted the main role of the activators in the vulcanization process (both in terms of efficiency and distribution) and it was demonstrated that the mechanical properties of rubber can be suitably tuned by modulating the nature of the vulcanization reagents (in this case the activator).

Bibliography

1.   Kim, B. H. & C.R., J. Single specimen test method for determining frecture energy (Jc) of highly deformable materials. *Eng. Fract. Mech.* **32,** 155–161 (1989).

2.   Fröhlich, J., Niedermeier, W. & Luginsland, H. D. The effect of filler-filler and filler-elastomer interaction on rubber reinforcement. *Compos. Part A Appl. Sci. Manuf.* **36,** 449–460 (2005).

3.   Boyce, M. C. & Arruda, E. M. Constitutive models of rubber elasticity: a review. *Rubber Chem. Technol.* **73,** 504–523 (2000).

4.   Bokobza, L. & Rapoport, O. Silica and carbon black reinforcement of natural rubber. *Macromol. Symp.* **194,** 125–133 (2003).

6

Influence of structural properties

on the reactivity of the activators

In the previous chapters, the introduction of two new activators with different morphology in rubber NCs was highlighted to have a strong impact on the efficiency of the vulcanization reaction and in the mechanical properties of rubber, compared to m-ZnO. Besides, their use in the model compound vulcanization reaction also evidenced the development of different reaction mechanisms.

In the catalytic field, the structural parameters of the materials are reported to play a fundamental role in the determination of the catalysts reactivity[1]. In fact, the structural properties can influence steric and electronic characteristics of the catalytic centres, especially metal centres, that oversee their reactivity.

In this case, with both the activators, structural changes were introduced, compared to m-ZnO, that can be responsible for the different behaviour in the vulcanization process. Regarding ZnO/SiO_2, the introduction of ZnO NPs instead of m-ZnO particles, increased the surface/volume ratio of the catalyst, enhancing the surface contact of ZnO with the other reagents. Furthermore, based on recent studies about catalyst-support interactions, the formation of Si-O-Zn bonds with SiO_2 surface during the synthetic procedure, could change the Zn Lewis acidity and consequently its tendency to react with the accelerant and sulphur, typical electron rich ligands that interact more easily with acidic metal centres. The study of the extent of the catalyst-support interaction in influencing ZnO reactivity in the vulcanization process was the main goal in the first section of the chapter. Moreover, the cooperation of Zn(II) with other metals (such as magnesium) was preliminarily investigated, as explained later. The work was performed at the University of Stanford, in collaboration with prof. Cargnello Matteo.

In the case of $Zn_YA_X-SiO_2$, the introduction of isolated Zn(II) centres was allowed thanks to a suitable anchoring agent, APTES, that favoured a 1:2 coordination between Zn and APTES, with other two free positions on Zn(II) centres. This structure was supposed to enhance the availability of Zn to react

with the vulcanization agents, reducing the time and the number of steps involved for the formation of active intermediate zinc complexes. As a consequence, low t_{90} were registered, accompanied to lower scorch time. Nevertheless, the very low scorch time of vulcanization can be an industrial issue, due to the low handling properties of rubber in the production phase. The availability of Zn(II) was here studied as a function of the different coordination that Zn(II) could develop in the system and to the different electronic properties that they could assume. In fact, the coordination of Zn(II) centres could be suitably changed by modifying the anchoring agents used in the synthetic process; direct consequences on the availability and stability of the so-formed Zn(II) centres are expectable, with changes in the kinetic parameters of the vulcanization reaction. In this study, the influence of different anchoring agents, having different functional groups to coordinate Zn(II) centres, in the determination of Zn coordination and reactivity was studied. These materials were applied in the rubber vulcanization process, focusing especially on the consequences on the reaction scorch time.

6.1 Effect of structural parameters on ZnO/SiO$_2$ reactivity

The influence of the catalyst-support interaction on ZnO reactivity in the vulcanization reaction is herein studied. The optimization of this structural parameter was supposed to be determinant for the achievement of highly reactive ZnO NPs in the present system.

In fact, the support has shown to modify the catalytic performances of different metal centres, in several reactions[2,3]. Support-catalyst interactions can modify the electronic neighbourhood of metal centres, causing a change in the aptitude of these centres to interact with the reagent involved in the catalytic reaction. As a consequence, the synergy between support and supported phases are determinant for the properties of catalysts. Supports can be classified as "active supports" or "inert supports", on the basis of their ability to increase the rates of the catalytic reactions. As an example, Ceria (CeO$_2$) is generally considered an active support for Pt NPs, because it shows a favourable effect for reactions involving redox steps, such as CO oxidation and water-gas shift (WGS) reactions, in the presence of Pt NPs[4]; in this case, a migration of oxygen atoms from the support to the metal particles was supposed, based on model systems. Besides, Morales *et at.*[5] claimed that a strong interaction can establish between Pt NPs and doped SnO$_2$, resulting in the occurrence of charge transfer from tin (and its substituting ions) towards platinum, responsible for the enhanced electro-catalytic activity of Pt NPs.

Supports of different acidity were also reported to influence the acidic properties of supported metal particles and their catalytic response: Au/Pd NPs supported on aluminosilicate with varied alumina content (0 to 100%, increasing the acidity of the support) were tested in the aromatic's hydrogenation reaction in the presence of S-compound[6]. The enhancement of the activity was related to modifications of the electronic properties of the metal atoms upon interaction with the acid sites and upon intermetallic interactions.

In the case of the vulcanization reaction, as Zn ions, generated in the vulcanization reaction, behaves as Lewis acids, interacting mainly with sulphur-based ligands, the effect of supports of different acidity was studied on ZnO reactivity. No detailed studies are reported on ZnO Lewis acidity effect in the rubber vulcanization process, that can be possibly changed by using supports with different degrees of acidity, compared to SiO_2. Thus, SiO_2 support to ZnO NPs was compared to alumina (Al_2O_3), a more acidic support, that could increase Zn centres acidity and consequently their reactivity in the vulcanization reaction.

Finally, an additional support, magnesium oxide (MgO) was used to support ZnO NPs, to get preliminary information about metal cooperation in the vulcanization reaction. In fact, the basic character of this metal oxide support should lead to a decreased activity of Zn. Nevertheless, Roy *et al.*[7] claimed that Mg(II) ions could be possible substitutes to Zn(II) ions in the vulcanization reaction and could participate to the formation of active intermediate complexes, as zinc. Moreover, $Zn_{1-X}Mg_XO$ NPs were synthesized by Guzmàn et al.[8], getting a faster vulcanization process with a higher cross-linking degree calculated at the end of the reaction. In this study, the use of MgO as a support for ZnO NPs was performed to demonstrate that the cooperation between Zn and Mg metals can effectively increase the vulcanization efficiency.

The model system was chosen in order to study the catalyst-support interaction effect in the reaction, exploiting the use of analytical techniques as MS and ^{1}H-NMR for the determination of cross-linking products formation. All the supported samples were tested in the MCV reaction, in order to discriminate the reactivity of the different systems.

6.1.1 Study of catalyst-support interaction effect

To study the catalyst-support interaction effect, ZnO NPs of different sizes (3, 6, 9 nm) were synthesized and characterized, with the aim of achieving a high control on the synthesis of ZnO NPs to be supported onto different supports.

In the first part of the study, ZnO monodispersed nanocrystals were synthesized using a hydrothermal method, in the presence of a complex system of capping agents, in which nucleation and growth process of ZnO NPs are controlled by the presence of suitable surfactants[9-11]. Capping agents are reported to selectively adhere to certain facets of nanocrystals, that ensure a slow growth rate and prevent particles agglomeration, as well as confer stability to the resulting nanocrystals. Typically, oleyl amine and oleic acid are used as the main surfactants for the syntheses of metal nano-colloids[12]. In this study, the two surfactants were substituted by stearic acid and octadecylamine, the respective saturated organic ligands, with the same functional groups and carbon chain lengths, but without any double bonds, to avoid any possible interferences during the MCV reaction (competition with TME molecules), due to impurities derived from the synthesis. An additional ligand, 1,2-dodecanediol was employed, to further control the spherical growth of ZnO NPs, preventing the preferential growth on the c-axis, typical of ZnO NPs[13]. The hot injection method (injection of one reagent at high temperature) was exploited, as it provokes a fast nucleation process of NPs, followed by a short growth time; it has already demonstrated to led to metal and metal oxide NPs formation with controlled size and shape[14]. ZnO NPs stabilized by surface organic ligands were formed.

The three sizes were chosen to get highly reactive ZnO NPs, considering that the highest reactivity for other metal centres NPs were reported in the range 1-10 nm; moreover, it was considered that: i) particles below 3 nm could not be formed, due to the intrinsic nature of ZnO to grow as nanocrystals, in the wurtzite crystalline phase; ii) particles above 10 nm were characterized by a high inhomogeneity, caused by the inability to fully control both the shape and the

size of ZnO NPs; in fact, ZnO NPs tend to grow in a preferential direction, along the c-axis[13], phenomena that decrease the homogeneity of particles size inside the sample when the size is increased. Different synthetic parameters were tested to get ZnO NPs of different sizes (role of 1,2-dodecanediol, amount of zinc precursor, concentration of the reagents in the reaction solution), as explained in the experimental procedure.

In the second part, to study the possible influence of the interaction between catalysts NPs and the support, the synthesized NPs were supported onto two different support: SiO_2, a typical inert support already used for the tyre applications as reinforcing filler, and alumina (Al_2O_3), characterized by a more acidic character. Due to its intrinsic properties, alumina support could favour the formation of Zn(II) catalytic centres on the surface of ZnO NPs with a higher Lewis acidity, that would facilitate the reaction with the other vulcanization agents and have an impact on the kinetic of the vulcanization process.

The synthesis of ZnO supported NPs was studied and the optimization of the experimental conditions performed. Due to the presence of the organic ligand on the surface of ZnO NPs an additional cleaning step of ZnO NPs surface was required, before testing the catalyst in the MCV reaction. In fact, the interaction of ZnO with the other vulcanization reagents starts with the "solubilization" process of ZnO by stearic acid (the co-activator), a ZnO surface reaction, in which Zn^{2+} ions are generated, to be further coordinated by the other reagents in solution (accelerator and sulphur). The presence of surface organic ligands could prevent Zn surface atoms from interacting with the co-activator, for example due to steric hindrance of the long carbonic chains. Thus, the removal of the covalently bonded stearic molecules on ZnO NPs was necessary to make ZnO available to the surface reaction with the co-activator and achieve a bare ZnO surface for the efficient formation of Zn^{2+} ions, the real catalytic form of ZnO NPs. For this reason, two main pathways were selected to support ZnO NPs:

i) the NPs were first treated through a ligands exchange procedure and then supported through an impregnation method on the different support materials. The ligands exchange method was necessary to get bare ZnO NPs, in which stearic acid molecules were substituted by BF_4^- ions. The presence of weakly coordinating BF_4^- groups on the surface of nanocrystals, through electrostatic interactions, was mandatory to guarantee repulsive interactions between ZnO NPs (instead of the steric repulsions generated by stearic acid molecules) and good dispersion of ZnO NPs, that otherwise would agglomerate. An investigation on the ligands exchange procedure is described in paragraph 6.1.1.3, even though a further optimization of this procedure is still undergoing to obtain bare ZnO NPs and future perspectives are presented at the end of the study;

ii) the NPs were first supported trough an impregnation procedure and in a second step treated through a thermal treatment to remove the organic ligands from the surface of ZnO NPs. The experimental parameters were studied focusing on the reaction time and calcination conditions. These two parameters were essential to control the reaction yield and the removal organic ligands, respectively, as described in paragraph 6.1.1.4.

6.1.1.1 Synthesis of ZnO NPs

Materials: zinc acetate dihydrate ($Zn(CH_3COO)_2 * 2H_2O$, ≥ 98%) was used as zinc precursor and purchased by Sigma Aldrich; stearic acid ($C_{18}H_{36}O_2$, 97%, SA) and octadecylamine ($C_{18}H_{39}N$, 90% tech., ODA) by Acros Organics; 1,2-dodecanediol (90%, DDD) from Sigma Aldrich. 1-octadecene (90%, ODE) and acetone were purchased from Acros Organics and Fisher Scientific, respectively.

Procedure: the syntheses are performed in a standard air-free Schlenk line. In a three necks flask (25 mL), suitable amounts of zinc acetate dihydrate, SA and DDD are added (Table 6.1, solution A); ODE was used as solvent (20 mL). The solution is degassed at 100°C for 30 minutes, under vigorous stirring. In the meantime, in another flask, a suitable amount of ODA is dissolved in 4 mL of

ODE and degassed at 100°C for 30 minutes (Table 6.1, solution B). The molar ratio SA:ODA was always 1:1, as it is reported in the literature as the optimal molar ratio between capping agents to get homogeneous samples[12,15]. In both the two flasks, the complete dissolution of all the solid components is achieved and two clear solutions are obtained.

Solution A is then heated up to reflux condition (270°C) under nitrogen atmosphere. When the solution is refluxing, and a typical orange colour is visible, solution B is quickly added to solution A through a syringe (hot injection method) and left under stirring for 5 minutes at 270°C; later on, the solution is cooled down to room temperature. The formation of solid particles is generally visible in solution below 100°C; the particles are separated through centrifugation, after the addition of acetone as antisolvent (1:1 volume ratio). At last, the solid precipitate is washed twice with fresh hexane (5 mL) and again reprecipitate with acetone (1:1 volume ratio) and eventually stored in hexane (5 mL). The suspension is generally stable enough without the addition of further surfactants for one week.

Figure 6.1. A typical sample of ZnO NPs. The suspension in hexane was stable up to one week.

The optimization of the synthesis was done in order to get reproducible ZnO NPs of different sizes. To achieve this goal, the subsequent parameters were changed: i) role of 1-dodecanediol; ii) amount of zinc acetate dihydrate; iii) concentration of the reagents inside the reaction solution (Table 6.1). In all cases, the molar ratios between stearic acid and octadecylamine was maintained constant and equal to 1.

Table 6.1. Amount of the reagents used for the preparation of ZnO NPs, during the optimization step.

Sample	Zn(CH₃COO)₂*2H₂O (mmol)	SA (mmol)	ODA (mmol)	DDD (mmol)
Z_D0	2	4	4	-
Z_D5	2	4	4	5
Z_D10	2	4	4	10
Z_1	1	4	4	10
Z_2	2	4	4	10
Z_2.5	2.5	4	4	10
Z_3	3	4	4	10
Z_4	4	4	4	10
Z_1(1:2:2)	1	2	2	10
Z_2	2	4	4	10

6.1.1.2 Characterization of ZnO NPs

Particles sizes were determined through TEM images; the particles size distribution was calculated by manually measuring 100 particles randomly chosen in each sample. UV-Vis spectroscopy and XRD were used to assure the formation of crystalline ZnO NPs. FTIR-ATR was employed to confirm the presence of surface ligands, derived from the synthesis. The amount of ligands bond to the surface of ZnO NPs and the reaction yields were calculated thanks to TGA.

Morphological study TEM. Thanks to the controlled synthetic conditions, the recipe allowed the formation of ZnO NPs in all the samples prepared in Table 6.1, as demonstrated by TEM images, reported in the following. Both stearic acid and octadecylamine demonstrated to behave as good capping agents, able to

hinder the further growth of NPs to micro-crystalline materials, in a molar ratio 1:1. The hot injection method guaranteed a sudden and rapid nucleation mechanism at high temperature, followed by a short growth time (5 min), after which the reaction was cooled down.

First, the role of DDD was studied by performing three synthesis in which its amount was changed from 0 to 10 mmols (Z_D0, Z_D5, Z_D10). In the literature, diols are claimed to control the growth process of ZnO NPs in all the direction, hindering the preferential growth on the c-axis and promoting spherical instead of elongated structures[13].

In Figure 6.2, TEM images show that DDD played a main role in the formation and in the control of the growth of ZnO NPs, promoting the generation of a more homogeneous system. In fact, when no DDD was added to the reaction solution, no particles could be separated from the surnatant and the TEM image did not show any particles (Figure 6.2a).

Whereas, both 5 and 10 mmols of DDD led to ZnO NPs separation and the relative TEM highlighted the formation of NPs of about 7-8 nm (Figure 6.2 b,c). Moreover, the higher the amount of DDD (10 mmol), the less the particles size distribution, with an improvement in terms of sample homogeneity (Figure 6.2 e,f).

The highest amount of DDD tested in this set of reactions (10 mmol) was chosen as optimal value for the synthesis of the other ZnO NPs.
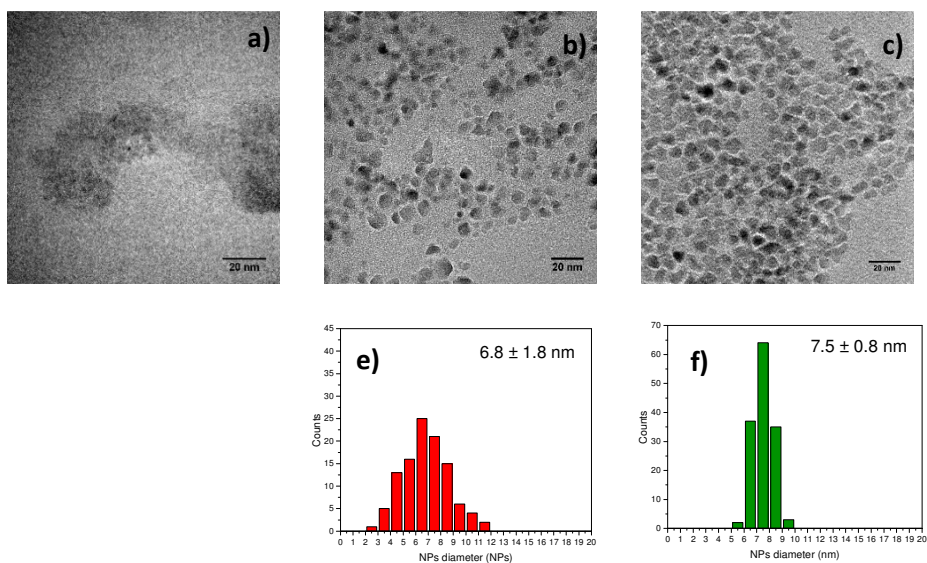
Figure 6.2. TEM images of ZnO NPs, synthesized with different amount of 1,2-dodecanediol as follows: a) 0 mmols, b) 5 mmols, c) 10 mmols; particles size distribution of b) and c) are reported in e) and f), respectively.

The second tested parameter was the amount of zinc precursor. Different amounts of zinc acetate led to the formation of ZnO NPs of different sizes, as demonstrated by the TEM images showed in Figure 6.3; a specific trend was detected, as by increasing the amount of zinc acetate from 1 to 4 mmols, bigger ZnO NPs were formed, moving from 5.2 nm to 16.7 nm NPs. Besides, together with the particles size, also the particles size distribution followed the same trend, so that smaller NPs were characterized by higher homogeneity. Based on the TEM results, it can be hypothesized that the less the amount of zinc acetate, the more the nucleation and growth process mechanism were controlled; in fact, only when a reduced amount of zinc acetate was used (samples Z_1, Z_2, Z_2.5), small and homogeneous ZnO NPs could be produced. This hypothesis was reflected also in the shape of ZnO NPs: with higher amount of Zn precursor (samples Z_3 and Z_4) more disordered structures were formed instead of spherical NPs, there were instead detected on samples Z_1 and Z_2.
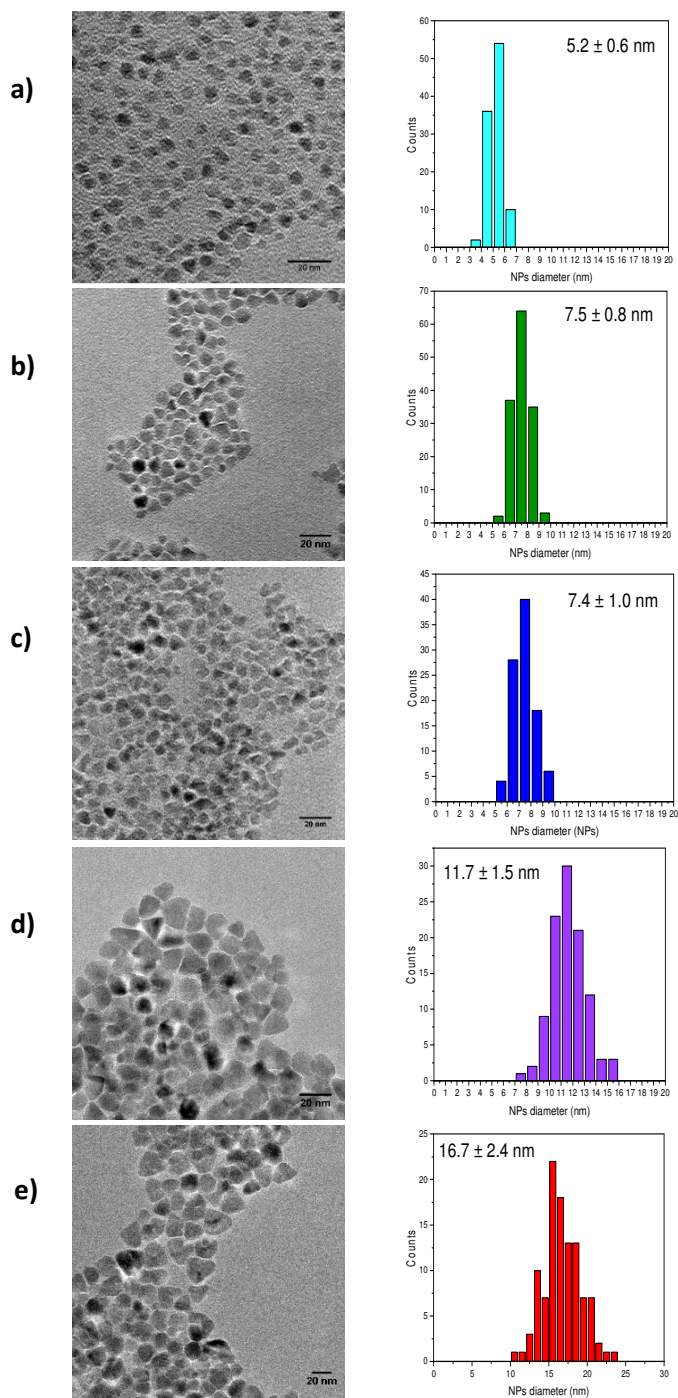
Figure 6.3. TEM images and particles size distributions of ZnO NPs, synthesized by increasing the moles of zinc precursor from a) to e) (Table 6.1.).

At last, the role of the concentration of the reagents was studied, especially concerning the concentration of the zinc precursor and of the other two surfactants (SA and ODA), keeping constant the amount 1,2-dodecanediol (10 mmols). Sample Z_2 (molar ratio Zn : SA : ODA equal to 1:2:2) was compared with a sample in which, keeping constant the molar ratio of the above-mentioned reagents, the concentration was divided by two (Z_1(1:2:2), Table 6.1.). Surprisingly, from sample Z_2, to sample Z_1(1:2:2), the size of ZnO NPs was divided by two as well as the concentration of the reagents, leading to the formation of 4 nm NPs, with a very low particles size distribution, that means a very homogeneous system (Figure 6.4).
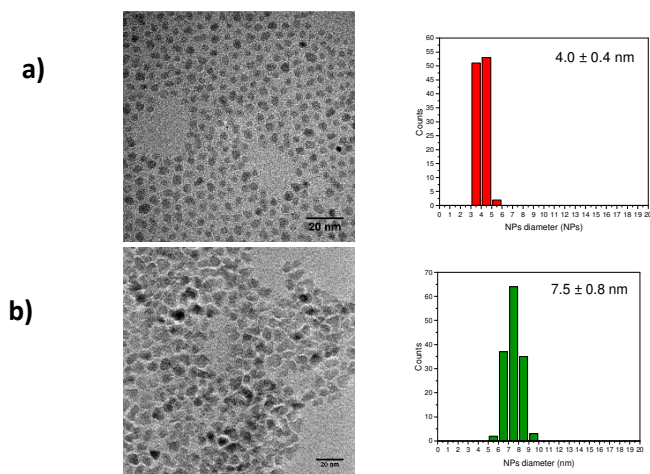
Figure 6.4. Effect of the total concentration of reagents on ZnO NPS size and particles size distributions. In a) the amount of zinc acetate, stearic acid and octadecylamine was half of the same reagents used in b).

In conclusion, a fundamental effect was assigned to 1,2-dodecanediol in influencing both the nucleation and growth process of ZnO NPs; different ZnO NPs were synthesized by changing the amount of zinc precursor and the total concentration of the reagents inside the system. For the subsequent characterization and application, three main sizes were chosen: 4.0 nm, 5.2 nm, 7.5 nm (Table 1, sample Z_1(1:2:2), Z_1 and Z_2).

UV-Vis spectroscopy. As a semiconductor, ZnO (band gap ~ 3.2 eV) has a strong absorption edge at ~ 370 nm, that can be highlighted irradiating the sample in the UV-Vis wavelength range. The absorption spectra of the nanoparticles dispersed in hexane are reported in Figure 6.5. (after dilution in hexane 1:3).
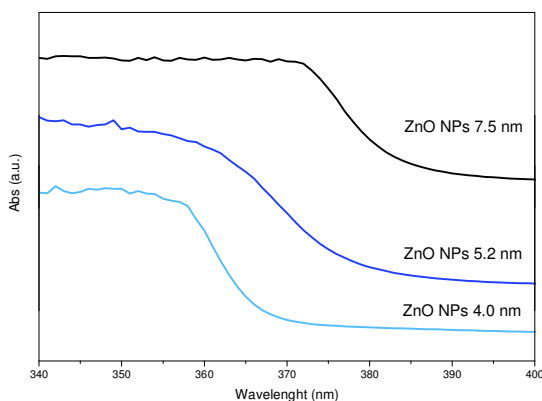
Figure 6.5. Absorption spectra of ZnO NPs dispersed in hexane of different sizes.

In the absorption spectra, all the samples showed the typical absorption band of ZnO, confirming the presence of ZnO particles in the dispersions. Moreover, moving from sample ZnO NPs 7.5 nm to 4.0 nm, the absorption edge shifted to lower wavelength values, that means higher frequencies. The band gap values were calculated by the inflection point, obtained from the minimum in the first derivative curve of the absorption spectrum (Table 6.2.). The band gaps systematically increased by decreasing the particles size, as expected[16], confirming the size trend estimated by TEM images, previously reported.

Table 6.2. Shift of the bandgaps of ZnO NPs, measured by the adsorption spectra.

Sample	Inflection point (nm)	Inflection point (eV)
ZnO NPs 7.5 nm	376	3.29
ZnO NPs 5.2 nm	368	3.37
ZnO NPs 4.0 nm	360	3.44

XRD. XRD analysis confirmed the crystalline structure of the synthesized ZnO NPs; in fact, in these experimental conditions, the growth of nanocrystals was favoured as demonstrated by the typical ZnO peaks detected in XRD diffractograms (2θ = 31.8, 34.5, 36.4). As an example, the XRD of Z_1 is reported in Figure 6.6.
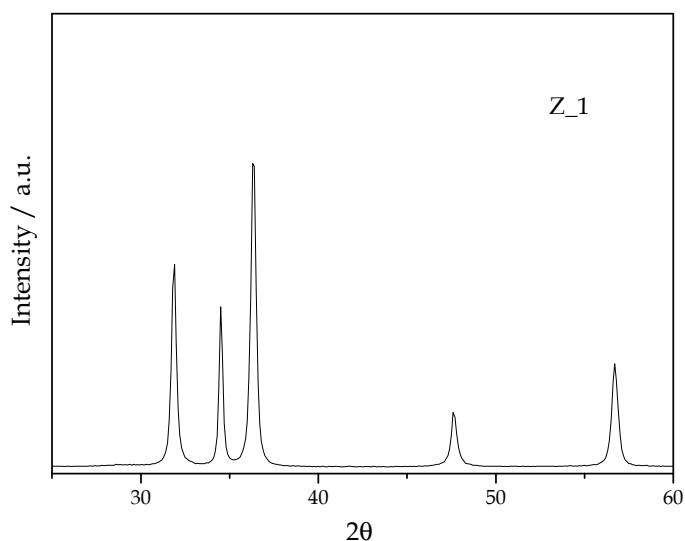
Figure 6.6. X-Ray diffractogram registered for Z_1 sample.

FTIR-ATR. The FTIR spectra were collected for the three selected samples with sizes of 4.0, 5.2 and 7.5 nm (Figure 6.7.) to analyse the NPs surface nature. In all the spectra, the typical peaks due to the stretching of CH_2 groups were detected at 2940 and 2860 cm^{-1}, that could be easily assigned to the carbon chains of the surfactants (either stearic acid or octadecylamine). Moreover, peaks at 1538, 1464 and 1398 cm^{-1} could be related to the symmetric and asymmetric stretching of the carboxylate groups of the zinc stearate structure, that correspond in this case, to stearic acid molecules that coordinate zinc atoms on the surface of ZnO NPs.

Through this analysis, it was deduced that the main ligands on the surface of ZnO NPs were stearic acid molecules, instead of octadecylamine. Besides, no free stearic acid was detected, whose main carboxylic stretching should be at

around 1700 cm^{-1}, thus confirming that all the stearic acid present in this sample was bond to Zn centres on ZnO NPs.

Nevertheless, an additional peak was always detectable between 1600 and 1580 cm^{-1}: the position of this peak suggested the presence of an amide group, that could be formed during the synthesis of ZnO NPs. In fact, the mechanism of formation of ZnO NPs, reported in the literature[17], suggests that an aminolytic reaction could take place between zinc acetate (or zinc-stearic acid complexes previously formed) and the amine (in this case octadecylamine) that is hot injected, thus leading to the formation of an amidic intermediate, that later on is able to decompose to zinc oxide, releasing the amide ligand.

For this reason, it can be reasonably supposed that some amide ligands are still present on the surface of ZnO NPs, as they are present on the solution and may interact with the surface of zinc oxide.

Another worthwhile observation is that the intensity of the peaks related to the ligands (the asymmetric and symmetric stretching of CH$_2$ groups) seemed higher for the sample Z_1 (5.2 nm), compared to the other two samples, in which the intensity was almost the same. This observation is in agreement with the synthetic parameters, because Z_1 was synthesized with a higher content of surfactants to zinc precursor (Zn : SA : ODA) (Table 6.1.). This parameter will be further discussed in the TGA paragraph (quantification of ligands and reaction yields).
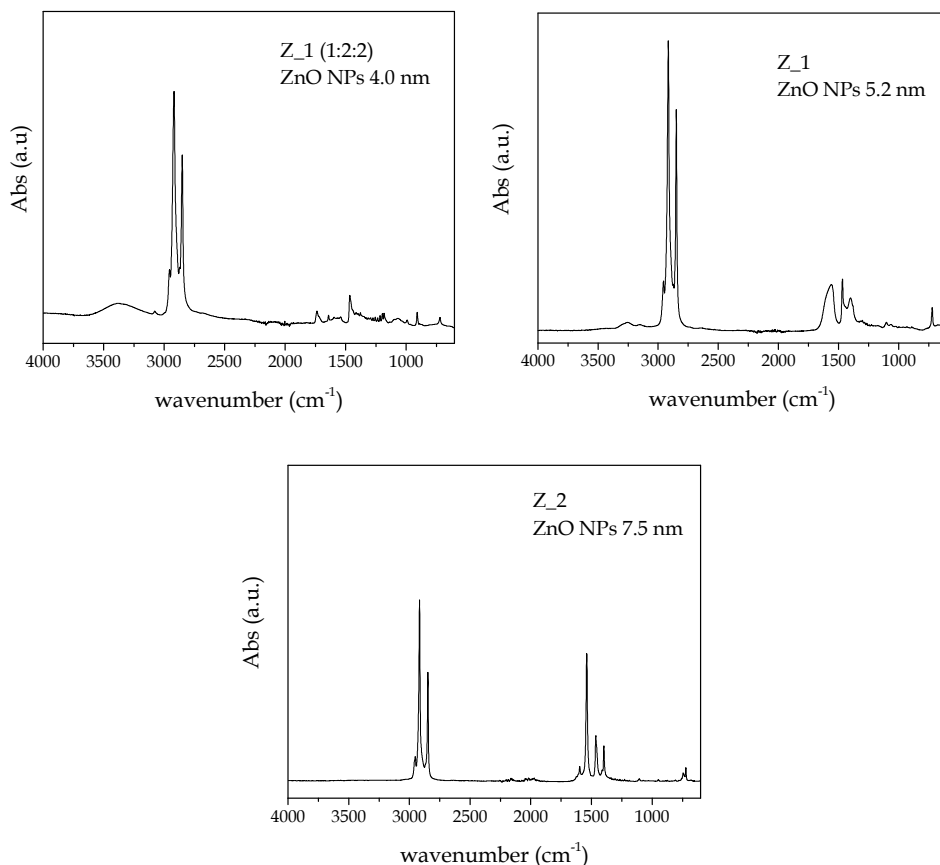
Figure 6.7.   FTIR-ATR of ZnO NPs of different sizes.

TGA analysis. Thermogravimetric analysis was performed in order to get a double information: the amount of organic material present in the sample, that are mainly stearic acid molecules bond to the surface of zinc oxide (as suggested by FTIR spectroscopy) and the calculation of the reaction yields. The analyses were performed on 100 µL of ZnO suspension in hexane, heating from room temperature to 500°C. The weight loss between 150 and 500°C was ascribed to the organic material bond to ZnO; ZnO concentration in hexane was determined from the residual inorganic material after the heating treatment at 500°C and the reaction yields calculated by the total mass of ZnO contained in 5 mL of hexane

(considering a homogeneous dispersion). Typical TGA curves are reported in Figure 6.8., between 150 and 500°C.
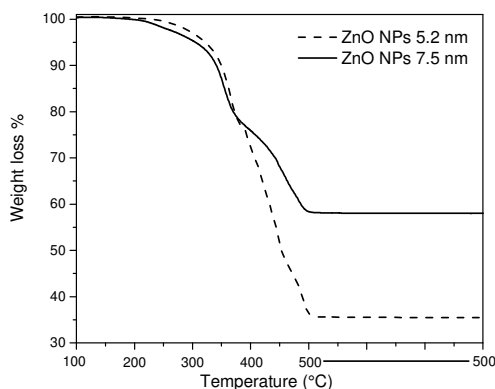
Figure 6.8. TGA curves of Z_1 (ZnO NPs 5.2 nm) and Z_2 (ZnO NPs 7.5 nm) in hexane.

The amounts of ligands estimated from TGA analysis are reported in Table 6.3., expressed as the ratio between the number of moles of ligand (nR) and ZnO. From the comparison, it appears that the amount of ligand in the samples reflects the amount of surfactant used during the reaction: Z_1 sample, synthesized with a molar ratio Zn : SA : ODA equal to 1:4:4 was characterized by a higher weight loss percentage and then a higher amount of ligands on the surface; with the other two samples, synthesized using a molar ratio of 1:2:2, a similar amount of ligand on the surface was calculated, lower than Z_1, as expected.

Table 6.3. Molar ratios of ligands on ZnO NPs (n_R/n_{ZnO}) and the reaction yields, measured by TGA analysis.

Sample	nR/nZnO	$Zn(CH_3COO)_2*2H_2O$ (mmol)	ZnO (mol) from TGA	Reaction yield (%)
Z_1 (1:2:2) (4.0 nm)	0.20	1	0.80 ± 0.04	80 ± 4
Z_1 (5.2 nm)	0.52	1	0.70 ± 0.03	70 ± 3
Z_2 (7.5 nm)	0.20	2	1.57 ± 0.06	78 ± 6

High reaction yields were calculated for all the three synthesized ZnO NPs (Table 6.3). The values, calculated as a medium value between three reproduction of the same synthesis, showed that the syntheses were indeed highly reproducible also in terms of reaction yields.

Summary on the synthesis of ZnO NPs with controlled size

As a conclusion, ZnO NPs were successfully synthesized using a typical hydrothermal procedure for nano-colloids preparation, achieving highly reproducible samples with high reaction yields. Hot injection method demonstrated a great importance on the development of a very fast nucleation process, followed by a very short growth time.

TEM images showed that both SA and ODA, together with DDD play a fundamental role in the control of NPs size and aggregation. ZnO NPs surrounded by stearic acid molecules were formed (FTIR, TGA). Three different sizes (4.0, 5.2, 7.5 nm) of ZnO NPs were prepared by changing the amounts of zinc precursor and varying the concentration of the reagents (Zn precursor, SA and ODA) inside the reaction solvent. These samples were considered for the further studies in MCV reactions.

6.1.1.3 Ligands exchange procedure of ZnO NPs

In the first method, the ligands exchange procedure was first used to remove the organic ligands from the surface of ZnO NPs, in order to get bare NPs to be supported through an impregnation method. In the proposed method, stearic acid molecules were substituted by BF_4^- ions as follows.

Materials: nitrosyl tetrafluoroborate ($NOBF_4$, 95%, Sigma Aldrich) was used as BF_4^- source; acetonitrile (AcN) was purchased from Acros Organics; dichloromethane from Sigma Aldrich.

Procedure: the ligands exchange was performed using a procedure reported in the literature, by Dong *et al.*[18]. 3 mL of NPs dispersion in hexane was mixed with 3 mL of dichloromethane solution of $NOBF_4$ (0.01 M) at room temperature and

left under vigorous stirring for 10 minutes. After addition of 3 mL of AcN to facilitate the separation of the two phases and substituted BF_4-ZnO NPs, the dispersion was centrifugated twice and washed with hexane. The resulting powder was dispersed in 3 mL of AcN.

Characterization of BF$_4$-ZnO NPs: the effective removal of the organic ligands (SA molecules) from ZnO NPs was studied through FTIR and TGA analysis (data not reported). Both the two analyses showed that the ligands were still present on the surface of ZnO NPs; by comparing FTIR spectra of the same sample before and after the treatment of $NOBF_4$, the same peaks were detected. Almost the same weight loss percentage was measured through TGA analysis, compared to the same sample before the treatment, confirming the non-efficient removal of stearic acid.

For this reason, this procedure was not followed to support ZnO NPs.

6.1.1.4 Synthesis of supported ZnO NPs on SiO$_2$ and Al$_2$O$_3$

Materials: SiO_2 support was synthesized following a conventional Stober method reported in the literature[19], using tetraethyl orthosilicate (TEOS, 0.28 M) as silica precursor, in a basic EtOH solution (H_2O = 6 M, NH_4OH = 0.17 M); particles of 150 nm ± 10 nm were obtained. Commercial Al_2O_3 (SasolTH100/ 150), calcined at 900°C for 24h, specific surface area 97 m^2g^{-1}, mainly in the γ phase. Hexane (≥ 95%) was purchased from Sigma Aldrich. ZnO NPs suspensions in hexane were used as received from the previous synthesis. Only the particles of intermediate size (5.2 nm) were chosen as probe to test the support effect, as the sintering process was not easily checked through TEM analysis and the size of ZnO NPs was hardly measured after the calcination process.

Procedure: ZnO NPs were supported through a wet impregnation method. 100 mg of support are dispersed in 3 mL hexane and left under stirring for 30 minutes, to achieve a good dispersion. Later on, a suitable amount of ZnO NPs suspension in hexane (depending on the amount of ZnO dispersed, previously calculated by TGA), is added to the support dispersion and left under stirring

for 2 hours. The amount of ZnO dispersion to be added is chosen in order to get a ZnO weight percentage on the final material equal to 2 wt%. After 2 hours, the powder is separated by centrifugation, dried for 2 hours in an oven at 80°C and finally calcined for 15 minutes at 500°C (to remove the surface ligands on ZnO NPs). Both the time necessary for the complete interaction between zinc oxide and the support and the calcination process were optimized, in order to have reproducible samples.

Herein the two supported ZnO NPs samples will be labeled as $Z\_1\_SiO_2$ and $Z\_1\_Al_2O_3$.

Impregnation time

Since ZnO NPs have a typical absorption edge under UV-Vis irradiation (as seen before), the presence of suspended ZnO NPs in solution can be monitored by measuring the UV-Vis solution absorption spectra. In this case, by analysing the absorption spectra of the solutions during the impregnation process of ZnO NPs onto different supports, it was possible to determine the impregnation time required to fully support ZnO NPs on the different supports. In fact, due to the interaction between ZnO and the support, the absorption band of ZnO NPs in solution should disappear after all ZnO NPs have interacted with the support. Moreover, the solution should change from whitish to clear solutions. Thus, the UV-Vis spectra of the solutions were registered during the impregnation process, every 10 minutes. In Figure 6.9, UV-Vis spectra of $Z\_1\_SiO_2$ solution are reported after 30″, 10′ and 120′ of mixing.
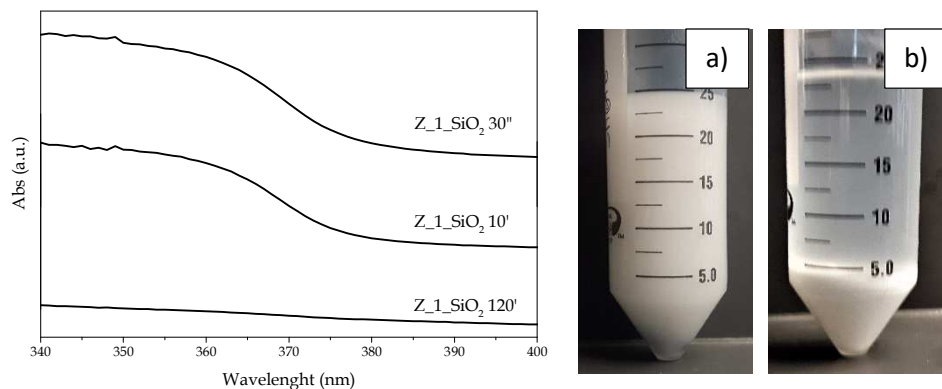
Figure 6.9. UV-Vis spectra of Z_1_SiO$_2$ solution after 30″, 10′ and 120′. Picture of 8a)
Z_1_SiO$_2$ system after 10′ of stirring. 8b) Z_1_SiO$_2$ system after 120′
stirring.

The ZnO absorption edge was clearly visible after 30″ and 10′ mixing time and
the solution appeared white (Figure 6.9a). After 2 hours, both the solution was
clear (Figure 6.9b) and the UV-Vis spectra showed no ZnO absorption band. The
same impregnation time was used for the preparation of Z_1_Al$_2$O$_3$; the UV-Vis
spectra of these two systems at the beginning (30″) and after two hours of
stirring are reported in Figure 6.10.
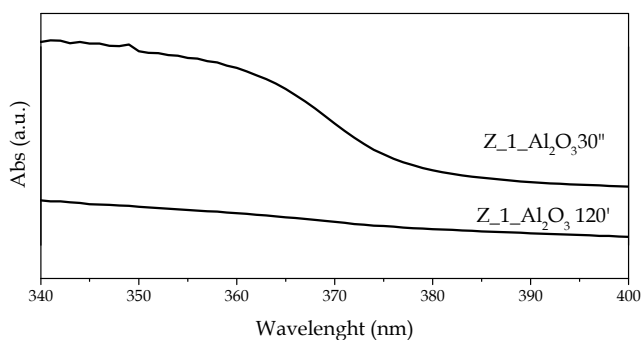
Figure 6.10. UV-Vis spectra of the ZnO NPs supported on Al2O3 solution, after 30″ and
120′ of stirring.

Calcination process

The calcination process was optimized by analysing the calcined powder through FTIR spectra. This process was necessary to create a covalent bond between ZnO NPs and the support and to remove the ligands that are bond to the surface of ZnO NPs. Only when no peaks due to the ligands were detected on the samples on FTIR spectra, the samples were considered clean.

Different temperatures and times were tested: i) fast calcination treatment (700°C, 30 s), as it has already demonstrated the highest performances for Pd particles, avoiding at the same time the sintering of the NPs[20]; ii) 700°C 1'; iii) 700°C 2'; iv) 500°C 15'.

FTIR spectra were collected for the supported samples after each treatment. As an example, FTIR of Z_1_SiO$_2$ after the different calcination treatments are reported in Figure 6.11, where the two peaks at 2941 cm^{-1} and 2860 cm^{-1} are highlighted, as they can be considered the main probes to point out the presence of carbonic chains (due to stearic acid) on the inorganic ZnO NPs.

Only after a longer treatment (500°C, 15'), all the ligands were fully removed; instead, when the sample was treated at high temperature (700°C) for 30", 1' and 2', the ligands were still present. A reduction of the amounts of ligands seems to be evident when the sample is treated for 2' instead of 30", but, in conclusion, the fast calcination treatment was not effective for ZnO NPs. A longer treatment at lower temperature (500°C, 15') showed high efficiency to remove organic ligands from ZnO NPs. The same result was registered with Z_1_Al$_2$O$_3$.
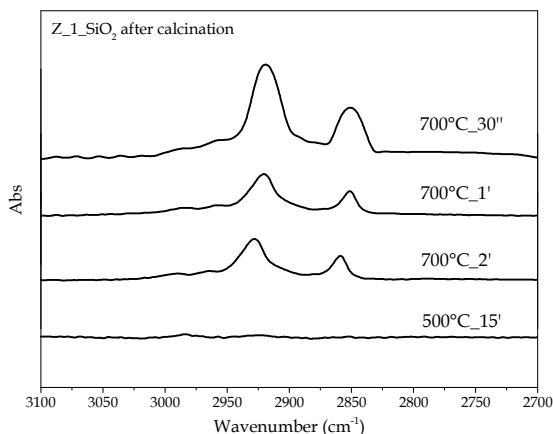
Figure 6.11. FTIR-ATR spectra of Z_1_SiO$_2$ after different calcination treatments in the range 3100-2700 cm^{-1}.

TGA analysis was further performed on the calcined samples, to confirm the results given by FTIR technique. In Figure 6.12, the thermogravimetric curves for ZnO NPs supported on SiO$_2$ are reported. The percentage of weight loss is compared to the weight loss of the bare sample (SiO$_2$) and of the same sample before calcination; from the comparison, Z_1_SiO$_2$ after calcination showed a similar behaviour to the bare sample, while before calcination a higher weight loss was registered.
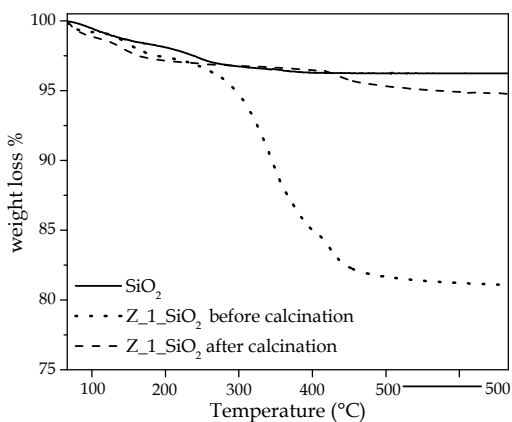
Figure 6.12. TGA profile for Z_1_SiO$_2$ sample after calcination, compared to bare SiO$_2$ and Z_1_SiO$_2$ before calcination.

6.1.1.5 Characterization of Z_1_SiO$_2$ and Z_1_Al$_2$O$_3$

ZnO NPs supported on SiO$_2$ and Al$_2$O$_3$ were characterized first to assess the effective presence of ZnO on the surface of the solid support, through ICP, UV-Vis spectroscopy and XRD analysis. A morphological characterization using TEM microscopy was further performed.

ICP, UV-Vis, XRD. ICP analysis on the calcined samples confirmed that the amount of ZnO detected onto the surface of the two supports was 2.1wt% ± 0.2wt%, as expected (nominal value 2.0wt%). The effective deposition of ZnO was confirmed by UV-Vis analysis, through the measurement of the typical absorption edge of ZnO, as seen before, at ~ 370 nm (data not reported). Moreover, the typical peaks of ZnO were measured in the XRD diffractograms (data not reported).

TEM analysis. TEM images were recorded on Z_1_SiO$_2$ and Z_1_Al$_2$O$_3$ before and after calcination process and compared to the bare supports. In the case of Al$_2$O$_3$, ZnO was not easily detected through TEM analysis, due to an inadequate contrast with the support material and the images were not useful for the description of the samples' morphology (data not reported). Whereas, the series collected for SiO$_2$ support is shown in Figure 6.13. Both before and after calcination treatment, the presence of ZnO NPs was confirmed, as well distributed NPs around the surface of SiO$_2$ particles. After calcination, no evident aggregation of SiO$_2$ particles seems to occur, but the measured size of ZnO NPs increased from 5.2 nm to 11 nm ± 1.2 nm, as a proof of a partial sintering between ZnO NPs.

Since aggregation phenomena of ZnO NPs occurred after calcination process on SiO$_2$ support, the same process would be reasonable to happen in the presence of Al$_2$O$_3$, even though no direct evidence was reported. As a consequence, supporting ZnO NPs of different sizes was not performed, because the size of the NPs could not be easily controlled.
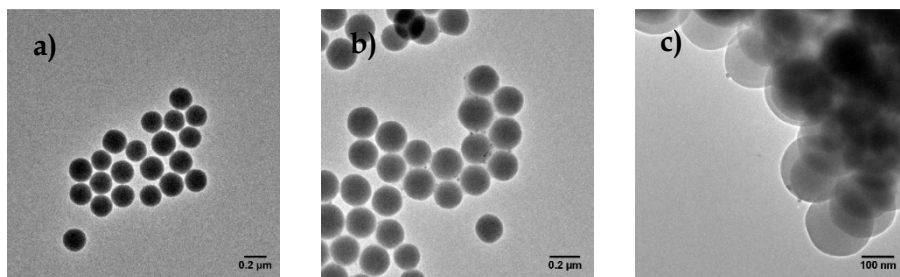
Figure 6.13. TEM images of a) bare SiO$_2$ (synthesized through Stober method), b) Z_1_SiO$_2$ before calcination and c) Z_1_SiO$_2$ after calcination process.

6.1.1.6 Tests in model compound vulcanization (MCV)

The catalytic activities of ZnO NPs supported on SiO$_2$ and Al$_2$O$_3$ were preliminarily tested in the model compound vulcanization reaction (MCV), using 2,3-dimethyl-2-butene (TME) as model compound.

Materials and procedure: the reactions were performed in the same experimental conditions described in Chapter 4, using CBS (1.6phr), sulphur (3phr) and a suitable amount of ZnO NPs supported samples, to have 1.85 phr of ZnO in the reaction (T = 120°C, different reaction time equal to 5, 10 and 20 minutes). The liquid portion recovered from these experiments were analyzed through Mass Spectrometry (MS) to measure the relative intensity of the cross-linking products (TME-S$_X$-TME) to an internal standard (N-diethylamine, m/z = 74, added just before the MS analysis).

MS results should not be compared with the previous results obtained in the presence of ZnO/SiO$_2$ and ZnA-SiO$_2$, because i) the data were registered with a different MS instrument (as explained in the appendix), so that changes in the absolute values of relative intensities could be connected to different instrumental conditions; ii) the presence of different supports materials could affect the reaction yields, because of absorption phenomena that could happen on the surface of either commercial SiO$_2$, synthesized SiO$_2$ or commercial Al$_2$O$_3$. These data are considered as an independent package of measurements, to collect information about catalysts-support interactions.

MS results. Preliminary MS data collected from MCV experiments, illustrated in Figure 6.14, showed that the two samples both worked in the vulcanization reaction. They both allowed the formation of mono- and di-sulphide bridges products already at 5 minutes, but their relative intensities increased at 20 minutes, demonstrating that the reaction is proceeding. The concentration of all the other species generally decreased or remained almost stable during the reaction time, with only few exceptions (as TME-S_X-TME with X=3, measured with Z_1_SiO$_2$), confirming that the reaction is based on a progressive degradation of poly-sulphur bridges products mechanism towards shorter sulphur chains, as discussed in Chapter 4.
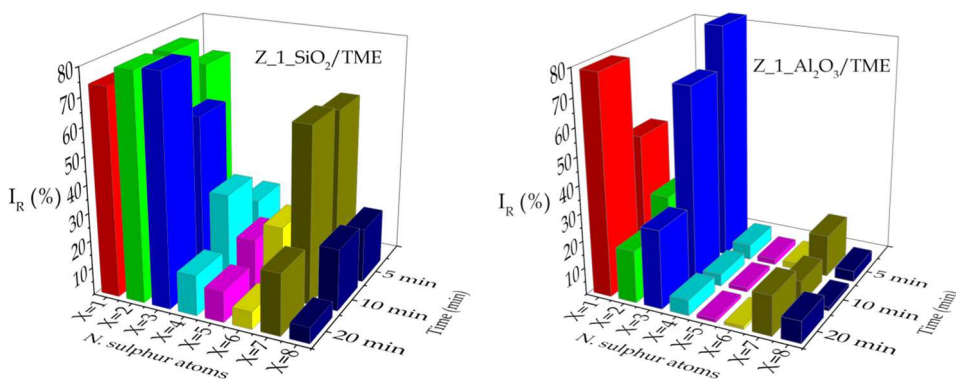
Figure 6.14. MS results obtained from MCV experiments performed with Z_1_SiO$_2$ (left) and Z_1_Al$_2$O$_3$ (right).

In general, the absolute values of the relative intensities of all the species were increased compared to the previous package of measurements, reported in Chapter 4. Another main difference was that none of these two samples showed an intermediate situation at 10 minutes, in which TME-S_X-TME (with X > 6) were totally consumed, but all the species were detected at all the reaction times. As explained before, both instrumental parameters and the different nature of the materials were probably responsible of the different experimental measurements.

From the comparison of the samples, it can be noticed that the concentration of TME-S_X-TME products with X = 7, 8 at the three reaction times was lower with Z_1_Al$_2$O$_3$ sample, even though the concentration of the other cross-linking products was comparable. This observation suggested that the degradation of poly-sulphide TME-S_X-TME products could take place with an improved kinetic of the reaction with Z_1_Al$_2$O$_3$, instead of Z_1_SiO$_2$.

The different behaviour of the two samples could be explained considering that the acidic site of Al$_2$O$_3$ could increase the acidic character of Zn(II) ions supported on alumina, thus increasing their reactivity as Lewis acids towards the other vulcanization agents, with an impact on the kinetic of degradation of poly-sulphur bridges products.

6.1.2 Metals cooperation effect

The effect of ZnO cooperation with other metals in the vulcanization reaction was studied in the presence of magnesium oxide (MgO). This oxide could generate Mg(II) ions, that together with Zn(II) could modify the vulcanization mechanism and efficiency, as previously reported. MgO was introduced in the system as support for ZnO NPs.

6.1.2.1 Synthesis of ZnO NPs supported on MgO

Materials: commercial MgO (≥ 97%) used as support and hexane (≥ 95%) were purchased from Sigma Aldrich.

Procedure: ZnO NPs were supported through a wet impregnation method, as explained in paragraph 6.1.1.4, followed by a thermal treatment to remove the organic ligands from the surface of ZnO NPs. The amount of ZnO dispersion to be added was chosen to get a ZnO weight percentage on the final material equal to 2wt%. The reaction time was fixed at 2 hours, based on the previous optimization of the synthetic procedure, as well as the calcination conditions (500°C, 15'). As before, only the particles of intermediate size (5.2 nm) were

chosen as probe to test the coordination effect, as the sintering process was not easily checked through TEM analysis and the size of ZnO NPs was hardly measured after the calcination process.

Herein the supported ZnO NPs samples on MgO will be labelled as Z_1_MgO.

6.1.2.2 Characterization of Z_1_MgO

The same characterization employed on ZnO NPs supported on SiO_2 and Al_2O_3 was used to characterized Z_1_MgO. Herein, data from the experimental characterization are not reported, as the results are comparable to the other two supports. At first, ICP, UV-Vis spectroscopy and XRD analysis confirmed the effective deposition of ZnO crystalline NPs on MgO. Lately, FTIR of calcined sample and TGA analysis assessed the total removal of organic ligands from ZnO NPs after the calcination process. TEM images were registered before and after the impregnation treatment, but as for Al_2O_3, ZnO was not easily detected through TEM analysis, due to an inadequate contrast with the support material and the images were not useful for the description of the samples' morphology.

6.1.2.3 Tests in model compound vulcanization

For the preparation of MCV experiments refers to paragraph 6.1.1.6. MS results of Z_1_MgO/TME are presented in Figure 6.15.
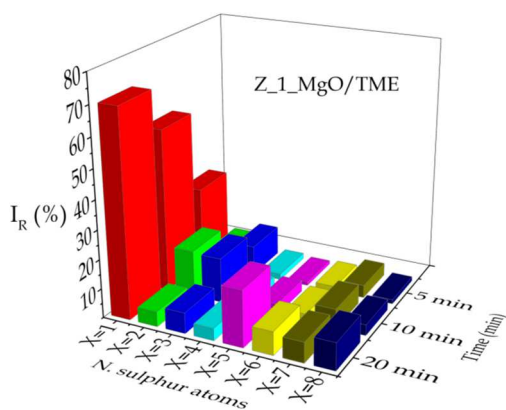
Figure 6.15. MS results of the MCV experiment performed in the presence of Z_1_MgO.

When ZnO NPs were supported on MgO, the concentration of S1 species increased during time, achieving the same concentration as the other catalysts by 20 minutes of reaction and suggesting that the reaction was efficiently proceeding during the reaction time. Nevertheless, a very different behaviour of the reaction was evident, by comparing the concentration of the other species: in fact, at all the reaction times all the other species were always detected, with a very low intensity, even at 5 minutes of reaction and seemed not to change during the whole reaction.

From these observations, it could be affirmed that Mg are likely to cooperate with Zn ions during the reaction performed in these experimental conditions; in particular, the presence of Mg together with Zn seems to increase the kinetic of the degradation process of long sulphur bridges products ($X \geq 6$) to mono- and di-sulphide bridges, compared to the rate of the formation of long sulphur bridges products. In fact, if the degradation process is supposed to be faster than the formation of cross-linking products, it could be reasonable to have stable concentrations of all the long sulphur bridges products during the reaction time.

6.1.3 Summary of the effect of structural parameters on ZnO/SiO_2 reactivity

The influence of catalyst-support interaction and metal-metal cooperation on ZnO/SiO_2 reactivity was studied. For this reason, model ZnO crystalline NPs of controlled size (4.0, 5.2 and 7.5 nm) were synthesized by using a high temperature colloidal synthesis. The amount of zinc precursor and the total concentration of the reagents in the reaction solution showed to influence the size of the synthesized NPs.

Between the two different procedures tested to support ZnO NPs on the three different materials (SiO_2, Al_2O_3 and MgO), the method composed of an impregnation step, followed by a thermal treatment to remove the organic ligands was successful and allowed the formation of bare homogeneously

dispersed ZnO NPs, characterized from a structural (XRD, UV), surface (FTIR, TGA) and morphological point of view (TEM).

The removal of the organic ligands from the surface of ZnO NPs before the impregnation step was also studied, through the exchange ligands technique. Nevertheless, the optimization of this step is still undergoing, with the use of different reaction conditions, as explained in the future perspectives.

As preliminary results, the presence of supports with different acidic properties (Al_2O_3 as acidic support, compared to the inert SiO_2) appeared to improve the Zn Lewis acidity and consequently its tendency to react faster with the other vulcanization agents. MgO, due to release of Mg(II) ions in the system, demonstrated to collaborate with Zn in the vulcanization process, increasing the kinetic of the shortening process of poly-sulphide products towards shorter sulphur bridges.

6.1.4 Future perspectives

A deeper study of the ligands exchange procedure needs to be performed, in order to get bare ZnO NPs. In fact, the ligands exchange procedure with $NOBF_4$ was employed to remove organic ligands from ZnO surface, but the reaction did not provide the expected results. Different small variations of the experimental conditions in the procedure (paragraph 6.1.1.3) were tested, such as change of the reaction temperature, time or solvent, without obtaining a full substitution of the ligands, assessed by TGA and FTIR analyses.

Future perspectives will focus on the possible use of different reagents as sources of exchangeable ligands, such as the Meerwein's salt[21-23], trialkyl oxonium salts, that thanks to their superior alkylating character could rapidly and efficiently remove a broad spectrum of native ligand types while leaving the surface of the nanocrystal bare, with weakly coordinating agents as BF_4^- of PF_6^-.

The optimization of this procedure could be interested in order to conclude the present study on the catalyst-support interaction effect, to synthesize supported

ZnO NPs avoiding the thermal treatment that could be responsible for the increased NPs size. Besides, the development of a direct method to get bare ZnO NPs of different sizes could pave the way to the study of the NPs size effect on the vulcanization reaction.

By reducing the particles size, a higher surface contact of ZnO with the chemical environment is expected and a possible enhancement of ZnO availability and catalytic activity achievable. Several examples are reported in the literature, in which the reduction of catalysts NPs size was claimed to improve their catalytic performances[24,25]. Nevertheless, in previous studies, detrimental effects were reported with very small metal NPs (such as Pt), applied as catalysts for gas-phase reactions[26,27]. As an example, 1 nm Pt NPs were less active compared to 3 nm Pt NPs in the hydrogen oxidation reaction, probably due to modified edge/facets sites ratios in the NPs[26].

In the case of ZnO NPs, decreasing NPs size would imply a modification of the number of surface atoms available in the reaction, the speciation of surface defects and the exposed surface faces of the NPs. In fact, ZnO NPs are generally characterized by surface oxygen and zinc defects, whose formation and amount strictly depend on the synthetic conditions[28,29]. Moreover, different surface exposed faces ratios can be achieved, with terminal polar (001) and (001) faces the more active surfaces than the non-polar surfaces perpendicular to them (i.e. 100, 101)[30,31]. All these parameters could contribute to differentiate the catalytic activity of different sized ZnO NPs. So far, luminescence properties and photocatalytic activity were discussed in the presence of ZnO NPs with different size[32-35]; thus, synthesis of nanostructures similar in morphology but with different crystallite sizes have shown a great importance on disclosing the effects of size on ZnO NPs performances. Nevertheless, no indications are reported in the literature about ZnO NPs size effect in the vulcanization process.

6.2 Effect of structural parameters on ZnA-SiO₂ reactivity

The reactivity of ZnA-SiO$_2$ strictly depends on the availability and reactivity of Zn(II) centres. These two parameters, determined by the chemical neighbourhood of Zn(II) centres, can be suitably tuned by changing both steric and electronic properties of Zn(II), which in turn are related to the type of coordination that these Zn(II) centres develop with the anchoring agents to SiO$_2$ surface. A modification of the functional groups that interact with Zn(II) to create the isolated metal centres distributed onto SiO$_2$, could produce a change in the coordination of Zn(II) and consequently in their stability, availability and reactivity. This change can be particularly important in first phase of the reaction: in fact, the highly availability of Zn(II) centres has already demonstrated to strongly reduce the scorch time of the vulcanization reaction of rubber NCs. By tuning the availability of Zn(II) centres, higher scorch times could be achieved, solving one main technological problem related to the management of rubber NCs.

As a result, APTES, used in Chapter 2 for the synthesis of ZnA-SiO$_2$, was here substituted by two other silane molecules, having different terminal functional groups (Figure 6.16).
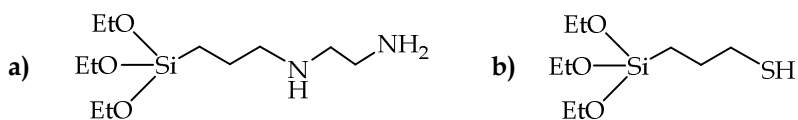
Figure 6.16. Two different anchoring agents used to coordinate Zn(II) centres to SiO$_2$, instead of APTES; on the left the structure of N-[3-(Trimethoxysilyl) propyl]ethylendiamine (EDTMS) and on the right the structure of (3-Mercaptopropyl)trimethoxysilane (MPTMS).

A silane with a double amino functionality, N-[3-(Trimethoxysilyl)propyl]ethyl-endiamine (EDTMS, Figure 6.16a), was proposed to verify whether a chelating or bridging coordination could be established between either one or two silane molecules with each Zn(II) centre. It was proposed that for example a chelating coordination of two EDTMS molecules on each Zn centre could favour a higher

stability of Zn(II), that would be less available to react with the other vulcanization agents (Figure 6.17), at least during the first phase of the reaction.
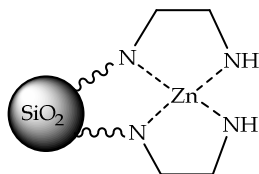
Figure 6.17. Possible coordination that could be promoted in the presence of EDTMS as anchoring agent of Zn(II) centres to SiO_2.

Whereas, the use of a sulphur-based functional group, (3-Mercaptopropyl)tri-methoxysilane (MPTMS), was connected to the possible change of the electronic properties of Zn(II) to tune its reactivity. In fact, there was no reason to suppose that the coordination of Zn(II) centres should change moving from APTES to MPTMS; on the contrary, the presence of a sulphur atom instead of nitrogen, could modify: i) the Lewis acidity of Zn(II) centres, ii) the involved bond energies between the heteroatoms and Zn. These changes could both participating in promoting or slowing down the reactivity of Zn(II) towards the vulcanization reagents.

In the following, the synthesis, characterization and application of these systems as activators of the rubber vulcanization process will be described.

6.2.1 Synthesis of ZnF-SiO$_2$

Materials: the same materials indicated in paragraph 2.2.1 were employed. Instead of APTES, N-[3-(Trimethoxysilyl)propyl]ethylendiamine (($CH_3O)_3$Si $(CH_2)_3NHCH_2CH_2NH_2$ 97%, EDTMS) and (3-mercaptopropyl)trimethoxysilane ($HS(CH_2)_3Si(OC_2H_5)_3$, 95%, MPTMS) were purchased from Sigma Aldrich.

Procedure: first, SiO$_2$ NPs are functionalized with EDTMS and MPTMS. The same functionalization procedure in toluene (120°C, 24h, paragraph 2.2.1) was employed for the preparation of the functionalized samples, labelled as D-SiO$_2$, in the case of EDTMS and M-SiO$_2$ with MPTMS. Only one molar ratio between the silanes and hydroxyl groups of silica was used, equal to 0.50, because this

value has already demonstrated to achieve the highest functionalization degree and high reaction yields with APTES ($A_{0.50}$-SiO_2 paragraph 2.2.2). These materials will be called as F-SiO_2 where F represents the functional agents dispersed on SiO_2. F corresponds to D and M for EDTMS and MPTMS silane respectively, in which D recalls the Double amino functionality and M the Mercaptan group.

With MPTMS, the following additional functionalization procedure was used: in a solution of cyclohexane (50.0 mL) with MPTMS (1.0% vol/vol) and n-propylamine (2.0% vol/vol), 1.0 g of SiO_2 is added. The mixture is left under stirring in reflux conditions (90°C) for 24 h. Later on, the reaction is cooled down and the product recovered through centrifugation, washed twice with fresh hexane and dried in an oven at 80°C. Herein, this sample will be labelled as M_{CH}-SiO_2, where CH means that the reaction was performed in cyclohexane.

In a second step, the functionalized SiO_2 samples were reacted with a Zn precursor, to get the formation of Zn(II) onto the surface of SiO_2, following the same experimental method explained in paragraph 2.2.1. The amount of Zn precursor was varied using different Zn/silane molar ratio, on the basis of the amount of silane molecules anchored to SiO_2 NPs surface (Table 6.4). Here after these samples will be labelled as Zn_YF-SiO_2, where Y is the molar ratios of Zn over silane (n_{Zn}/n_{silane}) and F is the silane, corresponding to D, M or M_{CH} for the three different functionalized SiO_2 samples prepared in the previous step.

Table 6.4. Different Zn/APTES molar ratios tested for each F-SiO_2 sample, where F corresponds to D (EDTMS), M (MPTMS, M_{CH} (MPTMS in cyclohexane) functionalization

	Y (n_{Zn}/n_{APTES})
	0.5
Zn_YF-SiO_2	1.0
	2.0

6.2.2. Characterization of F-SiO$_2$ and Zn$_Y$F-SiO$_2$

The samples were characterized following the previous characterization performed on A$_X$-SiO$_2$ and Zn$_Y$A$_X$-SiO$_2$ samples. First, the effective functionalization of F-SiO$_2$ samples was confirmed by FTIR-ATR on SiO$_2$ powder; besides, TGA and elemental analysis (CHNS) were used to quantify the amount of silane effectively deposited onto the surface of SiO$_2$. These analyses were repeated on the same samples after the treatment with the zinc precursor, to assess that the reaction did not modify the nature of the functionalized samples. Later on, ICP was used to measure the Zn content on Zn$_Y$F-SiO$_2$.

FTIR-ATR spectroscopy. FTIR spectra of D-SiO$_2$, M-SiO$_2$ and M$_{CH}$-SiO$_2$, compared to bare SiO$_2$ confirmed the efficient functionalization of SiO$_2$. In fact, the spectra showed the typical evidences illustrated before for the functionalization of SiO$_2$ surface: i) shift of 954 cm^{-1} peak (Si-OH stretching vibration) to higher wavenumber, due to the partial substitution of surface -OH groups of SiO$_2$; ii) CH$_2$ antisymmetric and symmetric stretching vibrations at 2948 cm^{-1} and 2864 cm^{-1}; iii) in the case of D-SiO$_2$, an additional peak at 1459 cm^{-1} was connected to the secondary amino group of the carbonic chain. In Figure 6.18, as an example, the FTIR spectra of D-SiO$_2$ and M$_{CH}$-SiO$_2$ are shown.
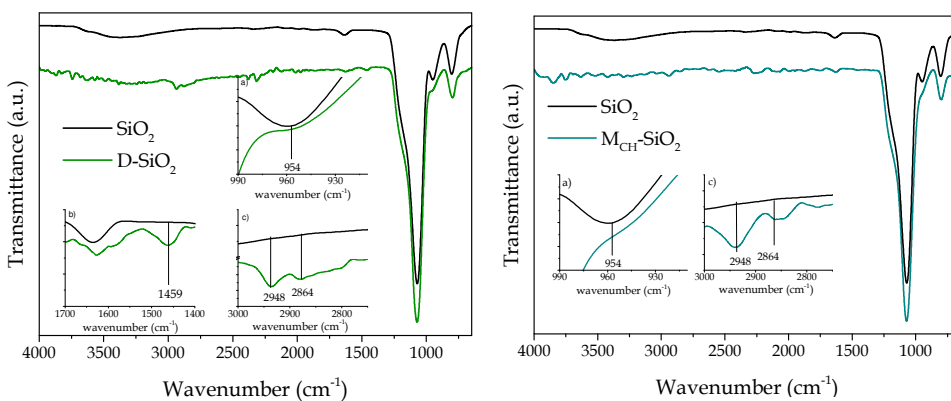
Figure 6.18. FTIR of D-SiO$_2$ (left) and M$_{CH}$-SiO$_2$ (right). In the insets: a) Si-OH stretching, b) NH$_2$ bending (secondary amine), c) antisymmetric and symmetric CH$_2$ stretching.

The FTIR spectra registered on the same samples after the reaction with the Zn precursor were comparable (data not reported), meaning that the reaction did not affect the first functionalization step, both with EDTMS and MPTMS.

TGA and CHNS analysis. Quantification of the amounts of functionalizing agents on SiO_2 surface was calculated starting from the TGA profiles registered between 150 and 1000°C (Figure 6.19), as previously described (paragraph 2.2.2).
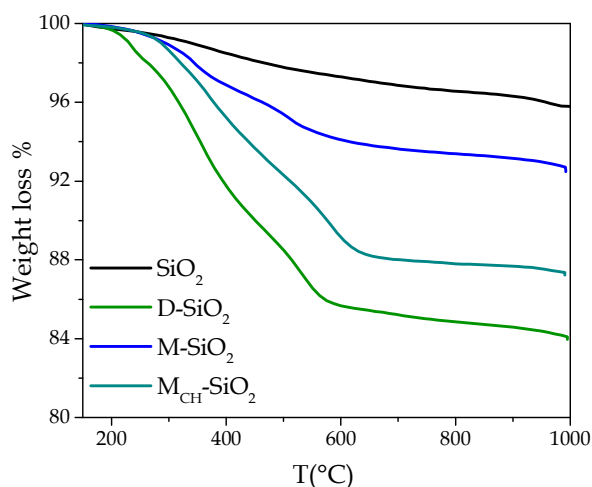
Figure 6.19. TGA profiles of D-SiO_2, M-SiO_2, M_{CH}-SiO_2 samples, compared to bare SiO_2 (black).

The calculated coverage degrees, reaction yields and the estimated number of EDTMS and MPTMS over SiO_2 surface are reported in Table 6.5. Each value is here calculated as the average value of three samples, with the relative standard deviations. From the comparison, D-SiO_2 was characterized by the high reaction yield (90%), whereas M-SiO_2 led to the lower reaction yield, not comparable to D-SiO_2 and A-SiO_2, synthesized in the same reaction conditions. For this reason, SiO_2 functionalization with MPTMS was repeated with another experimental setup (M_{CH}-SiO_2), that guaranteed higher yield value (47%). Both A-SiO_2, D-SiO_2 and M_{CH}-SiO_2 were characterized by a number of silane molecules over SiO_2

surface between 5 and 6 molecules nm^{-2}; these three samples were used for the subsequent reaction with the Zn precursor.

Table 6.5. Experimental weight loss percentages between 150-1000°C measured from TGA profiles of the functionalized SiO_2 with four different silanes and bare silica. From this data, the coverage degrees, reaction yields and an estimation of number of APTES molecules over silica surface were calculated.

Sample	% weight loss (150-1000°C)	Coverage degree (wt %)	Reaction yield	Number of silane molecules/nm²
SiO_2 Rhodia	4.2	-	-	-
$A_{0.50}$-SiO_2	10.4 ± 0.2	7.6 ± 0.2	76	5.2 ± 0.2
NN-SiO_2	15.8 ± 0.1	15.3 ± 0.1	90	6.2 ± 0.1
S-SiO_2	7.2 ± 0.2	3.6 ± 0.2	29	2.0 ± 0.2
S(CH)-SiO_2	12.2 ± 0.2	10.5 ± 0.2	47	5.6 ± 0.2

CHNS analysis gave a further confirmation about SiO_2 functionalization and confirms the quantification performed with TGA. In fact, nitrogen content (N%) calculated from TGA was comparable to the amount measured in the elemental analysis (Table 6.6).

Table 6.6. Weight percentage of nitrogen measured by CHNS analysis and determined through the previous quantification with TGA.

Sample	N% (TGA)	N% (CHNS)	S%(TGA)	S% (CHNS)
SiO_2	0.00	0.03	-	-
$A_{0.50}$-SiO_2	1.78	1.51	-	-
D-SiO_2	4.25	3.74	-	-
M-SiO_2	-	-	3.85	3.62
M_{CH}-SiO_2	-	-	5.34	4.29

TGA and CHNS of the same samples after the interaction with the Zn precursor did not show any significant changes, demonstrating that the samples are not affecting by the second step of the reaction.

ICP analysis. Zn content was evaluated through ICP analysis; three amounts of Zn precursor were tested (Table 6.4) for D-SiO$_2$ and M(CH)-SiO$_2$, to establish the possible coordination that Zn(II) could develop in the presence of the two different ligands. ICP results are reported in Table 6.7.

Table 6.7. Weight percentage of zinc measured by ICP analysis for the Zn$_Y$D-SiO$_2$ and Zn$_Y$M$_{CH}$-SiO$_2$ samples

Samples	Y (n$_{Zn}$/n$_{APTES}$)	Measured Zn (wt%)	Zn (molecules nm^{-2})	Zn/silane (molecules nm^{-2})
Zn$_Y$A$_{0.50}$-SiO$_2$	0.5 1.0 2.0	3.1 ± 0.1	2.58 ± 0.2	0.50
Zn$_Y$D-SiO$_2$	0.5	3.5 ± 0.2	3.58 ± 0.2	0.57
	1.0	5.9 ± 0.2	6.2 ± 0.2	1.00
	2.0	6.6 ± 0.2	7.1 ± 0.1	1.14
Zn$_Y$M$_{CH}$-SiO$_2$	0.5 1.0 2.0	3.3 ± 0.3	2.84 ± 0.2	0.51

The ICP results showed that both APTES and MPTMS favour the deposition of a fixed amount of Zn to SiO$_2$ surface, as the effective Zn weight percentage measured in the presence of the two silanes was always fixed and did not depend on the amount of Zn precursor used in the reaction. The ratio between Zn and silane molecules over SiO$_2$ surface (n. molecules nm^{-2}) was calculated equal to 0.5 for both APTES and MPTMS, suggesting that the two silanes could promote the same Zn(II) coordination. In this hypothesis, as explained in Chapter 2, each Zn(II) would be coordinated to two molecules of APTES or two molecules of MPTMS, with two free positions for each Zn(II) centres. To

synthesize this sample, the stoichiometric amount of Zn precursor (Y = 0.50) was used for further applications.

Whereas, D-SiO$_2$ sample showed a different behaviour: in this case, the Zn content in the sample depended on the amount of Zn precursor (Table 6.7) and the ratios between Zn and EDTMS molecules over SiO$_2$ surface changed for each Zn$_Y$D-SiO$_2$ sample. Zn$_{0.5}$D-SiO$_2$ was characterized by a number of molecules Zn/EDTMS ratio of about 0.5 over the surface, suggesting that each Zn(II) centres is coordinated by two molecules of silane and consequently four nitrogen atoms. A coordination similar to the one proposed in Figure 6.17. was likely formed in this sample. The formation of a structure that involves two EDTMS molecule is reasonable considering the proximity of the silane molecules on SiO$_2$ surface; moreover, the increased chain length of EDTMS (compared to APTES and EDTMS) would favour the higher mobility of silane chains.

Moreover, Zn/silane molecules ratio over silica surface was about 1 for Zn$_{1.0}$D-SiO$_2$ and Zn$_{2.0}$D-SiO$_2$ samples; in these latter two cases, each Zn(II) was suggested to coordinate to one EDTMS molecule, equivalent to two nitrogen atoms. Each EDTMS molecule is supposed to create a chelating coordination to each Zn centres.

Due to the different coordination to Zn(II) centres, Zn$_{0.5}$D-SiO$_2$ was tested as activator in the vulcanization process of rubber NCs, to evaluate whether the stability of Zn(II) centres was increased and the availability decreased. In addition, Zn$_{0.5}$M$_{CH}$-SiO$_2$ was used as activator, to evaluate the possible consequences of the substitution of nitrogen with sulphur both in the Zn reactivity and in the formation of a filler-rubber interaction. The results are reported in the next paragraph.

6.2.3 Vulcanization tests in IR NCs

Materials and procedure: refer to paragraph 3.2. The composites were prepared with a Zn content of 1.49 phr, correspondent to 1.85 phr of ZnO, already used for the preparation of IR NCs, in Chapter 3.

The NCs were labelled as $Zn_{0.5}F-SiO_2/IR$ on the basis of the silane (F) used for SiO_2 functionalization (Table 6.8.). In these NCs, no stearic acid and TESPD were required, due to the intrinsic nature of the activators, as explained before with APTES.

Table 6.8. Composition of $Zn_{0.50}F-SiO_2/IR$ NCs

	F = D			F = M_{CH}		
	Phr	Zn (phr)	SiO_2 (phr)	phr	Zn (phr)	SiO_2 (phr)
$Zn_{0.5}F-SiO_2/IR$	42.5	1.49	35.0	-	-	-
	-	-	-	44	1.49	38.7

Reference NCs were prepared using bare SiO_2 and m-ZnO, keeping constant the Zn content (1.49phr) and adding a suitable amount of SiO_2, in order to have the same SiO_2 content, compared to the tests in the presence of $Zn_{0.50}F-SiO_2/IR$ NCs. The NCs were labelled m-ZnO/IR (K SiO_2) where K is the SiO_2 content, equal to the two NCs reported in Table 6.8. In the reference samples, the addition of TESPD (equal to 8wt% of bare SiO_2) and stearic acid (2phr) was required.

Characterization: the influence of EDTMS and MPTMS in the vulcanization process was preliminarily studied by evaluating the vulcanization curves of IR NCs in the presence of the two materials, in particular considering the possible effect on the scorch time of the reaction, as explained before.

The curves, reported in Figure 6.20., were compared to the respective reference samples, prepared with m-ZnO, but a direct comparison between the moduli values registered for all the different NCs was not possible because of the different SiO_2 content.

$Zn_{0.5}D-SiO_2$ activator promoted a high vulcanization efficiency, with the achievement of high modulus values and a shorter t_{90}, compared to its reference

(Figure 6.20., left). The activator demonstrated a similar behaviour to the same material prepared with APTES, showing that the reactivity of Zn(II) was not decreased with EDTMS. Compared to $Zn_{0.5}A_{0.50}$-SiO_2/IR NC, a small scorch time with $Zn_{0.5}D$-SiO_2/IR was detected: the vulcanization started after ~ 30″, a delay time that was not observed in the case of APTES based material.
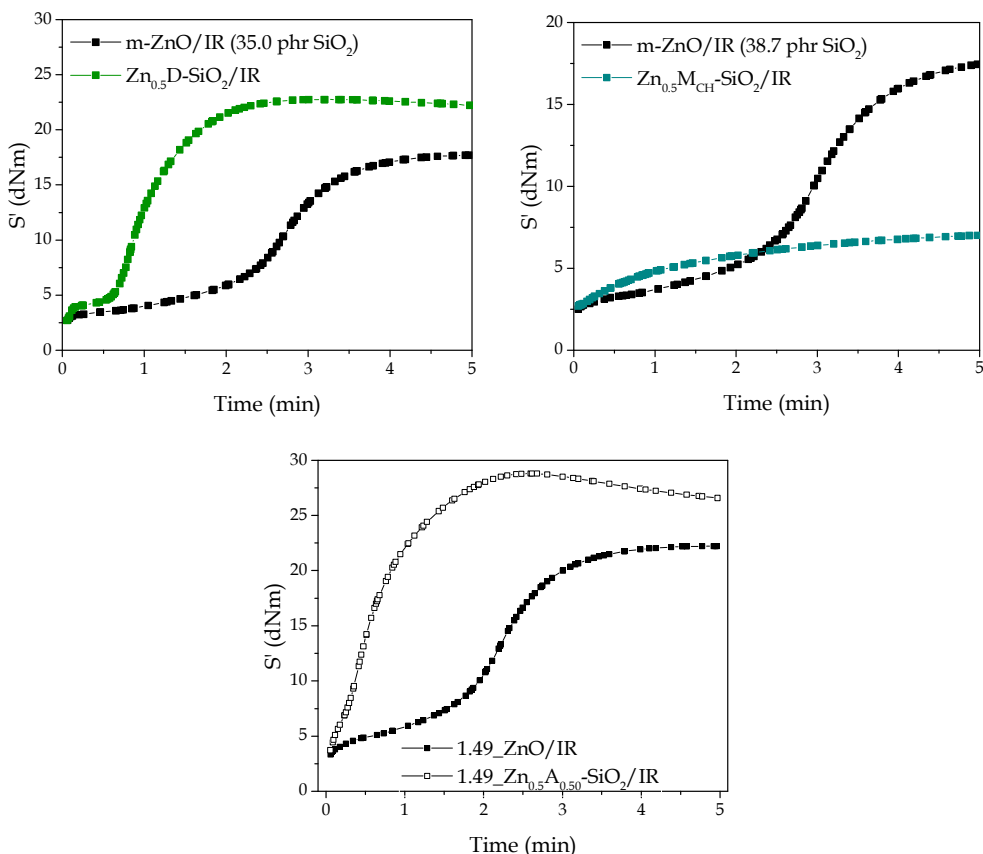
Figure 6.20. Vulcanization profiles measured for $Zn_{0.5}F$-SiO_2/IR NCs and their relative reference NCs, prepared with the same Zn and SiO_2 content. At the bottom, the vulcanization curves of 1.49_$Zn_{0.5}A_{0.50}$-SiO_2/IR and its reference are reported, as a comparison of APTES with the other two anchoring agents.

This observation was consistent with the structure of the two Zn(II)-based materials: when APTES is used as anchoring agent, the presence of two free positions on Zn(II) guarantees the high availability of Zn(II) to interact with the vulcanization agents; the reaction can start as soon as the vulcanization

temperature is reached, and the cross-linking formation suddenly increases. In the case of EDTMS, the chelating coordination of four nitrogen atoms on each Zn(II), forms a more closed structure around Zn(II) and reduces their availability at the beginning of the reaction, due to a less favourable steric neighbourhood around Zn(II) centres, that hinders the approach by the other vulcanization agents. At high temperature, the mobility of the chains of anchoring agents increases and the closed structure around Zn(II) centres can assume different conformations, so that Zn(II) may become more available to the reaction during the process.

Instead, the vulcanization curves of $Zn_{0.5}M_{CH}$-SiO_2/IR were less performant than the reference sample; in this case, the vulcanization profile was typical of a system in which the vulcanization did not take place through the classical ionic mechanism that involves Zn(II), but only a radical process happened. Thus, the addition of a sulphur-based anchoring agent instead of an amino-based agent has strongly modified the Zn reactivity. Different hypotheses could be formulated: on the one hand, the sulphur ligand could have changed the electronic properties of Zn, reducing its affinity towards the other vulcanization reagents; on the other hand, the introduction of an additional sulphur source in the rubber NCs could have modified the interaction inside the rubber matrix, with the formation of additional filler-rubber interactions that could have isolated the zinc centres, thus reducing their availability and reactivity in the overall reaction. These hypotheses need to be further studied and validated trough suitable MCV studies, that could clarify possible different mechanisms involved in the reaction.

6.2.4. Summary of the effect of structural parameters on ZnA-SiO$_2$ reactivity

The use of different anchoring agents for the formation of Zn(II) centres on SiO$_2$ surface was carried out to study the possible effects on Zn stability, availability and reactivity in the vulcanization reaction. A special focus was dedicated to the

tunability of the scorch time of the reaction, an industrial issue of $Zn_Y A_X$-SiO_2 material, due to the low handling time of the correspondent rubber NC, characterized by an extremely low scorch time.

EDTMS and MPTMS were used as possible different anchoring agents, that could promote various structural and electronic properties on Zn(II) centres and consequently tunable Zn(II) availability during the reaction. The use of these functionalizing agents has shown to play a fundamental role in the determination of Zn(II) availability.

First, optimized functionalization processes with EDTMS and MPTMS were developed on SiO_2, with coverage degrees similar to the one achieved with $A_{0.50}$-SiO_2. The treatment with Zn precursor allowed the formation of Zn(II) centres on the surface of SiO_2, as observed with APTES. EDTMS materials showed that different Zn(II) coordination structures could be originated by treating D-SiO_2 with different amount of Zn precursor (ICP analysis). $Zn_{0.5}D$-SiO_2 sample, in which a coordination 1:4 between Zn and nitrogen atoms was calculated, was used as activator for the rubber vulcanization process, leading to an increased scorch time, connected to the low availability of Zn(II) in the first phases of the reaction.

Also MPTMS caused different reactivity of Zn(II) centres during the reaction, even though deeper investigation on the structural and electronic properties of Zn(II) centres are required to give an univocal explanation on the different behaviour of Zn(II) in this system.

6.3 Bibliography

1.   Cargnello, M., Montini, T., Smolin, S. Y., Priebe, J. B., Delgado Jaén, J. J., Doan-Nguyen, V. V. T., McKay, I. S., Schwalbe, J. A., Pohl, M.-M., Gordon, T. R., *and others*. Engineering titania nanostructure to tune and improve its photocatalytic activity. *Proc. Natl. Acad. Sci.* **113**, 3966–3971 (2016).

2.   Cargnello, M., Fornasiero, P. & Gorte, R. J. Opportunities for tailoring catalytic properties through metal-support interactions. *Catal. Letters* **142**, 1043–1048 (2012).

3.   Murata, K., Mahara, Y., Ohyama, J., Yamamoto, Y., Arai, S. & Satsuma, A. The Metal-

Support Interaction Concerning the Particle Size Effect of Pd/Al $_2$ O $_3$ on Methane Combustion. *Angew. Chemie* **129**, 16209–16213 (2017).

4.   Cargnello, M., Doan-Nguyen, V., Gordon, T., Diaz, R., Stach, E., Gorte, R., Fornasiero, P. & Murray, C. Control of Metal Nanocrystal Size Reveals Metal-Support Interface Role for Ceria Catalysts. *Science (80-.).* **341**, 771–773 (2013).

5.   Jiménez-Morales, I., Cavaliere, S., Jones, D. & Rozière, J. Strong metal-support interaction improves activity and stability of Pt electrocatalysts on doped metal oxides. *Phys. Chem. Chem. Phys.* **20**, 8765–8772 (2018).

6.   Venezia, A. M., La Parola, V., Pawelec, B. & Fierro, J. L. G. Hydrogenation of aromatics over Au-Pd/SiO2-Al2O3catalysts; Support acidity effect. *Appl. Catal. A Gen.* **264**, 43–51 (2004).

7.   Roy, K., Alam, M. N., Mandal, S. K. & Debnath, S. C. Preparation of zinc-oxide-free natural rubber nanocomposites using nanostructured magnesium oxide as cure activator. *J. Appl. Polym. Sci.* **132**, 1–7 (2015).

8.   Guzman, M., Reyes, G., Agullo, N. & Borros, S. Synthesis of Zn/Mg oxide nanoparticles and its influence on sulfur vulcanization. *J. Appl. Polym. Sci.* **119**, 2048–2057 (2011).

9.   Thanh, N. T. K., Maclean, N. & Mahiddine, S. Mechanisms of nucleation and growth of nanoparticles in solution. *Chem. Rev.* **114**, 7610–7630 (2014).

10.   Lamer, V. K. & Dinegar, R. H. Theory, Production and Mechanism of Formation of Monodispersed Hydrosols. *J. Am. Chem. Soc.* **72**, 4847–4854 (1950).

11.   Polte, J. Fundamental growth principles of colloidal metal nanoparticles - a new perspective. *CrystEngComm* **17**, 6809–6830 (2015).

12.   Bu, W., Chen, Z., Chen, F. & Shi, J. Oleic acid/oleylamine cooperative-controlled crystallization mechanism for monodisperse tetragonal bipyramid nala(moO4)2nanocrystals. *J. Phys. Chem. C* **113**, 12176–12185 (2009).

13.   Ludi, B. & Niederberger, M. Zinc oxide nanoparticles: Chemical mechanisms and classical and non-classical crystallization. *Dalt. Trans.* **42**, 12554–12568 (2013).

14.   De Mello Donegá, C., Liljeroth, P. & Vanmaekelbergh, D. Physicochemical evaluation of the hot-injection method, a synthesis route for monodisperse nanocrystals. *Small* **1**, 1152–1162 (2005).

15.   Cozzoli, P. D., Snoeck, E., Garcia, M. A., Giannini, C., Guagliardi, A., Cervellino, A., Gozzo, F., Hernando, A., Achterhold, K., Ciobanu, N., *and others*. Colloidal synthesis and characterization of tetrapod-shaped magnetic nanocrystals. *Nano Lett.* **6**, 1966–1972 (2006).

16.   Viswanatha, R., Sapra, S., Satpati, B., Satyam, P. V, Dev, B. N. & Sarma, D. D. Understanding the quantum size effects in ZnO nanocrystals. *J. Mater. Chem.* **14**, 661–668 (2004).

17.   Zhang, Z., Liu, S., Chow, S. & Han, M. Y. Modulation of the morphology of ZnO nanostructures via aminolytic reaction: From nanorods to nanosquamas. *Langmuir* **22**, 6335–6340 (2006).

18.   Dong, A., Ye, X., Chen, J., Kang, Y., Gordon, T., Kikkawa, J. M. & Murray, C. B. A generalized ligand-exchange strategy enabling sequential surface functionalization of colloidal nanocrystals. *J. Am. Chem. Soc.* **133**, 998–1006 (2011).

19.   Greasley, S. L., Page, S. J., Sirovica, S., Chen, S., Martin, R. A., Riveiro, A., Hanna, J. V., Porter, A. E. & Jones, J. R. Controlling particle size in the Stöber process and incorporation of calcium. *J. Colloid Interface Sci.* **469**, 213–223 (2016).

20. Cargnello, M., Chen, C., Diroll, B. T., Doan-Nguyen, V. V. T., Gorte, R. J. & Murray, C. B. Efficient removal of organic ligands from supported nanocrystals by fast thermal annealing enables catalytic studies on well-defined active phases. *J. Am. Chem. Soc.* **137**, 6906–6911 (2015).

21. Rosen, E. L., Buonsanti, R., Llordes, A., Sawvel, A. M., Milliron, D. J. & Helms, B. A. Exceptionally mild reactive stripping of native ligands from nanocrystal surfaces by using Meerwein's salt. *Angew. Chemie - Int. Ed.* **51**, 684–689 (2012).

22. Milliron, D. J., Buonsanti, R., Llordes, A. & Helms, B. A. Constructing functional mesostructured materials from colloidal nanocrystal building blocks. *Acc. Chem. Res.* **47**, 236–246 (2014).

23. Papadas, I. T., Vamvasakis, I., Tamiolakis, I. & Armatas, G. S. Templated Self-Assembly of Colloidal Nanocrystals into Three-Dimensional Mesoscopic Structures: A Perspective on Synthesis and Catalytic Prospects. *Chem. Mater.* **28**, 2886–2896 (2016).

24. Lu, Y. & Chen, W. Size effect of silver nanoclusters on their catalytic activity for oxygen electro-reduction. *J. Power Sources* **197**, 107–110 (2012).

25. Reske, R., Mistry, H., Behafarid, F., Cuenya, B. R. & Strasser, P. Particle Size Effects in the Catalytic Electroreduction of CO 2 on Cu Nanoparticles. **6986**, 4–12 (2014).

26. Sun, Y., Dai, Y., Liu, Y. & Chen, S. A rotating disk electrode study of the particle size effects of Pt for the hydrogen oxidation reaction. *Phys. Chem. Chem. Phys.* **14**, 2278–2285 (2012).

27. Tan, T. L., Wang, L. L., Zhang, J., Johnson, D. D. & Bai, K. Platinum nanoparticle during electrochemical hydrogen evolution: Adsorbate distribution, active reaction species, and size effect. *ACS Catal.* **5**, 2376–2383 (2015).

28. Schmidt-Mende, L. & MacManus-Driscoll, J. L. ZnO - nanostructures, defects, and devices. *Mater. Today* **10**, 40–48 (2007).

29. Zhang, X., Qin, J., Xue, Y., Yu, P., Zhang, B., Wang, L. & Liu, R. Effect of aspect ratio and surface defects on the photocatalytic activity of ZnO nanorods. *Sci. Rep.* **4**, 4–11 (2014).

30. McLaren, A., Valdes-Solis, T., Li, G. & Shik, C. T. Shape and size effects of ZnO nanocrystals on photocatalytic activity. *J. Am. Chem. Soc.* **131**, 12540–12541 (2009).

31. Boppella, R., Anjaneyulu, K., Basak, P. & Manorama, S. V. Facile synthesis of face oriented ZnO crystals: Tunable polar facets and shape induced enhanced photocatalytic performance. *J. Phys. Chem. C* **117**, 4597–4605 (2013).

32. Joo, J., Kwon, S. G., Yu, J. H. & Hyeon, T. Synthesis of ZnO nanocrystals with cone, hexagonal cone, and rod shapes via non-hydrolytic ester elimination sol-gel reactions. *Adv. Mater.* **17**, 1873–1877 (2005).

33. Zhou, J., Zhao, F., Wang, Y., Zhang, Y. & Yang, L. Size-controlled synthesis of ZnO nanoparticles and their photoluminescence properties. *J. Lumin.* **122–123**, 195–197 (2007).

34. Kalita, A. & Kalita, M. P. C. Effects of size reduction on microstructural, optical, vibrational, magnetic and photocatalytic properties of ZnO nanocrystals. *Mater. Charact.* **137**, 109–118 (2018).

35. Li, G. R., Hu, T., Pan, G. L., Yan, T. Y., Gao, X. P. & Zhu, H. Y. Morphology-function relationship of ZnO: Polar planes, oxygen vacancies, and activity. *J. Phys. Chem. C* **112**, 11859–11864 (2008).

7

Applications
of the innovative activators
to different systems

In this last chapter, different applications of the innovative activators were evaluated.

In the first part, the growth of ZnO NPs and Zn(II) centres was studied on elongated silica particles and natural supports, as layered silicates. These systems, thanks to their intrinsic anisotropic character, are industrially employed as reinforcing filler. The combination of the anisotropy effect and of a more efficient vulcanization promoted by innovative activators is here preliminary investigated.

In the second section, the use of Zn(II) based activators was studied in a polymeric matrix, in which organic functionalities were previously added to the organic chains. The presence of organic functional groups is connected to the necessity to improve the filler-rubber interaction in the NCs; especially in silica filled NCs, the addition of compatibilizing agents to the filler NPs (as TESPD) can be substituted by suitable organic functionalities on the polymer chains, that could increase the compatibilization between the two phases. The presence of metal centres (Zn(II)) supported on SiO_2 surface is here studied as a possible way to further improve the interactions between filler NPs and rubber chains.

7.1 Anisotropic fillers as supports for zinc-based activators

The characteristics of fillers that mainly influence the properties of NCs are the dimension of the primary particles, the specific surface area, the chemical surface nature of particles and the structure of aggregates and agglomerates. Nowadays, the use of nanofiller, compatibilized with suitable compatibilizing agents to increase the affinity with the polymer chains, able to form a filler networking inside the NC, is spread all over the world in the rubber industries. Together with these parameters, recently a main role was assigned to the shape and morphology of filler NPs: Scotti *et al.*[1,2], synthesized shape controlled silica NPs with different aspect ratio (AR, equal to 1, 3, 5, 7), using a sol-gel approach, showing that the intrinsic anisotropy of these particles and their alignment in the rubber matrix could promote high percentage of immobilized rubber at the filler-rubber interface, with a consequent high reinforcement degree in the NC.

In this *scenario*, with the aim of exploiting materials already available in the nature, several studies have been done on the use of clay-layered silicates (LS) as filler for rubber NCs. The employment of materials naturally available has become nowadays an added value for the production processes of industries, including rubber industries for tyre applications. Natural layered silicates are a typical example of natural resources that can be used in rubber industries as highly reinforcing fillers. The interest in these materials is connected to: i) low environmental impact (environmentally friendly materials); ii) easy availability in nature; iii) high amount available; iv) reduced costs.

The possible use of elongated filler NPs (both SiO_2 NPs with high AR and LS) as supports for the Zn-based activators arose because of the possibility to develop high reinforced materials, that can simultaneously promote highly efficient vulcanization processes, thanks to the innovative activators studied in this Thesis. The synthesis of the "next generation double function fillers" was here considered, in order to mix the advantages coming from the intrinsic anisotropy

of filler NPs and the high reactivity of the Zn-based activators in determining the properties of rubber NCs.

In the following a brief introduction about natural layered silicates is illustrated, especially focusing on sepiolite, used for the present study. Later on, the synthesis of the materials, their full characterization and their application as double function fillers in the formulation of rubber NCs is described. The effects on the vulcanization efficiencies and the mechanical properties of rubber NCs are shown.

7.1.1 A natural layered silicate: sepiolite

Clays are a class of minerals with a general chemical formula $(Ca, Na, H)(X)_2(Si, Al)_4O_{10}(OH)_{2-n}H_2O^3$, where X is a metal like Al, Mg, Fe, Zn; they are composed of fine-grained particles, with a spherical diameter less than 2 µm and include natural and synthetic clays (such as mica, bentonite, etc.). Most of clays belong to the category of LS or phyllosilicates as they are composed of alternating sheets of tetrahedral SiO_2 and octahedral layers of XO_6 in a 1:1 ratio, such as halloysite and kaolinite, or 2:1 ratio such as montmorillonite and sepiolite (Sep).

Sepiolite is a magnesium layered silicate with a chemical formula $Mg_8Si_{12}O_{30}(OH)_4(H_2O)_4 \cdot 8H_2O$, characterized by high surface area (up to 300 m^2 g^{-1}), thanks to the structural periodic interval along *b*-axis and microporous tunnels along *c*-axis with a dimension of 0.37x1.06 nm. It is characterized by an organized structure in two-dimensional sheets (continuous in one direction) based on tetrahedral silica, that include a central MgO sheet, in an octahedral configuration. In the third direction, the sheets show a thickness of about 1.34 nm, sharing the edges with the closest sheets and producing a structural pattern known as "checkboard". As the sheets are covalently bonded, they cannot be exfoliated, as it usually happens after the interaction between polymer and LSs; in general, intercalated or exfoliated structures are formed with LSs, depending on the length of the organic chains and their dispositions in the interlayer space,

giving rise to different degree of intercalation[4] and therefore different spacing of the layers.

In general, the 2:1 type of LSs are characterized by a moderate negative surface charge, due to the partial replacement of Si^{4+} for Al^{3+} in the tetrahedral sheets and Al^{3+} for Mg^{2+} in octahedral sheets. To counterbalance the excess of negative charges, positive charges are usually distributed in the tunnels and they can be exchanged by bulkier organic cations, typically alkyl ammonium ions, that represents the principal approach to disperse the clay nanofillers in polymer matrix. Nevertheless, due to the low cationic exchange concentration (CEC) of sepiolite, the possibility to functionalize this material with the traditional ways used for LSs is limited; on the contrary, the silica layer at regular intervals in the *b*-axis undergoes an inversion of the tetrahedral sheets[5]. It results in the presence of silanol groups at the edge of the channels and makes Mg^{2+} exposed to the external surface. About 33% of the total amount of Mg^{2+} in pristine sepiolite is supposed to be exposed[6].

The elemental particles of sepiolite appears as tiny fibers 1-10 µm length and 40-150 nm width (Figure 7.1.); these fibers are usually stick together in bundles with a diameter between 0.1 and 1 µm, forming randomly-oriented aggregates (10-100 µm). These peculiar dimensions give rise to highly anisotropic systems (high Aspect Ratios), that make sepiolite one of the main LS materials usable in the nano-filler role in rubber NCs. Rubber-sepiolite NCs represent one possible attractive alternative to improve the microscopic properties of polymers, such as rigidity, wear resistance and hardness, without changing any parameters in the present processing technologies used in tyres industries.
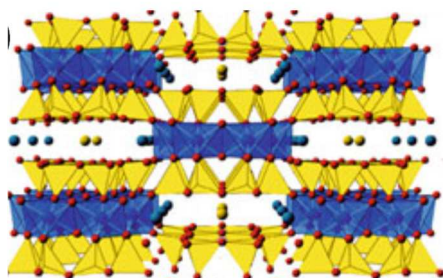
Figure 7.1. Fibrous structure of Sep.

In this work, Sep Pangel S9 (SepS9) was supplied by Tolsa and extracted from the landfill of Vallecas (Spain).

In the following, the possible use of sepiolite, together with silica anisotropic NPs as support for the development of the "next generation double function fillers" was studied.

7.1.2 Synthesis of Zn-based activators supported onto anisotropic fillers

The growth of ZnO NPs and Zn(II) centres on the surface of anisotropic supports (anisotropic SiO_2 and SepS9) is here described.

First, SiO_2 spherical (AR=1) and anisotropic NPs (AR=5) were synthesized using a procedure reported in the literature[7]. Later on, the synthesized SiO_2 NPs were used together with SepS9, as supports for ZnO NPs and Zn(II) centres growth.

7.1.2.1 Synthesis of SiO₂ NPs

SiO_2 NPs (AR=1,5) were prepared through a sol-gel approach, based on a co-condensation reaction of molecular precursors, mediated by a surfactant in the role of the Structure Directing Agent (SDA).

Materials: tetraethyl orthosilicate (TEOS, 99%), (3-mercaptopropyl)trimethoxy-silane (MPTMS, 95%), and cetyltrimethylammoniumbromide (CTAB, 98%) were purchased from Sigma Aldrich and were used without further purification. Milli-Q water was used with a resistivity 418.2 MΩ·cm.

Procedure: for the synthesis of 7 g of SiO_2 NPs: in a solution of 14 mL of NaOH 2 M and 1920 mL of Milli-Q water, 4 g of CTAB (SDA) are dissolved at 60°C. After 30 min of vigorous stirring (necessary for the achievement of a homogeneous temperature in the reaction solvent), 24 mL of TEOS and a suitable amount of MPTMS (0, 2.0 mL, for SiO_2 NPs with AR=1 and AR=5, respectively) are added. MPTMS molecules are deprotonated by the basic solution and as anions substitutes the bromide ions of CTAB micelles; this interaction was crucial to get a structural control on SiO_2 NPs growth. After 2 h the mixture is filtered and the powder dispersed in a solution of 40 mL of HCl (37 wt%) and 300 mL of ethanol, to remove the surfactant; the mixture is left under stirring for 24 h at 60°C (reflux). A further washing step is performed in the same experimental condition for 2 h; 98% of CTAB removal was guaranteed from the literature. Then, the precipitated silica is re-suspended in water (5.0 wt%) and the slurry equilibrated to pH 7.0 ± 0.2 by small amounts of ammonium hydroxide. Finally, silica powder is filtered and dried in an oven at 120°C for 24 h.

Hereafter the different shaped silica particles will be labelled SiO_2-X where X refers to the different aspect ratios of the silica particles (X=1 spherical shape; X = 5 rod-like shape, with AR=5).

7.1.2.2. Synthesis of ZnO NPs on anisotropic filler supports

ZnO NPs were synthesized on the surface of SiO_2-1, SiO_2-5 and SepS9.

Materials and procedure: refer to paragraph 2.1.1. Only samples with a ZnO loading on the supports equal to 10wt% were prepared (Table 2.2). The samples are labelled as ZnO/Z, where Z is the support used (SiO_2-1, SiO_2-5 and SepS9).

With sepiolite an additional initial step in a basic environment was performed, to remove the impurities and enhance the number of surface hydroxyl groups of sepiolite, activating the material: in a typical procedure, 1g of SepS9 is dispersed in 50 mL of NaOH solution (0.01 M) and left under stirring at room temperature for 24h. The powder is recovered through centrifugation, re-dispersed in H_2O to remove NaOH residual concentration and again re-centrifuged. The washing

treatments are repeated until the pH of the surnatant is 7.0 ± 0.2. The final SepS9 is dried using the freeze-drying method.

7.1.2.3 Synthesis of Zn(II) centres on anisotropic filler supports

Zn(II) centres were synthesized on the surface of SiO_2-1, SiO_2-5 and SepS9.

Materials and procedure: refer to paragraph 2.2.1. In the first step, the anisotropic supports were functionalized with APTES, using a molar ratio APTES over hydroxyl groups of the supports (n_{APTES}/n_{OH}) equal to 0.50. This APTES content has already shown the highest coverage degree, with high reaction yields. n_{OH} were previously calculated for each support, through a TGA analysis of the bare support.

In the second step, the reaction with Zn precursor was performed using a molar ratio of Zn over APTES molecules (n_{Zn}/n_{APTES}) equal to 0.5.

The samples are labelled as ZnA-Z, where Z is the support used in the reaction (SiO_2-1, SiO_2-5 and SepS9).

7.1.3 Characterization of Zn-based activators supported onto anisotropic fillers

The effective formation of ZnO NPs and Zn(II) centres onto the three different supports (SiO_2-1, SiO_2-5 and SepS9) and their relative structural properties are studied in this paragraph.

The characterization techniques reflected the same methods used for the characterization of ZnO NPs and Zn(II) grown on bare SiO_2 Rhodia (Chapter 2).

7.1.3.1 Characterization of ZnO NPs on anisotropic fillers

The characterization of ZnO NPs on anisotropic supports (10wt%) is here reported. SiO_2-1 is here shown as a reference sample with a high porosity. The samples were characterized to confirm the identity of the synthesized materials, as done in paragraph 2.1.3. The quantification of ZnO was measured with ICP-AES; structural, optical and morphological characterizations of ZnO NPs on

SiO$_2$ were performed with FTIR-ATR spectroscopy and XRD diffraction, UV-Vis reflectance and TEM analysis, respectively. In addition, due to the high porosity of the systems, the specific surface areas were measured before and after the reaction with Zn precursor.

ICP-AES. The Zn contents, determined through ICP-AES analysis, are shown in Table 7.1 with the different supports. In all the three samples, the effective ZnO loading is about 10wt% and the reaction yields over 80%, as expected. The same reaction conditions used for SiO$_2$ Rhodia could be translated to other systems, without changing the reaction performances.

Sample	Nominal ZnO wt%	Effective ZnO wt%	Reaction yield (%)
ZnO/SiO$_2$-1	12.2	10.4	**85**
ZnO/SiO$_2$-5	12.2	9.8	**81**
ZnO/SepS9	12.2	10.5	**86**

Table 7.1. ZnO wt% measured through ICP-AES for SiO$_2$-1, SiO$_2$-5 and SepS9 supports loaded with ZnO NPs.

FTIR spectroscopy. The FTIR-ATR spectra of ZnO/SiO$_2$-1 and ZnO/SiO$_2$-5 confirmed the effective presence of NPs bond to the surface of SiO$_2$. As shown with ZnO NPs loaded on SiO$_2$ Rhodia, FTIR spectra presented a typical shift of the Si-OH stretching vibration (954 cm^{-1}) of bare SiO$_2$, towards lower wavenumbers (~ 965 cm^{-1}). As illustrated in Figure 7.2, this peak became a shoulder of the main peak at 1050 cm^{-1}, due to a partial substitution of surface OH groups with a Si-O-Zn bond. In SiO$_2$-5 the peaks at ~ 2950 cm^{-1} and 2840 cm^{-1} were probably connected to some residual MPTMS used in the synthetic conditions, that disappeared after ZnO NPs reaction formation.
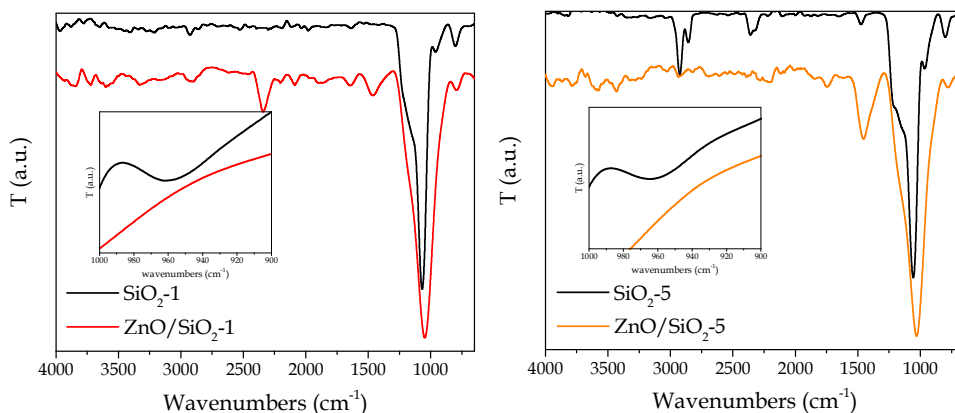
Figure 7.2. FTIR spectra of ZnO/SiO₂-1 and ZnO/SiO₂-5, compared to the respective bare SiO₂.

FTIR gave also a confirmation of ZnO NPs deposition on SepS9: FTIR-ATR spectra of ZnO/SepS9 was characterized by the strong reduction of signals at 3762-3578 cm⁻¹, compared to bare SepS9, assigned to the presence of OH groups in the octahedral sheet and the OH stretching vibration in the external surface of sepiolite[8]. The reduction of these peaks' intensities can be partially ascribed to a substitution of surface hydroxyl groups with a Si-O-Zn bond, analogously to SiO₂ supports.

Figure 7.3. FTIR spectra of ZnO/SepS9, compared to the respective bare SepS9.

XRD. The structural characterization of ZnO/SiO_2-1 and ZnO/SiO_2-5 proved that at this ZnO loading on SiO_2, amorphous ZnO NPs are formed (Figure 7.4), as observed on SiO_2 Rhodia. Nevertheless, traces of peaks related to the crystalline ZnO wurtzite phase are here detected, testifying the partial formation of ZnO crystalline NPs on these supports.
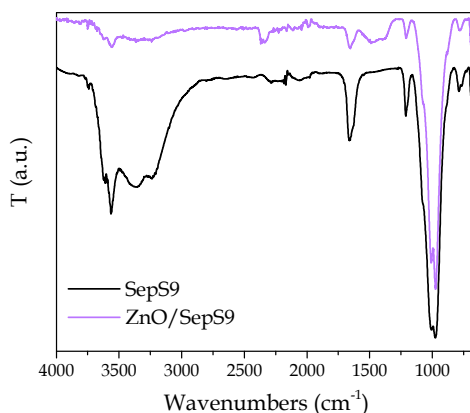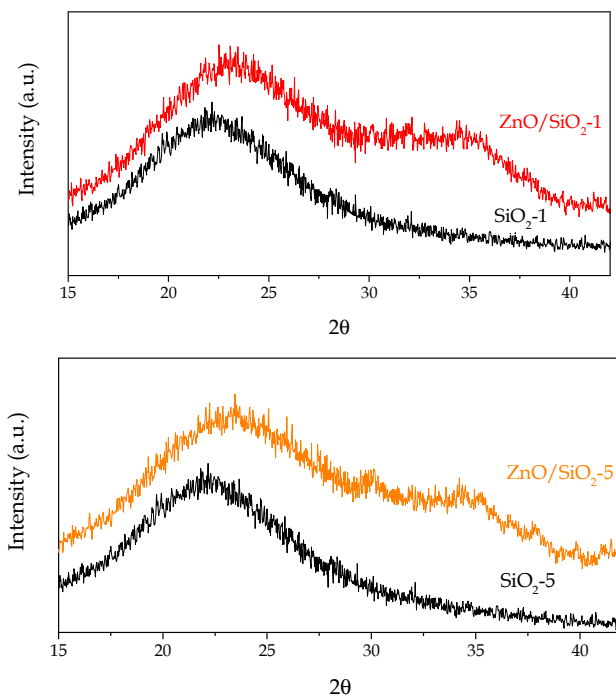

Figure 7.4. XRD spectra of ZnO-SiO₂-1 and ZnO-SiO₂-5, compared to the respective bare SiO₂.

On ZnO/SepS9 diffractogram, the presence of two additional peaks at 32° and 47° compared to SepS9, was evidenced. These peaks can be attributed to the crystallographic planes (100) and (102) of crystalline ZnO. Due to their low intensities, a possible suggestion is that both crystalline and amorphous ZnO NPs are formed on sepiolite surface. The formation of crystalline ZnO NPs is probably connected to the intrinsic crystallinity of SepS9, opposed to the amorphous character of SiO_2

Figure 7.5. XRD of ZnO/SepS9 and SepS9.

UV-Vis spectroscopy. In the UV-Vis reflectance spectra, the presence of the typical absorption edge of ZnO with all the three supports confirmed the formation of ZnO in all the cases (spectra not reported). The band gap values of ZnO, calculated starting from the UV-Vis profiles, using the Kubelka-Munk method[9], suggested that the size of ZnO is nanometric (higher band g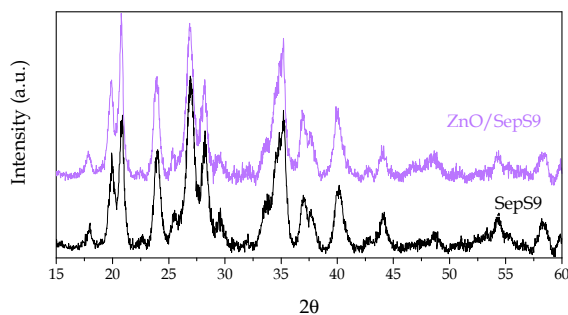ap values, compared to m-ZnO, ~ 3.2eV) and that the NPs are all characterized by the similar size (similar band gap values, Table 7.2).

Table 7.2. Band gap values of ZnO NPs supported on the three different supports, calculated from the UV-Vis reflectance spectroscopy

Sample	Band gap (eV)
ZnO/SiO$_2$-1	3.39
ZnO/SiO$_2$-5	3.40
ZnO/SepS9	3.33

Morphology study: TEM. TEM images of ZnO NPs supported on SiO$_2$-1, SiO$_2$-5 and ZnO/SepS9 (Figure 7.6) showed amorphous ZnO NPs in all the samples, with a size of 5-6 nm. Only in ZnO/SiO$_2$-5 and ZnO/SepS9 some crystalline NPs were evident, due to the crystalline planes assigned to wurtzite crystalline phase. A good distribution was evidenced especially in ZnO/SepS9, where

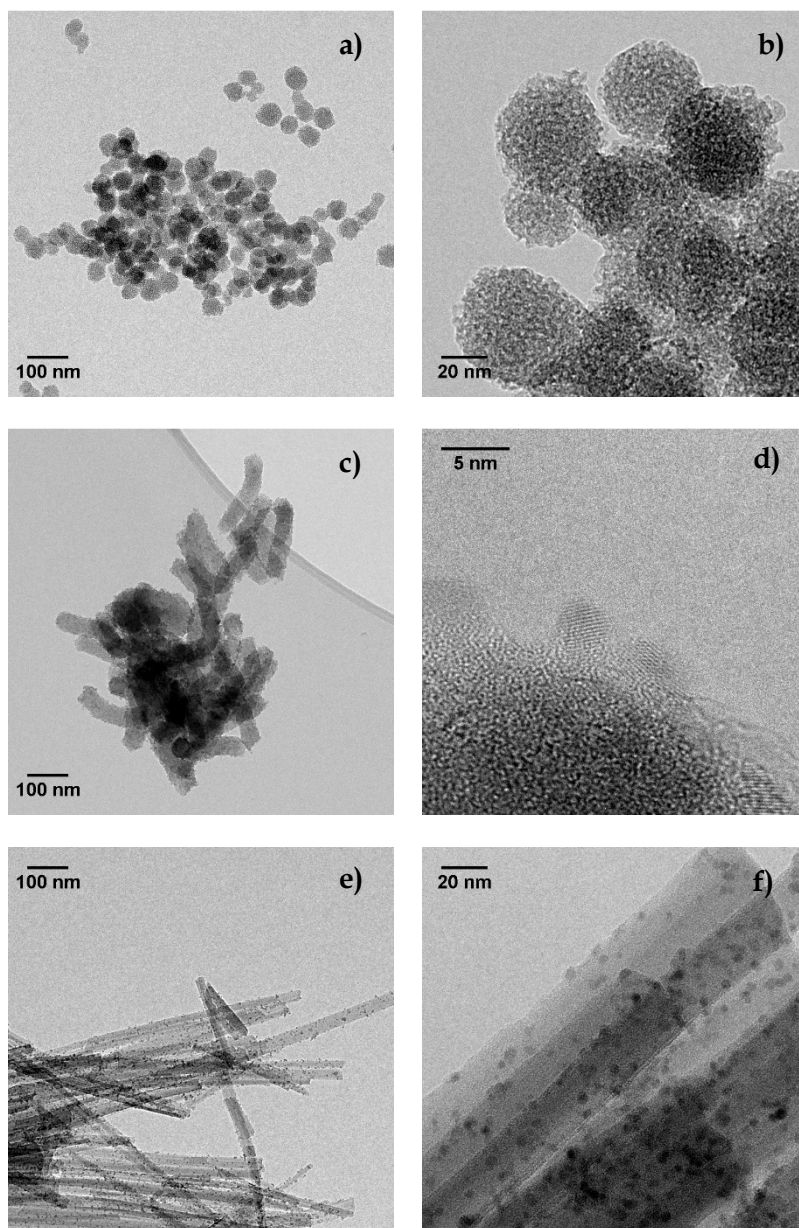small ZnO NPs were highlighted all over the surface of sepiolite fibres (Figure 7.6 e, f).

Figure 7.6. TEM images of ZnO/SiO$_2$-1 (a, b), ZnO/SiO$_2$-5 (c, d) and ZnO/SepS9 (e, f), at low magnification (left) and high magnification (right).

7.1.3.2 Characterization of Zn(II) centres supported on anisotropic fillers

Based on the previous studies in the presence of SiO_2 Rhodia, the functionalization of the three supports with APTES was studied through FTIR-ATR analysis and the quantification of APTES was calculate by TGA and CHNS technique. A confirmation of Zn coordination with APTES molecules was evaluated through ICP analysis, to quantify the Zn content in the samples, as explained in Chapter 2.

FTIR-ATR. The effective functionalization of both SiO_2-1 and SepS9 with APTES was confirmed by the appearance in FTIR-ATR spectra of two more peaks at 2864 and 2948 cm^{-1}, connected to the symmetric and asymmetric stretching of CH_2 groups, typical of the propyl chain of the APTES molecules. In A-SepS9, the presence of a broad peak at ~ 3200 cm^{-1} partially hidden the two peaks and a shoulder of this broad peak can be evidenced (Figure 7.7b).

Since in A-SiO_2-5 these two peaks could be assigned to MPTMS used in the synthetic procedure, in SiO_2 functionalized samples (AR=1,5), the shift of the peak related to Si-OH stretching vibration (954 cm^{-1}) to higher wavenumbers further confirmed the partial substitution of hydroxyl surface groups of bare SiO_2 with other bonds on the surface (Si-O-Zn, Figure 7.7a). This observation confirmed the effective functionalization of SiO_2 samples. In the case of sepiolite, the same substitution process happened, as confirmed by the reduction of signals at 3762-3578 cm^{-1} in A-SepS9, compared to bare SepS9, assigned to the presence of OH groups external surface of sepiolite[8] (Figure 7.7b).
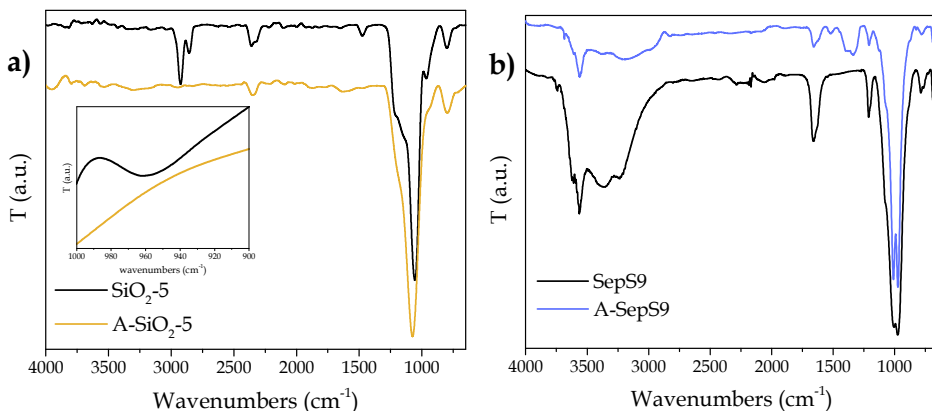
Figure 7.7. FTIR spectra of bare and functionalized A-SiO$_2$-5 and A-SepS9.

TGA and CHNS analysis. The quantification of APTES ligands on the surface of the three supports was calculated starting from the TGA profiles (for more details, see paragraph 2.2.2). In Figure 7.8 the TGA curves registered for A-SepS9, in comparison to bare SepS9, is shown as an example.
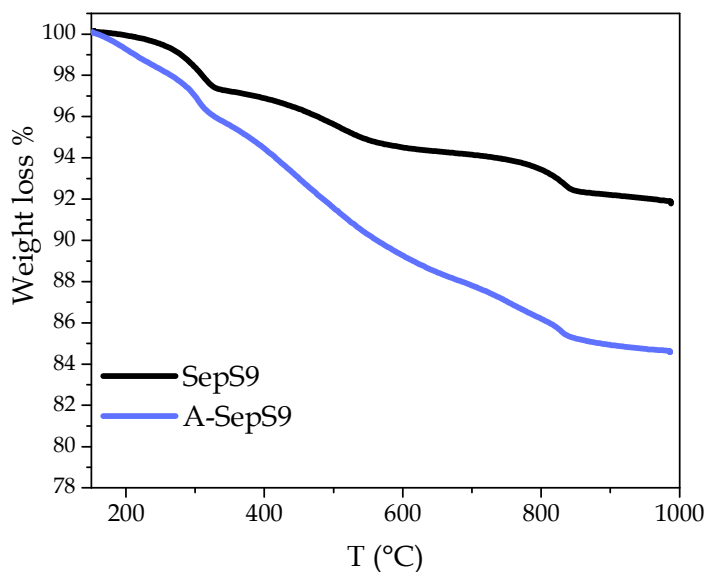
Figure 7.8. TGA profiles of A-SepS9, compared to SepS9.

In Table 7.3. the experimental data extrapolated from TGA curves are listed, expressed as the medium values between three repetitions of the same sample.

The coverage degrees with the three supports were a little increased to that obtained for $A_{0.50}$-SiO_2 (SiO_2 Rhodia).

Table 7.3. Experimental weight loss percentages between 150-1000°C measured from TGA profiles of the three functionalized supports. From this data, the coverage degrees, reaction yields and an estimation of number of APTES molecules over the supports were calculated.

| Sample	% weight loss (150-1000°C)	Coverage degree (wt %)	Reaction yield	SSA_{BET} (m^2g^{-1})	Number of APTES molecules/nm^2
$A_{0.50}$-SiO_2	10.4 ± 0.2	7.6 ± 0.2	76	107	5.2 ± 0.2
SiO_2-1	10.2 ± 0.2	-	-	1107	-
A-SiO_2-1	16.8 ± 0.1	8.1 ± 0.1	81	120	5.1 ± 0.1
SiO_2-5	15.8 ± 0.1	-	-	1336	-
A-SiO_2-5	22.2 ± 0.2	7.8 ± 0.1	78	150	4.9 ± 0.1
SepS9	7.9 ± 0.1	-	-	330	
A-SepS9	15.4 ± 0.3	9.1 ± 0.3	91	160	5.6 ± 0.3

The number of APTES molecules over the surface of the supports was calculated considering the surface areas of the supports. The specific surface area values (SSA_{BET}) were calculated from nitrogen physisorption measurements before and after the functionalization of the supports (**Figure 7.8**). A drastic decrease of SSA_{BET} values was observed after the functionalization process, confirming the efficient functionalization of the supports with APTES, due to the partial obstruction of the internal porosity.

While the coverage degrees were a little increased by using different supports, the number of APTES molecules over the surface of the supports were comparable; with higher surfaces available, higher amounts of APTES were able to bind to the surface support, as expected. Nevertheless, the maximum number of APTES molecules over the surface cannot exceed a certain saturation level, that depends on the steric hindrance of APTES molecules.

TGA results were further confirmed by CHNS data. The percentage of nitrogen calculated from TGA was comparable with the experimental measurements from CHNS analysis (data not reported).

ICP-AES. ZnA-Z samples were prepared using a molar ratio between APTES and Zn (n_{Zn}/n_{APTES}) equal to 0.5. The measurement of Zn content through ICP-AES analysis revealed higher Zn amounts with the three anisotropic supports, as expected from the higher coverage degrees detectable through TGA (Table 7.4.). The ratios between Zn and APTES molecules over the surface of the support were stable for the three supports, suggesting that the coordination of Zn to APTES ligands was unchanged by the modification of the nature of the support.

Table 7.4. Specific surface area measured for the three supports before and after the functionalization with APTES

Sample	Zn content (wt%)	Zn/APTES (molecules nm^{-2})
ZnA-SiO$_2$-1	3.2	0.55
ZnA-SiO$_2$-5	3.1	0.56
ZnA-SepS9	3.4	0.56

7.1.3.3 Summary of the materials characterization

ZnO NPs and Zn(II) centres NPs were successfully supported on anisotropic SiO$_2$ (AR=5) and sepiolite.

ZnO NPs of 5-6 nm covalently bonded to the surface of the supports (FTIR) were formed; the nanometric size was confirmed both by morphological analysis (TEM) and optical spectroscopy (UV-Vis analysis). High reaction yields were achieved, over 80%, confirming the high reproducibility of the synthesis (ICP). Compared to amorphous ZnO NPs detected on SiO$_2$, both amorphous and crystalline ZnO NPs were formed on anisotropic filler, especially with sepiolite, due to the intrinsic crystalline structure of sepiolite, as suggested with XRD.

Zn(II) centres were anchored on the supports after a first functionalization step with APTES of the anisotropic materials. The functionalization, confirmed by FTIR, involved the condensation reaction of APTES on the surface of the supports, through the interaction with the hydroxyl groups of the supports. The amounts of functionalizing agents were quantified through TGA and CHNS and confirmed the high reaction yields obtained with SiO_2 Rhodia. The coordination of Zn to APTES molecules was supposed to be unaffected by the change of the support, as suggested by the calculation based on ICP measurement.

7.1.4 Tests in rubber NCs

The combined effect of the anisotropy of the supports (SiO_2-5 and SepS9) to the NCs reinforcement properties and of the highly efficient Zn-based activators to the vulcanization process, is here presented. The vulcanization curves and the mechanical properties were considered as the main parameters in this comparison study.

Materials and procedure: refer to paragraph 3.2. The NCs were prepared by keeping constant the Zn content, equal to 1.49 phr. Filler content was equal to 40.0 phr when ZnO NPs were supported, 43 phr when Zn centres were anchored.

The NCs will be labelled with the name of the activator (as described previously in this chapter), followed by IR.

Effect of SiO_2-5 support

The vulcanization curves were strongly influenced by the change of the nature of SiO_2 filler: the substitution of the commercial SiO_2 Rhodia with SiO_2-1 and SiO_2-5 dramatically decreased the M_{max} values and the vulcanization hardly took place (Figure 7.9., left side). This trend respects the trend of the surface area values of the three supports and of their relative porosity: in fact, SiO_2-5/IR, with the highest SSA_{BET} filler (1337 m^2g^{-1} and high meso-porosity) was the less performant in the vulcanization conditions. The high porosity could be

responsible for the absorption of the vulcanization agents, that consequently decreased the efficiency of the vulcanization process. The same trend was detected when ZnO NPs were supported onto the surface of the three SiO_2 supports, in which ZnO/SiO_2-5/IR was the less performant in the vulcanization process (Figure 7.9., right side). This observation suggested that the nature of the support was still playing the main role in the determination of the vulcanization curves shape, despite the presence of the anchored ZnO NPs.
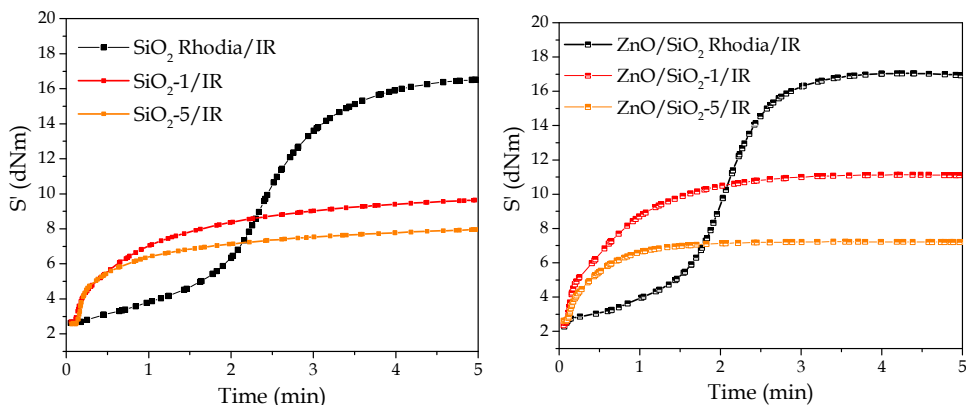
Figure 7.9.   Vulcanization curves registered in the presence of three different SiO_2 NPs (commercial SiO_2 Rhodia, SiO_2-1 and SiO_2-5) on the left; the effect ZnO NPs supported onto the three different supports on the vulcanization process is shown on the right.

As a result, the mechanical properties of these composites were dramatically decreased, as illustrated in Figure 7.10., where as an example the G′ curves of vulcanized NCs are reported in the presence of the bare and ZnO NPs modified SiO_2 support. The apparent reduction of the Payne Effect in SiO_2-1 and SiO_2-5 based NCs is justified due to the stable values of $G′_0$, that did not increase after the vulcanization process. The same results were also observed in the presence of Zn centres anchored to SiO_2-5 and SiO_2-1 (data not reported), with a strong decrease in the vulcanization efficiency and mechanical properties of the vulcanized NCs.
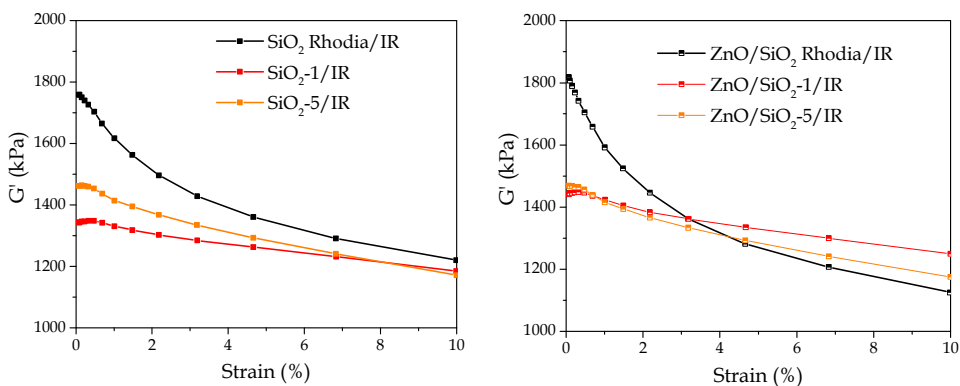
Figure 7.10. G′ values of vulcanized rubber NCs in the presence of the three different SiO₂ supports (left) and ZnO NPs anchored to the three SiO₂ supports.

Effect of SepS9 support

When ZnO NPs and Zn(II) centres were anchored to the surface of SepS9, the activators showed a high activity, leading to higher vulcanization efficiency, compared to m-ZnO (Figure 7.11.). A reduction of t_{90} and increased M_{max} values were measured with both ZnO/SepS9 and ZnA-SepS9, as shown in Table 7.5. Reduced scorch times were detected with ZnA-SepS9, as already noticed with ZnA-SiO₂ Rhodia, consistently with the structure of this activator and with the previous observations described in Chapter 3.

The presence of SepS9 did not affect the vulcanization efficiency, in comparison to the commercial SiO₂ Rhodia, despite the higher SSA_{BET} measured for SepS9 ($330 m^2 g^{-1}$); in this case, the small pore size of SepS9 hindered the strong absorption of the vulcanization agents, as demonstrated also by the higher vulcanization efficiencies achieved with the reference samples SepS9/IR, compared to SiO₂-1/IR and SiO₂-5/IR.
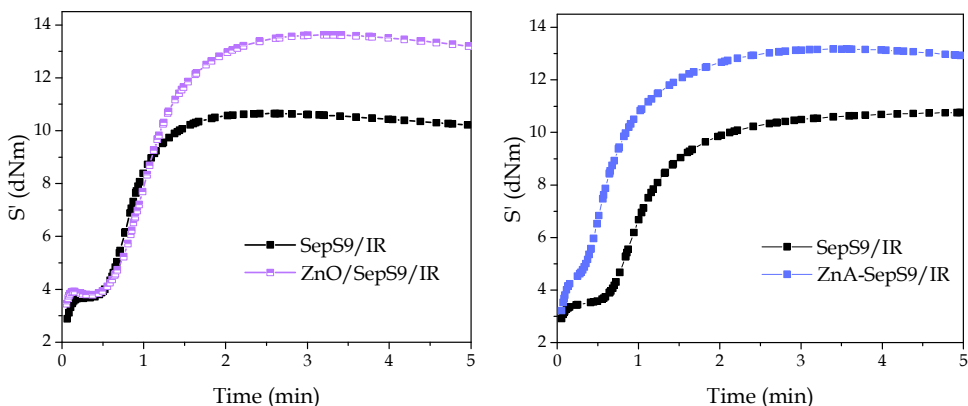
Figure 7.11.   Vulcanization curves registered for IR NCs containing ZnO/SepS9 (left) and ZnA-SepS9 (right) with their respective references NCs (SepS9).

Table 7.5. Vulcanization characteristics for ZnO/SepS9/IR and ZnA-SepS9/IR, compared to the reference SepS9/IR.

NCs	M_{max} (dNm)	M_{min} (dNm)	ΔM (dNm)	t90 (min)
SepS9/IR	10.6	2.8	7.8	1.4
ZnO/SepS9/IR	13.6	3.3	10.3	1.7
SepS9/IR	10.7	2.9	7.8	2.1
ZnA-SepS9/IR	13.2	3.2	10.0	1.6

The mechanical properties of vulcanized NCs with ZnO/SepS9 and ZnA-SepS9 were both improved compared to their reference samples. A slight shift of G′ curves to higher values, together with a reduction of G′′ and tanδ values were registered with both the two activators (Figure 7.12). Moreover, a strong reduction of the Payne Effect was highlighted in both cases (Table 7.6), due to an enhancement of G′∞ values. A strong filler-rubber interaction was developed in the presence of the ZnO/SepS9 and ZnA/SepS9 fillers, higher than what obtained before in the presence of SiO_2 Rhodia (Chapter 3).
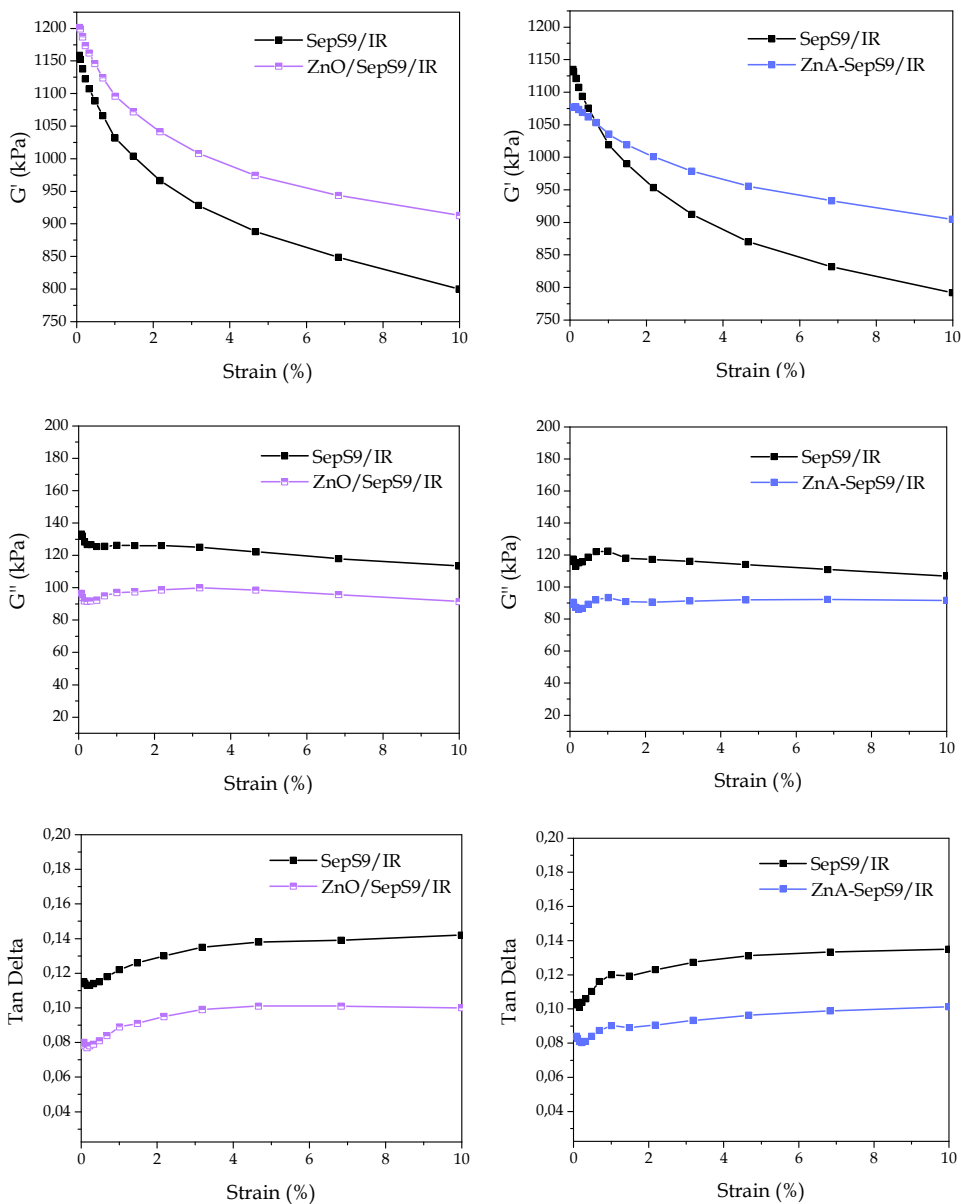
Figure 7.12. Mechanical properties (G′, G″, tanδ) of IR NCs prepared with ZnO/SepS9 (left) and ZnA-SepS9 (right) and their relative reference samples (SepS9).

Table 7.6. Payne Effects of ZnO/SepS9/IR and ZnA-SepS9/IR, compared to the reference SepS9/IR.

NCs	G'_0 (kPa)	$\Delta G'_{3\%-9\%}$ (kPa)
SepS9/IR	1158	111
ZnO/SepS9/IR	1200	88
SepS9/IR	1136	115
ZnA-SepS9/IR	1076	69

In conclusion, the use of SepS9 as a support for ZnO NPs and Zn(II) centres allowed the formation of IR NCs with improved vulcanization efficiencies and higher mechanical properties, with a strong reduction of tanδ values. A good combination between the anisotropy effect of SepS9 and highly reactive Zn-based activators was achieved. Further morphological and mechanical studies will be prosecuted to understand whether the distribution of the vulcanization process could be modified by the presence of Zn activator on the surface of SepS9, compared to SiO_2. In fact, as explained before, SepS9 tends to form fibres aggregates in the rubber matrix, that are responsible of the higher reinforcement properties; surface modification of SepS9 could favour the formation of highly vulcanized regions, closed to the SepS9 aggregates, responsible for the overall enhancement of the mechanical properties.

7.2 Use of ZnA-SiO$_2$ double function filler in organically modified polymers

In this section, the advantages of the use of a double function filler (ZnA-SiO$_2$) as a reinforcing filler and highly reactive activator in functionalized polymers is discussed. First, a brief introduction on polymers functionalization is described; later on, the interaction between Zn(II) centres and the organic functionalities is evaluated. In the end, the mixing process of functionalized polymers and ZnASiO$_2$ filler will be considered for the preparation of rubber NCs.

7.2.1 Functionalized polymers: use of Ph-TAD

In rubber NCs production, the functionalization of polymers has attracted more attention in the last few years, as a possible alternative to increase the interaction between the polymer and the reinforcing fillers. In the scientific research, the filler-rubber interaction has always been studied from the filler point of view, trying to modify the surface of these inorganic materials to make them more compatible with the polymer matrix (i.e. compatibilizing agents with SiO$_2$ filler)[10,11]. Nevertheless, recently more and more rubber industries have started to develop alternative technologies, that starting from the polymer side, could improve its compatibility towards fillers of different nature, used for the NCs formulation.

Among the scientific procedures for the polymers' functionalization, both the functionalization of the polymeric precursor and the post-polymerization functionalization are possible feasible paths. The latter is always preferred, since a higher number of accessible positions are available and a wider range of products synthesizable. As an example, pendent groups can be added to the polymers through post-polymerization functionalization, but not on the monomers, since their presence would favour collateral reactions during the polymerization process.

Nowadays, the introduction of functional groups can be guided to different polymeric positions, thanks to the use of advanced processes developed in the field of organic chemistry. Among the infinite number of available functionalities and polymer's positions, only those reactions that respect the concept of the "click chemistry" are usually employed: fast, harmless, up-scalable to industrial processes, giving high reaction yields, highly efficient in equimolar conditions, are some of the prerogatives for a good functionalization reaction of polymers in the rubber field.

In the literature, several different functional groups have been tested, including ester and thiol-based functionality[12]. In recent works, an urazol complex, the phenil-triazolidinone (Ph-TAD, Figure 7.13, left) has been used as a possible functionalizing group, thanks to the simple and small structure, and to the possible formation of stable bonds with the polymer in its oxidized form. The oxidation is performed in dichloromethane (CH_2Cl_2), in the presence of dimethoxybenzene, to give a very reactive molecule towards the double bonds of the polymer (Figure 7.13).
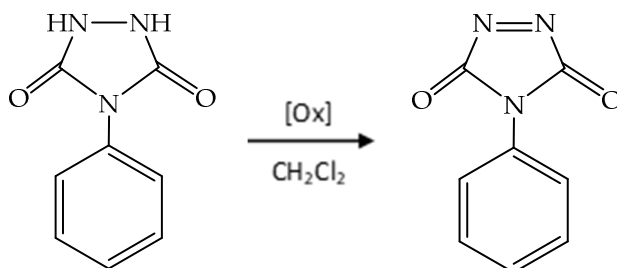
Figure 7.13. Ph-TAD oxidation in CH_2Cl_2.

The oxidized form can then react with the polymer following a very fast reaction shown in Figure 7.14. The completion of the reaction (5 minutes, room temperature) is indicated by the disappearance of the typical colour of the oxidized form (red) in solution, that becomes colourless after the interaction with the polymer[13,14].
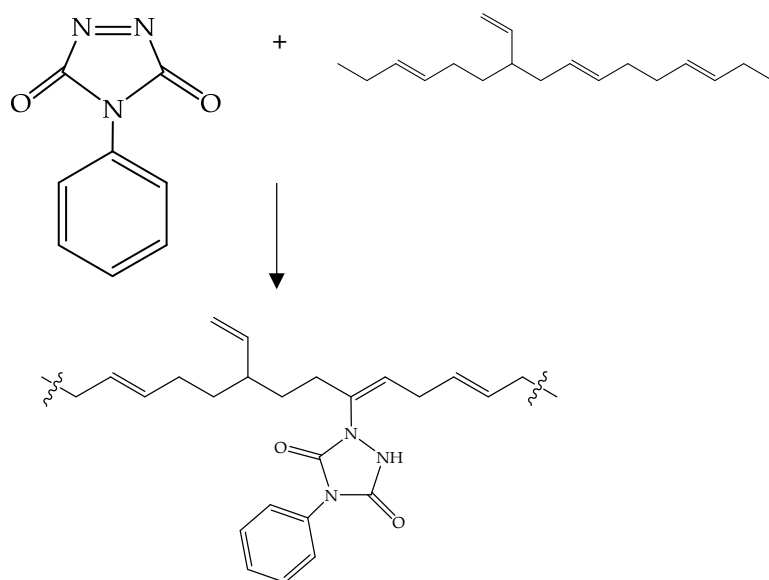
Figure 7.14. Reaction of the oxidized form of Ph-TAD with the polymer.

Furthermore, once connected to the polymer, Ph-TAD molecules present an amino group, that modify the hydrophilic character of the polymer and increase the affinity towards the more hydrophilic nanofillers as SiO_2. Possibly, hydrogen bonds develop between the Ph-TAD units dispersed in the polymer matrix and the hydroxy groups of SiO_2, enhancing the distribution of SiO_2 NPs.

Nevertheless, a main drawback is connected to the possible hydrogen bonds that could form in-between the polymer chains, through two amino groups of two Ph-TAD units, causing a stiffening of the polymeric matrix (Figure 7.15).
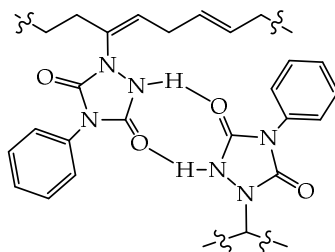
Figure 7.15. Hydrogen bonding interaction between two Ph-TAD units.

In most cases, this latter interaction prevents SiO_2 NPs from cooperating with Ph-TAD units, resulting in a scarce SiO_2 distribution in the polymer matrix and in the formation of SiO_2 aggregates, with a reduced filler-rubber networking.

As a consequence, the industrial application of Ph-TAD as a functional agent for polymer chains in SiO_2 filled NCs, requires an improvement of SiO_2 NPs affinity towards Ph-TAD units, to reduce the competition with other Ph-TAD units. The final aim is to increase the SiO_2-polymer compatibility and the filler distribution. For this reason, the application of ZnA-SiO_2 as a filler inside a Ph-TAD modified polymeric matrix was considered. In fact, Zn(II) centres are known to interact with amino groups, forming either covalent or coordinating bonds; the different energy bonds involved were exploited, in order to preferentially bond Ph-TAD units to SiO_2, through Zn(II) centres. Moreover, the presence of the highly reactive Zn(II) centres could promote a more efficient vulcanization process of the rubber NCs.

This project was realized in collaboration with Prof. Papagni, University of Milano Bicocca, responsible of the production of the organic materials.

First, the interaction of Zn(II) centres with Ph-TAD units was verified using both Zn(II) complexes and ZnA-SiO_2; later on, the introduction of ZnA-SiO_2 in the polymer matrix was studied through the synthesis of masterbatches, as explained later.

7.2.2 Zn(II) interaction with Ph-TAD

Zinc acetate and zinc stearate were used as examples of zinc complexes for the interaction with PhTAD, together with ZnA-SiO_2.

Materials: zinc acetate dihydrate (ZA, ≥ 98%) and zinc stearate (ZS, tech. grade) were purchased from Sigma Aldrich. Ph-TAD was provided from the Org. Chem. Labs, Prof. Papagni and used as received. Zn_YA_X-SiO_2 was synthesized as described in paragraph 2.2.1, with Y and X = 0.50. Sodium hydroxide (NaOH, 98%) and ethanol (EtOH, puriss, p.a., absolute, ≥ 99.8%) from Sigma Aldrich.

Procedure: in 5.0 mL of NaOH solution (0.1 M) in ethanol, 0.200 g of Ph-TAD are added. After 10 minutes, the Zn precursor (ZA, ZS, ZnA-SiO$_2$) is added and the reaction left under stirring for 2h. A molar ratio Zn : Ph-TAD equal to 1:1 is used to favour the coordination of each functional group with each Zn atom. The powder is filtered through Hirsch filter, washed with fresh ethanol and dried in an oven at 80°C for 12h.

Characterization: TGA and FTIR analyses were used to assess the effective coordination of Ph-TAD with ZA, ZS and ZnA-SiO$_2$.

TGA curves of Ph-TAD/ZA and Ph-TAD/ZS (Figure 7.16) showed different patterns compared to the bare Ph-TAD, with a decomposition process that starts at higher temperatures and leads to a lower weight loss percentage in both samples. This data confirmed the presence of inorganic material (Zn metal) and consequently the high ability of Zn centres to coordinate with Ph-TAD, leading to the formation of Zn complexes of different nature.
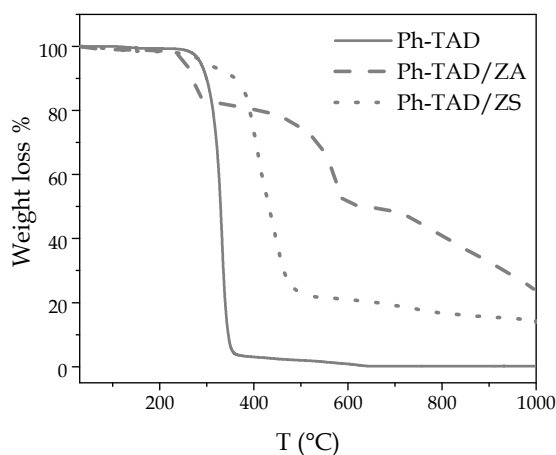

Figure 7.16. TGA profiles of Ph-TAD after interaction with ZA and ZS, in comparison to bare Ph-TAD.

Supposing that at 1000°C, the only residual materials is composed of inorganic species (in this case Zn), the weight loss% registered for Ph-TAD/ZS (86%) and for Ph-TAD/ZA (76%) were indicative of a Zn content equal to 14wt% and

24wt%, respectively. Since the maximum Zn weight percentage in the two samples would be equal to 27wt%, considering the maximum reaction yield and no other organic residual ligands on Zn (coming from acetate and stearate anions), in Ph-TAD-ZA the Zn content was almost equal to the stoichiometric value. The small difference could be ascribed to the presence of acetate moieties in the sample. In Ph-TAD-ZS, apparent Zn content can be correlated to the presence of stearate moieties, with a molecular weight five times higher than acetate moieties.

In parallel, the TGA curve of Ph-TAD/ZnA-SiO$_2$ (Figure 7.17) showed a weight loss percentage lower than bare Ph-TAD, but higher than bare ZnA-SiO$_2$, confirming the presence of additional organic material on the surface of SiO$_2$.
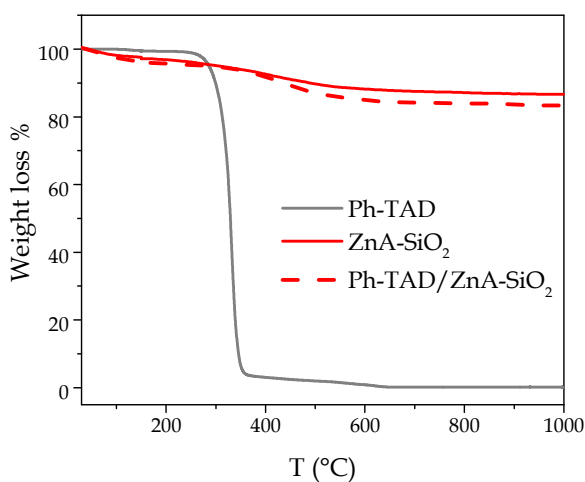
Figure 7.17. TGA profiles of Ph-TAD after interaction with ZA and ZS, in comparison to bare Ph-TAD.

In this case, since the maximum weight loss % ascribable to Ph-TAD (considering the highest reaction yield) is equal to 7.7wt%, the measured 4.2wt% from TGA curve is indicative of a lower coordination of Ph-TAD by isolated Zn(II) centres anchored to SiO$_2$. This observation is consistent with the structure of ZnA-SiO$_2$, as each Zn(II) centre has a limited free space available for the

coordination of other organic molecules and Ph-TAD has a notable steric hindrance. Moreover, the presence of free Zn(II) ions, not coordinated to Ph-TAD, is an advantage in the formulation of rubber NCs, so that Zn(II) can behave as activator centres for the vulcanization reaction.

As a further confirmation, Ph-TAD/ZnA-SiO$_2$ was characterized with FTIR-ATR analysis. The coordination between SiO$_2$ and Ph-TAD was confirmed through the appearance of the peaks at 1440 cm^{-1} and 1673 cm^{-1}, attributed to the stretching vibrations of C-N and C=O of urazole molecule, respectively.

As a conclusion, this first part confirmed the possible interaction of Zn(II) centres, both as free ions species and as supported isolated centres, with Ph-TAD unities. The coordination is probably due to the nitrogen atoms present in the urazole moiety of Ph-TAD.

7.2.3. Introduction of ZnA-SiO$_2$ in a Ph-TAD modified rubber NC

The introduction of ZnA-SiO$_2$ in an organically modified rubber NC was studied in a blend polyisoprene (IR)/polybutadiene (BR) 50:50; the functionalizing agent (Ph-TAD) was previously added to the PB phase in an *ex-situ* method, through an optimized procedure[13,14], and mixed to IR in a mixing chamber, together with the other ingredients of the rubber NC. The choice of this blend was connected to a technological issue, due to the natural tendency of SiO$_2$ to diffuse into IR phase when added to BR/IR rubber blend, creating non-homogeneous regions in the NC. By the addition of Ph-TAD to BR phase, the aim was to obtain a higher distribution of SiO$_2$ in the blend.

The preparation of a masterbatch between the polymer and the filler was applied in order to favour the pre-distribution of SiO$_2$ inside the BR phase. The mixing process with IR phase was performed in a second step in a mixing chamber.

Materials: polybutadiene (Europrene Neocis BR 40, 1,4-cis content ≥ 97%) was purchased from Polimeri Europa Eni. Dichloromethane (DCM, ≥ 99.9%) from

Sigma Aldrich. The other ingredients were purchased as described in paragraph 3.2.

Procedure: in a first step, the preparation of the masterbatch between BR and $ZnASiO_2$ is performed as follows. 30 g of BR polymer is first added to 2.5 L of DCM and left under mechanic stirring until the complete dissolution of BR is achieved. Then, Ph-TAD is added to the solution (0.5 phr of BR); after 30 minutes, the functionalization process is ended and ZnA-SiO_2 is added to the solution (78.2 phr of BR, correspondent to 1.3 phr of Zn and 35 phr of SiO_2 in the final NC, with both IR and BR, 50:50). The composite is extracted only when the solvent is completely evaporated, under mechanical stirring, and dried in an oven at 80°C for 12h.

The masterbatch was used in a second step for the preparation of a rubber NC with IR, blend IR/BR 50:50 phr. The mixing procedure was divided into two steps: in a first step, the masterbatch is mixed with IR and 6-PPD (2.5phr) at 90°C. In the second step, the NC is re-loaded in the mixing chamber and CBS (3 phr) and S_8 (1 phr) were added at 90°C. Lately, the composites were further mixed in a two-rolling mill at 50°C for 3 minutes, to improve the homogeneity of the composites. The composites were then vulcanized in a hydraulic press at 170 °C and 100 bar for 5 minutes (frequency = 1.670 Hz, Angle = 6.980%). This sample was labelled as $ZnASiO_2$/MBR(0.5)/IR where M means masterbatch.

A reference sample was prepared using bare SiO_2 for the preparation of the masterbatch. The masterbatch was used in the second step as previously described; the further addition of stearic acid (1 phr) and ZnO (1.3 phr) was required during the first step of the mixing procedure. No silane was used, because the functionalization of BR with Ph-TAD was supposed to replace the use of compatibilizing agents. This sample was labelled m-ZnO/MBR(0.5)/IR.

Characterization of the rubber NC: the vulcanization efficiency and the mechanical properties of rubber NCs were evaluated as follows.

The vulcanization curve of ZnA-SiO$_2$/MBR(0.5)/IR showed a good process efficiency, comparable to the reference systems (Figure 7.18). Despite the partial coordination of Zn(II) centres with Ph-TAD units, part of Zn(II) centres was still available to interact with the other vulcanization agents. Compared to the NC in IR (ZnA-SiO$_2$/IR), a higher scorch time was measured, probably due to the higher steric hindrance around Zn(II) centres, caused by the proximity of organic ligands and of the polymer chains.
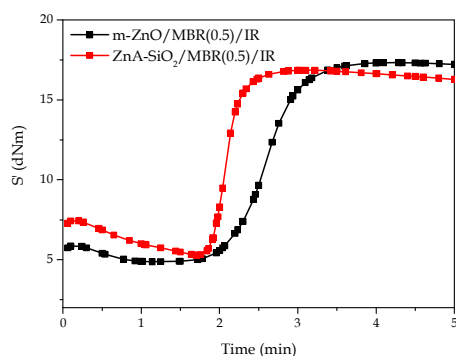
Figure 7.18. Vulcanization curves of BR/IR NCs (50:50) prepared through masterbatch technologies, using ZnA-SiO$_2$ (red curve) and bare SiO$_2$ (black curve).

The mechanical properties of ZnA-SiO$_2$/MBR(0.5)/IR showed opposing behaviours (Figure 7.19): a shift of the G' curve towards higher values could be connected to the enhancement of the strain-independent contributions to the curve (i.e. the polymer network). On the contrary, a slightly increased Payne Effect indicated a similar filler-rubber interaction, that was not affected by the introduction of ZnA-SiO$_2$ NPs. Besides, the increased G'' values and tanδ, suggested the necessity to further study this system, in order to improve the filler-rubber interactions inside the organically modified BR/IR blend.
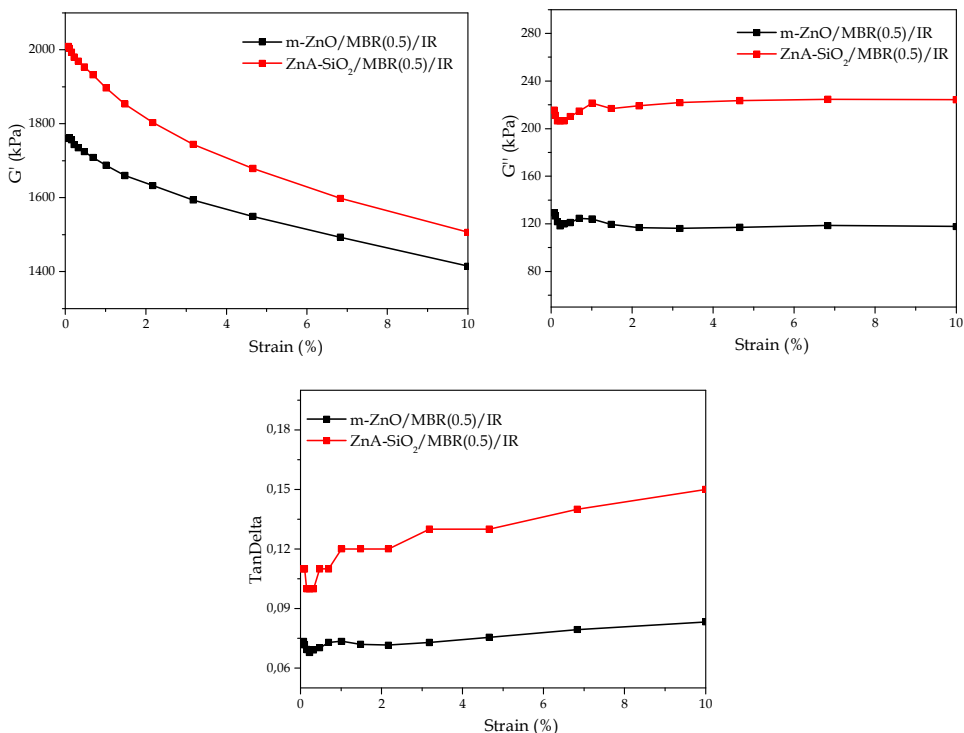
Figure 7.19. Mechanical properties (G', G'', tanδ) measured for BR/IR NCs (50:50) prepared through masterbatch technologies, using ZnA-SiO$_2$ (red curve) and bare SiO$_2$ (black curve).

In conclusion, the use of ZnA-SiO$_2$ in the Ph-TAD modified BR/IR blend led to a more efficient vulcanization process, with an increased reinforcement of the rubber NCs. Nevertheless, the high G'' values and tanδ values were representative of the necessity to deeper study the existing filler-rubber interactions and how to increase their compatibility in this system.

7.3 Summary of the application of the activators to different systems

The use of different supports to prepare anchored ZnO NPs and Zn(II) centres was employed as a method to improve the vulcanization process and the mechanical properties of the rubber NCs. Anisotropic fillers were used, including silica anisotropic particles and layered silicates (SepS9). Highly reinforced rubber NCs were prepared in the presence of anisotropic SepS9 particles as support for ZnO and Zn(II) centres. Improved mechanical properties and low energy dissipation were obtained thanks to the synergetic effect of the more efficient vulcanization and the more reinforcing anisotropic shape of the sepiolite particles.

In a second step, the versatility of ZnA-SiO$_2$ was tested by introducing the material in an organically modified polymer rubber (BR functionalized with Ph-TAD), to produce a reinforced NCs. Zn(II) centres anchored to SiO$_2$ surface react with the polymer functionalized groups behaving as centres for the cross-linking formation, improving at the same time the filler-rubber interactions and the efficiency of the vulcanization process.

7.3 Bibliography

1. Tadiello, L., D'Arienzo, M., Di Credico, B., Hanel, T., Matejka, L., Mauri, M., Morazzoni, F., Simonutti, R., Spirkova, M. & Scotti, R. The filler–rubber interface in styrene butadiene nanocomposites with anisotropic silica particles: morphology and dynamic properties. *Soft Matter* **11**, 4022–4033 (2015).

2. Scotti, R., Conzatti, L., D'Arienzo, M., Di Credico, B., Giannini, L., Hanel, T., Stagnaro, P., Susanna, A., Tadiello, L. & Morazzoni, F. Shape controlled spherical (0D) and rod-like (1D) silica nanoparticles in silica/styrene butadiene rubber nanocomposites: Role of the particle morphology on the filler reinforcing effect. *Polym. (United Kingdom)* **55**, 1497–1506 (2014).

3. Velde, B. *Clay Minerals: A Phisio-Chemical Explanation of their Occurence.* (1985).

4. Alexandre Michael & Dubois Philippe. Polymer-layered silicate nanocomposites: preparation, properties and uses of a new class of materials. *Mater. Sci. Eng.* **28**, 1–63 (2000).

5. Kotal, M. & Bhowmick, A. K. Polymer nanocomposites from modified clays: Recent advances and challenges. *Prog. Polym. Sci.* **51**, 127–187 (2015).

6. Esteban-Cubillo, A., Pina-Zapardiel, R., Moya, J. S., Barba, M. F. & Pecharromán, C. The role of magnesium on the stability of crystalline sepiolite structure. *J. Eur. Ceram. Soc.* **28**, 1763–1768 (2008).

7. Du, X. & He, J. Elaborate control over the morphology and structure of mercapto-functionalized mesoporous silicas as multipurpose carriers. *Dalt. Trans.* **39**, 9063–9072 (2010).

8. Alkan, M., Tekin, G. & Namli, H. FTIR and zeta potential measurements of sepiolite treated with some organosilanes. *Microporous Mesoporous Mater.* **84**, 75–83 (2005).

9. Susanna, a., Armelao, L., Callone, E., Dirè, S., D'Arienzo, M., Di Credico, B., Giannini, L., Hanel, T., Morazzoni, F. & Scotti, R. ZnO nanoparticles anchored to silica filler. A curing accelerator for isoprene rubber composites. *Chem. Eng. J.* **275**, 245–252 (2015).

10. Edwards, D. C. Polymer-filler interactions in rubber reinforcement. *J. Mater. Sci.* **25**, 4175–4185 (1990).

11. Fröhlich, J., Niedermeier, W. & Luginsland, H. D. The effect of filler-filler and filler-elastomer interaction on rubber reinforcement. *Compos. Part A Appl. Sci. Manuf.* **36**, 449–460 (2005).

12. Blasco, E., Sims, M. B., Goldmann, A. S., Sumerlin, B. S. & Barner-Kowollik, C. 50th Anniversary Perspective: Polymer Functionalization. *Macromolecules* **50**, 5215–5252 (2017).

13. Chen, T. C. S. & Butler, G. B. Chemical Reaction on Polymers. III. Modification of diene polymers via the ene reaction with 4-substituted-1,2,4-triazoline-3,5-diones. *J. Macromol. Sci. Part A - Chem.* **16**, 757–768 (1981).

14. Leong, K.-W. & Butler, G. B. Chemical Reactions on Polymers. II. Modification of Diene Polymers with Triazolonediones via the Ene reaction. *J. Macromol. Sci. Part A - Chem.* **14**, 287–319 (1980).

8

Conclusions

The topic of the present study was the design and preparation of innovative zinc-based activators for the vulcanization process of rubber. These activators materials were developed, by exploiting the concept of double function filler, a material which behaves both as reinforcing filler of the rubber NCs and as activator of the vulcanization process. Starting from the dispersion of ZnO NPs on the surface of SiO_2 nanofiller (ZnO/SiO_2), the anchoring of Zn(II) centres on SiO_2 was studied ($ZnA-SiO_2$), to get highly available and reactive activator centres of the vulcanization reaction, dispersed in the rubber matrix.

ZnO/SiO_2 was synthesized optimizing a procedure in which the hydrolysis and condensation of a zinc precursor (zinc acetate) take place in the presence of SiO_2, in a basic environment. ZnO NPs were dispersed on the surface of SiO_2, with the possibility to tune the ZnO loading and size.

The synthesis of $ZnA-SiO_2$ consisted of two phases; a first step was represented by the silica surface functionalization with a silane (APTES), able to react both with the silica through the ethoxy groups and with zinc, thanks to the amine groups. In the second step, Zn (II) centres were anchored to silica by the coordination with two amine groups. The coordination of the Zn(II) centres was completed by the presence of more labile groups, probably nitrate or hydroxy groups, from reagents or solvent, which guarantee a high reactivity of the single-site catalytic centres.

The application of the two activators $ZnA-SiO_2$ and ZnO/SiO_2 in the vulcanization process of IR NCs demonstrated that higher vulcanization efficiencies and improved cross-linking densities were obtained, compared to the conventionally used activator m-ZnO. Noteworthy, the higher curing efficiency were obtained by using half of the amount of zinc, compared to the loading usually used in the industrial rubber vulcanization process.

In particular, the two activators showed to induce faster kinetics of the cross-linking reactions, following different reaction pathways. ZnO/SiO_2 relies on the reaction with the co-activator SA to form an active Zn(II) complexes, which

diffuse in the rubber matrix giving rise to sulphurating complexes with the curatives, which further react to form the cross-link between the polymer chains. Nanosized dimension of ZnO particles and the supporting on silica surface, favour the availability of zinc centres to react.

In ZnA-SiO$_2$, Zn(II) centres showed high reactivity without the use of the co-activator SA, confirming that the single Zn(II) centres are the real active species involved in the catalytic process of the vulcanization. Zn(II) centres behave as heterogeneous catalytic sites, reacting with the curatives and promoting the cross-linking reactions, anchored on the surface of SiO$_2$ particles. This mechanism implies a very high reaction rate since no steps for Zn(II) complex formation are present. Besides, the anchoring on the silica surface, implicate that no zinc leaching occurs during the whole vulcanization process.

The different vulcanization mechanism and the different location of the zinc active centres in the rubber matrix (close to silica filler in ZnA-SiO$_2$ and dispersed in the rubber matrix in ZnO/SiO$_2$) were proved to influence the process of cross-linking formation in the rubber matrix. In particular, with ZnA-SiO$_2$ higher cross-linking densities were detected in the area next to the rubber SiO$_2$ interface. This structural change in the polymer network inside the rubber was connected to a different mechanical behaviour of the NC, with changes both in the strain/stress behaviour under low and high strain and fracture phenomenology compared to m-ZnO based NCs.

The reactivity of the two activators ZnA-SiO$_2$ and ZnO/SiO$_2$ was shown to be properly modulated by changing the structural parameters of the materials. Regarding ZnO based activator, the catalyst-support interaction was demonstrated to play a main role in the determination of the ZnO NPs activity, thanks to the possibility to tune the acidity of the Zn centres, and therefore the reactivity towards the electron donor ligands, depending on the acidity of the supporting oxides. In the case of ZnA-SiO$_2$, the nature of the anchoring agents and in particular of the functional groups that interact with Zn(II) centres, was

recognized as the main parameter to modulate the zinc stability, reactivity and availability during the reaction. By introducing sulphur or diamine groups (MPTMS or EDTMS, respectively), different performances were achieved in the vulcanization process; in particular, the presence of EDTMS allowed the achievement of increased scorch times.

The procedure to prepare ZnO/SiO_2 and $ZnA-SiO_2$ was extended to other silicate-based fillers, as a method to improve the vulcanization process and the mechanical properties of the rubber NCs. In particular, highly reinforcing anisotropic sepiolite SepS9 particles as support for ZnO and Zn(II) centres. High reinforcing mechanical properties and low energy dissipation were obtained thanks to the synergetic effect of the more efficient vulcanization and the more reinforcing anisotropic shape of the sepiolite particles.

The high versatility of $ZnA-SiO_2$ was preliminary tested also by introducing $ZnA-SiO_2$ in an organically modified polymer rubber (BR functionalized with Ph-TAD), to produce a reinforced NCs. in which the zinc centres anchored on the silica surface react with the polymer functionalized groups behaving also as centres for the cross-linking formation, improving at the same time the filler-rubber interactions and the efficiency of the vulcanization process.

These outcomes demonstrated that $ZnA-SiO_2$ and ZnO/SiO_2 are potentially effective alternative activators for the vulcanization process. The main advantages were the higher vulcanization efficiency, with a reduced consumption of zinc oxide for the preparation of rubber NCs; besides, in the case of $ZnA-SiO_2$, a potential reduction of zinc leaching was highlighted, with a main benefit in the environmental perspective.

Their promising interest for the industrial application was evidenced by a filed patent in Italy (2018), title "Processo per la preparazione di mescole per pneumatici e pneumatici che che le comprendono".

Appendix A:

Characterization methods

In this Appendix, the analytical techniques used in this work are resumed and briefly described.

A1. Fourier Transformed Infrared Spectroscopy (FTIR)

The analysis was performed with a Perkin Elmer Spectrum 100 instrument by a single reflection Attenuated Total Reflection (ATR) method (1 cm^{-1} resolution spectra, 650–4000 cm^{-1} region, 16 scans). The spectra were further analysed through baseline correction and normalized for obtaining the final presented spectra.

This technique was exploited to i) characterize inorganic support NPs (SiO$_2$ and SepS9) after the synthesis of ZnO/SiO$_2$, A$_X$-SiO$_2$ and Zn$_Y$A$_X$-SiO$_2$ and the relative zinc-based activators on SepS9; ii) study the vulcanization mechanism through MCV approach, by registering the spectra of liquid aliquots of the MCV reactions carried out in TME at 120°C, after filtration. FTIR spectra were also registered on ZnO/SiO$_2$ and Zn$_Y$A$_X$-SiO$_2$, after the MCV reaction, to evaluate the evolution of the two activators during the vulcanization reaction.

A2. Thermogravimetric analysis (TGA)

TGA analyses were carried out using a TGA/DCS1 STARe SYSTEM (Mettler Toledo) at constant air flux (50 mL min^{-1}). The sample holder was an alumina pan with 75 µL of volume, used without pan, filled at least until half of its . The temperature range was fixed between 30 and 1000°C, with a heating rate of 10°C min^{-1} and two isotherms at 150°C and 1000°C of 15 minutes. The analyses allowed the registration of the weight loss percentage of the samples during the heating treatments, due to decomposition reaction, oxidation and physical processes as vaporization and desorption. The isotherm steps were necessary to stabilize the weight percentages at 150°C and 1000°C, considered as the initial and final temperature for the weight loss of organic materials covalently bond to inorganic materials ($\Delta W_{150-1000°C}$).

This analysis was applied to measure the amount of organic material deposited onto the surface of inorganic supports and was extremely useful for the

estimation of the amount of silane (APTES, EDTMS, MPTMS) on the surface of SiO_2 and other natural supports, as Sep.

A3. Elemental analysis (CHNS)

The elemental analysis was performed in a heating furnace (CHNS analyser PerkinElmer Instruments) for the combustion of small aliquots of the sample (few mg, up to 1000°C); in this technique, typically used for organic materials, the main elements of organic structures (carbon, nitrogen, oxygen and sulphur) are converted into volatile molecules, that are separated through gas-chromatography, identified and quantified.

This measurement was useful for the quantification of organic ligands on the surface of inorganic supports, as a confirmation of the TGA analysis.

A4. X-Ray Diffraction (XRD)

Room temperature XRD patterns between 20 and 60° were registered with a Rigaki-Miniflex 600 diffractometer, that operates with a Bragg-Brentano geometry. In this geometry, the X-Ray source and the detector lie on a circle centred on the sample holder; slits collimate the incident X-rays, which hit the specimen at an angle θ. During the analysis, the sample position was fixed and a mobile X-Ray source (Cu Kα radiation λ_1 = 1.5406 Å, λ_2 = 1.54443 Å) was used. The sample was located in an amorphous holder, with crystallites in a random orientation, to avoid the generation of systematic errors. After passing through receiving slits, the diffracted X-rays are detected.

This analysis was employed for the study of the crystalline structure of ZnO NPs, both as bare NPs and supported, to understand whether ZnO is formed in an amorphous or crystalline structure during the synthetic procedures.

A5. Reflectance UV-Vis analysis

Reflectance UV-Visible analysis was performed with a UV Lambda 900 Perkin Elmer spectrometer on powder samples, in the range 800-200 nm, with an accuracy of 0.08 nm.

The sample is irradiated with a beam generated by a double source, composed of a deuterium lamp and a halogen lamp. After the emission from the source, the beam is reflected by a series of mirrors and monochromators to reach the sample. A typical quartz window was used as a sample holder, where the incident beam collides and is then reflected to the detector. The signal is consequently converted to a current signal by the photomoltiplicator.

This analysis was used for the characterization of powdered ZnO NPs, to determine the band gap energy of ZnO, as a semiconductor material. The calculation of the band gaps was done using the Kubelka-Munk treatment, exploiting the following equation:

$$F_R = \frac{(1 - R)^2}{2R}$$

where R is the measured reflectance and FR is the absorption coefficient. Starting from this parameter, the absorption onset can be obtained by plotting $\ln^2(I_t/I_0)$ versus the energy[1,2].

A6. High Resolution Transmission Electron Microscopy (HRTEM)

Morphological characterization of ZnO/SiO_2 and ZnO/SepS9 powders was performed on a Jeol 3010 High Resolution Transmission Electron Microscope (TEM) operating at 300 kV with a high-resolution pole piece (0.17 nm point to point resolution) and equipped with a Gatan slow-scan 794 CCD camera. The powders were supported on 3 mm copper grid for TEM investigation.

The morphological investigation of vulcanized composites was carried out by TEM using the Zeiss EM 900 microscope. Ultrathin sections (about 50 nm thick) of composites were obtained with a Leica EM FCS cryo-ultramicrotome

equipped with a diamond knife, by keeping the samples at -130°C. The thickness of the specimens was of about ~40 nm.

TEM analysis, thanks to the electron beam (speed up to 100KeV), high resolved images of the sample can be registered, with an apparatus able to resolve features as small as few nanometers.

A7. Inductively Couple Plasma Atomic Emission Spectroscopy (ICP-AES)

ICP measurements were performed by using an ICP-AES Optima 7000 DV Perkin Elmer instrunment (Software control WinLab32), coupled with a microwave mineralizer.

Specimens for the analysis were prepared by thinly grinding 0.2 g of powdered sample, dissolving them in a Teflon beaker with an acid solution composed of 4 mL of HNO_3, 3 mL of HCl and 1 mL of HF. The sample was treated in the mineralizer in three subsequent steps, at different times and temperatures (power 1000W): i) 8 minutes, 160°C, ii) 5 minutes, 200°C, 20°minutes 200°C. Finally, a dilution with 12 mL of Milli-Q water and a centrifugation were used; 15 mL of this solution were further diluted 1:100 with Milli-Q water and introduced in the ICP instrument for the analysis. Inside the quartz tube of plasma source, a constant flux of argon of 20L min^{-1} was applied to transport the vaporized sample.

A8. Nitrogen Physisorption

The analysis was carried out by a Quantachrome Autosorb-1 apparatus.

The nitrogen physisorption was used as a non-destructive technique, based on the physisorption of a vapour (usually N_2) on the surface of a solid at constant temperature (-77 K), to determine the specific surface areas of the solid supports before and after the deposition of the zinc-based activators. The typical output is an adsorption isotherm, that relates the amount of the species in the bulk phase and in the interphase. Instead of a Langmuir isotherm, that is more typical

for chemical than physical interactions (coverage stops when the coverage degree is equal to 1), a more complex isotherm was developed to take into account the formation of multilayers (B.E.T. method). The isotherm reports the volume of adsorbed gas (V_{ads}) vs the relative pressure p/p_0 (p is the actual pressure, p_0 is the pressure at which condensation of the vapour occurs). The surface area of the solid can be derived from the quantity of adsorbed gas at monolayer coverage; moreover, the shape of the adsorption-desorption hysteresis curve is related to the shape and size of prevalently present pores.

A9. Electron Paramagnetic Resonance (EPR)

The spectra EPR were acquired by a Bruker EMX spectrometer operating at the X-band frequency and equipped with an Oxford cryostat with the following conditions: 130 K, modulation frequency 100 kHz, modulation amplitudes 5 G and microwave power 5 mW.

This analysis was used to evaluate the coordination of copper atoms inserted during the synthesis of $Zn_YA_X-SiO_2$ samples, as probe for the EPR spectra. Since Zn is not paramagnetic, Cu was added in small quantities ($Zn_{Y-J}Cu_JA_X-SiO_2$) as a probe to get an indirect information about the coordination structure of the metal centres with APTES.

A10. X-Ray Photoelectron Spectroscopy (XPS)

XPS is a technique based on the kinetic analysis of the photoelectron emitted by the superficial layers of a sample, after irradiation with X-Ray, in a Ultra High Vacuum ($p \leq 10^{-7}$ Pa).

In this work, the analysis was performed on a Perkin Elmer Φ 5600-ci spectrometer using non-monochromatized source at Al-Mg double anode. Samples were mounted on steel holders and introduced directly in the fast-energy lock system of the XPS analytical chamber. The analysis area was 800 µm in diameter and the working pressure was lower than 10-9 mbar. The spectrometer was calibrated by assuming the binding energy (BE) of the Au

4f7/2 line at 83.9 eV with respect to the Fermi level. The standard deviation for the Be values was fixed at 0.2 eV.

In the acquisition mode, a standard source (Al Kα) with an energy of 1486.6 eV was used. Survey scans were obtained in the 0-1350 eV range and detailed multiplex scans were recorded for the C1s, O1s, N1s, Si2p, Zn2p regions. Charging effects were corrected by assigning to the C1s peak associated with accidental hydrocarbons a value of 284.8 eV. The analysis involved Shirley-type background subtraction, non-linear least-squares curve fitting Gaussian-Lorentzian peak shapes and peak area determination by integration[3]. The atomic compositions were evaluated from peak areas using sensitivity factors supplied by Perkin Elmer, taking into account the geometric configuration of the apparatus. The experimental error on the reported atomic composition values did not exceed ±5%.

A11. Nuclear Magnetic Spectroscopy (^{1}H-NMR)

^{1}H-NMR spectra were recorded at 500 MHz on samples dissolved in $CDCl_3$ (1:10 vol:vol). Chemical shifts were determined relative to the residual solvent peak (CDCl3, δ 7.26 ppm).

This analysis was performed in the MCV approach, on liquid aliquots of vulcanized TME samples at different reaction times (5, 10, 20 min) to study the process of formation of cross-linking products of TME.

A12. Solid State Nuclear Magnetic Spectroscopy (Solid State NMR)

Solid state NMR analyses were carried out with a Bruker 400WB spectrometer operating at a proton frequency of 400.13 MHz. Magic Angle Spinning (MAS) NMR spectra were acquired with single pulse (SP) experiments and cross polarization (CP), under the following conditions: ^{29}Si frequency: 79.48 MHz, π/4 pulse 2μs, decoupling length 6.3 μs, recycle delay: 150 s, 3k scans; for CP: contact time 5ms, π/2 pulse 4μs 2k scans. ^{13}C frequency 100.52 MHz, CP, π/2 pulse, contact time 2ms, decoupling length 6.3 μs, recycle delay 4s, 2k scans. ^{1}H:

single pulse seq. π/2 pulse 5μs, recycle delay: 20 s, 32 scans. Samples were packed in 4 mm zirconia rotors, which were spun at 7 kHz (10kHz for proton) under air flow. Q_8M_8 and adamantane were used as external secondary references.

Solid state NMR were performed on A_X-SiO_2 and Zn_YA_X-SiO_2 samples, to study the structure of the Zn(II) centres anchored onto the surface of silica. The analyses were repeated after tests in the MCV reaction to study the behaviour of the Zn(II) centres during the catalytic reaction.

A13. Mass Spectroscopy

MS spectra were acquired in positive-ion mode on a Q-Star Elite instrument (AB Sciex), equipped with a nano-electrospray ion source and a time of flight analyser (TOF), employing the following instrumental setting: scan range 50–450, de-clustering potential 60 V, curtain gas 20 PSI and ion spray 1.1 kV.

The experiments were performed in the MCV approach, in order to study the process formation of the cross-linking products of TME. The products formation was studied at different reaction times on liquid aliquots of vulcanized TME samples, after filtration and dilution in acetonitrile (1:10 vol:vol). The relative quantification of the species at different reaction times was performed by adding an internal standard at fixed concentration before MS analysis (diethylamine, 48 μM) and normalizing peak intensities according to the standard signal. Water (H_2O, 4% vol/vol) was added to favour the protonation of the species during the analysis.

A14. Stress-strain measurements

The mechanical properties of vulcanized samples were analysed through strain sweep tests by using a Rubber Process Analyzer (RPA 2000, Alpha Technologies) in a shear stress mode. The samples were first vulcanized in the at 170°C for 5 minutes and then, in the same testing chamber, the experiments

were carried out at 70°C and 10Hz, from 0.2 to 10% elongation, after 10 minutes of cooling down with air.

Specimens were cut by using a Constant Volume Rubber Sample Cutter (CUTTER 2000, Alpha Technologies) with a dimension of 3.5 cm diameter and 0.2 cm of thickness. The weight of the sample should be always equal to 5.0 ± 0.3 g. Two measurements were performed for each sample and the average value was reported.

A15. Swelling experiments

Swelling experiments were applied to evaluate the cross-linking degree of the rubber NCs after the vulcanization process.

Samples of 20x20x3 mm³ (m_0 = 1.00 g ± 0.05 g) were immersed in closed vessels filled with 25 mL of toluene at 25°C in the dark to avoid photo-degradation reactions. The samples have been swollen for four days, changing the solvent daily with fresh toluene, to eliminate all the extracted fractions. At the end of the last day, the mass of the swollen sample was determined (m_{sw}). Then, the samples were dried for 24 hours at room temperature and the mass of the dried samples measured (m_D). The volumetric fraction of the swelled rubber V_R was calculated according to the following equation:

$$V_R = \frac{(m_D - f \cdot m_0) \cdot \rho_p^{-1}}{(m_D - fm_0) \cdot \rho_p^{-1} + m_{so} \cdot \rho_s^{-1}}$$

where m_{SO} is the weight of the solvent in the swollen mass (m_{SO} = m_{SW} – m_D), ρ_P = 0.94 g·cm⁻³ is the IR density, ρ_s= 0.87 g·cm⁻³ is the toluene density and f is the fraction of the filler in the composites as determined by TGA. From this value, it was possible to estimate the cross-linking density ν according to the Flory-Rehner equation:

$$\nu = \frac{[\ln(1 - V_R) + V_R + \chi \cdot V_R^2}{-2 \cdot \rho_p \cdot V_s \cdot (V_R)^{1/3}}$$

where V_S = 105.91 is the molar volume of toluene and χ is the Flory solvent-polymer interaction term [4], which is 0.43 for toluene-IR[5].

Bibliography

1. Monticone, S., Tufeu, R. & Kanaev, A. V. Complex Nature of the UV and Visible Fluorescence of Colloidal ZnO Nanoparticles. *J. Phys. Chem. B* **102,** 2854–2862 (1998).

2. Zhang, L., Yin, L., Wang, C., Qi, Y. & Xiang, D. Origin of Visible Photoluminescence of ZnO Quantum Dots : Defect-Dependent and Size-Dependent. *Society* 9651–9658 (2010).

3. Kowalczyc, S., Ley, L., Pollak, R. & Shirley, A. High Resolution XPS spectr of Ir, Pt and Au valence bands. *Phys. Rev. B* **5,** 4709–4714 (1972).

4. Flory, P. J. & Rehner, J. Thermodynamics of high polymer solutions. *J. Chem. Phys.* **10,** 51–61 (1942).

5. Orwoll, R. & Arnold, P. Polymer-solvent interaction parameter. in *Physical properties of polymers handbook* 233–257 (Springer, 2007).